

NANOFORMULATION OF PHYTOMOLECULE LOADED GUAR GUM AGAINST DIABETIC WOUND HEALING

**Thesis Submitted for the Award of the Degree of
DOCTOR OF PHILOSOPHY**

in

Botany

By

Debojyoti Mandal

Registration No. -12021159

Supervised By

Dr. Jeena Gupta,

Associate Professor

Department of Biochemistry

School of Bioengineering and Biosciences

Co-Supervised By

Dr. Jayanta Kumar Sarmah,

Associate Professor

Department of Chemistry

Rabindranath Tagore University



LOVELY PROFESSIONAL UNIVERSITY, PUNJAB

2025

DECLARATION

I, hereby declare that the presented work in the thesis entitled “**NANOFORMULATION OF PHYTOMOLECULE LOADED GUAR GUM AGAINST DIABETIC WOUND HEALING**” in fulfilment of the degree of **Doctor of Philosophy (Ph.D.)** is the outcome of research work carried out by me under the supervision of Dr Jeena Gupta, working as Associate Professor, in the Department of Biochemistry, School of Bioengineering and Biosciences of Lovely Professional University, Punjab, India. In keeping with the general practice of reporting scientific observations, due acknowledgements have been made whenever the works described here are based on the findings of other investigators. This work has not been submitted in part or whole to any other University or Institute for the award of any degree.

(Signature of Scholar)

Name of the scholar: Debojyoti Mandal

Registration No. : 12021159

Department/School: Department of Botany (School of Bioengineering and Biosciences)

CERTIFICATE

This is to certify that the work reported in the Ph. D thesis entitled “**NANOFORMULATION OF PHYTOMOLECULE LOADED GUAR GUM AGAINST DIABETIC WOUND HEALING**” submitted in fulfilment of the requirement for the award of the degree of **Doctor of Philosophy(Ph.D.)** in the Department of Botany, School of Bioengineering and Biosciences, is a research work carried out by Debojyoti Mandal (Reg. No.:12021159), is a bonafide record of his original work carried out under my supervision and that no part of the thesis has been submitted for any other degree, diploma or equivalent course.



(Signature of Supervisor)

Supervised By

Dr. Jeena Gupta

Associate Professor

Department of Biochemistry

School of Bioengineering and
Biosciences

(Signature of Co-Supervisor)

Co-Supervised By

Dr. Jayanta Kumar Sarmah

Associate Professor

Department of Chemistry

Rabindranath Tagore University

Abstract

The chronic metabolic condition known as Type 2 diabetes mellitus (T2DM) is distinguished by persistent hyperglycaemia caused by insulin resistance and insufficient insulin synthesis. This condition progressively leads to severe complications, including chronic microvascular, macrovascular, and neuropathic issues that can be life-threatening. The onset of T2DM can be attributed to several factors, including insufficient insulin secretion, damage to pancreatic β cells, and insulin resistance, a condition in which the body fails to use insulin efficiently. The rising prevalence of T2DM is closely linked to increasing sedentary lifestyles, which significantly contribute to the global epidemic. The disease manifests in a variety of complications, such as nephropathy, neuropathy, cardiovascular and renal disorders, retinopathy, and disorders related to food intake. The impairment of pancreatic beta cells in T2DM hampers the effective use of insulin, exacerbating the condition. The burgeoning prevalence of T2DM has profound implications for individuals, society, and the economy, imposing substantial human and financial burdens. The global increase in diabetes cases has led to a dramatic rise in healthcare costs, with expenditures for individuals aged 20-79 soaring by 316% over 15 years, from USD 232 billion in 2007 to USD 966 billion in 2021. The expanding range of anti-hyperglycaemic medications for T2DM, each with varied mechanisms of action and safety profiles, presents a challenge for clinicians, highlighting the need for a well-informed strategy in prevention and treatment. Wound care in diabetic patients is particularly challenging due to the complex pathophysiology of diabetes, which includes high blood glucose levels, persistent inflammation, impaired immune responses, and reduced vascular function. These factors collectively contribute to delayed or inadequate wound healing. Wounds resulting from physical, chemical, thermal, or immunological trauma alter tissue cell structure and integrity.

The conventional understanding of wound healing involves a "healing cascade" comprising hemostasis, inflammation, proliferation, and maturation. However, for diabetics, even minor injuries such as scrapes, bruises, and burns can lead to severe health issues due to impaired healing processes. Diabetes-induced physiological and metabolic disturbances slow wound healing significantly. The elevated blood glucose levels associated with diabetes exacerbate oxidative stress and inflammation, which further impede the healing process. Infected wounds can lead to complications such as tissue and bone infections, potentially becoming life-threatening if not promptly treated. Even without infection, prolonged wound healing in diabetic patients adversely affects health and quality of life. The International Diabetes

Federation (IDF) reported that approximately 537 million people aged 20–79 were living with diabetes in 2021, with this number expected to rise to 643 million by 2030 and 783 million by 2045. The high mortality rate associated with diabetes, with 1 in 5 deaths attributed to the condition in 2021, underscores the urgency of addressing this global health crisis. The escalating costs associated with diabetes treatment further highlight the need for innovative and effective management strategies. Conventional wound care approaches, while foundational, often fall short of addressing the specific needs of diabetic wound healing.

These treatments face limitations in efficacy and overall outcomes, prompting a search for alternative approaches. Nanotechnology represents a promising frontier in this field, offering the ability to address the complexities of diabetic wounds at the nanoscale. This technology allows for the precise manipulation and design of materials, potentially surpassing the effectiveness of conventional treatments. Guar gum, a natural polysaccharide derived from guar beans, has emerged as a promising nanocarrier in wound healing formulations. Its unique properties—such as biodegradability, mucoadhesiveness, and improved stability—make it an attractive candidate for encapsulating therapeutic agents within nanoparticles. Despite its potential, there has been limited research focusing on the effectiveness of guar gum nanoparticles in diabetic wound healing, particularly in combination with bioactive compounds like natural phenolic acids. Phenolic acids, known for their antioxidant, anti-inflammatory, and antimicrobial properties, offer significant advantages in diabetic wound healing. They mitigate oxidative stress and inflammation, enhance collagen synthesis, stimulate angiogenesis, and support tissue repair by modulating growth factors and matrix metalloproteinases. These combined actions improve wound healing and address common complications associated with diabetic wounds. This research explores the potential of drug-loaded guar gum nano-formulations incorporating phenolic acids in enhancing diabetic wound healing. The study involved optimizing these nano-formulations, characterizing their properties, and conducting *in vitro* and *in vivo* evaluations. Free radical scavenging assays, including DPPH and ABTS tests, demonstrated the nano-formulations' capacity to effectively neutralize free radicals, which is crucial for promoting wound healing. Antidiabetic assays, such as glucosidase and amylase activity tests, yielded promising results, indicating beneficial effects on glucose metabolism. *In vitro* cytotoxicity tests revealed that the nano-formulations exhibited minimal or negligible toxicity, an important factor for their safety profile. Significant improvements were observed in wound healing and angiogenesis, as evidenced by enhanced performance in scratch assays (measuring wound closure) and tube formation assays (assessing new blood

vessel development). These findings suggest that the nano-formulations effectively support both tissue repair and the formation of new vascular structures. Additionally, *in vitro* antioxidant assays—including lipid peroxidation (LPO), catalase, Superoxide-dismutase assay (SOD), and Glutathione-S-transferase assay (GST) assay—showed that the nano-formulations enhanced antioxidant activity, thereby restoring near-normal oxidative conditions in the test systems. Following these promising *in vitro* results, the two most effective nano-formulations, guar gum nanoformulation of Sinapic acid(NF2) and guar gum nanoformulation of o-Coumaric acid(NF3), were selected for *in vivo* studies. These studies demonstrated that the nano-formulations were highly effective in healing diabetic wounds. Specifically, high doses of the nano-formulations achieved complete wound healing comparable to that observed under normal conditions. Even at lower doses, the nano-formulations nearly achieved full wound closure in diabetic conditions. Moreover, the treatments significantly restored tensile strength to levels similar to those seen in non-diabetic conditions. Consistent with the *in vitro* antioxidant assays, the *in vivo* studies also indicated that the nano-formulations improved antioxidant activity, helping to normalize oxidative stress conditions in the healing wounds. In conclusion, the optimized guar gum nano-formulations demonstrated significant efficacy in diabetic wound healing. They exhibited controlled drug release, effective free radical scavenging, minimal toxicity, and substantial improvements in antioxidant activity, wound healing, and angiogenesis. *In vivo* validation further confirmed that optimized nanoformulation NF2 and NF3 achieved complete wound healing and restored tensile strength, highlighting their potential as effective and safer alternatives to conventional treatments. This highlights the importance of conducting pre-clinical studies to evaluate how various therapeutic dosages affect disease progression. Further research is crucial to advance this product to clinical trials and assess its potential applications in human health. It is essential to thoroughly understand the molecular, cellular, and biochemical mechanisms by which this bioactive compound promotes wound healing.

ACKNOWLEDGEMENT

"তোমার আত্মা যদি প্রবল হয়,
তবে তোমার বাধা যতই কঠিন হোক,
সবকিছু জয় করা সম্ভব।"

- স্বামী বিবেকানন্দ

(If your soul is strong, no matter the obstacles, everything can be conquered.)

I dedicate this thesis to my beloved **বাবা** and **মা**, whose unwavering support and boundless love inspire me every day. Your dreams became my guiding light, and I am deeply grateful for the values and aspirations you instilled in me.

I want to express my heartfelt gratitude to my respected Supervisor, **Dr. Jeena Gupta**, Associate Professor, Department of Biochemistry, School of Bioengineering and Biosciences, Lovely Professional University, for her vigilant guidance, insightful criticism, extensive knowledge, and helpful scientific advice. Her selfless support has been instrumental in completing this thesis, and working under her supervision has been both an honour and a pleasure.

I extend my deepest gratitude to my respected Co-Supervisor, **Dr. Jayanta Kumar Sarmah**, Associate Professor, Department of Chemistry, Rabindranath Tagore University, for his invaluable feedback and guidance, which helped me navigate my research challenges. His mentorship has been immensely beneficial.

I am also profoundly grateful to the respected **Dr. Sukhinder Cheema**, University Research Professor, Department of Biochemistry, Core Science Facility, Memorial University of Newfoundland, for her insightful feedback and support. Her guidance has been instrumental, and I am sincerely thankful for her mentorship.

I would also like to extend my deep gratitude to **Dr. Jyotirmoy Ghosh**, Principal Scientist, Molecular Biology Laboratory, Division of Physiology, National Institute of Animal Nutrition and Physiology (NIANP), Bangalore, for his unwavering support, invaluable guidance, and constant encouragement throughout my research. His profound expertise, insightful suggestions, and constructive feedback have greatly enriched my work. I am sincerely grateful

for his availability and assistance, which were essential in shaping the direction of this thesis. A special thanks to **Dr. Navneet Khurana**, Professor, Department of Pharmacology, School of Pharmaceutical Sciences, Lovely Professional University, for his invaluable help in completing my in vivo experiments and for generously sharing his time and expertise.

I would also like to express my sincere appreciation to **Dr. Vancha Harish**, an Assistant Professor at the School of Pharmaceutical Sciences at Lovely Professional University, for his diligent work assisting me in completing my formulation development experiments.

My heartfelt thanks go to **Dr. Ashok Mittal (Honourable Chancellor)**, **Mrs. Rashmi Mittal (Pro-Chancellor)**, **Dr. Lovi Raj Gupta (Pro Vice-Chancellor)**, and **Dr. Monica Gulati (Registrar)** for their leadership and for giving me the opportunity to be a part of such a prestigious institution.

I am also thankful to our dedicated lab technicians, **Mr. Rahul Sharma**, **Ms. Sandeep**, **Mr. Madan**, and **Malti Aunty**, who provided invaluable assistance at every step of my research.

My deepest thanks go to my parents, **Mr. Mahadev Mandal** and **Mrs. Banasri Mandal**, and my sister, **Madhurima Mandal**, for their unfailing love, unwavering support, and encouragement. Their trust in my abilities, endless sacrifices, and constant encouragement have been the foundation of my accomplishments. Their influence has shaped my academic journey and my character and values, for which I am forever grateful.

I am profoundly grateful to my best friend and partner, **Piyali Maity**, for her unwavering belief in me, countless hours of feedback, and moral support. Her friendship has been a strength throughout my academic and personal journey.

I extend my heartfelt gratitude to my dear friend Dr. Kriti Kushwaha, whose unwavering encouragement, support, and understanding were crucial throughout this journey. I would also like to thank my lab mates, Nancy Bhura and Aayushi Velingarkar, for their timely help during the animal study and exceptional support, which enriched this academic endeavor.

Finally, I sincerely thank my close friends Bata, Kolu, Lela, Pandit, Arun Kumar, Ritesh Mudage, Chandan Shinde, Keshav Anand, and Rohit Malhotra, whose companionship has illuminated my path during difficult times. To my brotherly friend Tonton, thank you for

always standing by me. Your unwavering support has been a constant source of strength throughout this journey.

To everyone who has contributed to this thesis, whether directly or indirectly, thank you for participating in this significant milestone in my academic journey. Your support has been the cornerstone of my achievement, and I am profoundly grateful for that.

TABLE OF CONTENTS

S. No.	Chapter titles	Page No.
1	Chapter 1: Introduction	1-8
2.	Chapter 2: Review of Literature (ROL)	9-49
	2.1 Pathophysiology	9-13
	2.2 Wound	13
	2.3 Types of Wounds	13-15
	2.4 Wound healing	15-17
	2.5 Diabetic Wound Healing	17-19
	2.6 Normal Wound Healing vs. Diabetic Wound Healing: A Comparative Overview	19-21
	2.7 Wound healing medications and treatments	21-31
	2.8 Disadvantages/Limitations of these Wound Healing Treatments:	31
	2.9 How Nanotechnology-Based Treatments are filling this gap ?:	31-37
	2.10 Polymeric nanotechnology in diabetic wound healing	37-38
	2.11 Guar gum as polymeric nanocarrier:	38-42
	2.12 Phenolic acid in wound healing	42-49
	Research Gap	50
3.	Chapter 3: Hypothesis	51-52
4.	Chapter 4: Aims and Objectives	53
5.	Chapter 5: Materials and Methods	54-75
	5.1 Chemicals and Reagents	54
	5.2 Nanoformulation Design	54-55
	5.3 Evaluation of the prepared nanoformulation	56-57
	5.4 Characterization of the prepared nanoformulation:	57-58
	5.5 In vitro studies	58-69
	5.5.1 Free radical scavenging activity of the prepared nanoparticles	58-59
	5.5.2 Anti-diabetic enzyme activity of the prepared nanoparticles	59-60
	5.5.3 Cytotoxicity activity	60-61
	5.5.4 In vitro scratch assay	61
	5.5.5 Tube formation assay	61-62
	5.5.6: In vitro induction of diabetes in cell line	62

	5.5.7: In Vitro model establishment (in 6-well plates)	62-63
	5.5.8 Cell lysis and preparation of cell lysate for protein array (6-well format)	63
	5.5.9 Preparation of tissue/cell homogenate	63
	5.5.10: Estimation of protein	64-65
	5.5.11: In vitro oxidative biomarkers analysis	65-69
	5.6 Antimicrobial tests	69-70
	5.6.1 Anti-microbial activity assay	69
	5.6.2 Enzyme Inhibition Assay: Cox-II	70
	5.6.3 Cytokine assay: Expression Analysis of TNF- α (with and without Bacterial infection condition)	70
	5.7 In vivo experiment	70-75
	5.7.1 Description of in vivo experiment:	70-73
	5.7.2: Parameters of evaluation of DM	73-74
	5.7.3: Wound Healing Parameters-	74-75
	5.8 Statistical analysis	75
Chapter 6: Results		76-165
6.	6.1 Optimization, Characterization of Zeta sizer, and SEM of placebo	76-77
	6.2 Optimization of guar gum nanoformulation of Syringic acid(NF1)	77-81
	6.3 Optimization of guar gum nanoformulation of Sinapic acid (NF2)	81-86
	6.4 Optimization of guar gum nanoformulation of o-Coumaric acid (NF3)	86-90
	6.5 Characterization of Zeta sizer and SEM of optimized nanoformulation of Syringic acid (NF1), optimized nanoformulation of Sinapic acid (NF2), optimized nanoformulation of o-Coumaric acid (NF3)	90-91
	6.6 DSC Analysis and Interpretation	91-95
	6.7 TGA Analysis and Interpretation	96-99
	6.8 FTIR Analysis and Interpretation	99-106
	6.9 Drug loading and release kinetics	106-111
	6.10 Determination of pH	112-115
	6.11 Determination of Spreadability	115-118

	6.12 Determination of Viscosity	118-121
	6.13 Determination of RI	121-124
	6.14 In vitro	124-142
	6.14.1 In vitro Free radical scavenging activity	124-127
	6.14.2 Anti-diabetic enzyme activity	127-130
	6.14.3 Cytotoxicity (MTT) assay	130-131
	6.14.4 Scratch assay	132-134
	6.14.5 Tube formation assay	134-136
	6.14.6 In vitro oxidative biomarkers analysis	136-142
	6.15 Antimicrobial tests	142-147
	6.15.1 Antimicrobial assay	142-145
	6.15.2 Assessment of Cox-II Activity	145
	6.15.3 TNF- α expression	146-147
	6. 16 In vivo results	147-165
	6.16.1 Evaluation of DM Parameters	147-149
	6.16.2 Evaluation of Wound Healing Parameters-	149-154
	6.16.3 Protein estimation in tissue homogenate using Lowry's method	154-155
	6.16.4 In vivo oxidative biomarkers analysis	155-159
	6.16.5 Estimation of hydroxyproline	159-161
	6.16.6 Estimation of Hexosamine	162-163
	6.16.7 Histopathology	164-165
7.	Chapter 7: Discussion	166-187
8.	Chapter 8: Conclusion	188-189
9.	References	190-231

LIST OF TABLES

S. No.	Description	Page no
Table 1:	Pathophysiology of Type 2 Diabetes (Type 2 DM)	11-12
Table 2:	Normal Wound Healing vs. Diabetic Wound Healing: A Comparative Overview	20-21
Table 3:	Some phenolic acids for diabetic wound healing	46-47
Table 4:	Reagents for protein estimation	65
Table 5:	The procedure of LPO estimation	66
Table 6 :	Reagent details for Catalase estimation	69
Table 7 :	GST estimation reagent details	70
Table 8 :	In vivo experimental groups and treatment	73
Table 9 :	Formulations of placebo (Guar gum nanoformulation/GGNP) with particle size (nm), PdI, and Zeta potential value (mV)	77
Table 10:	Results of optimized nanoformulation of Syringic acid (NF1) of BBD design	79-80
Table 11:	The F-value, p-value, and coefficient of regression (R^2) of the optimized nanoformulation of Syringic acid (NF1) optimized formulation	80
Table 12:	Results of optimized nanoformulation of Sinapic acid (NF2) of BBD design	83
Table 13:	The F-value, p-value and coefficient of regression (R^2) of the optimized nanoformulation of Sinapic acid (NF2) optimized formulation	84
Table 14:	Results of optimized nanoformulation of o-Coumaric acid (NF3) of BBD design	87-88
Table 15:	The F-value, p-value and coefficient of regression (R^2) of the optimized nanoformulation of o-Coumaric acid (NF3) optimized formulation	88
Table 16:	Kinetics Models of guar gum nanoformulation of Syringic acid (NF1), guar gum nanoformulation of Sinapic acid	112

	(NF2), optimized nanoformulation of o-Coumaric acid (NF3) (coefficient of regression R^2)	
Table 17.1:	Photographic representation of wound healing on different days (0, 3rd, 7th)	152-153
Table 17.2:	Photographic representation of wound healing on different days (10th, 14th)	153-154
Table 18:	Histopathological evaluation of the diabetic wound healing process before and after treatment in different groups	165-166

LIST OF FIGURES

S. No	Figure	Page No
Figure 1:	Different stages of wound healing	17
Figure 2:	Different types of nanomaterials and use in different stages of wound healing	37
Figure 3:	Schematic Representation of the Nanoformulation Process	57
Figure 4	In vivo study plan	74
Figure 5	a) Particle size b) Zeta potential of GGNP, c) SEM image (x75000) particle size of placebo	77-78
Figure 6	3D diagrams of a)Particle size, b)PdI, c)Zeta Potential, d)Drug loading values of guar gum nanoformulation of Syringic acid (NF1)	80-82
Figure 7	3D diagrams of a)Particle size, b)PdI, c)Zeta Potential, d)Drug loading values of guar gum nanoformulation of Sinapic acid (NF2)	85-86
Figure 8	3D diagrams of a)Particle size, b)PdI, c)Zeta Potential values, d)Drug loading of guar gum nanoformulation of o-Coumaric acid (NF3)	89-90
Figure 9:	A) Particle diameter of nanoformulations (measured in nanometers) (Malvern Zeta Nano S90). B)Zeta potential measurement of nanoformulations (mV) using Zetasizer (Malvern Zeta Nano S 90), C)FESEM of nanoformulations (20nm scale bar, x75,000 magnification) (JEOL-6610).	91-92
Differential Scanning Calorimetry (DSC) graphs		
Figure 10:	Differential Scanning Calorimetry (DSC) graphs of Guar gum (GG) and Guar gum nanoformulations (GGNP)	92-93
Figure 11:	Differential Scanning Calorimetry (DSC) graphs of Syringic acid (SRN) and Syringic acid loaded nanoformulation (NF1)	94
Figure 12:	Differential Scanning Calorimetry (DSC) graphs of Sinapic acid (SNP) and Sinapic acid loaded nanoformulations (NF2)	95

Figure 13:	Differential Scanning Calorimetry (DSC) graphs of o-Coumaric acid (OCA) and o-Coumaric acid loaded nanoformulations (NF3)	96
Figure 14:	Thermogravimetric analysis (TGA) graphs of different samples	99-100
FTIR spectra of different samples		
Figure 15:	FTIR spectra of GG and GGNP	101
Figure 16: B); C)	FTIR spectra of Syringic acid (SRN) and Syringic acid loaded nanoformulation (NF1) along with Guar gum (GG) and Guar gum nanoformulation (GGNP); Enlargement view of FTIR spectra of SRN, guar gum nanoformulation of Syringic acid (NF1)	103
Figure 17: A); B)	FTIR spectra of Sinapic acid (SNP) and Sinapic acid loaded nanoformulation(NF2)along with Guar gum (GG) and Guar gum nanoformulation (GGNP); Enlargement view of FTIR spectra of SNP, guar gum nanoformulation of Sinapic acid (NF2)	105
Figure 18: A); B)	FTIR spectra of o-Coumaric acid (OCA) and o-Coumaric acid loaded nanoformulation (NF3) along with Guar gum (GG) and Guar gum nanoformulation (GGNP); Enlargement view of FTIR spectra of OCA, guar gum nanoformulation of o-Coumaric acid (NF3)	107
Figure 19:	Different kinetics models of optimized guar gum nanoformulation of Syringic acid (NF1)	108-109
Figure 20:	Different kinetics models of optimized guar gum nanoformulation of Sinapic acid (NF2)	110
Figure 21:	Different kinetics models of optimized guar gum nanoformulation of o-Coumaric acid (NF3)	111-112
pH values of different samples		
Figure 22:	pH values of different run samples for optimized nanoformulation of Syringic acid (NF1) and optimized guar gum nanoformulation of Syringic acid (NF1)	113

Figure 23:	pH values of different run samples for optimized nanoformulation of Sinapic acid (NF2) and optimized guar gum nanoformulation of Sinapic acid (NF2)	114
Figure 24:	pH values of different run samples for optimized nanoformulation of Sinapic acid (NF2) and optimized guar gum nanoformulation of Sinapic acid (NF2)	115
Spreadability values of different samples		
Figure 25:	Spreadability values of different run samples for optimized nanoformulation of Syringic acid (NF1) and optimized nanoformulation of Syringic acid (NF1) (SR-Standard run used in BBD model)	117
Figure 26:	Spreadability values of different run samples for optimized nanoformulation of Sinapic acid (NF2) and optimized nanoformulation of Sinapic acid (NF2) (SR-Standard run used in BBD model)	118
Figure 27:	Spreadability values of different run samples for optimized nanoformulation of o-Coumaric acid (NF3) and optimized nanoformulation of o-Coumaric acid (NF3) (SR-Standard run used in BBD model)	119
Viscosity values of different samples		
Figure 28:	Viscosity values of different run samples for optimized nanoformulation of Syringic acid (NF1) and optimized nanoformulation of Syringic acid (NF1) (SR-Standard run used in BBD model)	120
Figure 29:	Viscosity values of different run samples for optimized nanoformulation of Syringic acid (NF1) and optimized nanoformulation of Syringic acid (NF1) (SR-Standard run used in BBD model)	121
Figure 30:	Viscosity values of different run samples for optimized nanoformulation of o-Coumaric acid (NF3) and optimized nanoformulation of o-Coumaric acid (NF3) (SR-Standard run used in BBD model)	122
RI (Refractive index) values of different run samples		

Figure 31:	RI values of different run samples for optimized nanoformulation of Syringic acid (NF1) and optimized nanoformulation of Syringic acid (NF1) (SR-Standard run used in BBD model)	123
Figure 32:	RI values of different run samples for optimized nanoformulation of Sinapic acid (NF2) and optimized nanoformulation of Sinapic acid (NF2) (SR-Standard run used in BBD model)	124
Figure 33:	RI values of different run samples for optimized nanoformulation of o-Coumaric acid (NF3) and optimized nanoformulation of o-Coumaric acid (NF3) (SR-Standard run used in BBD model)	125
Figure 34:	DPPH free radical scavenging activity of formulations	126
Figure 35:	ABTS free radical scavenging activity of formulations	128
Figure 36:	α -glucosidase enzyme activity of formulations	129
Figure 37:	α -amylase enzyme activity of formulations	130
Figure 38:	Cytotoxicity assay of formulations A) L929 cells; B) HaCaT	132
Figure 39:	In vitro scratch assay (A-D) (A= Before treatment with GGNP, 0hr; B=after treatment with GGNP, 24hr; C, D= Control/no treatment, E=Bar graph showing % of healing) *p<0. 05	133
Figure 40:	In vitro scratch assay (A-D) (A= Before treatment, 0hr; B=after treatment with SRN, 24hr; C= after treatment with guar gum nanoformulation of Syringic acid (NF1)) *p<0. 05	134
Figure 41:	In vitro scratch assay (A-D) (A= Before treatment, 0hr; B=after treatment with SNP, 24hr; C= after treatment with guar gum nanoformulation of Sinapic acid (NF2);24 hr) *p<0. 05	134
Figure 42:	In vitro scratch assay (A-D) (A= Before treatment, 0hr; B=after treatment with OCA, 24hr; C= after treatment with guar gum nanoformulation of o-Coumaric acid (NF3);24 hr) *p<0. 05	135
Figure 43:	Graphical representation of the in vitro scratch assay of all samples	135

Figure 44:	Graphical representation of the in vitro tube formation assay	136
Figure 45:	Photographs of Tube formation after being treated with different samples (A-Control, B-SRN, C-guar gum nanoformulation of Syringic acid (NF1), D-SNP, E-guar gum nanoformulation of Sinapic acid (NF2), F-OCA, G-guar gum nanoformulation of o-Coumaric acid (NF3))	137
Figure 46 :	Protein estimation using the Lowry method	137
Figure 47:	In vitro Lipid peroxidation (LPO) activity of different experimental samples	139
Figure 48:	In vitro Catalase activity of different experimental samples with the L929 cell line	140
Figure 49:	In vitro Superoxide dismutase (SOD) activity of different experimental samples with the L929 cell line	141
Figure 50:	In vitro Glutathione S-transferase (GST) activity of different experimental samples with the L929 cell line	143
Figure 51:	Antimicrobial activity graph of (A): <i>S. aureus</i> ; (B): <i>E. coli</i> ; (C): <i>C. albicans</i>	144-145
Figure 52:	Antimicrobial activity plate of (A) <i>S. aureus</i> ; (B) <i>E. coli</i> ; (C) <i>C. albicans</i>	145-146
Figure 53:	Enzyme Inhibition Assay for Cox-II (wrt- with respect to)	146
Figure 54:	A)-B) The protein expression of TNF- α is decreased in the presence of bacterial infection compared to the control group without infection, C)-D) Protein Expression (downregulation) of TNF- α with respect to (wrt) control (with bacterial infection) (positive control group (with LPS treatment), the negative control group (cells without LPS treatment))	147-148
Figure 55:	Body weight of groups on different days	149
Figure 56:	Evaluation of blood glucose on different days	150
Figure 57:	Graphical representation of wound healing in different in vivo experimental groups	151
Figure 58:	Graphical representation of tensile strength of wound healing in different in vivo experimental groups	155
Figure 59:	Protein estimation using the Lowry method	156

Figure 60:	In vivo Lipid peroxidation (LPO) activity of different experimental groups	157
Figure 61:	In vivo Catalase activity of different experimental samples with wounded skin	158
Figure 62:	In vivo Superoxide dismutase (SOD) activity of different experimental samples with wounded skin	159
Figure 63:	In vivo Glutathione S-transferase (GST)activity of different experimental samples with wounded skin	160
Figure 64:	Estimation of hydroxyproline content in wounded/healed skin tissue	162
Figure 65:	Comparison of hydroxyproline content in wounded/healed skin tissue	162
Figure 66:	Estimation of hexosamine content in wounded/healed skin tissue	164
Figure 67:	Comparison of hexosamine content in wounded/healed skin tissue	164
Figure 68:	Particle size variation	169

❖ Abbreviations

DM	Diabetes mellitus
LPO	Lipid peroxidation
SOD	Superoxide dismutase
GST	Glutathione s transferase
Cat	Catalase
HFD	High-fat diet
WHO	World Health Organization
ECM	Extracellular matrix
ROS	Reactive oxygen species
COX-2	Cyclooxygenase-2
TGF- β	Transforming growth factor- β
IDF	International diabetes federation
VEGF	Vascular endothelial growth factor
STZ	Streptozotocin
DPPH	1, 1 diphenyl-2-picrylhydrazyl
MTT	3- (4, 5-dimethylthiazol-2-yl)-2, 5-diphenyltetrazolium bromide
DMSO	Dimethyl sulfoxide
DMEM	Dulbecco's modified eagle medium
PBS	Phosphate buffer saline
EDTA	Ethylenediamine tetraacetic acid
BSA	Bovine serum albumin
CDNB	1-chloro-2, 4-dinitrobenzene
MDA	Malondialdehyde
TBA	Thiobarbituric acid
NBT	Nitroblue tetrazolium
HRP	Horseradish peroxidase
TMB	Tetra methyl benzidine
ANOVA	Analysis of variance
T2D	Type 2 diabetes
TNF- α	Tumor necrosis factor- α

TBA	Thiobarbituric acid
NF	Nanoformulation
GG	Guar gum extra pure
GGNP	Guar gum nanoformulation/Placebo
NF	Nanoformulation
NF1	Nanoformulation of Syringic acid
NF2	Nanoformulation of Sinapic acid
NF3	Nanoformulation of o-Coumaric acid
SRN	Syringic acid
SNP	Sinapic acid
OCA	o-Coumaric acid
ZP	Zeta potential
PdI	polydispersity index
BBD	Box-Behnken design
LPS	Lipopolysaccharides

Chapter 1

Introduction

Diabetes has been recognized as a serious and debilitating disease for over 2000 years. Its earliest descriptions trace back to ancient Egyptian, Indian, and Greek civilizations. In the 2nd century AD, the Greek physician Aretaeus coined the term *diabetes*, meaning "siphon," to describe the excessive urination observed in patients (Roony et al., 2009; Rizeq et al., 2008). Later, in the 17th century, Dr. Thomas Willis added *mellitus*—Latin for "honey-sweet"—after observing the sweet taste of diabetic urine, a result of high glucose levels (Marko et al., 2020; Karamanou et al., 2016). Until the discovery of insulin in the early 20th century, diabetes was a fatal condition. Patients were managed with low-calorie diets, which often left them malnourished and weak (Rennie et al., 1926). In 1921, a groundbreaking discovery by Canadian scientists transformed diabetes care—insulin therapy dramatically reduced blood sugar levels and restored life to near-death patients (Sanders et al., 2002; Gerstein et al., 2021). In the 1950s, diabetes was further classified into two types: insulin-sensitive (Type 1) and insulin-insensitive (Type 2) (Ahlqvist et al., 2022). Since then, continuous medical advancements have significantly improved the quality of life for diabetic patients (Singh et al., 2010). Despite these strides, the quest for a definitive cure continues. While insulin remains a milestone achievement, modern research is focused on uncovering newer, more effective treatments.

Among the various forms of diabetes, T2DM is the most prevalent, accounting for over 90% of all cases globally. The metabolic condition known as T2DM is distinguished by persistent hyperglycaemia caused by insulin resistance and decreased insulin production (DeFronzo et al., 2015). High blood glucose levels, the hallmark symptom of type 2 diabetes, are caused by either inadequate insulin synthesis by the pancreas or the body's inability to effectively use the insulin it produces (Rachdaoui et al., 2020). Genetic traits and lifestyle choices, like a sedentary lifestyle and eating poorly, can contribute to the development of diabetes. Without proper management, diabetes can lead to severe complications like vision impairment, kidney disease, and nerve damage (Wing et al., 2001). The increasing global incidence of T2DM underscores its significant impact on public health, highlighting the need to explore its diverse complications comprehensively. One particularly intricate and clinically meaningful manifestation is impaired wound healing (Murea et al., 2012).

The pathophysiology of T2DM is multifactorial and complex. At its core lies a progressive decline in pancreatic β -cell function combined with peripheral insulin resistance. In the early stages, insulin resistance is partially compensated by increased insulin production. However, over time, β -cell dysfunction leads to inadequate insulin secretion (LeRoith,2002). This imbalance results in chronic hyperglycaemia, which triggers a cascade of metabolic disturbances, including lipotoxicity, glucotoxicity, oxidative stress, and chronic inflammation. These disruptions contribute to endothelial dysfunction and impaired microcirculation, laying the groundwork for a host of complications such as cardiovascular disease, nephropathy, neuropathy, retinopathy, and delayed wound healing. The sustained hyperglycaemic state in T2DM patients interferes with normal cellular and molecular mechanisms, significantly impairing the wound healing process (Lima et al.,2022).

Any physical, chemical, thermal, or immunological damage that alters the framework and integrity of tissue cells is considered a wound (Han et al., 2023). The process of wound healing is commonly defined as the restoration of the skin. When the skin sustains damage, the body triggers an innate series of processes, commonly known as a "healing cascade, " to mend the injured tissue (Sorg et al., 2023). The healing process consists of four interrelated phases: haemodynamic equilibrium (Homeostasis), inflammation, proliferation, and maturation (Young et al., 2011). Occurrences of superficial injuries, bruises, and burns are regrettable yet unavoidable. Nevertheless, individuals with diabetes may experience severe health complications as a result of these injuries. Diabetes impairs wound healing through a multifaceted interplay of physiological and biochemical disruptions. The complex pathophysiology of diabetes involves elevated blood glucose levels, chronic inflammation, impaired immune responses, and compromised vascular function, all of which contribute to wound delayed or impaired healing (Burgess et al., 2021). Individuals with diabetes are prone to wounds that may heal slowly, inadequately, or, in some cases, fail to heal altogether. These wounds can become infected, potentially spreading to nearby tissues and bones or distant parts of the body. Without timely medical intervention, such infections can become life-threatening or fatal. Even without infection, delayed wound healing can negatively impact an individual's overall health and quality of life. Diabetes mellitus is a major global health concern, affecting approximately 537 million people aged 20–79 worldwide, with a global prevalence rate of 10.5% (IDF, 2021). This number is projected to rise to 643 million by 2030 and 783 million by 2045. About 75% of diabetic individuals reside in low- and middle-income countries, contributing to nearly 4 million deaths annually, especially among individuals aged 40–59

years (Sun et al., 2022; IDF, 2021). Additionally, 352 million people are currently at risk of developing Type 2 diabetes. The economic burden is significant. In 2021, global healthcare expenditure on diabetes reached approximately USD 966 billion, marking a 316% increase from USD 232 billion in 2007 (IDF Diabetes Atlas, 9th Edition, 2019). Diabetic individuals spend 2–3 times more on healthcare than non-diabetics, posing a severe socioeconomic impact, particularly in developing countries (Kowluru et al., 2015). In India, often referred to as the "Diabetes Capital of the World," the burden is especially high. The country is home to one in seven diabetic individuals globally (Kamani et al., 2017), with around 80 million cases currently and an expected rise to 130 million by 2045 (IDF, 2022). Type 2 diabetes accounts for nearly 90% of all cases (Pradeepa et al., 2003). Alarming, prevalence is rising across all age groups, with a >10% increase among youth. Beyond blood sugar regulation, diabetes is associated with numerous microvascular and macrovascular complications, including stroke, cardiovascular disease, impaired wound healing, foot ulcers, and coronary heart disease, making it a leading cause of morbidity and mortality (King et al., 2005).

They are observed to impact approximately 15% of individuals with diabetes, constituting more than 27% of the \$176 billion spent annually on healthcare services for diabetes in the United States (Gordois et al., 2003). Approximately 4–10% of individuals with diabetes are estimated to have diabetic foot ulcers (DFUs). Moreover, 56% of DFUs are prone to infection, with 20% of these cases requiring lower limb surgery (Wu et al., 2007). In the Indian context, approximately 12–25% of individuals with diabetes are susceptible to developing diabetic foot ulcers (DFUs). These ulcers are often complicated by cellulitis or osteomyelitis, which arise from the interaction between the immune system and colonising bacteria. DFUs significantly impact a patient's physical health, economic stability, and mental well-being. The situation worsens once infected, primarily by bacterial agents, often requiring hospitalisation. In India, it is estimated that 44–68% of hospitalized DFU patients develop osteomyelitis, which commonly results in amputation of the affected area. This highlights the severe burden of DFUs in the Indian healthcare system (Kale et al., 2023).

Conventional wound healing treatments—including topical antibiotics, growth factors, and dressings—offer symptomatic relief but often fail to address the underlying pathophysiological disturbances in diabetic wounds. Moreover, limitations such as low bioavailability, poor penetration, and high cost reduce their clinical efficacy. These shortcomings have led to the exploration of alternative approaches that can enhance healing while targeting multiple facets of the wound microenvironment. Conventional medication, while a cornerstone in managing

diabetic wound healing, is not without its drawbacks. These limitations encompass various aspects that can impact the efficacy and overall outcomes of the treatment. One significant challenge lies in the systemic nature of many conventional medications (Mandal et al., 2023). Administered throughout the entire body, these medications can give rise to systemic side effects that extend beyond the targeted wound site. Patients may experience discomfort and complications unrelated to the healing process. Another notable limitation is the lack of precision in targeting specific cells or tissues (Adepu et al., 2021). Conventional medications do not possess the ability to deliver therapeutic agents exclusively to the wound site. This lack of targeting precision may compromise the optimal concentration of drugs at the injury site, potentially diminishing their effectiveness. Paradoxically, certain conventional medications intended to address diabetic wound healing may inadvertently contribute to delayed healing. For instance, anti-inflammatory drugs prescribed for managing inflammation can interfere with the normal inflammatory response crucial for the initial phases of healing wounds (Salazar et al., 2016). The prolonged use of conventional antibiotics to treat wound infections can lead to the development of drug-resistant strains of bacteria (Pirvanescu et al., 2014). In diabetic patients, who may already face compromised immune function, this poses a serious challenge in managing infections over time. Achieving optimal bioavailability of drugs can be challenging, especially in chronic conditions like diabetic wounds, where impaired blood circulation may limit the effective delivery of medications to the wound site. This can result in suboptimal therapeutic effects. Interactions between medications are an additional concern, particularly in diabetic individuals who often require multiple medications for various aspects of their condition. Conventional medications for wound healing may interact with other drugs, leading to unpredictable effects and potential complications (Monika et al., 2022). While conventional medications may address symptoms, actively stimulating cellular responses essential for tissue regeneration is often limited. This can result in a slower and less effective healing process, especially in chronic wounds associated with diabetes. Allergic reactions to conventional medications can further complicate wound healing (Guo et al., 2010). Skin rashes, itching, or more severe allergic responses may occur, necessitating adjustments to the treatment plan. The lack of personalization in conventional medication approaches means treatments are often based on general protocols and standard dosages. This one-size-fits-all approach may not account for the unique characteristics of individual patients' wounds and overall health, potentially leading to suboptimal outcomes. Finally, the chronic use of some diabetic wound medications raises concerns about dependency and potential long-term effects (McLellan et al., 2000). A balance between managing wounds effectively and promoting

natural healing processes is crucial to ensure the best possible outcomes for patients. In light of these limitations, ongoing research is exploring alternative approaches, such as nanotechnology-based approaches.

Nanotechnology presents a promising frontier in diabetic wound healing, surpassing conventional treatments in several aspects. At its core, nanotechnology operates at the nanoscale, allowing for precise manipulation and design of materials to address the intricate challenges of diabetic wounds (Du et al., 2019). In terms of drug delivery, nanotechnology offers a groundbreaking approach. Engineered nanoparticles can be tailored to ferry therapeutic agents directly to the affected areas, ensuring a targeted and controlled release. An illustrative study showed that the controlled release of rhEGF enclosed in nanoparticles augmented the effects of rhEGF in promoting cell proliferation and accelerating wound healing (Chu et al., 2010). Wound dressings, a critical component in diabetic wound care, benefit significantly from nanotechnology. Nanomaterial integration enhances the properties of dressings, providing increased flexibility, porosity, and the ability to maintain an optimal, moist environment conducive to healing (Stoica et al., 2020; Liu et al., 2022). Nanofiber-based dressings, for instance, emulate the extracellular matrix, promoting cell adhesion and migration and facilitating tissue regeneration (Iacob et al., 2020). Additionally, certain nanomaterials, such as silver or gold nanoparticles, exhibit inherent antimicrobial properties, addressing the prevalent issue of infections in diabetic wounds (Sabarees et al., 2022; Qin et al., 2022). Diagnostic capabilities are also revolutionized by nanotechnology.

Innovative tools enable real-time monitoring of the healing process at the molecular level, allowing for tailored treatment plans based on individual patient needs (Huang et al., 2023). This personalized approach can significantly enhance the effectiveness of interventions. Moreover, the anti-inflammatory effects of nanomaterials contribute to creating a more favourable environment for tissue repair. Chronic inflammation, a common hindrance in diabetic wound healing, can be mitigated through the careful modulation of the inflammatory response using nanotechnology (Padmanabhan et al., 2015). Nanoparticles can serve dual roles by aiding in wound healing and providing diagnostic insights. They can be utilized for in vivo imaging and tracking of cells involved in the reparative process, offering valuable information on the dynamics of tissue repair (Gil et al., 2019). This capability enables healthcare professionals to make informed decisions and adjust treatment strategies based on real-time observations. While the potential of nanotechnology in diabetic wound healing is evident, it is crucial to acknowledge ongoing research efforts (Smith et al., 2017). Questions related to long-

term safety, efficacy, and the scalability of nanotechnology-based treatments remain, and addressing these aspects will be essential for the widespread clinical adoption of these innovative approaches. As an answer, biological macromolecule-based nanoformulations have gained significant interest in recent decades for improving wound healing (Garg et al., 2023). For example, active compounds such as vaccarin, curcumin, and melatonin have been effectively loaded into chitosan-based nanoformulations with potential wound healing effects (Hou et al., 2020; Fahimirad et al., 2021; Correa et al., 2020). Similarly, active compounds like Aloe vera extract have been successfully incorporated into xanthan gum-based nanoformulations for improved wound healing activity (Saravanakumar et al., 2023). These nanoformulations of macromolecules, such as xanthan gum, guar gum, and chitosan, offer unique advantages, including improved drug delivery, enhanced bioavailability, and targeted therapeutic effects (Baruah et al., 2022).

Guar gum, a natural polysaccharide derived from guar beans, is a promising nanocarrier in wound healing formulations. The unique properties of guar gum make it an attractive candidate for encapsulating therapeutic agents within nanoparticles, offering several advantages in wound care (Orsu et al., 2020). One of the key attributes contributing to the appeal of guar gum as a nanocarrier is its biocompatibility. Derived from a natural source, guar gum is well-tolerated by the human body, reducing the likelihood of adverse reactions (Verma et al., 2021). This is particularly crucial in medical applications, where compatibility with biological systems is essential for safety and effectiveness. Additionally, guar gum exhibits mucoadhesive properties, enabling it to adhere to mucosal surfaces. This quality is advantageous in wound healing formulations as it enhances the residence time of the nanocarrier at the wound site (Verma et al., 2021). The stability of encapsulated drugs or bioactive compounds is critical in pharmaceutical formulations. Guar gum, when used as a nanocarrier, contributes to improved stability, preserving the potency of therapeutic agents during storage and transportation (Verma et al., 2021). This is especially relevant in developing wound healing formulations intended for practical use. Moreover, guar gum's biodegradability aligns with the growing emphasis on environmentally friendly medical materials. The natural breakdown of guar gum over time supports the development of sustainable and biocompatible wound healing technologies. Formulating nanoparticles with guar gum is relatively straightforward, contributing to its attractiveness for drug delivery applications. This ease of formulation enhances the feasibility of incorporating guar gum-based nanocarriers into practical wound-healing solutions. The potential for enhanced bioavailability is another advantage offered by guar gum-based

nanocarriers. In scenarios where therapeutic agents have limited solubility, guar gum can improve bioavailability, ensuring better absorption and, consequently, more effective wound healing outcomes. Furthermore, the cost-effectiveness of guar gum adds to its appeal for large-scale applications. Guar gum is economically viable and readily available and contributes to the practicality and scalability of nanocarrier formulations for wound healing (Dodi et al., 2023).

Nevertheless, much focus is put on using guar gum in combination with other substances and drugs in diabetic wound healing treatments (Santos et al., 2016; Bhabani et al., 2021).

However, not much focus has been given to understanding the effectiveness of guar gum nanoparticles in diabetic wound healing, along with other bioactive compounds like natural phenolic acids (Santos et al., 2020).

Recent research has focused on the integration of phytochemicals, especially phenolic acids, into nanocarrier systems to exploit their antioxidant, anti-inflammatory, and antimicrobial properties in wound management. Phenolic acids, natural compounds found in plants, exhibit effectiveness in diabetic wound healing through diverse mechanisms (Kumar et al., 2019). In diabetic wounds, oxidative stress is a common challenge (Yang et al., 2023). The antioxidant properties of phenolic acids are significant as they effectively counteract reactive oxygen species (ROS) and mitigate oxidative stress (Kaurinovic et al., 2019). This protective effect creates a more favourable environment for healing and reduces inflammation. Chronic inflammation in diabetic wounds can impede healing (Zhao et al., 2016). The anti-inflammatory activities of phenolic acids involve the modulation of the inflammatory response and inhibiting pro-inflammatory molecule synthesis (Taofiq et al., 2015). This regulation contributes to a more balanced inflammatory environment for tissue repair. Certain phenolic acids, such as ferulic acid, stimulate collagen synthesis, a critical component of tissue repair (Kumar et al., 2020). Enhanced collagen production improves wound closure, tissue regeneration, and the overall structural integrity of the healed tissue. Phenolic acids with antimicrobial properties help combat infections, common complications in diabetic wounds (Du et al., 2022). By preventing or treating infections, phenolic acids contribute to a healthier wound environment, reducing the risk of complications and supporting the healing process. Angiogenesis, the development of new blood vessels essential for delivering nutrition and oxygen to the healing wound, is stimulated by phenolic acids. Improved blood flow enhances the delivery of essential elements to the wound site, facilitating faster and more efficient

healing (Tsakiroglou et al., 2019). The influence of phenolic acids on growth factors, such as transforming growth factor-beta (TGF- β), regulates cell proliferation, differentiation, and migration (Ashrafizadeh et al., 2020). These processes are essential for effective wound repair. Phenolic acids can modulate the activity of matrix metalloproteinases (MMPs), enzymes involved in tissue remodelling and wound closure. This modulation helps maintain a balanced extracellular matrix, supporting proper wound healing without excessive tissue breakdown (Hwang et al., 2006).

Anticipating the advantages of nanotechnology and the related favourable characteristics of guar gum and phenolic acids, this work explores the potential of active phenolics-loaded guar gum nano-formulation in diabetic wound healing.

Chapter 2: Review of Literature (ROL)

Diabetes mellitus is one of the most prevalent non-communicable diseases globally, with India accounting for approximately one-seventh of the world's diabetic population (Kamani et al., 2017). The condition has seen a marked rise across all age groups, with over a 10% increase observed among the younger population. As a major lifestyle-related disorder, diabetes poses serious short- and long-term health risks.

2.1 Pathophysiology Type 2 diabetes mellitus (T2DM)

The development and advancement of Type 2 diabetes mellitus (T2DM) are caused by a complicated interplay of hereditary, environmental, and lifestyle variables (Zheng et al., 2018). Unlike Type 1 Diabetes Mellitus, marked by the autoimmune destruction of insulin-producing beta cells, T2DM is primarily characterised by insulin resistance and reduced insulin secretion. Here is an overview of the critical elements in the pathophysiology of T2DM (Table 1):

- 1. Insulin Resistance:** A vital aspect of the pathophysiology of T2DM is insulin resistance, where body cells, especially those in the muscles, liver, and adipose tissue, become less responsive to insulin's effects. Usually, insulin, a hormone the pancreas produces, enables cells to absorb glucose for energy. In T2DM, this mechanism is impaired, resulting in elevated blood glucose levels (Goldstein et al., 2002).
- 2. Impaired Insulin Secretion:** As T2DM progresses, the pancreatic β cells that produce and secrete insulin may experience dysfunction and reduced responsiveness. Despite the pancreas's initial response of producing more insulin, β cells eventually become overwhelmed, and insulin levels fall dangerously low. This results in insufficient insulin to maintain normal glucose levels, contributing to hyperglycaemia (Maria Elizabeth et al., 2017).
- 3. Genetic Predisposition:** Genetic factors are crucial in determining susceptibility to T2DM. Certain genetic variations can affect insulin sensitivity, β -cell function, and various components of glucose metabolism, increasing the risk of developing the condition. Individuals with a family history of diabetes may be more predisposed to developing T2DM, although environmental factors also play a crucial role (Beck-Nielsen et al., 2003).
- 4. Lifestyle Factors:** Environmental factors, particularly lifestyle choices, contribute significantly to the development of T2DM. Sedentary lifestyles, unhealthy dietary habits, and obesity are significant contributors. Lack of physical activity and consuming

calorie-dense, nutrient-poor diets can lead to weight gain and exacerbate insulin resistance (Kolb et al., 2017).

- 5. Adipose Tissue Dysfunction:** Adipose tissue, particularly visceral fat, becomes dysfunctional in T2DM. This dysfunctional adipose tissue releases pro-inflammatory substances, including cytokines and adipokines, contributing to chronic inflammation. Inflammation further impairs insulin signalling and exacerbates insulin resistance (Sbraccia et al., 2021).
- 6. Glucose Production by the Liver:** The liver, the key regulator of glucose metabolism in hyperglycaemia, may overproduce glucose, especially during fasting periods. This overproduction contributes to elevated fasting blood glucose levels, further contributing to the overall hyperglycaemia seen in T2DM (Stone et al., 1985).
- 7. Chronic Inflammation:** Chronic low-grade inflammation is a hallmark of T2DM. Inflammatory signals emanating from adipose tissue and other sources contribute to systemic inflammation, which worsens insulin resistance and plays a role in the development of complications associated with diabetes (Sharif et al., 2021).

Table 1: Pathophysiology of Type 2 Diabetes (Type 2 DM)

Aspect	Description	Mechanism	Complications and Consequences	References
Insulin resistance	At first, cells' insulin sensitivity declines, which slows glucose uptake.	Reduced the ability of cells to utilise insulin for glucose uptake.	Elevated blood glucose levels and increased insulin production.	Cavaghan et al., 2000
Impaired Insulin Secretion	The pancreas loses effectiveness in producing and secreting insulin.	Dysfunction and reduced responsiveness of pancreatic beta cells.	Insufficient insulin leads to hyperglycaemia.	Kitabchi et al., 2009
Hyperglycaemia	Persistent elevation of blood glucose levels due to disrupted glucose homeostasis.	The imbalance between insulin supply and demand leads to glucose accumulation.	Microvascular and macrovascular complications, neuropathy, and nephropathy.	Szablewski, 2011
Adipose Tissue Dysfunction	Dysfunctional adipose tissue contributes to inflammation and worsens insulin resistance.	Release of pro-inflammatory cytokines and adipokines from adipose tissue.	Exacerbation of insulin resistance and systemic inflammation.	Ahmed et al., 2021 Derosa et al., 2020

Glucose Production by the Liver	Overproduction of glucose by the liver, especially during fasting periods.	Dysregulation of hepatic glucose output and gluconeogenesis.	Elevated fasting blood glucose increases glucose release by the liver.	Sargsyan et al., 2019
Genetic Predisposition	Genetic factors influence insulin sensitivity, beta cell function, and susceptibility.	Variations in genes related to insulin signalling and glucose metabolism.	Higher risk of developing T2DM based on genetic predisposition.	Ruchat et al., 2009
Lifestyle Factors	Sedentary lifestyles, unhealthy diets, and excess body fat exacerbate insulin resistance.	Lack of physical activity and unhealthy dietary choices lead to obesity.	Weight gain, exacerbation of insulin resistance, and increased inflammation.	Reis et al., 2011
Chronic Inflammation	Chronic low-grade inflammation from adipose tissue and other sources impacts insulin response.	Release of inflammatory mediators affects insulin sensitivity.	Aggravation of insulin resistance, increased risk of cardiovascular diseases.	Heilbronn et al., 2008

T2DM is linked to various complications (like nephropathy, neuropathy, diabetic wound healing, etc.), whether micro or macrovascular, occurring in target organs, and is associated with a reduction in the average lifespan. Atraumatic limb amputations are expected outcomes of chronic wounds in diabetes, which is a significant cause for fret (World Health Organisation, 2016). They are observed to impact approximately 15% of individuals with diabetes, constituting more than 27% of the \$176 billion spent annually on healthcare services for diabetes in the United States (CDC, 2017; Gordoio et al., 2003).

2.2 Wound

A wound is a physical injury to the body that damages the skin or underlying tissues. Wounds can occur due to a variety of causes, including accidents, trauma, surgery, or underlying health conditions (Eming et al., 2014). The severity of a wound can range from minor cuts and abrasions to more complex injuries involving deeper tissues. Wounds are typically categorised based on their characteristics, such as incised wounds (clean cuts), lacerations (tearing of tissue), abrasions (scrapes), or puncture wounds (penetration by a pointed object). Additionally, wounds can be acute, healing over a relatively short period, or chronic, persisting over an extended duration (Wolcott et al., 2010). The body's natural response to a wound involves a series of processes, including inflammation, tissue repair, and remodelling. Inflammation is the initial response to injury, involving blood clotting and immune cell activity. The subsequent phases focus on rebuilding damaged tissue through cell proliferation and collagen synthesis. Proper wound care facilitates optimal healing and prevents complications such as infections. It involves cleaning the wound, applying appropriate dressings, and sometimes seeking medical attention for more severe injuries. Wounds may also require specific interventions, such as sutures or staples for wound closure or surgical procedures to address underlying issues. Chronic conditions, impaired circulation, or compromised immune function can affect the body's ability to heal wounds, leading to complications (Rodrigues et al., 2019; Eming et al., 2014).

2.3 Types of Wounds

- 1. Incised Wounds:** Incised wounds result from sharp objects such as knives or glass. They cause clean, well-defined cuts in the skin. Due to the sharpness of the object, these wounds often have minimal tissue damage, and bleeding is generally more controlled than in other types of wounds (Davison, 2004).

2. **Lacerations:** Lacerations involve tearing the skin and underlying tissues. They often result from blunt force trauma or accidents. The irregular edges of lacerations can complicate the healing process, and the extent of tissue damage varies based on the force applied (Trott, 2012).
3. **Abrasions:** Colloquially known as scrapes, they occur when the skin rubs against a rough surface. They are characterised by removing the top layer of skin and exposing the underlying tissue. While typically not deep, abrasions can be painful and may take time to heal (Shrestha et al., 2020; Kramer et al., 2016).
4. **Contusions,** or bruises, develop when blood vessels beneath the skin rupture due to blunt force. The characteristic discolouration results from blood pooling beneath the skin. The severity of a contusion depends on the force of impact and the depth of tissue affected (Harris et al., 2010).
5. **Puncture Wounds:** Puncture wounds result from sharp, pointed objects like nails or needles penetrating the skin. These wounds may seem minor on the surface, but can be deceiving, as the risk of deep tissue damage and infection is higher due to the narrow entry point (Racz et al., 2010).
6. **Penetrating Wounds:** Penetrating wounds occur when an object enters and remains embedded in the body. These wounds may cause damage to internal organs or structures. The management of penetrating wounds involves assessing the depth and trajectory of the foreign object (Reginelli et al., 2015).
7. **Avulsions:** Avulsions involve the tearing away of skin and underlying tissues. They can occur during accidents or traumatic events, leading to significant tissue loss. Avulsions may require complex reconstructive procedures to restore form and function (Pope, 2009).
8. **Gunshot Wounds:** Gunshot wounds result from bullets or other projectiles penetrating the body. The extent of tissue damage can vary widely, depending on factors such as the type of firearm, bullet trajectory, and entry/exit points. Treatment often involves addressing the wound and potential internal injuries (Dicpinigaitis et al., 2006).
9. **Burns:** Burns are injuries resulting from exposure to heat, chemicals, electricity, or radiation. They are categorised into degrees according to their severity. First-degree burns affect the outer layer of skin, while third-degree burns extend into deeper tissues. Severe burns may require specialised care, including skin grafts (Schiestl et al., 2013).

- 10. Ulcers:** are open sores that can develop internally or externally. Conditions such as venous insufficiency, arterial disease, or infections can affect their formation. Chronic ulcers may resist healing and require ongoing management (Margolis et al., 2002).
- 11. Surgical Wounds:** Surgical wounds are intentional incisions made during surgical procedures. The manner of closure (e.g., sutures or staples) depends on the type of surgery. Proper postoperative care prevents complications like infections (Baxter, 2003).
- 12. Chronic Wounds:** Chronic wounds remain unresolved for prolonged periods, frequently due to underlying health conditions such as diabetes, vascular disorders, or immune system dysfunction. These wounds may exhibit delayed healing and are prone to infections (Falanga et al., 2022).
- 13. Crush Injuries:** Crush injuries occur when a body part experiences intense pressure. These injuries can damage muscles, blood vessels, and bones. Complications may include compartment syndrome or systemic issues like crush syndrome (Visha et al., 2010).

2.4 Wound healing

In reaction to tissue damage, the body undertakes a complicated and dynamic natural process called wound healing. The process entails a sequence of meticulously synchronised phases to heal injured tissues' functional and structural integrity (Rodrigues et al., 2019) (Visha et al., 2019; Hosgood et al., 2006; Enoch et al., 2008). The four stages of wound healing are (Figure 1):

1. Hemostasis:

- **Initiation:** Immediately after injury, blood vessels constrict to minimise blood loss.
- **Platelet Activation:** Platelets adhere to the wound, forming a temporary plug and releasing growth and clotting factors.
- **Blood Clot Formation:** A blood clot forms to seal the wound and stop bleeding.

2. Inflammation:

- **Vasodilation:** Blood vessels around the wound dilate, allowing immune cells, nutrients, and growth factors to reach the site.
- **Immune Cell Infiltration:** Upon arrival at the site, neutrophils and macrophages migrate to eliminate trash, pathogens, and injured tissue.

- Cytokine Release: Cells release signalling molecules (cytokines) that coordinate the immune response and tissue repair.

3. Proliferation:

- Angiogenesis: Angiogenesis is the process of forming new blood vessels to supply nutrients and oxygen to growing tissue.
- Fibroplasia: Migrating to the wound, fibroblasts synthesise collagen that establishes the structural basis for tissue regeneration.
- Reepithelialisation: Epithelial cells near the periphery of the wound undergo proliferation and migration to extend over the wound's surface.
- Granulation Tissue Formation: The wound space is filled with granulation tissue rich in fibroblasts and blood vessels.

4. Remodelling (Maturation):

- Collagen Remodelling: Collagen fibres are rearranged and cross-linked to strengthen the tissue.
- Scar Formation: Excess granulation tissue is reduced, and a mature scar is formed.
- Wound Contraction: The margins of the wound compress, diminishing the wound's dimensions.
- Tissue Maturation: Tissue undergoes maturation, becoming more organised and functional.

The stages of wound healing are not strictly linear, and there is often overlap between them. Additionally, the effectiveness of the healing process can be influenced by factors such as nutrition, oxygenation, infection control, and underlying health conditions. A well-coordinated and adequately functioning immune response is critical for the success of each stage in the wound-healing process.

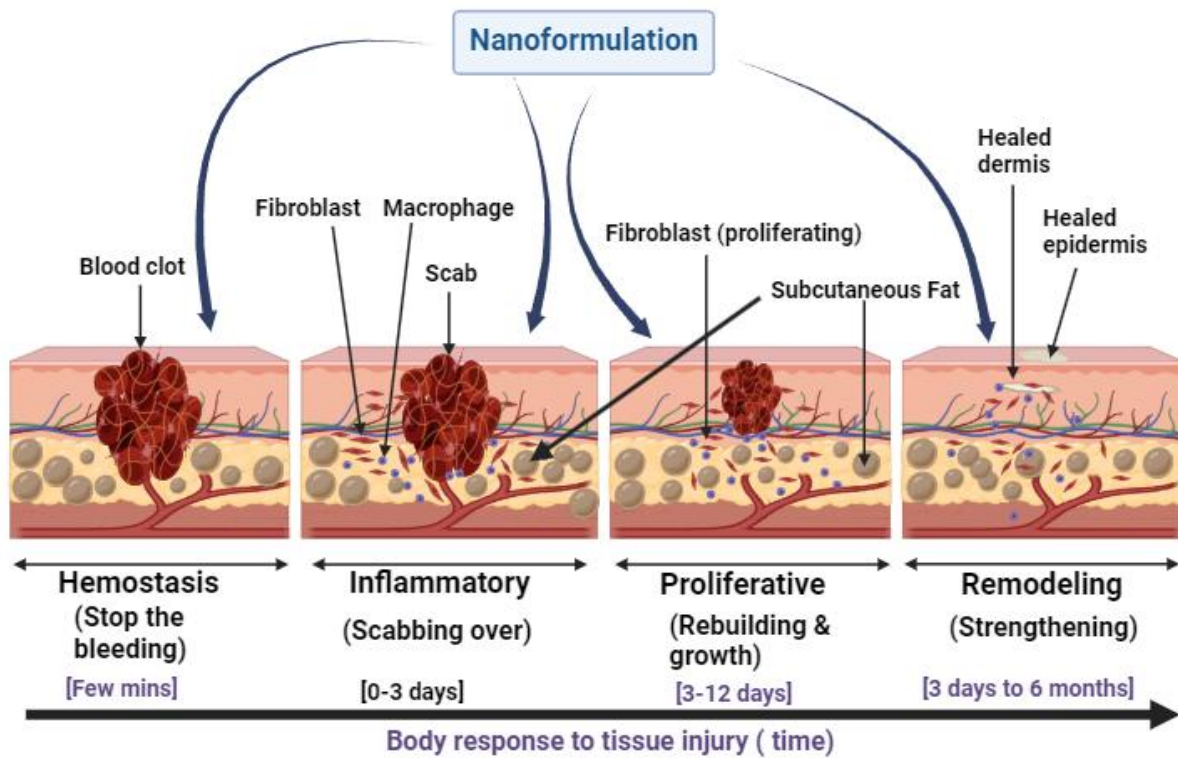


Figure 1: Different stages of wound healing

2.5 Diabetic Wound Healing

Diabetic wound healing presents a unique set of challenges, primarily stemming from the intricate web of factors associated with diabetes. The chronic nature of hyperglycaemia, coupled with impaired blood circulation, neuropathy, and compromised immune function, collectively contributes to delays and complications in the healing process (Chakraborty et al., 2022). A comprehensive understanding of these challenges is crucial for effective management and optimized outcomes in individuals with diabetes. The major problems associated with diabetic wound healing are as follows:

1. Delayed Inflammation:

In a typical wound-healing process, inflammation functions as a defensive mechanism, facilitating the removal of debris and pathogens. However, in diabetic individuals, chronic hyperglycaemia can disrupt this phase, leading to prolonged inflammation. This delay poses a significant challenge, as it impedes the timely progression to subsequent stages of healing (Pierce, 2001).

2. Impaired Angiogenesis:

The process of angiogenesis, the generation of new blood vessels, is vital for providing the necessary oxygen and nutrients to the wound site. Unfortunately, diabetes is often associated with impaired angiogenesis. This impairment restricts blood flow to the wound, creating an environment where tissue regeneration becomes challenging, further complicating the healing process (Kolluru et al., 2012; Okonkwo et al., 2017).

3. Deficient Fibroblast Function:

Fibroblasts serve a crucial function in collagen synthesis and tissue repair. However, individuals with diabetes may experience compromised fibroblast function. This compromise results in reduced collagen production, affecting the structural integrity of the wound and leading to impaired wound closure (Desta et al., 2010).

4. Reduced Growth Factor Activity:

Growth factors are essential in signalling cell proliferation and promoting tissue regeneration. In diabetic conditions, the activity of these growth factors may be diminished, creating a barrier to the effective progression of the healing process. This reduction in growth factor activity can significantly hinder the body's ability to repair and regenerate damaged tissue (Ojalvo et al., 2017).

5. Microvascular Complications:

Microvascular complications, which affect blood vessels on a small scale, are a hallmark of diabetes. In the framework of wound healing, these complications disrupt normal blood flow and nutrient delivery to the wound site. The compromised microvasculature contributes to an unfavourable environment for efficient tissue regeneration (Pfeiffer et al., 1995).

6. Neuropathy:

Diabetic neuropathy impacts sensory and autonomic nerves, leading to diminished pain perception. This reduction in sensitivity can result in delayed detection of wounds, as individuals with diabetes may not readily sense injuries. Delayed awareness poses a challenge in initiating timely wound care and intervention (Margolis et al., 2002).

7. Increased Risk of Infection:

Due to the elevated blood glucose levels in diabetic wounds, bacteria thrive. The increased risk of infections is a notable concern, as infections can further impede the healing process and lead to more severe complications if not promptly addressed (Lavery et al., 2006).

8. Poor Immune Response:

The compromised immune response in diabetes leaves individuals susceptible to infections and hampers the body's ability to clear pathogens from wounds effectively. This diminished immune function adds another complexity to the overall challenge of diabetic wound healing (Moura et al., 2019).

2.6 Normal Wound Healing vs. Diabetic Wound Healing: A Comparative Overview

Routine wound healing is a meticulously orchestrated process, seamlessly progressing through distinct phases to restore tissue integrity. In contrast, diabetic wound healing introduces a complex interplay of factors that intricately alter this natural course (Table 2).

2.6.1 Normal Wound Healing:

In a non-diabetic individual, the inflammatory phase initiates promptly after injury. This phase involves vasoconstriction, platelet activation, and blood clot formation. Neutrophils and macrophages swiftly move to clear debris, initiating the inflammatory response (Gonzalez et al., 2016). This inflammation is tightly regulated, allowing for an efficient transition to the proliferative phase. During angiogenesis, new blood vessels form to provide oxygen and nutrients essential for regenerating damaged tissues (Lee et al., 2021). Fibroblasts, the architects of healing, migrate to the wound site and synthesise collagen, forming a structural framework for tissue repair. Growth factors play a pivotal role in signalling cell proliferation, contributing to the regeneration of damaged tissue. The remodelling phase involves collagen rearrangement, scar formation, and wound contraction, ultimately resulting in the maturation of the healed tissue (Yun et al., 2010).

2.6.2 Diabetic Wound Healing:

In the diabetic context, wound healing encounters many challenges, primarily driven by chronic hyperglycaemia (Sorg et al., 2017). The inflammatory phase, intended to be a transient response, becomes prolonged due to persistent high glucose levels. This chronic inflammation can impede the orderly progression to subsequent phases. Angiogenesis, a critical aspect of wound healing, is hampered in diabetes (Schultz et al., 2003). Microvascular complications associated with the condition limit blood flow, reducing the delivery of oxygen and nutrients to the wound site (Borgquist et al., 2010). Fibroblast function may be compromised, leading to reduced collagen synthesis and delayed wound closure. Growth factor activity, essential for signalling cell proliferation, may be diminished in diabetes, hindering effective tissue repair.

Collagen remodelling in the diabetic wound healing process becomes aberrant, resulting in weak scars that are more susceptible to re-injury. Furthermore, diabetic neuropathy, affecting sensory and autonomic nerves, diminishes pain perception. This can lead to delayed wound detection, exacerbating wound management challenges. A higher risk of infection is associated with increased glucose levels because they foster bacterial development. The compromised immune response in diabetes further intensifies infection susceptibility (Feldman et al., 2019).

When a wound usually heals, standard wound care practices are generally effective. This includes maintaining cleanliness, applying appropriate dressings, and monitoring for signs of infection or delayed healing. In diabetic wound healing, the complexity of challenges necessitates a multifaceted approach. Tight glycaemic control becomes paramount, addressing the root cause of many diabetic complications. Meticulous wound care is crucial, often involving more frequent monitoring and specialised interventions. Advanced therapies, such as applying growth factors or hyperbaric oxygen therapy, may be considered for severe cases.

Table 2: Normal Wound Healing vs. Diabetic Wound Healing: A Comparative Overview

Aspect	Normal Wound Healing	Diabetic Wound Healing	Challenges
Inflammation	Well-coordinated and timely response; transitions efficiently to subsequent stages	Prolonged inflammation due to chronic hyperglycaemia; potential delay in transitioning to subsequent phases	Chronic inflammation, potential for impaired immune response
Angiogenesis	Adequate formation of new blood vessels; optimal oxygen and nutrient supply	Impaired angiogenesis due to microvascular complications; restricted blood flow hinders tissue regeneration.	Microvascular complications: diminished blood flow
Fibroblast Function	Optimal fibroblast function: practical collagen synthesis	Compromised fibroblast function; reduced collagen production; and delayed wound closure	Reduced collagen synthesis; compromised tissue repair
Growth Factor Activity	Adequate growth factor activity stimulates cell proliferation	Diminished growth factor activity hampers effective tissue repair	Impaired signalling for cell proliferation;

			slowed tissue regeneration
Remodelling	Organised collagen remodelling and scar formation; muscular and functional tissue	Aberrant collagen remodelling; weak scars prone to reinjury; compromised tissue strength	Weak scar formation; increased susceptibility to reinjury
Neuropathy	Sensory and autonomic nerves function correctly.	Diabetic neuropathy affects pain perception and the potential for delayed wound detection.	Diminished pain perception; risk of delayed wound identification
Risk of Infection	Lower risk of infection due to an efficient immune response	A higher risk of infections is associated with elevated glucose levels, which foster bacterial development.	Increased susceptibility to infections; compromised immune response
Immune Response	Robust immune response; effective infection control	Compromised immune response; increased susceptibility to infections	Reduced ability to combat pathogens; heightened infection risk
Management Strategies	Standard wound care practices are effective.	A multifaceted approach requires tight glycaemic control, meticulous wound care, and advanced therapies for severe cases.	Addressing root cause: specialised interventions for diabetes-related complications.

2.7 Wound healing medications and treatments

- 1) Antibiotics:** Antibiotics are a class of medications designed to combat bacterial infections. In wound healing, they prevent or treat infections that may compromise the healing process. Topical antibiotics, like neomycin and bacitracin, are applied directly to the wound surface to inhibit bacterial growth (Spann et al., 2003). Systemic antibiotics, such as amoxicillin and cephalexin, are administered orally or intravenously to address more extensive or systemic infections that can arise from wounds (Hernandez, 2006).

Mechanism of Action:

Antibiotics interfere with bacteria's growth and reproduction by killing them (bactericidal) or inhibiting their growth (bacteriostatic). Regarding wound healing, the goal is to prevent or treat bacterial infections that could impede the natural healing process (Etebu et al., 2016).

Topical Antibiotics:

- **Neomycin:** Neomycin is an aminoglycoside antibiotic commonly used topically. It works by disrupting bacterial protein synthesis. When applied directly to the wound, neomycin helps prevent or control localised bacterial infections, particularly in minor cuts, scrapes, and burns (Bikowski, 1999).
- **Bacitracin:** The polypeptide antibiotic Bacitracin hinders the formation of bacterial cell walls. It is often combined with other antibiotics in over-the-counter ointments, such as neomycin and polymyxin. B. Bacitracin is effective against various bacteria and is used to prevent and treat superficial skin infections (Werner et al., 1999).

Systemic Antibiotics:

- **Amoxicillin:** Amoxicillin is a broad-spectrum penicillin-type antibiotic commonly used orally to treat a wide range of bacterial infections, including those that may result from wounds. It interferes with bacterial cell wall synthesis, destroying the bacteria (El-Ela et al., 2019).
- **Cephalexin:** Cephalexin belongs to the cephalosporin class of antibiotics. It is effective against a broad spectrum of bacteria and is often prescribed for skin and soft tissue infections, including those related to wounds. Like other beta-lactam antibiotics, cephalexin disrupts bacterial cell wall synthesis (Moran et al., 2017).

Indications for Antibiotic Use in Wound Healing:

- **Prevention of Infection:** Antibiotics may be used prophylactically in clean surgical wounds to prevent bacterial contamination and subsequent infection (El-Ela et al., 2019).

- **Treatment of Existing Infections:** If a wound shows signs of infection, such as redness, swelling, or pus, antibiotics are prescribed to eradicate the bacteria causing the infection (Werner et al., 1999).
- **Secondary Infections:** Wounds that have become contaminated or infected with bacteria, particularly in the case of traumatic injuries, may require systemic antibiotics to prevent the spread of infection to surrounding tissues or into the bloodstream (Werner et al., 1999).

Considerations and Caution:

- **Resistant Strains:** Inappropriate or excessive usage of antibiotics can result in the emergence of antibiotic-resistant bacterial strains. This emphasises the importance of using antibiotics judiciously and only when necessary (English et al., 2010).
- **Allergies:** Some individuals may be allergic to certain antibiotics, leading to allergic reactions. Before administering antibiotics, healthcare practitioners must be informed of any known allergic reactions (El-Ela et al., 2019).
- **Systemic Effects:** Systemic antibiotics can affect the entire body and may have side effects, such as gastrointestinal upset or allergic reactions. Close monitoring by healthcare professionals is essential during antibiotic therapy (English et al., 2010).

2) Topical Antiseptics:

Topical antiseptics clean and disinfect wounds, reducing the risk of infection. Hydrogen peroxide, iodine solutions (like povidone-iodine), and chlorhexidine are commonly used (Atiyeh et al., 2009). These antiseptics kill or inhibit the growth of microorganisms on the skin and within the wound.

A. Hydrogen Peroxide:

- **Mechanism of Action:** Hydrogen peroxide (H_2O_2) is an oxidising agent that releases oxygen upon contact with the wound. This effervescence helps remove debris and dead tissue from the wound. Additionally, the oxygen released can have a bactericidal effect by damaging bacterial cell walls and proteins (Rai et al., 2023).
- **Application:** Hydrogen peroxide is commonly used to clean minor wounds. It is poured or sprayed onto the wound surface to clean and disinfect. However, its use has become

somewhat controversial, as excessive use can hinder the natural healing process by damaging healthy cells (Rai et al., 2023).

B. Iodine Solutions (Povidone-Iodine):

- **Mechanism of Action:** Povidone-iodine is a complex of iodine and a polymer carrier (povidone). It has broad-spectrum antimicrobial activity, killing bacteria, viruses, and fungi. Iodine disrupts microbial cell membranes and proteins (Bigliardi et al., 2017).
- **Application:** Povidone-iodine is often used as a preoperative skin antiseptic for wound cleaning. Solutions, ointments, and swabs are just a few of its forms. The concentration of iodine in these solutions may vary, with higher concentrations having greater antimicrobial efficacy.

C. Chlorhexidine:

- **Mechanism of Action:** Chlorhexidine is a chemical antiseptic with a broad spectrum of activity against bacteria and some fungi. It disrupts microbial cell membranes and has residual antimicrobial activity (Karpiński et al., 2015).
- **Application:** Chlorhexidine is commonly used as a surgical hand scrub, preoperative skin preparation, and wound cleanser. It is available in different concentrations, including solutions and wipes. Compared to other antiseptics, chlorhexidine is less likely to cause tissue irritation.

Considerations and Caution:

- **Cytotoxicity:** Some antiseptics, including hydrogen peroxide, can be cytotoxic to fibroblasts and other cells involved in wound healing. Excessive use or prolonged exposure may hinder routine healing (Karpiński et al., 2015).
- **Tissue Irritation:** Caution is needed to prevent irritation of healthy tissue surrounding the wound. This is particularly important in wounds with delicate or sensitive skin (Karpiński et al., 2015).
- **Allergic Reactions:** While rare, allergic reactions to antiseptics can occur. Healthcare providers should know any known allergies before selecting an antiseptic (Karpiński et al., 2015).

3) Wound Dressings:

Wound dressings are essential for establishing an ideal environment to promote healing. The selection of dressings—such as gauze, hydrocolloids, hydrogels, and foam—depends on the specific requirements of the wound (Rezvani Ghomi et al., 2019). For instance, hydrocolloid dressings maintain a moist environment and assist in the autolytic debridement of necrotic tissue, while gauze dressings are suitable for wounds with minimal exudate. The choice of dressing is influenced by factors including the size, depth, and stage of the wound. Some wound dressings are as follows-

A. Gauze Dressings:

Gauze dressings are woven or non-woven fabric made from materials like cotton or a combination of synthetic fibres. They come in various forms, including sterile pads, rolls, or sponges. Gauze dressings are versatile and commonly used for wounds with minimal to moderate exudate. It covers the incision and prevents further moisture loss while letting air flow. Gauze can be impregnated with antimicrobial agents for added infection control. Regular changing of gauze is necessary to prevent it from sticking to the wound bed, which could disrupt the healing process. This type of dressing is often used in the early stages of wound care (Jones et al., 2006).

B. Hydrocolloid Dressings:

Hydrocolloid dressings consist of a gel-forming agent, such as gelatin or pectin, embedded in a flexible, water-resistant outer layer. Hydrocolloid dressings create a moist environment that supports autolytic debridement, helping to remove necrotic tissue and promote granulation tissue formation. They are handy for wounds with moderate exudate. These dressings are semi-occlusive, which can contribute to a controlled moisture level. They are suitable for wounds in various stages of healing and can be worn for several days before changing (Pott et al., 2014).

C. Hydrogel Dressings:

Hydrogel dressings are water—or glycerine-based gels that keep the area surrounding the wound wet. They are effective for wounds with minimal to moderate exudate, promoting a moist wound environment that aids cell migration and autolytic debridement. They are often used for partial-thickness burns and necrotic wounds. Hydrogel dressings can be soothing and provide pain relief. A second dressing to keep them in place might be necessary, and the frequency of dressing changes depends on the level of exudate (Yang et al., 2021).

D. Foam Dressings:

The ingredients used to make foam dressings are silicone or hydrophilic polyurethane. Foam dressings keep the area wet while absorbing excess fluid. Pressure ulcers, leg ulcers, and surgical wounds are commonly used as they are appropriate for wounds with moderate to high exudate. Foam dressings provide thermal insulation, which can aid in maintaining an optimal wound temperature. They are breathable and conform well to wound areas, minimising the risk of maceration (Nielsen et al., 2015).

E. Alginate Dressings:

Alginate dressings consist of sodium or calcium alginate fibres sourced from seaweed. Because of their high absorption rate, alginate dressings are ideal for wounds that produce moderate to substantial amounts of exudate. When in contact with wound exudate, they form a gel, promoting autolytic debridement and aiding in hemostasis. These dressings are often used for wounds with irregular shapes, such as cavities or packing deep wounds. A second dressing might be necessary to keep them in place (Aderibigbe et al., 2018).

Considerations for Dressing Selection:

- **Wound Characteristics:** A dressing is selected based on factors such as wound size, depth, level of exudate, and the presence of infection or necrotic tissue (Yang et al., 2021).
- **Frequency of Changes:** Dressing changes are determined by the dressing type, the wound healing stage, and the amount of exudate. Frequent changes can disrupt the healing process, while infrequent changes may increase the risk of infection (Yang et al., 2021).

4) Superior Quality Wound Care Items:

Superior-quality wound Care Items encompass a range of innovative solutions aimed at promoting tissue repair and regeneration. These may include growth factors and proteins that stimulate cell proliferation and tissue formation. Platelet-derived growth factors (PDGF) and epidermal growth factor (EGF) are examples (Man et al., 2020). Tissue-engineered skin substitutes like Apligraf are designed to provide a scaffold for cell growth and aid in healing complex wounds.

A. Growth Factors:

Role in Wound Healing: Growth factors are signalling proteins crucial in regulating cell growth, proliferation, and tissue repair. In wound healing, growth factors stimulate the various cellular processes involved in tissue regeneration (Maddaluno et al., 2017).

Examples:

- **Platelet-derived Growth Factor (PDGF):** The PDGF family includes proteins secreted by several cell types, including platelets. Wound healing depends on PDGF's ability to stimulate cell migration, angiogenesis (creating new blood vessels), and the development of an extracellular matrix (Grazul-Bilska et al., 2003).
- **Epidermal Growth Factor (EGF):** Growth factor (EGF) promotes cell division, new blood vessel formation, and collagen production. It is crucial when fresh epidermal tissue is forming and wounds are just beginning to heal (Laato et al., 1987).
- **Application:** Growth factors may be applied topically or integrated into various formulations, such as gels or creams. They can also be delivered through advanced wound dressings.

B. Tissue-Engineered Skin Substitutes:

Bioengineered materials that mimic the skin's natural structure can repair or replace damaged skin. They often consist of living cells, extracellular matrix components, and synthetic or natural scaffolds (Goodarzi et al., 2018). Example: Apligraf is a commercially available skin substitute composed of living human keratinocytes (epidermal cells) and fibroblasts (dermal cells) placed on a bovine collagen matrix. Apligraf provides a three-dimensional structure that mimics the architecture of natural skin. The living cells in Apligraf contribute to tissue repair, and the collagen matrix acts as a scaffold for cell growth. Chronic wounds, where the body's natural healing processes have been impeded, are treated with Apligraf. These wounds include venous leg ulcers and diabetic foot ulcers (Eaglstien et al., 1998).

C. Extracellular Matrix (ECM) Products:

Supporting cells structurally and biochemically, the extracellular matrix (ECM) is a non-cellular component of tissues. In wound healing, ECM products aim to restore the

natural extracellular matrix and promote tissue regeneration. One of the many possible sources for ECM products is the submucosa of the small intestine of pigs (SIS), bovine dermis, or synthetic materials. In order to facilitate cell adhesion, migration, and proliferation, these products are administered to the wound bed. Wounds can be treated directly with or incorporated with sophisticated wound dressings (Solarte David et al., 2022).

D. Cellular Therapies:

Cellular therapies involve the use of living cells to promote tissue repair. This can include autologous (patient's own) or allogeneic (from a donor) cell sources. Autologous skin grafts, where a patient's skin is transplanted to cover a wound, are a traditional form of cellular therapy (Zelinka et al., 2022). More recent approaches involve mesenchymal stem cells (MSCs) or other cell types. Cellular therapies are used in cases where the body's natural regenerative capacity is insufficient. MSCs, for example, have anti-inflammatory and regenerative properties that can enhance wound healing (Casado-Díaz et al., 2020).

E. Bioengineered Dressings:

Bioengineered dressings are advanced wound dressings that may incorporate various materials, such as collagen, hyaluronic acid, or synthetic polymers, to enhance wound healing. These dressings provide a supportive environment for wound healing, promoting cell migration and tissue repair and, in some cases, releasing growth factors or antimicrobial agents. Bioengineered dressings are often used for chronic burns and complex surgical wounds. They may be applied to promote specific aspects of wound healing, such as angiogenesis or collagen synthesis (Mir et al., 2018).

Key Factors to Consider in Advanced Wound Care:

- **Patient Selection:** Advanced wound care products are often customised to suit the individual's treatment requirements and specific wound attributes.
- **Clinical Monitoring:** Healthcare professionals closely monitor the wound's response to these advanced therapies, adjusting the treatment plan as needed.
- **Cost and Accessibility:** Advanced wound care products may be more expensive than traditional options, and accessibility can vary depending on healthcare settings.

5) Negative Pressure Wound Therapy (NPWT)

Negative Pressure Wound Therapy (NPWT) is a sophisticated therapeutic regimen specifically developed to promote wound healing by applying regulated negative pressure to the wound

area using a specialised vacuum dressing (Blume et al., 2008). This innovative approach has been employed in various medical settings and has demonstrated efficacy in promoting the healing of complex wounds. Here is a more detailed elaboration of NPWT:

Mechanism of Action:

- **Vacuum Dressing:** NPWT involves applying a sealed dressing over the wound, creating an airtight seal. This dressing is connected to a vacuum pump, establishing a controlled hostile pressure environment (Agarwal et al., 2019).
- **Removal of Exudate:** NPWT assists in removing excess wound fluid (exudate) and reduces edema. This is crucial as excessive exudate can impede the healing process, and oedema can contribute to poor tissue perfusion (Normandin et al., 2021).
- **Enhanced Blood Flow:** The negative pressure enhances blood flow to the wound bed, promoting angiogenesis (formation of new blood vessels) and increasing the delivery of oxygen and nutrients essential for tissue repair (Ma et al., 2016).
- **Stimulation of Granulation Tissue:** Negative pressure wound therapy promotes the development of granulation tissue, an essential stage in wound healing. Granulation tissue contains a high concentration of blood vessels and fibroblasts, which facilitate tissue regeneration (Karam et al., 2018).

Uses for NPWT:

1. **Chronic Wounds:** NPWT is commonly used for persistent wounds, including diabetic ulcers, venous ulcers, and pressure ulcers that have shown a poor response to conventional wound management (Wynn et al., 2019).
2. **Surgical Incisions:** NPWT can be applied to closed surgical incisions to minimise the risk of postoperative complications, such as infections or wound dehiscence (separation of wound edges) (Hyldig et al., 2019).
3. **Traumatic Injuries:** Wounds resulting from traumatic injuries, including crushes or significant tissue defects, can benefit from NPWT to support healing (Wynn et al., 2019).

Clinical Considerations:

1. **Monitoring:** Healthcare professionals closely monitor patients undergoing NPWT to assess wound progress, ensure proper device function, and promptly address complications (Blume et al., 2008).

2. **Patient Comfort:** While generally well-tolerated, NPWT may cause discomfort for some patients. Adequate communication and pain management strategies are implemented to enhance patient comfort (Ma et al., 2016).
3. **Duration of Therapy:** The duration of NPWT varies depending on the wound's response and the healthcare provider's assessment. Some wounds may require extended therapy, while others may quickly improve (Blume et al., 2008).

6) Hyperbaric Oxygen Therapy (HBOT)

The medical procedure known as Hyperbaric Oxygen Therapy (HBOT) subjects patients to pure oxygen at increased atmospheric pressure inside a hyperbaric chamber. This therapeutic approach is based on the principle that increased oxygen levels can stimulate and enhance the body's natural healing processes (Mathieu et al., 2015). Here is a more detailed elaboration of Hyperbaric Oxygen Therapy:

Mechanism of Action:

1. **Hyperbaric Chamber:** Hyperbaric oxygen therapy (HBOT) involves placing the patient within a hyperbaric chamber pressurised to levels above atmospheric pressure. The patient inhales undiluted oxygen, leading to a markedly elevated relative pressure of oxygen in the bloodstream (Bessereau et al., 2017).
2. **Enhanced Oxygen Dissolution:** The increased atmospheric pressure allows oxygen to dissolve in the plasma, independent of haemoglobin. This means tissues receive an excellent oxygen supply, promoting oxygen delivery to wound areas with compromised blood flow (Bessereau et al., 2017).
3. **Promotion of Healing Processes:** The heightened oxygen levels support various healing processes, including:
 - **Angiogenesis:** Forming new blood vessels improves blood flow to damaged tissues (Thackham et al., 2008).
 - **Collagen Formation:** Enhanced collagen synthesis is essential for tissue repair (André-Lévigne et al., 2016).
 - **Reduced Edema:** Oxygen's anti-inflammatory effects can reduce swelling (Heyboer III et al., 2017).

4. **Combating Infections:** Oxygen at elevated levels has bactericidal and bacteriostatic effects. It can enhance the body's immune response and sometimes help fight specific infections (Çimşit et al., 2009).

Indications for HBOT:

1. **Non-Healing Wounds:** When other wound care methods have failed, such as diabetic foot ulcers or surgical incisions that refuse to heal, HBOT may be an option (Roeckl-Wiedmann et al., 2005).
2. **Compromised Grafts and Flaps:** HBOT improves the success rate of skin grafts or flaps used in reconstructive surgery (Phillips, 2005).
3. **Gas Gangrene and Infections:** Certain bacterial infections, especially those involving anaerobic bacteria, can be treated with HBOT (Çimşit et al., 2009).

Hyperbaric Oxygen Therapy offers a unique and powerful approach to support the body's healing processes by delivering increased oxygen levels under elevated atmospheric pressure. Its application is well-established for specific medical conditions, particularly those involving compromised tissue oxygenation.

While traditional wound healing treatments have been effective in many cases, they may have disadvantages. The potential disadvantages of traditional treatments are as follows:

2.8 Disadvantages/Limitations of these Wound Healing Treatments:

- A. **Limited Targeting:** Traditional treatments may not have specific targeting mechanisms, leading to a broader impact on healthy and damaged tissues. This lack of precision can slow healing (Boateng et al., 2015).
- B. **Infection Risk:** Despite antibiotics and antiseptics, there is still a risk of infection in wounds, especially in chronic or complex cases. Bacterial resistance can also be a concern with long-term antibiotic use (Howell-Jones et al., 2005).
- C. **Scar Formation:** Some wounds may heal with significant scarring, which impacts aesthetics and function. Scar tissue may not have the same mechanical properties as the original tissue (Brown et al., 2008).
- D. **Slow Healing:** Certain chronic wounds may exhibit slow or impaired healing despite standard treatments. This can lead to prolonged pain and healthcare costs (FrykbergRobert, 2015).

2.9 How Nanotechnology-Based Treatments are filling this gap ?:

Nanotechnology has several benefits and advantages over conventional, standard wound healing methods. The advantages are as follows.

- A. **Targeted Drug Delivery:** Nanoparticles can be engineered to deliver drugs directly to the wound site, reducing systemic adverse effects and maximising medication effectiveness. This directed approach enhances the therapeutic impact (Shamiya et al., 2022).
- B. **Antibacterial Nanomaterials:** Silver nanoparticles and other nano-sized materials are effective against germs. Wound dressings and topical preparations that combine these components can be more successful in fighting bacterial infections (Hamad et al., 2020).
- C. **Accelerated Healing:** Materials derived from nanotechnology have the potential to accelerate tissue regeneration by increasing angiogenesis and cellular responses. This could be especially helpful when conventional treatments have failed, such as persistent wounds (Augustine et al., 2019).
- D. **Reduced Scarring:** Nanomaterials may influence collagen deposition and organisation, potentially leading to less noticeable scars. By modulating the wound healing process at the molecular level, nanotechnology offers the potential for improved tissue remodelling (Kwan et al., 2011).
- E. **Enhanced Imaging:** By acting as contrast agents in imaging modalities, nanoparticles let doctors see the wound and track its healing progress in real-time. This can be useful for spotting problems early on (Zheng et al., 2021; He et al., 2020).
- F. **Biocompatibility:** Many nanomaterials used in wound healing applications are designed to be biocompatible, lowering the potential for localised tissue inflammation or undesirable effects (Wang et al., 2021).
- G. **Customized Therapies:** Nanotechnology allows for the design of personalised therapies based on the specific characteristics of a patient's wound. This tailoring enhances treatment effectiveness (Hamdan et al., 2017).
- H. **Regenerative Medicine:** Nanotechnology can be used as a carrier for growth factors or stem cells and as a scaffold for tissue regeneration and repair (Fathi-Achachelouei et al., 2019).
- I. **Healing Stages and Associated Nanomaterials:** Wound healing involves a series of well-coordinated stages where different nanomaterials can be strategically used to

enhance the process. Below is a breakdown of the wound healing stages along with the nanomaterials (Figure 2):

❖ Hemostasis

Stage Overview: Hemostasis is the first step in wound healing, where the body's mechanisms work to stop bleeding. This involves platelet aggregation and forming a fibrin clot to seal the wound (Yang et al., 2017).

Nanomaterials Used:

- **Polymeric Nanoparticles:** Polymeric nanoparticles can be engineered to deliver clotting agents or to provide a scaffold that aids in the rapid formation of a fibrin network. They help achieve quick hemostasis while providing a structure for cell attachment in subsequent stages (Rajangam et al., 2013; Pourshahrestani et al., 2020).
- **Ceramic Nanoparticles/CeO₂ nanoceria:** Ceramic nanoparticles, due to their inorganic nature, are bioactive and can interact with blood proteins to accelerate clot formation (Kailashiya et al., 2022). They can also provide a surface that supports the adhesion and aggregation of platelets, which is essential for clot stabilisation. CeO₂ nanoceria possesses antioxidant properties that protect cells and proteins from oxidative damage during clot formation. By reducing oxidative stress, they ensure that the clotting process is more efficient, helping to quickly seal the wound (Sadidi et al., 2020; Xue et al., 2024).

❖ Inflammation

Stage Overview: During inflammation, immune cells are recruited to the wound site to clear debris, fight infection, and set the stage for tissue repair. This stage is characterised by redness, heat, swelling, and pain (Martin et al., 2005).

Nanomaterials Used:

- **Polymeric Nanoparticles:** Polymeric nanoparticles can deliver anti-inflammatory drugs in a controlled manner, reducing excessive inflammation and promoting a balanced immune response. Their biocompatibility and degradability make them ideal for sustained-release applications (Gadde et al., 2014).
- **Ceramic Nanoparticles/CeO₂ Nanoceria:** Ceramic nanoparticles can modulate the inflammatory response by interacting with immune cells and cytokines, helping to reduce excessive inflammation that can lead to chronic

wounds. With their potent antioxidant properties, CeO₂ nanoceria help mitigate oxidative stress, thereby reducing the release of pro-inflammatory cytokines. This action prevents prolonged inflammation and facilitates the transition to the proliferation stage (Allu et al., 2023).

- **Gold Nanoparticles (AuNPs):** AuNPs effectively reduce inflammation by downregulating pro-inflammatory cytokines. They can also polarise macrophages to an anti-inflammatory state, promoting tissue repair (Cherng et al., 2022).
 - **Silver Nanoparticles (AgNPs):** AgNPs are well-known for their antimicrobial properties, which are crucial in preventing infections that could exacerbate the inflammatory response. Additionally, they can help modulate inflammation by reducing the activity of inflammatory cells (Younis et al., 2021).
 - **Carbon-based Nanomaterials:** These nanomaterials, such as graphene oxide and carbon nanotubes, can reduce inflammation by scavenging free radicals and promoting cellular responses that favour tissue regeneration (He et al., 2022).
 - **Hydrogel:** Hydrogels can be used as a delivery system for anti-inflammatory agents. They provide a moist environment conducive to healing while reducing inflammation. They also offer a physical barrier to protect the wound from external irritants (Huang et al., 2022).
 - **Nanofiber:** Nanofibers can be engineered to release anti-inflammatory drugs and provide a scaffold for cellular infiltration, aiding in the resolution of inflammation and preparation for tissue regeneration (Jiang et al., 2023).
 - **Zinc Nanoparticles (ZnNPs):** ZnNPs have both antimicrobial and anti-inflammatory properties. They can help modulate the immune response, ensuring the inflammation phase is practical but not prolonged (Ali et al., 2017).
- ❖ **Proliferation-** The proliferation phase is marked by tissue formation, where new blood vessels, collagen, and extracellular matrix components are synthesised to replace the damaged tissue (Gonzalez et al., 2016).

Nanomaterials Used:

- **Polymeric Nanoparticles:** Polymeric nanoparticles can be loaded with growth factors like VEGF and FGF to stimulate angiogenesis and fibroblast activity, which are critical for tissue formation and wound closure (Alavi et al., 2020).

- **CeO₂ Nanoceria:** CeO₂ nanoceria, which can reduce oxidative stress and support cell proliferation and collagen synthesis, is vital for new tissue formation (Nosrati et al., 2023; Allu et al., 2023).
- **Gold Nanoparticles (AuNPs):** AuNPs can enhance endothelial cell and fibroblast proliferation, forming new blood vessels and extracellular matrix during the proliferation phase (Pivodová et al., 2015).
- **Silver Nanoparticles (AgNPs):** AgNPs continue to provide antimicrobial protection during the proliferation phase, preventing infections that could derail tissue regeneration (Paladini et al., 2019).
- **Carbon-based Nanomaterials:** These nanomaterials enhance cell adhesion and proliferation, providing structural support to the newly forming tissue. They also contribute to the synthesis of collagen and other matrix components (Rahman et al., 2022; Sadat et al., 2022)
- **Hydrogel:** Hydrogels can encapsulate and release growth factors and cells to promote tissue regeneration. Their water-retaining properties ensure a moist environment, which is critical for cellular activity and tissue formation (Hillel et al., 2007).
- **Nanofiber:** Nanofibers serve as scaffolds that mimic the extracellular matrix, providing a conducive environment for cell growth and tissue formation. They can also deliver bioactive molecules that promote proliferation (Sell et al., 2007).
- **Zinc Nanoparticles (ZnNPs):** ZnNPs promote keratinocyte migration and proliferation, aiding in the re-epithelialization of the wound. They also support angiogenesis, which is crucial for supplying nutrients to the growing tissue (Sajjad et al., 2023).
- **Solid Lipid Nanoparticles (SLNs):** SLNs can encapsulate and deliver hydrophobic drugs or growth factors to promote cell proliferation and tissue regeneration. Their biocompatibility and controlled release properties make them effective in this phase (Aguilar et al., 2019).
- **Dendrimers:** Dendrimers are highly branched nanostructures with multiple therapeutic agents to promote cell proliferation and tissue regeneration. Their surface can be functionalised to target specific cells involved in the wound-healing process (Shaikh et al., 2022).

- **Micelles:** Micelles deliver hydrophobic drugs or growth factors that support cellular proliferation and angiogenesis. Their ability to encapsulate and release bioactive agents in a controlled manner enhances the proliferation phase (Zhao et al., 2022).
- **Copper Nanoparticles (CuNPs):** CuNPs are known for promoting angiogenesis and collagen synthesis. They enhance the formation of new blood vessels and extracellular matrix, which are critical for wound closure and tissue repair (Alizadeh et al., 2019).
- ❖ **Remodelling**—The remodelling phase involves maturing the wound, reorganising collagen fibres, and enhancing the tensile strength of the new tissue. This stage can last several weeks to months.

Nanomaterials Used:

- **Iron Oxide Nanoparticles:** Iron Oxide Nanoparticles can guide the alignment of collagen fibres, enhancing the mechanical strength of the healed tissue. Their magnetic properties can be harnessed for targeted therapy and controlled release of growth factors that promote tissue maturation (Sandoval et al., 2022; Pérez-Díaz et al., 2023).
- **Ceramic Nanocerria:** Ceramic nanocerria supports the remodelling process by providing a stable, bioactive surface that promotes the alignment and organisation of collagen fibres. Their antioxidant properties also help maintain a conducive environment for tissue maturation (Kargozar et al., 2018).

Integrating these nanomaterials at different stages of wound healing allows for a targeted and controlled approach to enhance each phase. These nanomaterials are critical in improving wound healing outcomes, from promoting rapid hemostasis to reducing inflammation, supporting tissue proliferation, and ensuring proper tissue remodelling.

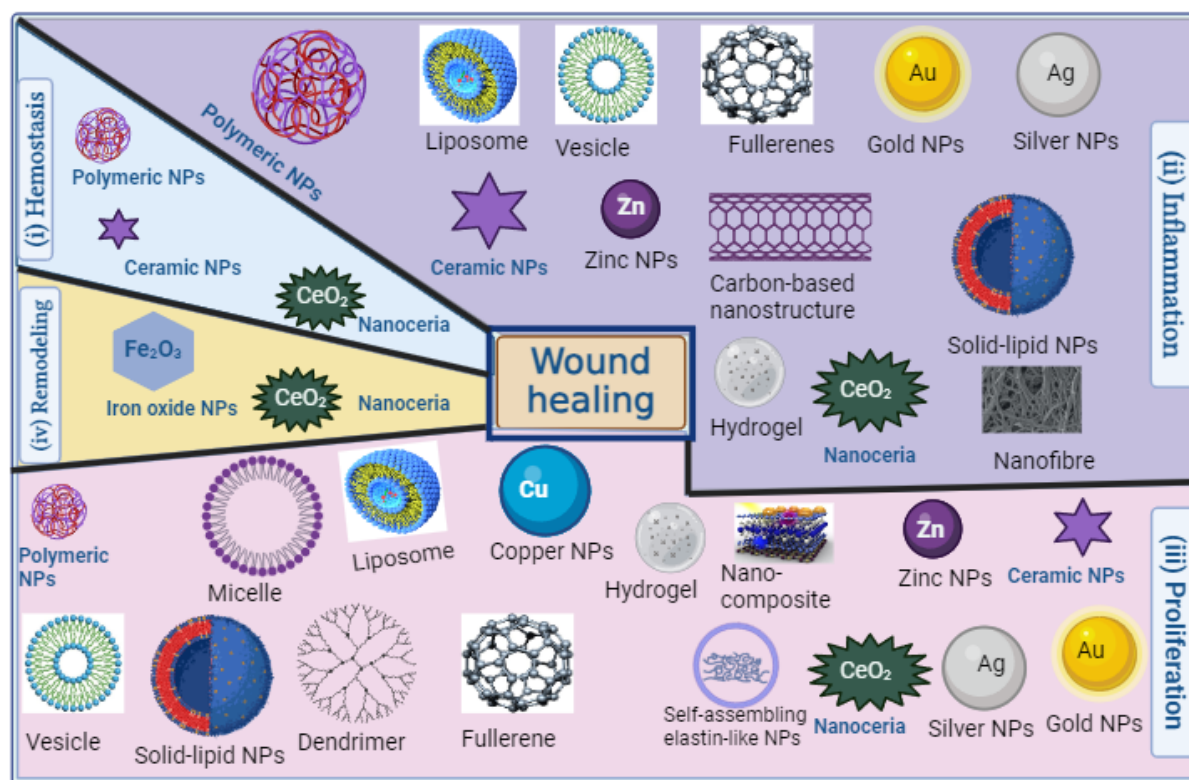


Figure 2: Different types of nanomaterials and their use in different stages of wound healing

2.10 Polymeric nanotechnology in diabetic wound healing

Polymeric nanotechnology has gained prominence in diabetic wound healing due to several advantages that make it a promising choice over other nanotechnologies. The unique properties of polymeric nanoparticles contribute to their effectiveness regarding the particular difficulties linked to diabetic wounds (Cavalu et al., 2019). Here are some reasons why polymeric nanotechnology is considered advantageous for diabetic wound healing:

A. Biocompatibility:

Many polymeric materials, like poly (lactic-co-glycolic acid) (PLGA), chitosan, and polyethylene glycol (PEG), are biocompatible and well-tolerated by the body. This reduces the risk of adverse reactions or inflammatory responses in diabetic patients with compromised immune systems (Bianchera et al., 2020).

B. Biodegradability:

Biodegradable polymeric nanoparticles may be engineered to gradually wear out with time, aligning with the natural healing process. This is important for diabetic wounds, which often require extended treatment (Mandal et al., 2023).

C. Controlled Drug Release:

Polymeric nanoparticles offer controlled and sustained drug release. Diabetic wound healing relies on this characteristic, as it allows for a continuous and controlled supply of therapeutic agents, such as growth factors or antimicrobial agents, optimising the treatment's efficacy (Kamaly et al., 2016).

D. Targeted Drug Delivery:

Engineering polymeric nanoparticles can achieve the targeted distribution of drugs to the region of the diabetic wound. In the case of compromised blood circulation, active targeting ligands on the nanoparticle surface can improve specificity, assuring that therapeutic medicines reach the desired cells or tissues (Madawi et al., 2023).

E. Incorporation into Dressings and Scaffolds:

Wound dressings or three-dimensional scaffolds can incorporate polymeric nanoparticles. This makes it easy to apply the dressing, which promotes wound healing by creating an optimum environment and bringing therapeutic agents straight to the area of the wound (Yu et al., 2019).

F. Encapsulation of Multiple Agents:

Polymeric nanoparticles allow for the simultaneous encapsulation of various therapeutic agents. This enables a multi-pronged approach to diabetic wound healing by coordinating the treatment of different aspects, such as inflammation, infection, and tissue regeneration (Morachis et al., 2012).

G. Stability and Shelf Life:

Polymeric nanoparticles can enhance the stability of encapsulated drugs, protecting them from degradation. This property is essential for ensuring the effectiveness of therapeutic agents during storage and transportation, especially in clinical settings (Kumari et al., 2010).

H. Imaging and Monitoring:

Polymeric nanoparticles can serve dual purposes by acting as imaging contrast agents. This allows healthcare professionals to monitor the wound healing process in real time, facilitating timely adjustments to the treatment plan (Elsabahy et al., 2015).

While polymeric nanotechnology offers these advantages, it is essential to note that the choice of nanomaterial depends on the specific requirements of the diabetic wound, the characteristics of the therapeutic agents, and the overall treatment goals. Other nanotechnologies, such as

metallic nanoparticles or lipid-based nanoparticles, may also find application in diabetic wound healing, depending on the specific context and objectives of the treatment.

2.11 Guar gum as a polymeric nanocarrier:

Guar gum is extracted from the seeds of the guar plant (*Cyamopsis tetragonoloba*), a leguminous plant native to India and Pakistan. The guar plant is known for its drought-resistant nature and is primarily cultivated for its seeds. A galactomannan, guar gum, is a polysaccharide containing galactose and mannose units. The ratio of mannose to galactose imparts unique properties to guar gum (Gresta et al., 2013). It is often classified as a high-molecular-weight carbohydrate.

Chemical Composition of Guar Gum: A Deeper Insight

- **Galactomannan Structure:** Guar gum, extracted from the endosperm of guar beans, is a galactomannan—a complex polysaccharide renowned for its intricate molecular arrangement. At its core, this polymer is constructed from mannose and galactose units. The galactomannan structure is a hallmark feature, distinguishing guar gum from other polysaccharides (Gresta et al., 2013).
- **Mannose-Galactose Ratio:** Guar gum's unique properties emerge from its molecular framework's specific ratio of mannose to galactose units. Typically, this ratio is approximately 2:1, indicating a predominance of mannose units. These units' arrangement contributes to guar gum's distinctive physicochemical characteristics, impacting its solubility, viscosity, and gel-forming capabilities (Sharma et al., 2018).
- **High-Molecular-Weight Carbohydrate:** Guar gum is categorised as a high-molecular-weight carbohydrate, highlighting its molecular structure's substantial size and complexity. This designation underscores the presence of numerous mannose and galactose units linked together through glycosidic bonds, forming a large and intricate macromolecule (Amjed et al., 2023).
- **Polymeric Backbone:** The guar gum backbone consists of mannose units connected by β -1, 4-glycosidic linkages in a linear fashion. These chains serve as the foundation of the galactomannan structure, providing stability and defining the polymer's overall architecture (Mary et al., 2019).
- **Branching with Galactose Units:** Intermittently along the mannose backbone, galactose units are attached through α -1,6-glycosidic linkages, creating branches within the polymer structure. This branching pattern introduces complexity and contributes to

the polymer's versatile properties, influencing its solubility, rheological behaviour, and interactions with other molecules (Mary et al., 2019).

- **Hydrophilic Nature:** Guar gum's galactomannan structure imparts a highly hydrophilic character. Multiple hydroxyl groups in mannose and galactose units enhance its water-absorbing capabilities, making guar gum readily soluble in water. This hydrophilicity is critical in its applications, particularly in industries where water-based formulations are essential (Sharma et al., 2018).
- **Functional Properties:** Beyond its role as a thickening or gelling agent, the specific arrangement of mannose and galactose units contributes to guar gum's functionality. The polymer's ability to form stable gels, its viscosity in solution, and its interaction with other molecules make it a versatile ingredient in various applications, ranging from food and pharmaceuticals to cosmetics (Tahmouzi et al., 2023).

Guar gum, derived from guar beans, has emerged as a promising polymeric nanocarrier for drug delivery. It offers a range of advantageous properties that make it suitable for various applications.

- **Biocompatibility and Biodegradability:** Guar gum is relatively safe because of its natural biocompatibility with humans. Moreover, its biodegradability ensures that it can be broken down into non-toxic components over time, contributing to environmentally friendly drug delivery systems (Soltani et al., 2021).
- **Hydrophilic Nature:** One notable characteristic of guar gum is its hydrophilic nature. This property enables effective interaction with water, making it particularly suitable for drug encapsulation and delivery in aqueous environments. It ensures that formulations can be readily dispersed and absorbed when administered (Thombare et al., 2016).
- **Mucoadhesive Properties:** Guar gum's mucoadhesive characteristics allow it to stick to surfaces coated with mucus. This property benefits drug transport to mucosal tissues, including the gastrointestinal tract. The mucoadhesive nature enhances residence time and drug absorption, improving therapeutic outcomes (Singh et al., 2010).
- **Polymer Matrix Formation:** Guar gum can form a stable polymer matrix, providing a structural framework for drug encapsulation. This matrix's dual function of protecting encapsulated medicines from degradation and facilitating regulated release makes sustained and prolonged therapeutic benefits possible.

- **Drug Encapsulation:** Guar gum's ability to encapsulate drugs within its matrix is crucial. This encapsulation offers protection to drugs, particularly those sensitive to environmental factors. It also ensures improved stability and bioavailability of the drugs during the delivery process (George et al., 2019).
- **Controlled Release:** Guar gum's viscosity and gelling properties contribute to controlled release mechanisms. This is essential for achieving desired pharmacokinetics, allowing for sustained drug release. Controlled release is precious in maintaining therapeutic drug levels and reducing the frequency of administrations (Verma et al., 2021).
- **Versatility in Formulation:** Guar gum's adaptability is evident in its capacity to be easily modified and processed into various forms, including nanoparticles and microparticles. This versatility allows tailoring the nanocarrier's size, surface characteristics, and drug-loading capacity to meet specific therapeutic requirements (Madni et al., 2021).
- **Enhanced Bioavailability:** Nanocarriers derived from guar gum have shown promise in increasing the bioavailability of medicines with low solubility. The nanoscale dimensions and surface modifications contribute to improved drug solubility and absorption, overcoming challenges associated with low drug bioavailability (George et al., 2019).
- **Cost-Effectiveness:** Guar gum's notable advantage is its cost-effectiveness. Being a natural polymer with widespread availability, it provides an economically viable option for drug delivery formulations. This cost-effectiveness is essential for large-scale production and commercial applications (Soltani et al., 2021).

Guar gum's unique combination of biocompatibility, hydrophilicity, mucoadhesive properties, controlled release mechanisms, and cost-effectiveness positions it as a valuable polymeric nanocarrier for drug delivery applications. Researchers continue to explore and refine its potential, increasing the reach of medication administration platforms and contributing to treatment advancements.

Guar gum nanoformulations have a broad spectrum of applications in various disease treatments. Their ability to enhance the solubility, stability, and bioavailability of drugs, along with providing controlled release and targeted delivery, makes them highly effective in treating conditions like diabetes, cancer, infections, gastrointestinal disorders, and neurodegenerative

diseases (Aravindaraj et al., 2022). The continued research in this area holds great promise for developing novel, effective, and patient-friendly therapies.

➤ **Diabetic Wound Healing**

Diabetes, particularly in its chronic form, impairs wound healing due to the presence of oxidative stress, high blood glucose levels, and reduced vascularisation. Guar gum nanoformulations have been explored for delivering antioxidants and anti-inflammatory agents to treat diabetic wounds, often combining guar gum with bioactive compounds like polyphenols (Mandal et al., 2024).

➤ **Cancer Therapy**

Cancer treatment faces several challenges, including the need for targeted delivery, reduction of systemic toxicity, and overcoming multidrug resistance (Amaldoss et al., 2022). Guar gum nanoformulations provide solutions to these challenges by acting as nanocarriers for chemotherapy drugs like doxorubicin (Yadav et al., 2022; Verma et al., 2022), Paclitaxel (Shah et al., 2019), Tamoxifen (TMX) (Day et al., 2020; Sarmah et al., 2022), or even phytochemicals with anticancer properties (Biganeh et al., 2023).

➤ **Antimicrobial and Antioxidant Applications**

Guar gum nanoformulations have shown efficacy in antimicrobial therapies, particularly in treating infections caused by resistant bacterial strains or biofilms. Guar gum's hydrophilic nature allows it to encapsulate antimicrobial agents, enhancing their bioavailability and stability (Bains et al., 2023; Aguilera-Correa et al., 2022; Trigo-Gutierrez et al., 2021).

➤ **Gastrointestinal Disorders**

Guar gum nanoformulations have shown promise in treating gastrointestinal (GI) disorders by delivering bioactive compounds that require protection from the stomach's acidic environment (Ghorani et al., 2018). Guar gum nanoformulations have an essential role in the treatment of colon cancer (Sharma et al., 2013). Conditions like inflammatory bowel disease (IBD) or irritable bowel syndrome (IBS) benefit from targeted delivery systems that ensure the drugs reach the intestines intact (Caban et al., 2023; Zhang et al., 2016; Mishra et al., 2020).

➤ **Neurological Disorders**

One of the challenges in treating neurological disorders is the inability of many therapeutic agents to cross the blood-brain barrier (BBB). GGNP have been investigated for their role in delivering neuroprotective drugs to the brain

(Bostanudin et al., 2021; Nampoothiri et al., 2023). Neuroprotective agents, such as curcumin, resveratrol, or quercetin, often suffer from poor bioavailability (Nampoothiri et al., 2023; Moballegh Nasery et al., 2020). GGNPs enhance their stability and provide sustained release, leading to prolonged neuroprotective effects.

➤ **Antidiabetic Activity**

Guar gum nanoformulations have been tested for their ability to regulate blood glucose levels by more effectively delivering antidiabetic drugs. Natural compounds with antidiabetic properties, like polyphenols and flavonoids, are often poorly absorbed but can enhance their bioavailability (Xu et al., 2022; Yadav et al., 2024).

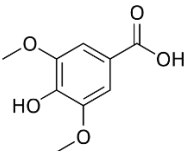
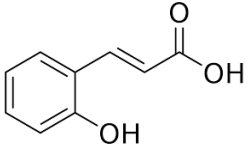
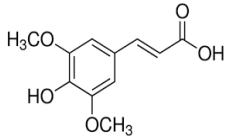
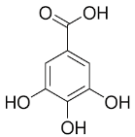
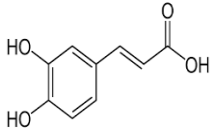
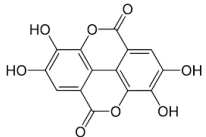
2.12 Phenolic acid in wound healing

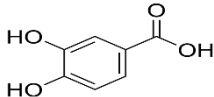
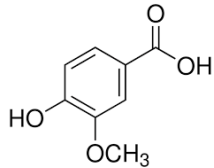
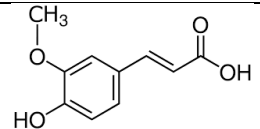
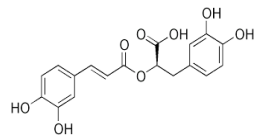
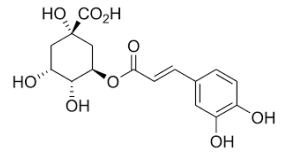
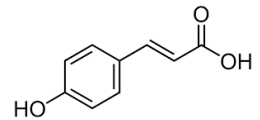
As a subgroup of plant compounds, Phenolic acids offer several potential benefits for wound healing through a multifaceted approach (Melguizo-Rodríguez et al., 2021) (Table 3). The mechanisms are as follows-

- **Antioxidant Defence Mechanisms:** A significant role in reducing oxidative stress linked to diabetes is played by phenolic acids, which are well-recognised for their antioxidant properties (Lin et al., 2016). By scavenging free radicals and reactive oxygen species, these compounds help maintain a balance in the cellular redox environment. This reduction in oxidative stress is pivotal for protecting cells from damage and creating an environment conducive to effective wound healing (Kaurinovic et al., 2019).
- **Immunomodulation and Anti-Inflammatory Effects:** Diabetes's chronic inflammatory state can impede routine wound healing (Zhao et al., 2016). Phenolic acids exert anti-inflammatory effects by modulating immune responses. They interact with immune cells, cytokines, and signalling pathways, promoting a regulated and controlled inflammatory environment. This modulation is essential for transitioning through the inflammatory phase of wound healing without undue delays (Costa et al., 2012).
- **Stimulation of Collagen Synthesis:** A crucial extracellular matrix constituent, collagen imparts structural stability to tissues. Phenolic acids, such as Syringic acid, O-Coumaric acid, and Sinapic acid, stimulate collagen synthesis. This effect is critical for enhancing the tensile strength of the healed tissue, helping to ensure that the wound heals appropriately (Alexandru et al., 2015).

- **Angiogenic Support:** A common complication of diabetes is the inability of blood to transport oxygen and nutrients to wound sites adequately. Phenolic acids have been associated with pro-angiogenic effects, fostering the development of new vascular systems. This angiogenic support is vital for reestablishing adequate blood flow, facilitating nutrient supply, and fostering an environment conducive to effective tissue regeneration (Diniz et al., 2017).
- **Antimicrobial Défense:** In diabetes, the compromised immune system increases susceptibility to infections, posing a significant challenge in wound healing. Phenolic acids exhibit antimicrobial properties, acting against a spectrum of bacteria. By preventing or managing infections, these compounds contribute to an environment that supports uninterrupted wound healing (Cueva et al., 2010).
- **Modulation of Growth Factors:** The expression and activity of essential growth factors involved in wound healing can be influenced by phenolic acids. For instance, they may enhance the effects of platelet-derived growth factor (PDGF) and transforming growth factor-beta (TGF- β). Crucial steps in the complex process of wound healing, these growth factors coordinate the development of cells, their differentiation, as well as the regeneration of tissue (Lin et al., 2010).
- **Regulation of Matrix Metalloproteinases (MMPs):** Proper tissue remodelling requires a delicate balance in matrix metalloproteinases (MMPs) activity. Phenolic acids regulate MMPs, ensuring a controlled degradation and synthesis of the extracellular matrix. This regulation contributes to the orderly progression through the remodelling phase of wound healing (Pluemsamran et al., 2012).
- **Neovascularization Facilitation:** Phenolic acids contribute to neovascularisation, a process essential for reestablishing vascular networks. These substances improve the wound's vascularisation by encouraging the growth of new blood vessels; this, in turn, facilitates the transport of nutrients as well as oxygen to the injured cells, which are essential for the repair process (Tsakiroglou et al., 2019; Li et al., 2018)
- **Enhancement of Cellular Proliferation:** Fibroblasts and keratinocytes are critical in tissue regeneration. Phenolic acids positively influence the proliferation of these cells, accelerating the closure of diabetic wounds. This upregulated cellular activity is aided by developing robust granulation tissue and the following lesion healing (Tsakiroglou et al., 2019; Melguizo-Rodríguez et al., 2021).

Table 3: Some phenolic acids for diabetic wound healing

Phenolic Acid	Source	Chemical Structure	Role in Wound Healing	Mechanisms in Wound Healing	Reference
Syringic Acid	Various plants, fruits, and medicinal plants		Antioxidant, Anti-inflammatory	Scavenging free radicals, Modulation of inflammatory pathways	Srinivasulu et al., 2018
O-Coumaric Acid	Fruits, vegetables, and grains		Antimicrobial Stimulation of Collagen Synthesis	Inhibition of microbial growth, Promotion of collagen production	Taofiq et al., 2017
Sinapic Acid	Cruciferous vegetables, fruits, and seeds		Antioxidant, Anti-inflammatory	Neutralisation of oxidative stress, Modulation of inflammatory responses	Rostami et al., 2022
Gallic Acid	Fruits, nuts, tea, and medicinal plants		Antibacterial, Antioxidant	Inhibition of bacterial growth, Scavenging of free radicals	Borges et al., 2013
Caffeic Acid	Coffee, fruits, vegetables, and medicinal plants		Anti-inflammatory Stimulation of collagen synthesis	Regulation of inflammatory pathways, Enhancement of collagen production	Huang et al., 2018
Ellagic Acid	Fruits, nuts, berries		Antioxidant, Contribution to angiogenesis	Protection against oxidative damage, Promotion of new blood vessel formation	Rozentsvit et al., 2017 Huang et al., 2011

Protocatechuic Acid	Fruits, vegetables, and medicinal plants		Anti-inflammatory, Antioxidant	Modulation of immune responses, Scavenging of free radicals	Li et al., 2011
Vanillic Acid	Vanilla, fruits, and plant-based foods		Antimicrobial Stimulation of Collagen Synthesis	Inhibition of microbial growth, Enhancement of collagen production	Rasheeda et al., 2018
Ferulic Acid	Grains, fruits, and vegetables		Antioxidant, Stimulation of collagen synthesis	Scavenging of free radicals, Promotion of collagen production	Cavalcanti et al., 2021
Rosmarinic Acid	Herbs (rosemary, basil, mint)		Anti-inflammatory, Antioxidant	Modulation of inflammatory pathways, Scavenging of free radicals	Rocha et al., 2015
Chlorogenic Acid	Coffee, fruits, and vegetables		Antioxidant, Anti-inflammatory	Neutralisation of oxidative stress, Regulation of inflammatory responses	Jiang et al., 2022
P-Coumaric Acid	Fruits, vegetables, and grains		Antimicrobial Stimulation of Collagen Synthesis	Inhibition of microbial growth, Promotion of collagen production	Selvakumar et al., 2023

Amongst these, the three active phytoconstituents (phenolic acid) were Syringic acid, Sinapic acid, and o-Coumaric acid, which can be effective against diabetic wound healing.

Syringic acid (SRN), a naturally occurring hydroxybenzoic acid derivative found in various plant sources, has emerged as a compound of interest in wound healing (Geana et al., 2023). The intricate tissue repair process, particularly in conditions like diabetes, where wound healing is often compromised, benefits from Syringic acid's diverse pharmacological properties (Padalkar et al., 2022). At the core of its contributions is the ability to modulate inflammation. Syringic acid demonstrates potent anti-inflammatory effects by regulating key pathways and reducing the production of pro-inflammatory molecules (Somade et al., 2023). This capacity is crucial in establishing a balanced inflammatory response at the wound site, promoting an environment conducive to optimal tissue repair. A noteworthy attribute of Syringic acid is its role as an antioxidant. As a scavenger of free radicals and reactive oxygen species, Syringic acid helps mitigate oxidative stress. This is significant in protecting cells from damage and creating a favourable milieu for the cellular processes involved in wound healing (John et al., 2021). Syringic acid's impact on collagen synthesis further underscores its potential in wound repair. Promoting the production of collagen by fibroblasts contributes to the formation of a robust extracellular matrix. This, in turn, enhances the tensile strength of the healing tissue, facilitating efficient wound closure and regeneration (Ren et al., 2019). In infection control, Syringic acid exhibits antimicrobial properties against a spectrum of bacteria and fungi. This antimicrobial action is instrumental in preventing or combating infections in the wound, an essential aspect of unimpeded healing (Zochedh et al., 2023). Moreover, Syringic acid has been associated with promoting angiogenesis and forming new blood vessels. This vascularisation is critical for ensuring an adequate blood supply to the wound and meeting the metabolic demands of cells involved in the regenerative process (Ren et al., 2019).

One naturally occurring phenolic component in plants and fruits, Syringic acid, shows promise as a wound healer. In a study (Ren et al., 2019) on type 2 diabetic rats using an incisional wound model, 2.5% and 5.0% SA accelerated wound closure and epithelisation. SA-treated diabetic wounds demonstrated reduced blood glucose levels, improved serum insulin, and addressed dyslipidemia. After 14 days, Syringic acid inhibited pro-inflammatory responses (NF- κ B p65, TNF- α , IL-1 β , IL-8, and IL-2), enhanced anti-inflammatory response (IL-10), lowered oxidative stress, and decreased matrix metalloproteinase concentrations while increasing tissue inhibitor of metalloproteinases levels—additionally, Syringic acid promoted angiogenesis, growth factor expression, collagen deposition, and re-epithelialization.

Histological analysis revealed improved skin structure. Based on these results, Syringic acid may be an excellent alternative to current synthetic medications for diabetic wound therapy.

Padalka et al. (2022) focus on developing a specialized wound-healing dressing system tailored for diabetic wounds. The approach combines curcumin, Syringic acid, and Aloe vera to address the distinctive pathophysiological changes associated with diabetic wounds, including hemostasis, inflammation, cell proliferation, and tissue remodeling challenges. Curcumin and Syringic acid are blended with Aloe vera juice, and the mixture is gelled using Carbopol 934. This formulation is then loaded into sterilized polyurethane foam to create the wound dressing system. Results indicate favourable characteristics of the dressing system. It demonstrates excellent folding endurance, suggesting durability and flexibility. Regarding antibacterial activity, the dressing system exhibits significant effectiveness against *Staphylococcus aureus* and *Escherichia coli*, as evidenced by a substantial zone of inhibition. Furthermore, the *in vitro* diffusion rates of curcumin and Syringic acid are noteworthy, indicating the potential for these components to permeate tissues effectively. The study also evaluates the dressing system's performance *in vivo*, utilizing diabetes-induced rats as a model. Remarkably, complete wound healing is observed within 14 days, highlighting the effectiveness of the dressing system in diabetic wound conditions.

Sinapic acid (SNP), a hydroxycinnamic acid derivative, is a notable phenolic compound in the Brassicaceae family (Hameed et al., 2016). It is present in various aromatic medicinal plants and foods, including blueberries, cherries, apples, nuts, rosemary, thyme, basil, and capsicum (Cherng et al., 2013; Nićiforović et al., 2014). Research has shown that Sinapic acid possesses numerous beneficial pharmacological effects both *in vivo* and *in vitro*, such as antioxidant, antihyperglycaemic, anti-inflammatory, neuroprotective, antimicrobial, anticancer, and anxiolytic properties (Cherng et al., 2013; Kikuzaki et al., 2002; Zou et al., 2002; Yun et al., 2008).

Due to these pharmacological effects, Sinapic acid is a potential candidate for treating various diseases, including wound healing (Kaltalioglu et al., 2023). For instance, Chandika et al., (2022) developed a multifunctional hydrogel incorporating Sinapic acid wound dressing. This formulation exhibited *in vitro* biocompatibility, antioxidant, and antimicrobial properties, along with significant enhancement of *in vivo* full-thickness wound closure, re-epithelialization, granulation tissue formation, and collagen deposition. These findings indicate the efficacy of Sinapic acid in promoting wound healing.

O-Coumaric acid (OCA), a hydroxycinnamic acid, is an organic compound and a hydroxy derivative of cinnamic acid. It is present in foods such as common wheat, dates, bilberries, and corn and in alcoholic beverages like beer and red wine (Contardi et al., 2021). As of now, there have been no studies focusing on the use of o-Coumaric acid for diabetic wound healing. Nevertheless, some isomers of Coumaric acid have been studied for their effects on diabetes and wound healing. For instance, studies have demonstrated that p-Coumaric acid has significant antihyperglycaemic and antioxidant properties in STZ-induced diabetic rats (Shairibha et al., 2014; Amalan et al., 2015). In 2023, Selvakumar et al. developed a collagen scaffold incorporated with p-Coumaric acid, which enhanced diabetic wound healing by modulating the expression of MMP-9 and TGF- β 3. Similarly, Arin et al. (2023) formulated a p-Coumaric acid-loaded liver ECM scaffold cross-linked with acellular marine kelp, concluding it to be a promising agent for wound healing. Additionally, in vitro studies have shown that trans-cinnamic and p-Coumaric acids can enhance fibroblast migration without adversely affecting cell viability (Viana et al., 2021).

While in vitro and in vivo studies have demonstrated promising results, translating these phenolic acids' potential into practical wound healing applications requires further exploration. Rigorous clinical trials are essential to validate their efficacy, establish safe dosage parameters, and determine their potential as therapeutic agents in human wound care.

Research Gap

Guar gum, a natural polysaccharide, has demonstrated excellent biocompatibility, biodegradability, and gel-forming properties, making it a promising candidate for drug delivery systems. Phenolic acids, conversely, are well-documented for their antimicrobial and anti-inflammatory properties, which are critical in managing diabetic wounds. However, the combination of guar gum as a drug carrier and phenolic acids for diabetic wound healing has not been explored. Existing polymeric nanoformulations, such as those using chitosan and xanthan gum, often suffer from limitations like low entrapment efficiency, reduced loading capacity, and higher production costs, which restrict their scalability and practical applications. Despite the individual potential of guar gum and phenolic acids, no safe, cost-effective, and efficient formulation has been developed that integrates these two components specifically for diabetic wound healing. This research gap highlights the need to design and develop a guar gum-based nanoformulation embedded with phenolic acids, aiming to leverage their synergistic antimicrobial and anti-inflammatory effects for a scalable and affordable diabetic wound healing therapy.

Chapter 3: Hypothesis

Diabetes, a metabolic disorder typically caused by deficiencies in insulin secretion or function, results from a complex interplay of genetic and environmental factors. According to the International Diabetes Federation (IDF), 537 million individuals aged 20–79 had diabetes worldwide in 2021. This number is projected to increase to 643 million by 2030 and 783 million by 2045. In 2021, one in five deaths was attributed to diabetes. The global rise in healthcare costs due to diabetes has been substantial, escalating from approximately USD 232 billion in 2007 to around USD 966 billion in 2021 for individuals aged 20–79 years, reflecting a growth rate of 316% over the past 15 years. Individuals with diabetes are at a greater risk of developing chronic wounds, especially on their feet, known as diabetic foot ulcers (DFU). The significant global increase in DFU incidence has considerable socio-economic implications. For instance, approximately 15% of the global health budget is allocated each year to treating diabetes and its complications, including DFU patients. Impaired glucose metabolism is believed to obstruct the wound-healing process in diabetics, leading to chronic wound formation. Additionally, elevated blood sugar levels hinder blood circulation, preventing essential nutrients from reaching the affected area and disrupting healing mechanisms. Chronic wounds are typically characterized by persistent inflammation and increased oxidative stress, contributing to significant damage to the host tissue. The approval of anti-diabetic wound drugs by the United States Food and Drug Administration has led to the widespread adoption of synthetic drugs worldwide for treating diabetic foot ulcers (DFU). Becaplermin and Omnigraft are common examples of drugs used in clinical practice to prevent DFU pathogenesis. However, concerns have been raised regarding the safety and effectiveness of these medications due to their adverse side effects, including blisters, skin peeling, intense itching, and redness. As mentioned earlier, while the use of synthetic drugs has reduced the risk of developing DFU, doubts about their safety and efficacy remain due to these unwanted effects. This highlights the need to explore safer alternatives with fewer or minimal side effects. Nanotechnology-based formulations have emerged as potential candidates to address these issues. Nanotechnology is revolutionizing our lives, particularly in the biological sciences, where it is being used innovatively to develop new frameworks, technologies, and systems that could transform how we approach illness, treatment, and diagnosis. Traditional medicines often involve costly and time-consuming treatments, unlike nanotechnology-based medications. Compared to conventional methods, nanotechnology-based drug delivery systems, especially polymeric nanoformulations, offer greater promise due to their controlled release and targeted activity.

Numerous studies have shown that polymeric nanoformulations, embedded with active phytoconstituents, can be effective for diabetic wound healing, though significant results are yet to be uncovered. Consequently, we hypothesize that naturally active constituents, when embedded in the polymeric macromolecule, could be effective for diabetic wound healing. To accomplish this, we will create a cutting-edge polymeric nanoformulation infused with active phytoconstituents, specifically designed for diabetic wound healing, under the hypothesis "Revolutionizing Diabetic Wound Healing: Innovative polymeric nanoformulation with Potent Phytoconstituents."

Chapter 4: Aims and Objectives

The use of synthetic medications for treating diabetic wounds has raised concerns about their safety and effectiveness due to adverse side effects such as blisters, skin peeling, intense itching, and redness. This underscores the need to explore safer alternatives with minimal or no side effects. Polymeric nanoformulations embedded with naturally occurring phytochemicals have emerged as strong contenders in diabetic wound healing. Based on previous studies, the natural biological macromolecule/polymer guar gum has been selected to create the nanoformulation. The active phytoconstituents were finalised through molecular docking and a thorough literature review. The optimized nanoformulations will be further evaluated to validate their potential in reducing diabetes-associated delayed wound healing, using both in vitro and in vivo diabetic wound models. Consequently, the following objectives were formulated to elucidate the potential of the selected phytochemicals in advancing wound healing:

- To explore, evaluate, and characterize potential phytochemicals embedded in Guar gum nanoparticles.
- To test the wound healing properties of nanoparticle-embedded phytochemicals in an in vitro skin cell culture system.
- To evaluate the efficacy of nanoparticle-embedded Phyto-molecules in the Streptozotocin-induced diabetic rat wound healing model.

Chapter 5: Materials and Methods

5.1 Chemicals and Reagents

Glutaraldehyde (25%, w/v) and HPLC-grade dichloromethane (DCM) were sourced from Merck Chemicals, Mumbai, India. Glycerol, HPLC-grade water, Span 80, and Tween 20 were obtained from HI Media Laboratories in Mumbai. Guar gum, with a molecular weight of approximately 110 kDa, was procured from SRL, Mumbai. Sigma-Aldrich, India, supplied Syringic acid, Sinapic acid, and o-Coumaric acid. Cholesterol was acquired from Hi Media Laboratories, Mumbai. Additionally, DL-methionine, carboxymethyl cellulose, and casein were sourced from Saras Casein (Orai), while a vitamin and mineral mix was purchased from a local vendor. Yeast powder was obtained from S. D. Fine Chemicals and HiMedia India Ltd. for use in the study.

5.2 Nanoformulation Design

Guar gum's nanoformulation (NF) was created using a slightly modified version of the in situ polymer crosslinking approach and oil-in-water emulsification (Sarmah et al., 2009). To create the oil phase, 10 mL of DCM (Drug for drug-loaded guar gum NF and without Drug for blank NF) (1: 6 drug: polymer ratio) and 1 mL of tween 80+Tween 20 were mixed in a 2-5%v/v, 1:1 ratio with Transcutol P, a co-emulsifier and solubiliser linked to improved skin penetration in topical dose formulations. The oil phase was introduced drop-by-drop to a 30 mL water-based guar gum continuously stirred using a magnetic stirring rod. Following the oil and continuous phase reaching mutual saturation, the mixture was subjected to sonication for 8-20 mins (30s On/10s Off, 40% amplitude). Subsequently, 10 mL of glycerol was added drop-wise. As a crosslinker, 1-3 mL of glutaraldehyde (25%) was added. The nanosuspension was then incubated at 37°C overnight to generate the nanoformulation. Nanoparticles were acquired by cold centrifugation at 20,000 revolutions per minute for 40 minutes, rinsed with 15 mL of high-performance liquid chromatography (HPLC) grade water, and then restored (Figure 3).

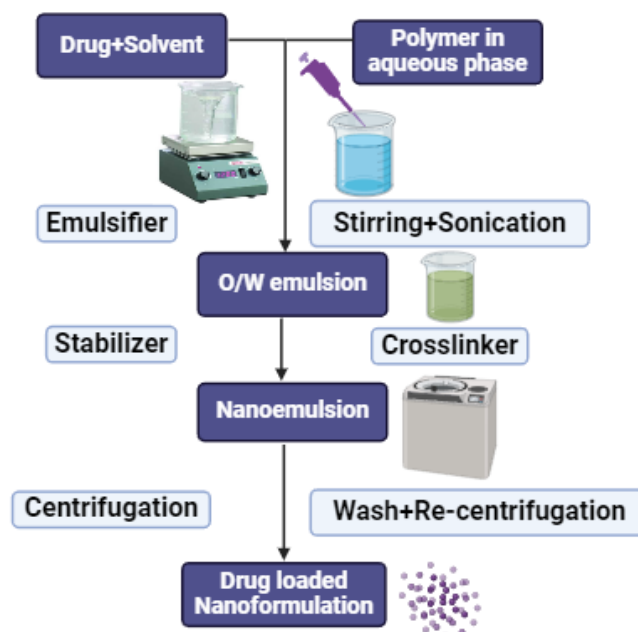


Figure 3: Schematic Representation of the Nanoformulation Process

Box-Behnken Design (3 factors, four levels) was selected to optimise the nanoformulation and to study the effect of various experimental variables. The experimental variables for applying BBD were selected based on the literature (Harish et al., 2023; Sarkar et al., 2019). The variables such as the amount of cross-linker (mL), time of sonication (min) and percentage of emulsifier (%) were selected as independent variables for the present study at three levels viz; low (-1), medium (0) and high (+1). The selected cross-linker, sonication time and emulsifier ranges were 1-3 mL, 8-20 min and 2-5 %, respectively. The effects of the independent variables on dependent variables such as size, polydispersity index (PDI), zeta potential (ZP), and drug loading were studied. The constraints were set as maximum for drug loading and minimum for size, PDI, and ZP, respectively. BBD has given 17 experiments with five centre points (table). The results were fitted to various linear, 2FI, quadratic, cubic, and residual models. The model, which was not aliased and significant for the model terms, was selected based on adjusted, predicted R-square value (highest) and p-value (<0.0001). Response surface methodology was applied to evaluate the effect of independent variables on dependent variables.

5.3 Evaluation of the prepared nanoformulation

5.3.1 Calculation of the pH level

The formulations were measured using a calibrated digital pH meter at a constant room temperature of $24 \pm 2^\circ\text{C}$.

5.3.2 Spreadability

This investigation utilises equipment originally suggested by Mutimer et al., 1956 and adapted for laboratory use to measure spreadability. A pulley was attached to one end of a wooden block, which forms the equipment. A substance's spreadability is defined by its 'Slip' and 'Drag' properties. An extra (about 2 gm) of the studied formulation was placed on a ground glass slide attached to this block. The nanoemulsion gel was encased between two identical glass slides, one with a hook. Place a single kilogram of weight on each slide to remove air and ensure the formulation was evenly distributed between the slides for 5 minutes. The borders were cleaned of any extra formulation. The top plate was subsequently pulled with an 80-gram rope from the hook, and the resulting time, in seconds, was recorded as the distance of 7.5 cm covered by the top slide. The spreadability is better when the time gap is shorter. A precise formula was used to determine spreadability (Mutimer et al., 1956)

$$S = \frac{M \times L}{T}$$

Here, S represents the spreadability of a substance, which measures how easily it spreads under a given set of conditions. The variables are defined as follows:

- M: The weight of the upper slide applies force to the substance.
- L: The length of the glass slides used in the measurement.
- T: The time taken for the two glass slides to separate from each other completely.

5.3.3 Viscosity

The viscosity of formulated samples was determined using a Brookfield viscometer (Brookfield Viscometer DV-E) at $25^\circ\text{C} \pm 2^\circ\text{C}$ at the rpm 4

5.3.4 Refractive index (RI)

At a temperature of 25°C, an Abbe refractometer was used to determine the system's refractive index. This was accomplished by depositing one drop of the formulation on the slide in triplicate.

5.4 Characterization of the prepared nanoformulation:

5.4.1 Investigation of particle size and zeta potential characteristics

The particle size of the prepared nanoformulation was evaluated using a particle size analyser (Malvern S90), which operates on the principle of dynamic light scattering (DLS). Millipore water was used for the DLS experiments, and the concentration of the particle emulsions was set at 1 mg/ml. Each measurement was conducted three times at a 90-degree angle, with the samples maintained at a temperature of 25°C. Additionally, the zeta potential was measured at 25°C using the Malvern zeta potential analyser, which determines the zeta potential by analysing the electrophoretic movement of particles in an electric field.

5.4.2 Differential Scanning Calorimetry (DSC)

The DSC 6000, Perkin Elmer (Waltham, MA, USA) was used to conduct the DSC analysis of the lyophilised guar gum (GG) and guar gum nanoformulation (GGNP) Syringic acid (SRN) and optimized Syringic acid loaded guar gum nanoformulation (SRNNP). The drug's crystalline behaviour in the formulations was the intended subject of the analysis. Indium, a 99.9% pure calibration reference was used to calibrate the device for melting point and heat of fusion. A 10 °C/min heating rate was employed within the 30–300°C temperature range. Experimentation was conducted with nitrogen gas purging at a 50 mL/min rate. A standard Aluminium pan held 4 mg of the sample, while an empty pan was kept as a control.

5.4.3 Fourier transform infrared spectroscopy (FTIR)

In order to monitor any modifications in nanoformulation, FTIR (Perkin Elmer Spectrum 2) spectra were acquired. Using a Nicolet iS50 FT-IR from Thermo Scientific, a thermally-controlled diode laser was used to record the FTIR spectrum in the 4000-500 cm⁻¹ spectral area.

5.4.3 Field Emission Scanning Electron Microscopy (FESEM)

Field Emission Scanning Electron Microscopy (FESEM) was employed to examine the surface morphology of nanoparticles of nanoformulations. The analysis used a FESEM (model JSM-

6610LV, JEOL, Peabody, MA, USA) known for its exceptionally high depth resolution. A thin layer of the nanoformulation was applied to an aluminium stub using double-sided adhesive carbon tape for sample preparation. The stub was coated in an argon atmosphere using a high-vacuum evaporator with a gold sputter module. Photomicrographs of the optimized nanoformulation samples were captured at magnifications ranging from 10X to 300,000X.

5.4.4 Drug loading and in vitro drug release

A stock solution of raw drugs was prepared to create a standard curve. The λ max of the active compounds was identified by scanning an appropriate dilution of the stock solution. To determine the drug loading of the drug/compound in nanoparticles, 5 mg of drug-loaded NPs were dissolved in a 1:1 mixture of DMSO and deionised water (totalling 5 ml). The samples were rotated at 50 rpm for 24 hours to ensure complete dissolution. The drug loading percentage was calculated using the following formula:

All samples were analysed in triplicate. The drug loading percentage was calculated as follows:

$$\text{Drug loading (\%)} = (\text{Weight of drug loaded in NF} / \text{Weight of initial drug IN NF}) \times 100$$

The release experiments were conducted using the dialysis technique. To determine the release profiles of the drug/active compound, 20 mg of drug-loaded nanoformulations were suspended in 2 mL of phosphate-buffered saline (PBS) at pH 7.4 and placed into a dialysis bag with a 5 kDa molecular weight cutoff. The dialysis bag was then immersed in 100 ml of PBS (pH 7.4) and incubated at 37°C with continuous magnetic stirring at 50 rpm. The release medium was periodically removed and replaced with a fresh buffer. The concentration of the drug or active compound in the release medium was measured using the UV detection method as previously described.

The optimized formulation's in vitro drug release kinetics were evaluated and fitted to various drug release models, including the zero-order, first-order, and Higuchi models.

5.5 In vitro studies

5.5.1 Free radical scavenging activity of the prepared nanoparticles

A. DPPH assay-

The antioxidant activity of the samples was assessed using the DPPH free radical scavenging assay, based on a modified version of the method by Nithianantham et al. 2011. Briefly, 50 μ L of each sample at concentrations of 20 μ g/mL, 40 μ g/mL, 60 μ g/mL, 80 μ g/mL, and 100 μ g/mL was added to test tubes containing 5 mL of a 0.004% (w/v) DPPH solution. The mixture was vortexed and incubated in the dark at room

temperature for 30 minutes. Absorbance readings were taken at 517 nm using a spectrophotometer. An 80% (v/v) methanol solution served as the blank, and ascorbic acid was used as the reference standard. Each measurement was repeated three times, and DPPH scavenging activity was calculated with the formula:

$$\text{DPPH scavenging activity(\%)} = \frac{A_0 - A_1}{A_0} \times 100$$

A_0 is the absorbance of the negative control (0.004% DPPH solution), and A_1 is the absorbance of the test sample.

B. ABTS assay

The ABTS radical cation decolourisation assay, following the protocols outlined by (Re et al., 1999; Chandan et al., 2020), was employed to evaluate the free radical scavenging activity of the nanoparticles, with ascorbic acid serving as the standard. This method combined a seven mM ABTS solution with a 2.5 mM ethanolic Potassium Persulfate ($K_2S_2O_8$). The mixed solution had been stored in the dark at room temperature for 12-16 hours to generate the $ABTS^{\cdot+}$ cation radical. After the incubation period, the solution was diluted until its absorbance at 743 nm reached 0.7. The produced solution was subsequently applied to a 100 μ l sample, incubated at ambient temperature for 30 minutes, and the absorbance was quantified at 734 nm utilizing a Shimadzu UV-1800 UV/Visible Scanning Spectrophotometer. The inhibition% was subsequently computed using the given equation.

$$\text{ABTS scavenging activity(\%)} = \frac{A_0 - A_1}{A_0} \times 100 \quad (2)$$

A_0 represents the absorbance of the ABTS solution used as a negative control, and A_1 represents the absorbance of the test sample. Various concentrations, such as 20 μ g/ml, 40 μ g/ml, 60 μ g/ml, 80 μ g/ml, and 100 μ g/ml, were used for the test.

5.5.2 Anti-diabetic enzyme activity of the prepared nanoparticles

A. Inhibition of the enzyme activity of α -glucosidase

The α -glucosidase inhibition capacity of the nanoparticles was assessed utilizing a standard testing method with minor changes (Shai et al., 2011). A reaction mixture comprising 50 μ l of phosphate buffer (100 mM, pH 6.8), 10 μ l of α -amylase (2 U/ml), and 20 μ l of nanoparticles at different concentrations (20, 40, 60, 80, and 100 μ g/ml) was pre-incubated in a 96-well plate

at 37°C for 20 minutes. The substrate, 20 µl P-NPG (5 mM), was added, and the mixture was further incubated for 20 minutes at 37°C. 50 µl of 0.1 M Na₂CO₃ was added to stop the reaction. Using a Multiplate Reader, the absorbance of the freed p-nitrophenol was measured at 405 nm. Acarbose at different concentrations (20, 40, 60, 80, and 100 µg/ml) was included as a standard. A control sample without GGNP was set up in parallel, and each experiment was performed in triplicate. Percentage inhibition is calculated as follows (equation 3)

$$\alpha - \text{glucosidase scavenging activity (\%)} = \frac{A_0 - A_1}{A_0} \times 100 \quad (3)$$

A₀ is the absorbance of the negative control (α -glucosidase solution), and A₁ is the absorbance of the test sample. Acarbose was used as the reference drug in the α -Glucosidase assay because it acts as an α -Glucosidase inhibitor, which can help glycemic management in diabetes by reducing the rise in blood glucose after meals and enhancing the utilization of insulin.

B. Inhibition of the enzyme activity of α -Amylase

The α -amylase inhibitory activity of nanoparticles was assessed using a modified standard protocol (Ademiluyi et al., 2013). A reaction mixture of 50 µl phosphate buffer (100 mM, pH 6.8), 10 µl α -amylase (2 U/ml), and 20 µl nanoparticles (20-100 µg/ml) was pre-incubated at 37°C for 20 minutes in a 96-well plate. Then, 20 µl of 1% soluble starch was added as the substrate, followed by incubation for 30 minutes. Afterwards, 100 µl of DNS reagent was added, and the mixture was boiled for 10 minutes. Absorbance was measured at 540 nm using a Multiplate Reader. Acarbose (20-100 µg/ml) served as the standard, and all tests were run in triplicate with controls. The inhibitory activity was calculated using Equation 4.

$$\alpha - \text{Amylase scavenging activity (\%)} = \frac{A_0 - A_1}{A_0} \times 100 \quad (4)$$

Where A₀ is the absorbance of the negative control (α -Amylase), and A₁ is the absorbance of the test sample.

5.5.3 Cytotoxicity activity

A modified version of the MTT colorimetric assay, based on the method by Bruggisser et al., 2002, was utilised to assess cell viability in a 96-well plate. Each well received 200 µl of MTT solution, which was yellowish due to the absence of phenol red (5 mg/ml in PBS). The plates were then incubated at 37°C with 5% CO₂ for approximately seven hours, allowing the metabolically active cells to reduce the MTT. This reduction process involves glucose-

metabolizing enzymes that generate reducing equivalents, such as NADH and NADPH. The intracellular formation of purple formazan crystals resulted from this process. Following incubation, the supernatants were removed, and 100 µl of DMSO was added to each well to dissolve the formazan crystals. The plates were shaken for 15 minutes to ensure complete dissolution. Optical density (OD) readings were then taken at 595 nm using a scanning multiwell spectrophotometer (Bio-Rad, Model 680, Japan), with DMSO as the blank. The formazan produced, measured at 595 nm, was directly proportional to the number of viable cells in the culture. Each experiment was conducted in triplicate to ensure reproducibility. Relative cell viability (%) was determined by comparing the experimental wells, with and without nanoparticles as carriers, using the following equation.

$$\text{Cell viability(\%)} = \frac{A_{\text{control}} - A_{\text{test}}}{A_{\text{control}}} \times 100 \quad (5)$$

A_{test} is the absorbance of the test sample, and A_{control} is the absorbance of the control sample.

5.5.4 In vitro scratch assay

The HaCaT cells were spread out in 24-well plates with a density of 3×10^6 cells/ml and left to grow for 24 hours at 37°C with 5% CO₂. Using sterile p200 pipette tips, a small linear scratch was carefully scraped into the confluent monolayer. During the scratching process, great attention was taken to ensure that all samples were of the same size and distance. Before adding the media containing various treatment solutions, the cells were thoroughly washed with PBS to eliminate any remaining cell debris. The images were taken at various intervals (0 and 24 hours) after the incubation period of 24 hours. The experiment was performed in triplicate, and the wound healing rate was analysed using ANOVA followed by post-hoc tests to determine statistical significance. Care was taken to maintain consistent pressure and angle when creating scratches to standardise the scratch width. The wound healing rate was determined using equation 6 (Syarina et al., 2015)

$$\text{Wound healing (\%)} = \frac{\text{Initial Area} - \text{Final Area}}{\text{Initial Area}} \times 100 \quad (6)$$

5.5.5 Tube formation assay

This assay is commonly employed to study angiogenesis, the process by which endothelial cells form capillary-like structures resembling blood vessels. The procedure emphasises sterile techniques and optimal cell recovery conditions. After incubating the HUVECs under optimal

conditions, the culture medium is changed to remove residual dimethyl sulfoxide (DMSO). As the cell culture approaches confluency, the medium volume is doubled, and cells are subcultured when reaching 80% confluency. In preparation for the tube formation assay, Geltrex® LDEV-Free reduced growth factor basement membrane matrix is thawed and applied to the growth surface. This matrix provides a three-dimensional environment conducive to the formation of capillary-like structures. The cells are then diluted in a supplemented medium, and angiogenesis inducers or inhibitors may be added as needed. The cell suspension is gently added to the gel-coated wells, and the plate is incubated overnight for tube formation. After incubation, the cells are visualised directly using a light microscope to assess the formation of capillary-like structures (Arnaoutova et al., 2010; DeCicco-Skinner et al., 2014)

5.5.6: Establishment of type 2 diabetes in cell line: an in vitro study

Materials:

- Dulbecco's Modified Eagle Medium (DMEM)
- Mannitol
- Glucose
- Antibiotics (AB)
- Fetal Bovine Serum (FBS)
- Phosphate Buffered Saline (PBS)
- Distilled Water (DW)

➤ Protocol

The NCCS, Pune cell bank supplied the L929 and HaCaT cell lines. Cells were cultured in Dulbecco's Modified Eagle Medium (DMEM), either with low/average glucose (5 mM plus 20 mM mannitol for osmotic balance) or high glucose (25 mM), following standard procedures and protocols. They were maintained with 10% fetal bovine serum and antibiotics (Penicillin at 100 IU/ml and Streptomycin at 100 mg/ml) in a 5% CO₂ atmosphere at 37°C. Once the cells reached 80–90% confluency, they were induced to enter the G₀ phase to simulate hyperinsulinemia and hyperglycaemia. The entire process was carried out in triplicate.

5.5.7: Establishment of an in vitro model using six healthy plates

Upon achieving 70% confluency, the high glucose plate seed cells were grown in a 6-well plate containing 30 mmol of glucose, with distinct treatments administered to each group.

5.5.8 Protocol for Cell lysis and preparation of cell lysate for protein estimation

Protease and phosphate inhibitors were added to the lysis solution to prevent protein breakdown and modification, ensuring the highest protein yield during cell lysis. After treating the cells on a 6-well plate according to the experimental protocol, they were rinsed with ice-cold phosphate-buffered saline (PBS). 5 mM sodium butyrate was incorporated into the lysis solution to maintain acetylation levels. The lysis buffer was then applied to the plate, and the cells were scraped off using a cell scraper. The resulting lysate was transferred to microcentrifuge tubes and centrifuged at 1700 rpm for 7 minutes in a cold microcentrifuge. The supernatant was retained for further analysis, while the pellet was discarded.

5.5.9 The method of preparing tissue and cell homogenate

A Dounce homogeniser was used to prepare the homogenate using a buffer solution consisting of 0. 1M Ethylenediamine tetraacetic acid (EDTA) and 0. 1M Tris chloride was mixed and adjusted to a pH of 7.4. Beta-mercaptoethanol was added to the buffer before homogenising the cells and tissues. The homogenising tube was kept in an ice-filled beaker throughout the process. Cells were homogenised using a motor-driven Teflon pestle rotating at 3000 revolutions per minute. The resulting homogenate was then filtered through cotton gauze and stored in labelled plastic vials in a refrigerator at -18°C until needed. This 10% homogenate (1g of cells in 9 ml of buffer) was used as the starting material for further dilutions with appropriate buffers to obtain the working homogenate fraction as required.

A. Post-nuclear supernatant preparation (PNS)

The cell homogenate was centrifuged using a C-24 REMI cold centrifuge at 10,000 rpm for 5 minutes at 4 °C to separate the nuclear pellet from the supernatant. The post-nuclear supernatant (PNS) was then collected and stored at -18°C for future use.

B. Post mitochondrial supernatant (PMS)

After removing the nuclear pellet, the supernatant was centrifuged at 10,000 g for 10 minutes at four °C to obtain the mitochondrial pellet and the post-mitochondrial supernatant (PMS). The PMS was then stored at -18°C for subsequent analysis.

5.5.10: Protocol for protein estimation

The protein content was quantified following the standardized method established by Lowry et al., 1951, employing a standard curve derived from bovine serum albumin (BSA).

Principle

This method is based on the presence of the amino acids tyrosine and tryptophan. Folin's reagent, which reacts with proteins to form a coloured complex, was used. The aromatic amino acids in the protein interact with copper (in an alkaline environment), leading to the reduction of phosphomolybdate and resulting in colour production. The intensity of the colour is proportional to the amount of aromatic amino acids present.

Reagents:

- **Reagent A:** 2% sodium carbonate in 0. 1N NaOH
- **Reagent B:** 1% CuSO₄ in double-distilled water
- **Reagent C:** 2% sodium potassium tartrate in double-distilled water

Lowry's Reagent: Mix Reagent A, Reagent B, and Reagent C in a ratio of 49: 0. 5: 0.5 (v/v)

Folin's Ciocalteu's Reagent: Dilute with double-distilled water in a ratio of 1:1 (v/v)

Stock Protein Standard: Dissolve 20 mg of bovine serum albumin (BSA) in 1 ml of double-distilled water (Table 4).

Table 4: Reagents for protein estimation

Reagent	Blank (ml)	Standard (ml)	Test (ml)
Double-distilled water (DDW)	1	0.9	0.9
Standard	-	0. 1	-
Test Sample	-	-	0. 1
Lowry's Reagent	5 ml	5 ml	5 ml

Sample Preparation:

1. **Add Reagents:** For each sample, add the appropriate volumes of DDW, standard, or test sample to the respective tubes.
2. **Add Lowry's Reagent:** Add 5 mL of Lowry's Reagent to each tube.

3. **Incubate:** Incubate the tubes at 37°C for 15 minutes.
4. **Add Folin's Reagent:** Add 0.5 ml of Folin's Ciocalteu's Reagent to each tube.
5. **Incubate Again:** Incubate the tubes for 30 minutes at 37°C.

5.5.11: In vitro oxidative biomarkers analysis

L929 was utilised to evaluate in vitro antioxidant activity. Different groups were used for all the *in-vitro* estimation of antioxidant activities: control (without treatment), hyperglycaemia (treatment with high glucose), HG/HD (Treatment with 100 µg/ml as the high dose of experimental samples in the high glucose condition), and HG/LD (Treatment with 50 µg/ml as the low dose of experimental samples in the high glucose condition).

A. Estimation of lipid peroxidation (LPO):

It is quantified using the criteria established by Beuge and Aust in 1978.

Principle

Free radicals can induce damage to polyunsaturated fatty acids primarily through peroxidation, primarily by the action of OH⁻ and O₂⁻ ions. Peroxidation yields Malondialdehyde (MDA), which has been studied to undergo a reaction with Thiobarbituric acid (TBA), resulting in a faint red absorbance at 535nm.

Reagents:

- 150 mM Tris-HCl buffer (pH 7.1)
- 1.5 mM Ascorbic acid
- one mM FeSO₄
- 10% Trichloroacetic acid
- 0.375% Thiobarbituric acid (pH 7)

Protocol

Table 5: Procedure of LPO estimation

Reagent	Blank (ml)	Test (ml)
Tris-HCl buffer	0.1	0.1
FeSO ₄	0.1	0.1
Ascorbic acid	0.1	0.1
Double-distilled water (DDW)	0.7	0.6
Sample	-	0.1

In a total volume of 1000 µl, the reaction mixture included 100 µl of homogenate, 100 µl of ferrous sulphate (1 mM), and 100 µl of ascorbic acid (1.5 mM), together with 1000 µl of Tris-HCl buffer (pH 7.1;150 mM). Adding 1000 µl of 10% trichloroacetic acid terminated the incubation of the reaction mixture at 37°C after an hour. The tubes were sealed and left in boiling water for 15 minutes after adding 1000 µl of 0.375% thiobarbituric acid. Subsequently, these samples were placed on ice and spun at 3000×g for 10 minutes. By comparing the absorbance of the supernatant at 535 nm to that of a reagent blank, the amount of TBARS (lipid peroxidation) was determined. The molar extinction value of $1.56 \times 10^{-5} \text{ M}^{-1} \text{ cm}^{-1}$ was used to express the results as nM MDA formed/min/mg tissue at 37°C (Mani et al., 2022) (Table 5).

B. Estimation of Superoxide dismutase (SOD) activity:

Principle

The underlying concept is converting Nitroblue Tetrazolium dye into formazon, a blue-coloured compound regulated by superoxide radicals. The generation of these radicals occurs through the auto-oxidation of hydroxylamine hydrochloride. Furthermore, it prevents the reduction of NBT by substrate oxidase (SOD) and is facilitated by hydroxylamine hydrochloride. Quantification of enzyme activity is based on the degree of inhibition.

Reagents:

- 50 mM Sodium Carbonate buffer in 0.1 mM EDTA (pH 10.8)
- 96 µM Nitro Blue Tetrazolium (NBT) in 95% ethanol
- 0.6% Triton X-100 in double-distilled water (DDW)
- 20 mM Hydroxylamine HCl (pH 6.0)

Procedure for SOD Estimation:

1. Prepare the Reaction Mixture:

○ For the Blank:

- 1.35 ml of 50 mM Sodium Carbonate buffer (pH 10.8) in 0.1 mM EDTA
- 0.1 ml of 20 mM Hydroxylamine HCl (pH 6.0)
- 0.1 ml of 0.6% Triton X-100 in DDW

- 0.5 ml of 96 μ M Nitro Blue Tetrazolium (NBT) in 95% ethanol
- For the Test:
 - 1.3 ml of 50 mM Sodium Carbonate buffer (pH 10.8) in 0.1 mM EDTA
 - 0.1 ml of 20 mM Hydroxylamine HCl (pH 6.0)
 - 0.1 ml of 0.6% Triton X-100 in DDW
 - 0.5 ml of 96 μ M Nitro Blue Tetrazolium (NBT) in 95% ethanol
 - 0.05 ml of the sample

2. Incubation minutes at room temperature.

To estimate SOD activity, the reaction in which hydroxylamine hydrochloride produces superoxide radicals and reduces nitro blue tetrazolium (NBT) dye was replicated according to the protocol laid out by Beyer and Fridovich. In 1.3 ml of sodium carbonate (50 mM, pH 10.0), there was 500 μ L of NBT (96 μ M, Sigma Aldrich) and 100 μ L of Triton X-100 (0.6%) in the reaction mixture. The reaction was started by adding 100 μ L of hydroxylamine hydrochloride (20 mM, pH 6.0) and 70 μ L of lysate. The UV-VIS spectrophotometer was used for 5 minutes at 60-second intervals to record the rise in absorbance caused by the lowering of NBT. The wavelength used was 560 nm. The blue colour that was developed was measured. The quantity of enzyme needed to produce a 50% inhibition in the reduction of NBT is referred to as one unit of SOD activity.

C. Estimation of Catalase (CAT)

Principle: Catalase is an enzyme that catalyzes the decomposition of hydrogen peroxide (H_2O_2) into water (H_2O) and oxygen (O_2).

Reagents:

- Phosphate Buffer (0.2 M, pH 7.0):
 - Solution A: Dissolve 1.79 g of KH_2PO_4 in 200 ml of double-distilled water (DDW).
 - Solution B: Dissolve 3.52 g of $\text{NaHPO}_4 \cdot 2\text{H}_2\text{O}$ in 300 ml of DDW.
 - Phosphate Buffer: Mix Solution A and Solution B in a ratio of 3: 7 to achieve a pH of 7.0.

- **Working Phosphate Buffer:** Add 160 μl of H_2O_2 to 100 ml of the phosphate buffer prepared above to create the working phosphate buffer solution. This solution will be used in the catalase activity assay (Table 6).

Procedure

Table 6: Reagent details for Catalase estimation

Reagents	Blank	Test
Sample	25 μl	25 μl
Phosphate buffer+ H_2O_2	-	3.0 ml
Phosphate buffer- H_2O_2	3.0 ml	-

The optical density (O.D.) was measured at 240 nm over 2 minutes, with readings taken at 30-second intervals. The enzyme activity for catalase was calculated using a molar extinction coefficient of $43.6 \text{ M}^{-1}\text{cm}^{-1}$. The results were expressed in terms of the amount of hydrogen peroxide (H_2O_2) decomposed, measured in micromoles per minute per milligram of protein ($\mu\text{moles H}_2\text{O}_2$ decomposed/min/mg protein or U/ mg protein).

The method for determining catalase activity was based on that of Chance and Maehly, 1955. The reaction mixture consisted of 3000 μl of 50 mM phosphate buffer with a pH of 5, 25 μl of PMS sample and 5.9 mM of H_2O_2 . The absorbance change was monitored at 240 nm every 30 seconds for 2 minutes. Using the molar extinction coefficient, the enzyme activity was determined. The results are presented as the amount of hydrogen peroxide degraded each minute per milligram of protein.

D. Estimation of Glutathione-S-Transferase (GST)

Principle: Glutathione-S-Transferase (GST) is an enzyme that catalyses the conjugation of 1-chloro-2, 4-dinitrobenzene (CDNB) with the sulfhydryl group of reduced glutathione (GSH). The resulting CDNB-Glutathione conjugate absorbs light at 340 nm, which can be measured spectrophotometrically.

Reagents:

- **100 mM Potassium Phosphate Buffer (pH 6.5):** Prepare a 100 mM potassium phosphate buffer solution and adjust the pH to 6.5.
- **one mM GSH (Reduced Glutathione) (pH 6.5):** Prepare a one mM solution of reduced glutathione, adjusted to pH 6.5.

- **1 mM CDNB (1-Chloro-2, 4-Dinitrobenzene):** Dissolve 61 mg of CDNB in 50 mL of distilled alcohol to obtain a 1 mM solution (Table 7).

Procedure

Table 7: GST estimation reagent details

Reagents	Blank (ml)	Test (ml)
Buffer	1	1
DDW	1.65	1.55
GSH	0.3	0.3
Sample	-	0.1
CDNB	0.05	0.05

In order to evaluate GST activity, the methodology proposed by Habig et al., 1974 was employed. In a total volume of 2000 µl, the reaction mixture included 1000 µl of phosphate buffer (pH 6.5; 0.1 M), 300 µl of reduced glutathione (1 mM), 50 µl of 1-chloro-2,4-dinitrobenzene (CDNB) (1 mM), and 100 µl of PMS. The UV-VIS spectrophotometer measured the absorbance at 340 nm for 5 minutes at 60-second intervals, which increased due to the production of the glutathione conjugate. This enzyme activity was determined by measuring the CDNB conjugate generated per minute per milligram of protein, with a molar extinction coefficient of $9.6 \times 10^3 \text{ M}^{-1} \text{ cm}^{-1}$.

5.6 Antimicrobial tests

5.6.1 Assay for antimicrobial properties

Antimicrobial capacity had been assessed using the Zone Inhibition Method, also known as the Kirby-Bauer protocol. The Mueller Hinton Agar (MHA) dishes were inoculated by evenly distributing 100 µl of microbial culture throughout the surface (cell count 1.5×10^8 CFU/mL). A disc containing 10 µg of Ciprofloxacin was employed as the positive control for the antibacterial assay, while a disc loaded with 25 µg of Amphotericin B served as the positive control for the antifungal assay. Sample concentrations vary from 0 to 1000 µg/ml. The dishes had been incubated (Basil et al., India) at 37 °C for 24 hrs. The dimensions of a clean zone surrounding the disc have been assessed and documented. The following microorganisms had been selected for study: *Staphylococcus aureus* (MTCC 96), a gram-positive bacterium;

Escherichia coli (MTCC 452), a gram-negative bacterium; and *Candida albicans* (MTCC 854), a fungal species.

5.6.2 Cox-II Inhibition Assay

The protocol is outlined with minor alterations. Different concentrations (0-200 µg/ml) had been prepared in a Buffer solution (Tris-HCl, 100 mM, pH 8.0). The enzyme, dissolved in a solution of Tris/heme/phenol with a concentration of 100mM/1µM/1µM correspondingly, was mixed with a reaction buffer. This mixture was then applied to a designated well of a 96-well plate containing THP-1 cells. The reaction was initiated by adding five µl of the substrate (Arachidonic acid, 10 mM) and five µl of TMPD solution (17 mM) to the plate. Subsequently, the plate was stored at ambient temperature for 10 minutes, and the degree of light absorption was quantified at a wavelength of 595 nm utilising a microplate reader (iMark, Bio-Rad). An inhibitor, Celecoxib (25 µM final concentration), has been employed as a positive control.

5.6.3 TNF- α (Cytokine) assay (in the presence or absence of a bacterial infection)

The study used protocol guidelines described in the GENLISATM Human TNF α ELISA kit (Cat No.: KB1145). LPS (200 microliter) was used to simulate a bacterial infection, while cells lacking LPS were used to represent the normal condition. Untreated wells were designated as the negative control, while wells solely exposed to LPS were designated as the positive control.

5.7 In vivo experiment

5.7.1 Description of in vivo experiment: The in vivo evaluation of nanoformulations was performed under IAEC approval Number: [LPU/IAEC/2023/41]

- A. **Experimental animals:** For this study, the animals were female Sprague Dawley rats of weight 180-220 grams (Rats were procured from NIPER, Mohali, which were 7 weeks of age). They were placed in polypropylene cages, which are maintained at standard conditions (12-hour light/dark cycles, 25±5 °C in paddy husk beds. A high-fat diet with a single dose of Streptozotocin (40 mg/kg of body weight) induces Type 2 diabetes, which causes pancreatic insulinitis as well as resistance to insulin-producing diabetes in rats. It is believed that the mechanism behind this is the pathogenic involvement of the pancreas, leading to low insulin production. This method is beneficial for the IIDDm type of diabetes or Type 2 diabetes.

B. Steps for the Induction of diabetes and treatment

1. Diabetes (Type 2) was induced via HFD, administering a fresh aqueous medium of STZ (40 mg/kg of body weight) in phosphate buffer pH 7.4 through the intraperitoneal (i.p.) route.
2. Seven days after STZ administration, serum was collected from fasting rats via the tail vein to analyse plasma glucose. The fasting glucose levels in rats ranged from 301-330 mg/dl, which indicated clear signs of polyphagia, polyuria, and polydipsia, which is a consideration of diabetes.
3. After the induction of diabetes, the Excision wounds were created on the skin of diabetic mice.

C. Experimental procedure

After acclimatisation for one week, the rats were allocated into two dietary regimens: either a regular pellet diet (NPD) controls or HFD (58% fat, 25% protein, and 17% carbohydrate, as a percentage of total kcal) *ad libitum*, for 4 weeks. On the seventh day, a single dose of STZ (40 mg/kg) was injected into HFD-fed rats. After 7 days, blood glucose will be evaluated, and rats with blood glucose levels more than 250 mg/dl will be considered diabetic. In the diabetic rats, excision wounds were created per the reported procedure on the 15th day of the protocol and will be considered as 0 days of wound. The mice were anaesthetised by administering an intraperitoneal injection of a combination of xylazine and ketamine at 90 mg/kg and 5 mg/kg body weight, respectively. The dorsal surface of the mice was then shaved and sterilised using a 5% povidone-iodine solution. A circular full-thickness cutaneous wound measuring 8 mm in diameter was created on the dorsal surface of each mouse using a biopsy punch.

The next day after creating a wound will be considered as day 1 of wounded diabetic rats, and from day 1 to day 14 (days 16th to 29th of the protocol), treatment will be given as follows:

HFD + Raw drug one or Raw drug 2 (high dose), HFD + NF1/NF2 (high dose) (NF1 of Sinapic acid)/ (NF2 of o-Coumaric acid), HFD + NF1/NF2 (low dose) (NF1 of Sinapic acid)/ (NF2 of o-Coumaric acid), HFD + placebo (Guar gum nanoformulation/GGNP), HFD + Positive (5% povidone/iodine solution). According to Gaikwad et al. (2010), the composition and preparation of HFD are the same. Body weight will be recorded weekly from the beginning to the end of the study. Blood biochemical parameters, such as glucose, lipid profile, and kidney function tests, will be measured at the start and end of the study for NPD groups, on day 14, and at the end for HFD groups. At the end of the study, animals will be sacrificed by cervical dislocation after anaesthesia (Table 8) (Figure 4).

Table 8: In vivo experimental groups and treatment

S. No	Group Name	Diet + Dose and route of drug treatment	No. of animals
Group 1	Non-diabetic wounded control	NPD for 4 weeks	6
Group 2	Diabetic wounded Placebo	HFD for 4 weeks+ 40 mg/kg STZ (i.p)+Placebo (topical)	6
Group 3	Diabetic wounded+ Positive control	HFD for 4 weeks + 40 mg/kg STZ (i.p)+5% povidone-iodine solution (topical)	6
Group 4	Diabetic wounded + Drug 1 (Sinapic acid) (H. D)	HFD for 4 weeks + 40 mg/kg STZ (i. p) + 40 mg/kg of Drug 1 (topical)	7
Group 5	Diabetic wounded+NF of Sinapic acid (H. D)	HFD for 4 weeks + 40 mg/kg STZ (i. p) + 40 mg/kg of NF1 (topical)	7
Group 6	Diabetic wounded+NF of Sinapic acid (L. D)	HFD for 4 weeks + 40 mg/kg STZ (i. p) + 20 mg/kg of NF1 (topical)	7
Group 7	Diabetic wounded +Drug 2 (o-Coumaric acid) (H. D)	HFD for 4 weeks + 40 mg/kg STZ (i. p) + 40 mg/kg of Drug 2 (topical)	7
Group 8	Diabetic wounded+NF of o-Coumaric acid (H. D)	HFD for 4 weeks + 40 mg/kg STZ (i. p) + 40 mg/kg of NF2 (topical)	7
Group 9	Diabetic wounded+NF of o-Coumaric acid (L. D)	HFD for 4 weeks + 40 mg/kg STZ (i. p) + 20 mg/kg of NF2 (topical)	7 Total =60

Treatment Schedule

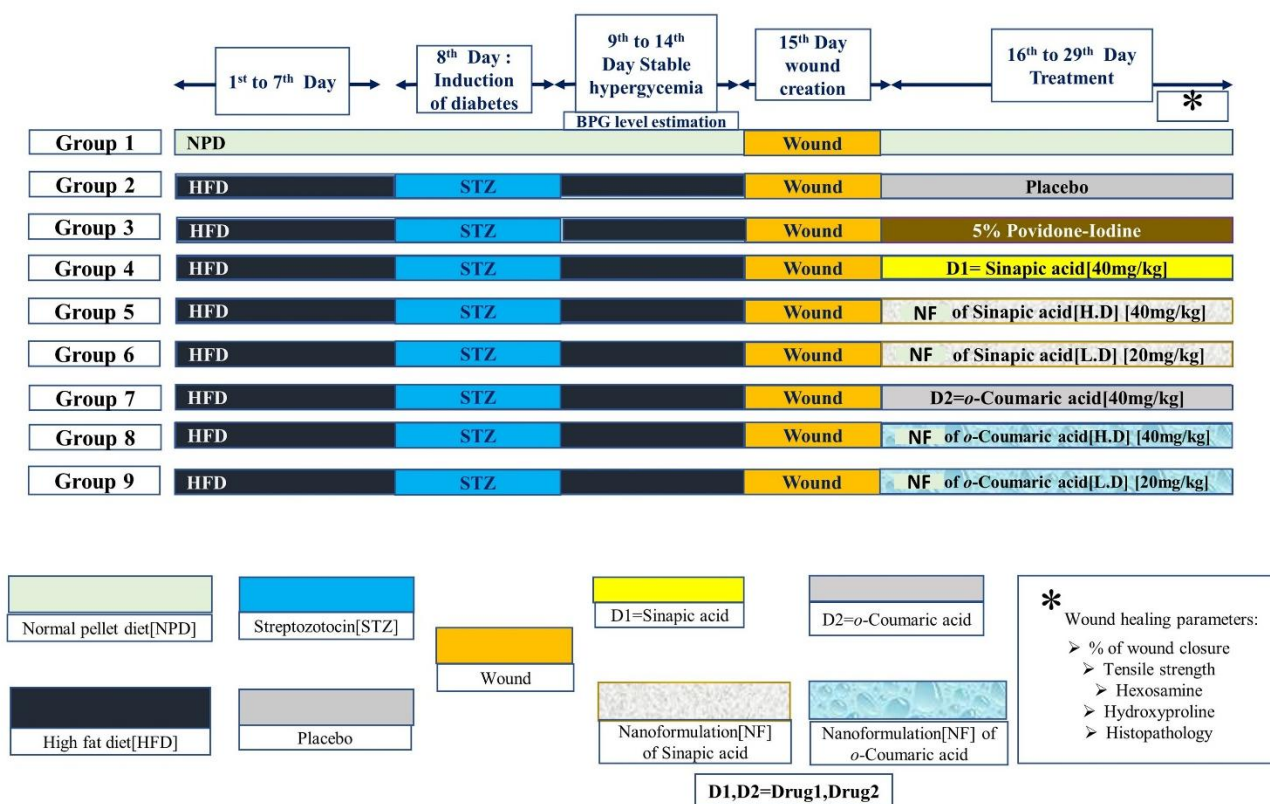


Figure 4: In vivo study plan

5.7.2: Parameters of evaluation of DM

The following parameters were assessed after the experiments to determine the treatment's effect:

- A. Estimating body weight:** The rats' body weight was estimated before the in vivo experiments, and after that, body weights were routinely checked every week before behaviour evaluation. Estimations were conducted in triplicate.
- B. Estimation of glucose in Blood:** The blood glucose measurement was conducted utilising the counter appliance Accu-Check by extracting 0.1 mL of blood from the tail of experimental mice.
- C. Biochemical parameters (Oxidative biomarkers)**

Oxidative Biomarkers: Upon completion of the study, animals designated for biochemical analysis were sacrificed by cervical dislocation on the final day of treatment.

The tissues were excised and homogenised to prepare a 10% (w/v) homogenate in 0.1 M phosphate buffer (pH 7.4). The homogenate was then centrifuged at 3000 rpm for 15 minutes, and the resulting clear supernatant was used for various biochemical assays to measure the levels of SOD, CAT, GST, and LPO.

5.7.3: Wound Healing Parameters-

- A. % Wound Closure:** The percentage of wound contraction will be calculated based on the percentage of wounds reduced from the original wound size. The percentage of wound closure will be measured on days 3rd, 7th, and 14th.

Percentage wound closure = $\frac{\text{Wound area on day 0} - \text{wound area on day } (n)}{\text{Wound area on day 0}} \times 100$

Wound area on day 0

where n = number of days (3, 7, and 14).

- B. Tensile Strength:** Tensile strength was measured using the Universal Testing Machine (UTM) (Zwick et al. 2010) CRF-IITD at the Sonipat Campus.
- C. Estimation of Hydroxyproline content:** On the 10th day, wounded tissues were analysed for hydroxyproline content, a key component of collagen. The tissues were dried in a hot air oven at 60–70°C until a constant weight was achieved. They were then hydrolysed in 6 N hydrochloric acid at 130°C for 4 hours in sealed tubes. After hydrolysis, the solution was neutralised to pH 7.0. Chloramine-T oxidation was performed for 20 minutes, and the reaction was stopped by adding 0.4 M perchloric acid. Colour development was achieved using the Ehrlich reagent at 60°C, and the absorbance was measured at 557 nm using a UV/Vis spectrophotometer, following the method described by Dwivedi et al., 2017.
- D. Estimation of Hexosamine content:** Weighed granulation tissues were hydrolysed in 6 N HCl for 8 hours at 98°C. After hydrolysis, the solution was neutralised to pH 7 with 4N NaOH and diluted with water. The diluted solution was then mixed with acetylacetone and heated to 96°C for 40 minutes. After cooling, 96% ethanol was added, followed by r-dimethylamino-benzaldehyde solution (Ehrlich's reagent). The mixture was thoroughly mixed and allowed to stand at room temperature for 1 hour. Absorbance was measured at 530 nm using a UV/Vis spectrophotometer. The amount of hexosamine was determined by comparing the results with a standard curve and was expressed as mg/g dry tissue weight, following the method described by Dwivedi et al., 2017.
- E. Histopathology:** After sacrifice and decapitation, rats were dissected, and the skin around the wounds was quickly excised and fixed in 10% neutral buffered formalin

for 48 hours. The fixed skin was then processed for wax embedding and sectioning. Sections were cut at a thickness of 5 μm using a microtome, processed through a xylene-alcohol series, and stained with alum hematoxylin and eosin (H&E). The stained sections were examined microscopically to evaluate histopathological changes, as described by Ahmed et al. (2017).

5.8 Statistical analysis

Statistical analysis was conducted using GraphPad Prism Software (Version 8.1.0, San Diego, USA), employing one-way ANOVA followed by Tukey's nonparametric test. Data were expressed as mean \pm standard error of the mean (SEM), and differences were considered statistically significant at $p < 0.05$.

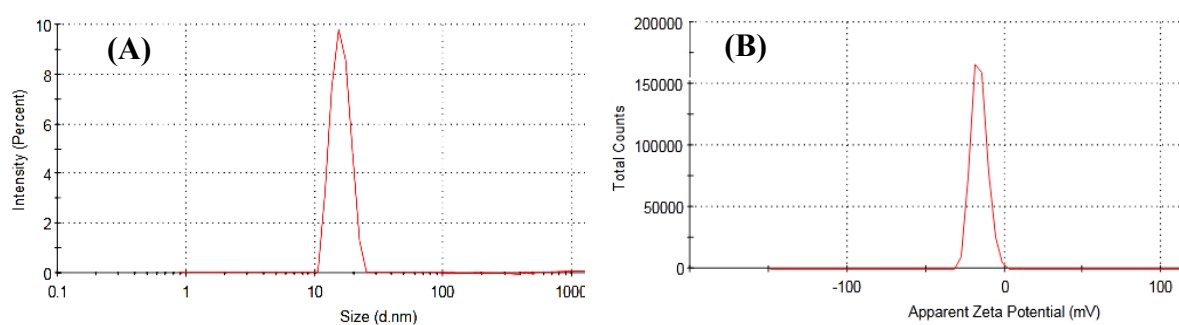
Chapter 6: Results

6.1 Optimization, Characterization of Zeta size, and SEM of placebo

Table 9 and Figure 5 present the particle size distribution and the zeta potential values of the various nano-formulations (S1-S5). Table 2 and Figure 2 show that formulation S2 obtained the lowest particle size of 18.4 nm. The corresponding zeta potential was found to be -16 mV. The zeta potential of all other formulations was in the range of -18 to -24 mV. The PDI values ranging from 0.09 to 0.21 indicate a relatively narrow size distribution.

Table 9: Formulations of placebo (Guar gum nanoformulation/GGNP) with particle size (nm), PDI, and Zeta potential value (mV)

Sample	Particle size (nm) \pm SEM	PDI \pm SEM	Zeta Potential (mV) \pm SEM
S1	36.3 \pm 2.44	0.091 \pm 0.02	-18.6 \pm 1.3
S2	18.4 \pm 3.21	0.105 \pm 0.05	-17.6 \pm 2.6
S3	28.3 \pm 2.4	0.105 \pm 0.04	-18.0 \pm 1.7
S4	22.2 \pm 4.5	0.121 \pm 0.07	-24.7 \pm 1.9
S5	29.3 \pm 6.3	0.217 \pm 0.05	-18.4 \pm 1.1



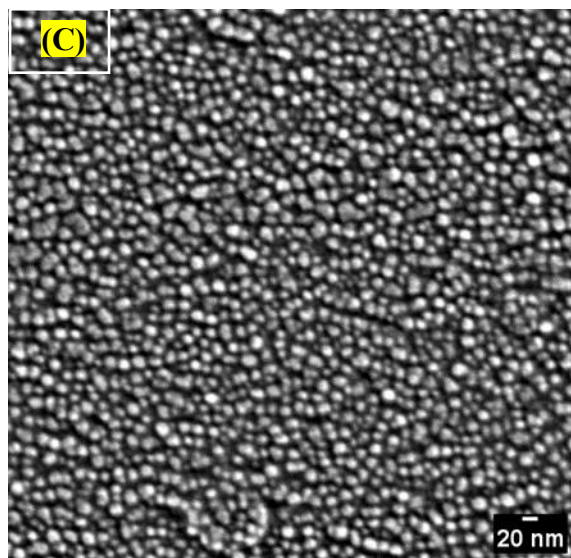


Figure 5: Characterization of placebo (Guar gum nanoformulation/GGNP) A) Particle size, B) Zeta potential of GGNP, C) SEM image (x75000)

6.2 Optimization of guar gum nanoformulation of Syringic acid (NF1)

All the 18 experiments given by BBD were formulated accordingly and characterised individually for their size, PDI, ZP and drug loading (table 10) for studying the effects of the cross-linker, sonication time and emulsifier percentage on their size, PDI, ZP and drug loading. The size, PDI, ZP and drug loading ranges was found to be between 19.2 nm (run 14) - 41.7 nm (run 11), 0.149 (run 8) – 0.562 (run 10), -24.1mV (run 17) - -31.2 mV (run 9) and 67.69 % (run 4) -93.95 % (run 9), respectively (Table 10). 3D diagrams of individual responses show the effects of independent variables on dependent variables (Figure 6). Different statistical tools such as F-value, r-square, model summary, p-value, lack of fit test and sequential model sum of squares were applied for DoE to identify the design space and formulation optimisation. Further, to understand the level of significance, ANOVA was applied.

The F-value, p-value, and coefficient of regression (r^2) indicate the quadratic model for size, PDI, and drug loading (%), whereas the model is linear for ZP (Table 11). The analysis of the terms of multiple regression revealed that the model has predicted values—adequate precision measurement given a ratio of signal to noise as four, which is desirable. Therefore, the model can navigate the design space based on the above values. BBD also determines the mathematical equations for each response in terms of coded equations. These coded polynomial equations have positive and negative signs, indicating synergistic and antagonistic effects, respectively (Table 11). The equations are as follows:

$$\text{Size} = +26.25 - 0.3250 \times A + 2.57 \times B - 4.80 \times C - 3.28 \times AB - 2.88 \times AC - 6.33 \times BC + 7.94 \times A^2 + 1.24 \times B^2 + 0.3875 \times C^2$$

$$\text{PDI} = +0.3467 + 0.0871 \times A + 0.1815 \times B + 0.0211 \times C + 0.1028 \times AB - 0.1440 \times AC - 0.0568 \times BC - 0.0008 \times A^2 + 0.0004 \times B^2 - 0.0018 \times C^2$$

$$\text{ZP} = -27.79 - 2.94 \times A - 0.7375 \times B + 0.2000 \times C$$

$$\text{Drug loading (\%)} = +86.69 + 9.34 \times A + 3.66 \times B + 1.16 \times C - 3.60 \times AB - 1.95 \times AC + 0.0850 \times BC - 3.42 \times A^2 + 1.16 \times B^2 - 0.3025 \times C^2$$

A, B, and C are crosslinkers, sonication times, and emulsifiers (%).

Table 10: Size, PDI, Zeta Potential, and Drug loading efficacy results of optimized nanoformulation of Syringic acid (NF1) of BBD design

	Response 1	Response 2	Response 3	Response 4
Run	Size	PDI	Zeta potential	Drug loading
	nm		mV	%
1	36.9	0.092	-27	69.49
2	41.5	0.338	-24.2	83.72
3	25.1	0.347	-27.9	87.01
4	29.7	0.181	-24.3	67.69
5	23.9	0.085	-26.5	83.95
6	26.5	0.308	-30.6	92.54
7	26.8	0.242	-26.9	85.3
8	35.9	0.149	-30.3	92.33
9	34.6	0.717	-31.2	93.95
10	41.6	0.562	-28.6	89.61
11	41.7	0.555	-31	93.33
12	26.5	0.346	-27.5	86.9
13	27.1	0.345	-28	86.65
14	19.2	0.492	-29.9	91.3
15	26.3	0.347	-27.7	86.6
16	26.2	0.348	-27.3	86.52
17	33.2	0.421	-24.1	76.49

18	26.3	0.347	-27.2	86.43
----	------	-------	-------	-------

Table 11: The F-value, p-value and coefficient of regression (R^2) optimized nanoformulation of Syringic acid (NF1) optimized formulation.

Responses	Model	P-value	Adjusted R^2	Predicted R^2	F- value
Size	Quadratic	<0.0001	0.9935	0.9910	338.29
PDI	Quadratic	0.0296	1.0000	0.9998	5.07
ZP	Linear	<0.0001	0.8545	0.7598	34.27
Drug loading	Quadratic	0.0009	0.9795	0.8496	16.17

Design-Expert® Software
Factor Coding: Actual

(A)

Size (nm)

● Design points above predicted value

○ Design points below predicted value

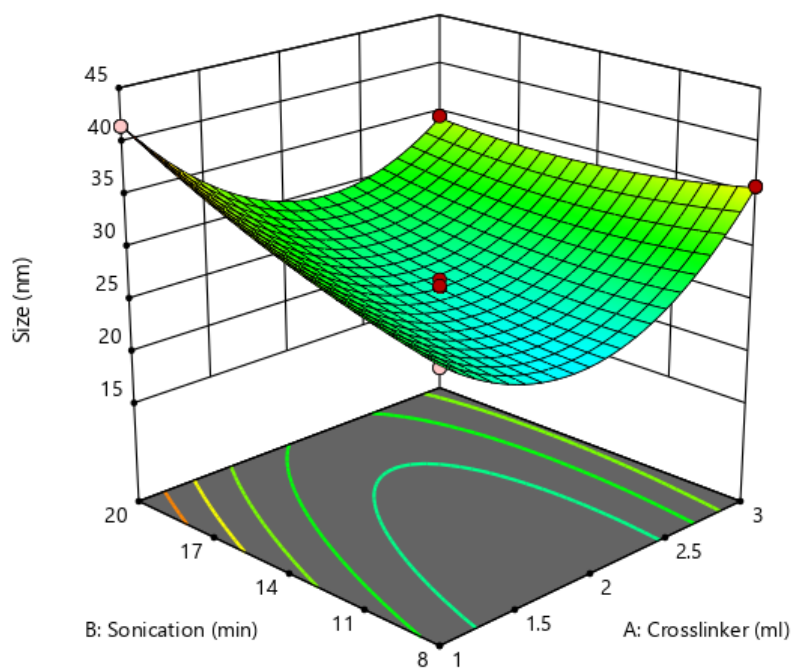
19.2 41.7

X1 = A: Crosslinker

X2 = B: Sonication

Actual Factor

C: Emulsifier = 3.5



Design-Expert® Software
Factor Coding: Actual

(B)

Pdl

● Design points above predicted value

○ Design points below predicted value

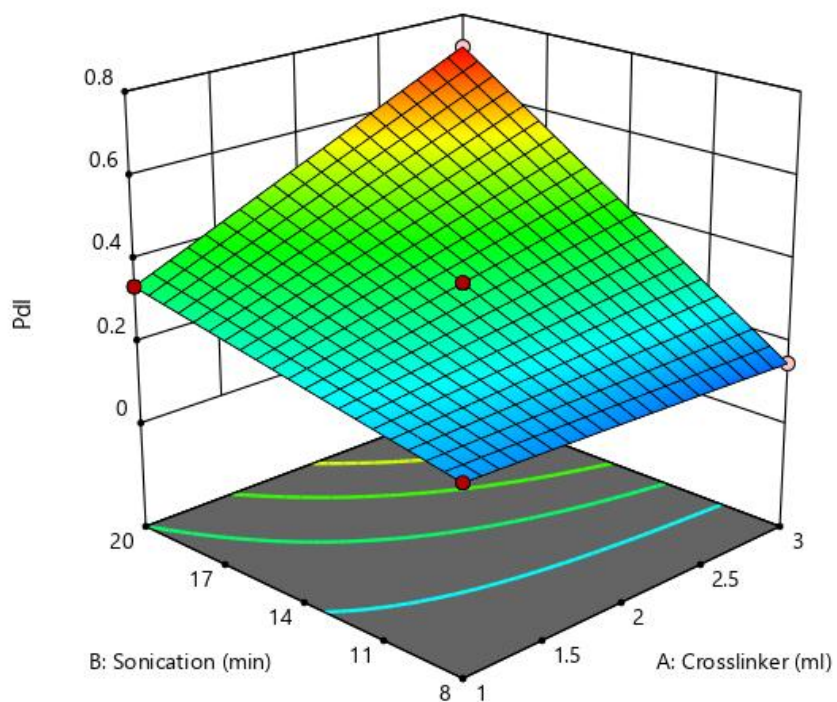
0.085 0.717

X1 = A: Crosslinker

X2 = B: Sonication

Actual Factor

C: Emulsifier = 3.5



Design-Expert® Software (C)
Factor Coding: Actual

Zeta potential (mV)

● Design points above predicted value

○ Design points below predicted value

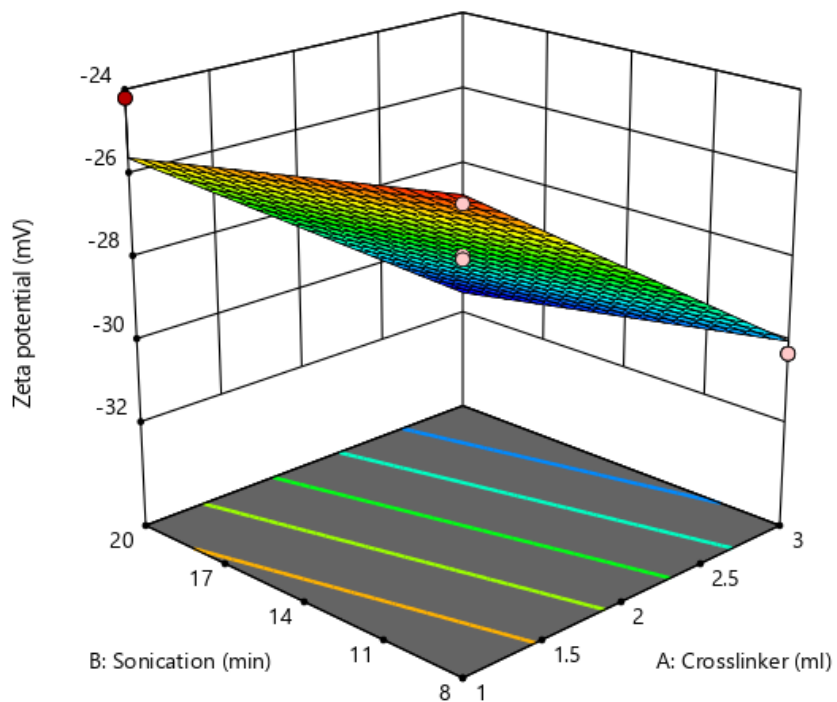
-31.2 -24.1

X1 = A: Crosslinker

X2 = B: Sonication

Actual Factor

C: Emulsifier = 3.5



Design-Expert® Software (D)
Factor Coding: Actual

Drug loading (%)

● Design points above predicted value

○ Design points below predicted value

67.69 93.95

X1 = A: Crosslinker

X2 = B: Sonication

Actual Factor

C: Emulsifier = 3.5

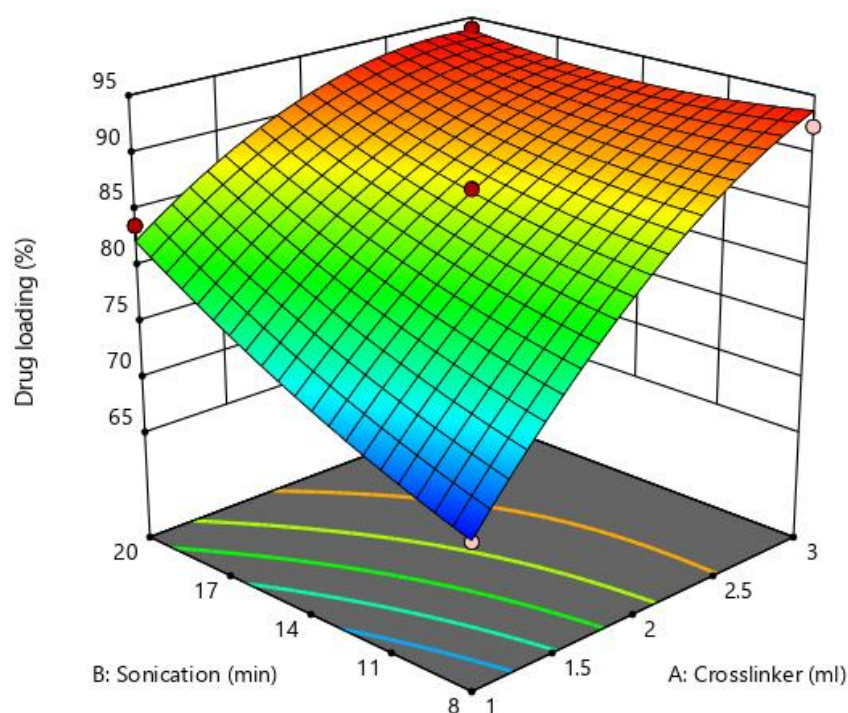


Figure 6: 3D diagrams of guar gum nanoformulation of Syringic acid (NF1): A) Particle size, B) PDI, C) Zeta Potential, D) drug loading

6.3 Optimization of guar gum nanoformulation of Sinapic acid (NF2)

All the 18 experiments given by BBD were formulated accordingly and characterised individually for their size, PDI, ZP and drug loading for studying the effects of the cross-linker, sonication time and emulsifier percentage on their size, PDI, ZP and drug loading. The size, PDI, ZP and drug loading ranges was found to be 19.2 nm (run 14) - 40.5 nm (run 2), 0.092 (run 1) – 0.34 (run 15), -23.2 mV (run 1) - -31mV (run 11) and 77.69 % (run 4) -96.9 % (run 9) respectively (Table 12) (Figure 7). Different statistical tools such as F-value, r-square, model summary, p-value, lack of fit test and sequential model sum of squares were applied for DoE to identify the design space and formulation optimisation. ANOVA was applied to understand the significance level (Harish et al., 2023).

Table 12: Size, PDI, Zeta Potential, and Drug loading efficacy results of optimized nanoformulation of Sinapic acid (NF2) of BBD design

Run	Response 1	Response 2	Response 3	Response 4
	Size (nm)	PDI	Zeta potential (mV)	Drug loading (%)
1	36.9	0.092	-23.2	78.49
2	40.5	0.11	-24.2	84.2
3	25.1	0.309	-27.3	88.01
4	29.7	0.12	-25.3	77.69
5	23.9	0.095	-26	83.9
6	26.5	0.3	-30.6	92.54
7	26.8	0.25	-26.9	85.3
8	35.9	0.151	-30.1	92.33
9	34.6	0.276	-29.2	96.9
10	39.1	0.253	-28.6	89.61
11	38	0.2	-31	93.33
12	26.5	0.309	-27.5	88.9
13	27.1	0.313	-28	88.65
14	19.2	0.271	-28.9	91.3
15	26.3	0.34	-27.7	86.6
16	26.2	0.309	-27.3	86.52
17	33.2	0.17	-24.1	83.49
18	26.3	0.32	-27.2	86.43

The F-value, p-value, and coefficient of regression (R^2) indicate the quadratic model for size, PDI, and drug loading (%), whereas the model is linear for ZP (Table 13). The analysis of the terms of multiple regression revealed that the model has predicted values. Adequate precision measurement gave the ratio of signal to noise as four, which is desirable. Therefore, based on the above values, the model can navigate the design space. BBD also determines the mathematical equations for each response in terms of coded equations. These coded polynomial

equations have positive and negative signs indicating synergistic and antagonistic effects, respectively. The equations are as follows:

$$\text{Size} = +26.25 - 0.6625A + 2.1375B - 4.025C - 3.025AB - 1.95AC - 5.7BC + 7.6625A^2 + 1.2625B^2 - 0.2625C^2$$

$$\text{Pdl} = +0.317 + 0.054A + 0.037B + 0.0439C + 0.03375AB + 0.0055AC - 0.03425BC - 0.0895A^2 - 0.0628B^2 - 0.03658C^2$$

$$\text{Zeta potential} = -27.39 - 3.0125A - 0.325B - 0.2125C$$

$$\text{Drug loading} = +87.45 + 6.41A + 2.855B + 0.9125C$$

Table 13: The F-value, p-value and coefficient of regression (R²) optimized nanoformulation of Sinapic acid (NF2) optimized formulation

Responses	Model	P-value	Adjusted R ²	Predicted R ²	F- value
Size	Quadratic	<0.0001	0.9754	0.8637	100.09
PDI	Quadratic	0.0296	0.9759	0.9023	125.34
ZP	Linear	<0.0001	0.8612	0.7691	36.17
Drug loading	Linear	0.0009	0.9451	0.9210	98.64

Design-Expert® Software
Factor Coding: Actual

(A)

Size (nm)

● Design points above predicted value

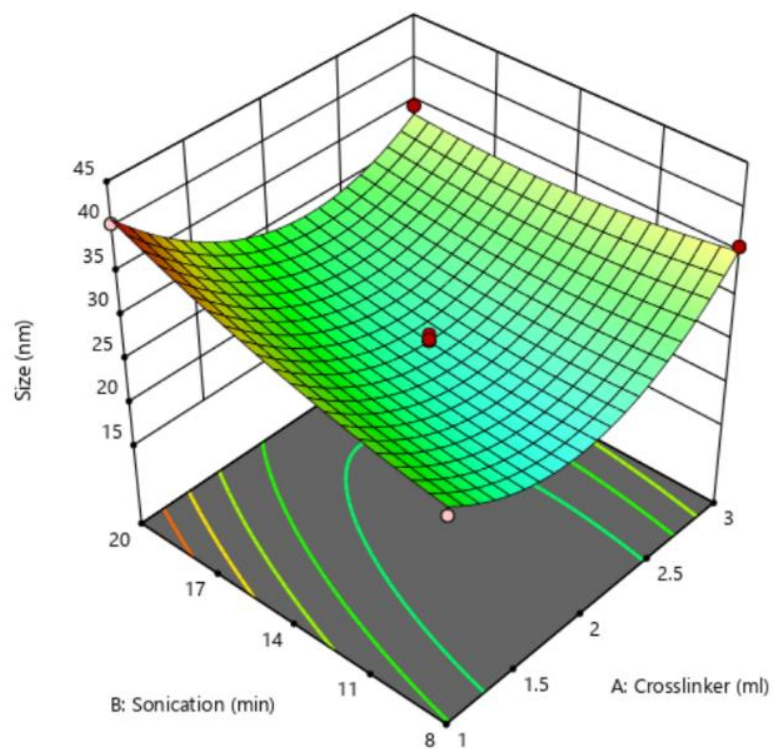
○ Design points below predicted value

19.2 40.5

X1 = A: Crosslinker
X2 = B: Sonication

Actual Factor

C: Emulsifier = 3.5



Design-Expert® Software
Factor Coding: Actual

(B)

PdI

● Design points above predicted value

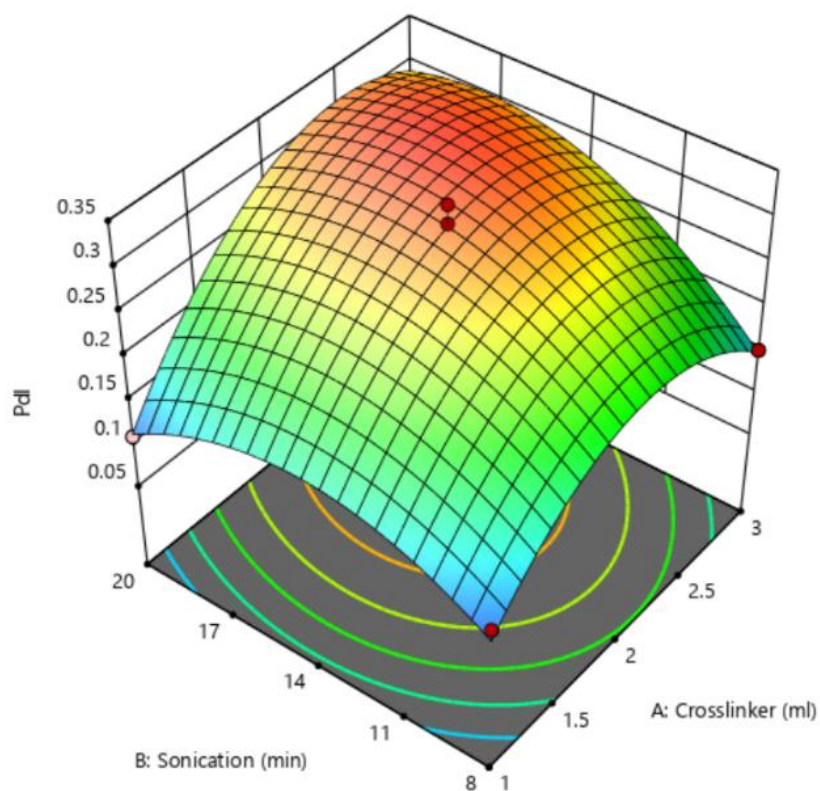
○ Design points below predicted value

0.092 0.34

X1 = A: Crosslinker
X2 = B: Sonication

Actual Factor

C: Emulsifier = 3.5



Design-Expert® Software
Factor Coding: Actual

(C)

Zeta potential (mV)

● Design points above predicted value

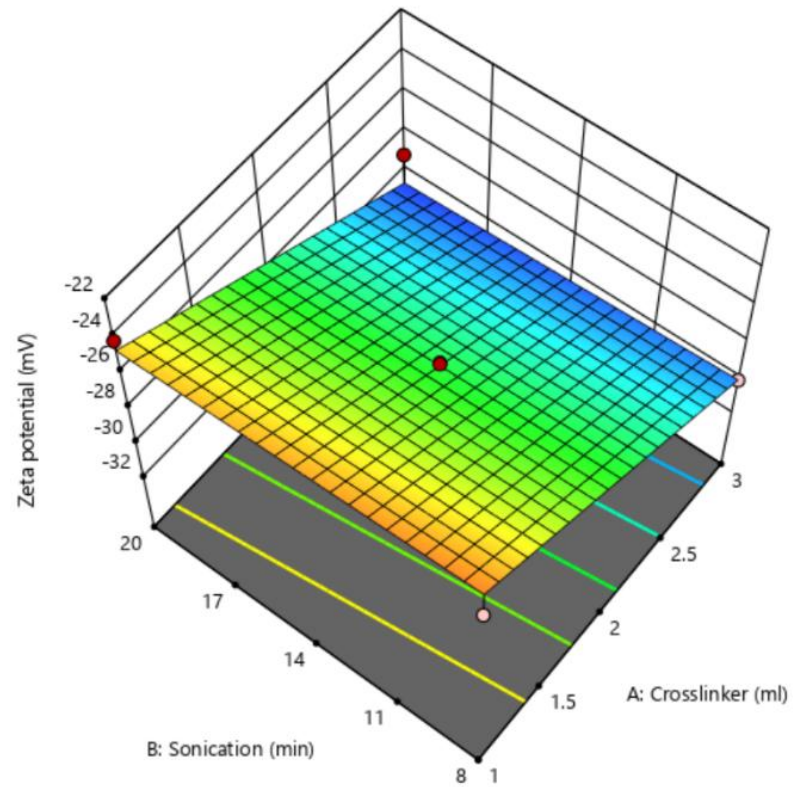
○ Design points below predicted value

-31  -23.2

X1 = A: Crosslinker
X2 = B: Sonication

Actual Factor

C: Emulsifier = 3.5



Design-Expert® Software
Factor Coding: Actual

(D)

Drug loading (%)

● Design points above predicted value

○ Design points below predicted value

77.69  96.95

X1 = A: Crosslinker
X2 = B: Sonication

Actual Factor

C: Emulsifier = 3.5

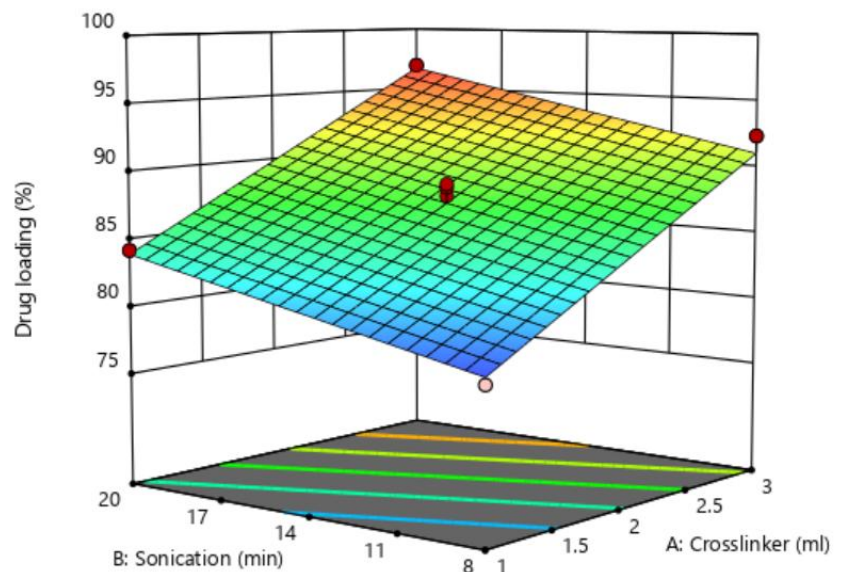


Figure 7: 3D diagrams of guar gum nanoformulation of Sinapic acid (NF2): A)Particle size, B)PDI, C)Zeta Potential values, D)drug loading

6.4 Optimization of guar gum nanoformulation of o-Coumaric acid (NF3)

All the 18 experiments given by BBD were formulated accordingly and characterised individually for their size, PDI, ZP and drug loading for studying the effects of the cross-linker, sonication time and emulsifier percentage on their size, PDI, ZP and drug loading. The size, PDI, ZP and drug loading ranges was found to be 24.2 nm (run 14) - 43.9 nm (run 2), 0.099 (run 5) – 0.32 (run 18), -21.8 mV (run 1) - -31mV (run 18) and 77.6 % (run 4) -97.91 % (run 9) respectively (Table 14) (Figure 8). Different statistical tools such as F-value, r-square, model summary, p-value, lack of fit test and sequential model sum of squares were applied for DoE to identify the design space and formulation optimisation. ANOVA was applied to understand the significance level (Harish et al., 2023).

Table 14: Size, PDI, Zeta Potential and Drug loading efficacy results of optimized nanoformulation of o-Coumaric acid (NF3) of BBD design

Run	Response 1	Response 2	Response 3	Response 4
	Size (nm)	PDI	Zeta potential (mV)	Drug loading (%)
1	39.8	0.102	-21.8	80.9
2	43.9	0.16	-28.2	86.7
3	32.1	0.29	-27.3	88.01
4	30.3	0.17	-25.3	77.6
5	24.3	0.099	-26	86.51
6	37.1	0.224	-30.1	92.54
7	37.1	0.118	-26.1	85.3
8	34.4	0.178	-25.7	92.33
9	34.8	0.212	-30.1	97.91
10	40.4	0.117	-28.6	91.45
11	37.8	0.21	-31	94.21
12	31.9	0.284	-27.1	88.9
13	35.8	0.28	-27.8	88.65

14	24.2	0.2	-28.2	91.3
15	33.7	0.281	-27.7	92.6
16	32.2	0.285	-28.3	86.52
17	36.9	0.229	-29.1	83.49
18	42.3	0.32	-31.2	90.55

The F-value, p-value, and coefficient of regression (R^2) indicate the quadratic model for size, PDI, and drug loading (%), whereas the model is linear for ZP (Table 15). The analysis of the terms of multiple regression revealed that the model has predicted values. Adequate precision measurement gave the ratio of signal to noise as four, which is desirable. Therefore, based on the above values, the model can navigate the design space. BBD also determines the mathematical equations for each response in terms of coded equations. These coded polynomial equations have positive and negative signs, indicating synergistic and antagonistic effects, respectively. The equations are as follows: A, B and C are crosslinkers, sonication time and emulsifier (%), respectively.

$$\text{Size} = +34.67 - 0.85A + 2.15B - 0.875C - 3.3AB + 0.55AC - 7.25BC + 3.791A^2 - 2.608B^2 - 0.558C^2$$

$$\text{PDI} = +0.29 + 0.020375A + 0.0155B + 0.030375C + 0.011AB - 0.02825AC + 0.016BC - 0.026125A^2 - 0.083875B^2 - 0.072625C^2$$

$$\text{Zeta potential} = -27.76 - 1.5625A - 1.5B - 0.7625C$$

$$\text{Drug loading} = +89.205 + 8.17A + 2.46B - 0.18C + 0.635AB - 0.814AC + 0.265BC - 2.83A^2 + 0.775B^2 - 1.34C^2$$

Table 15 The F-value, p-value and coefficient of regression (r^2) optimized nanoformulation of o-Coumaric acid (NF3) optimized formulation

Responses	Model	P-value	Adjusted R^2	Predicted R^2	F- value
Size	Quadratic	0.0004	0.9188	0.4812	100.09
PDI	Quadratic	0.0296	0.9759	0.9023	125.34
ZP	Linear	<0.0001	0.8612	0.7691	36.17
Drug loading	Linear	0.0009	0.9451	0.9210	98.64

Design-Expert® Software
Factor Coding: Actual

(A)

Size (nm)

● Design points above predicted value

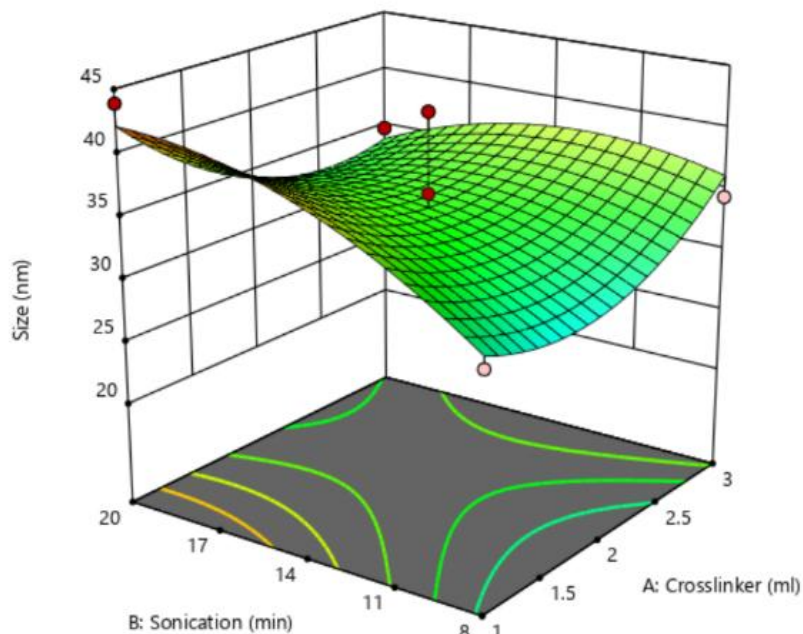
○ Design points below predicted value

24.2 43.9

X1 = A: Crosslinker
X2 = B: Sonication

Actual Factor

C: Emulsifier = 3.5



Design-Expert® Software
Factor Coding: Actual

(B)

PdI

● Design points above predicted value

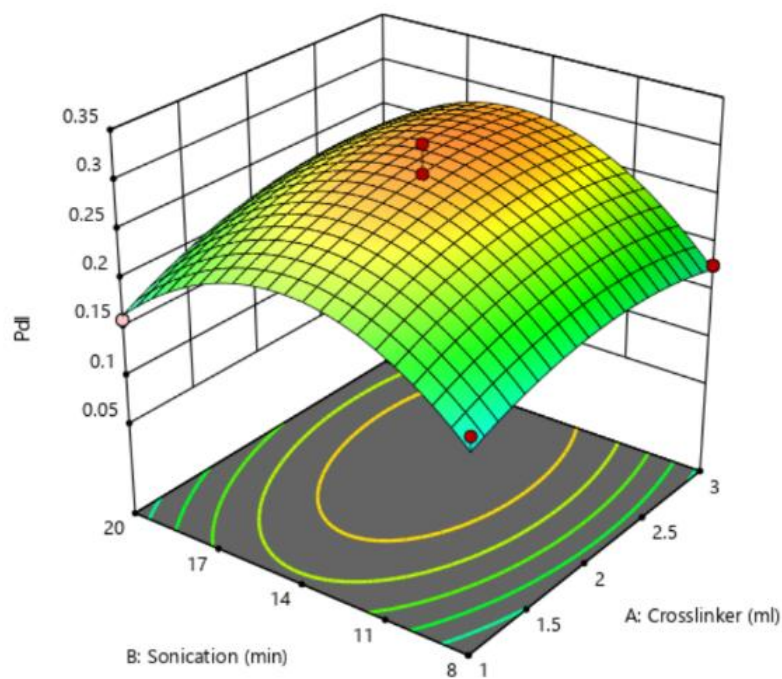
○ Design points below predicted value

0.099 0.32

X1 = A: Crosslinker
X2 = B: Sonication

Actual Factor

C: Emulsifier = 3.5



Design-Expert® Software
Factor Coding: Actual

(C)

Zeta potential (mV)

● Design points above predicted value

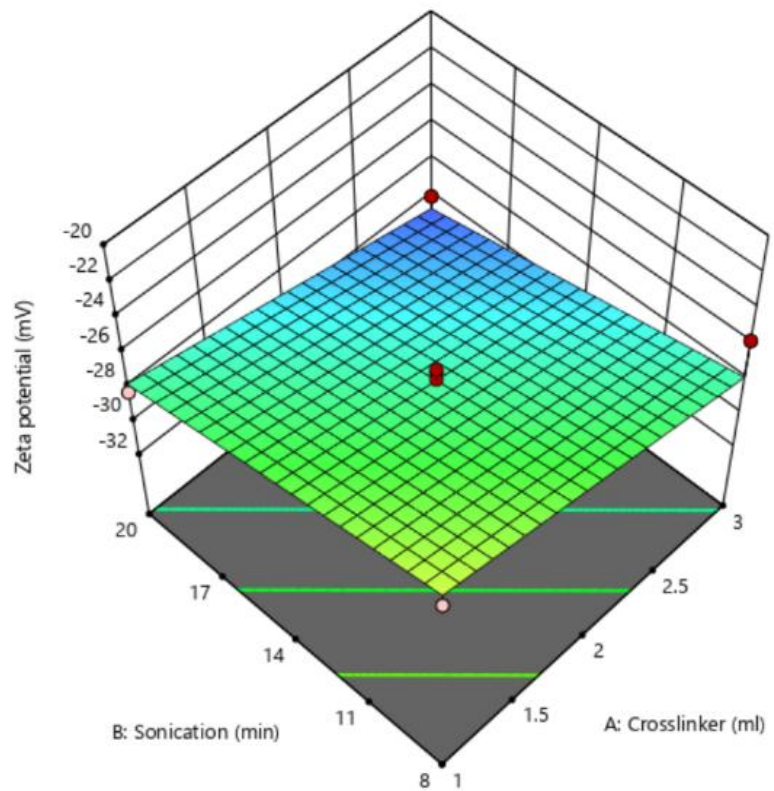
○ Design points below predicted value

-31.2  -21.8

X1 = A: Crosslinker
X2 = B: Sonication

Actual Factor

C: Emulsifier = 3.5



Design-Expert® Software
Factor Coding: Actual

(D)

Drug loading (%)

● Design points above predicted value

○ Design points below predicted value

77.6  97.97

X1 = A: Crosslinker
X2 = B: Sonication

Actual Factor

C: Emulsifier = 3.5

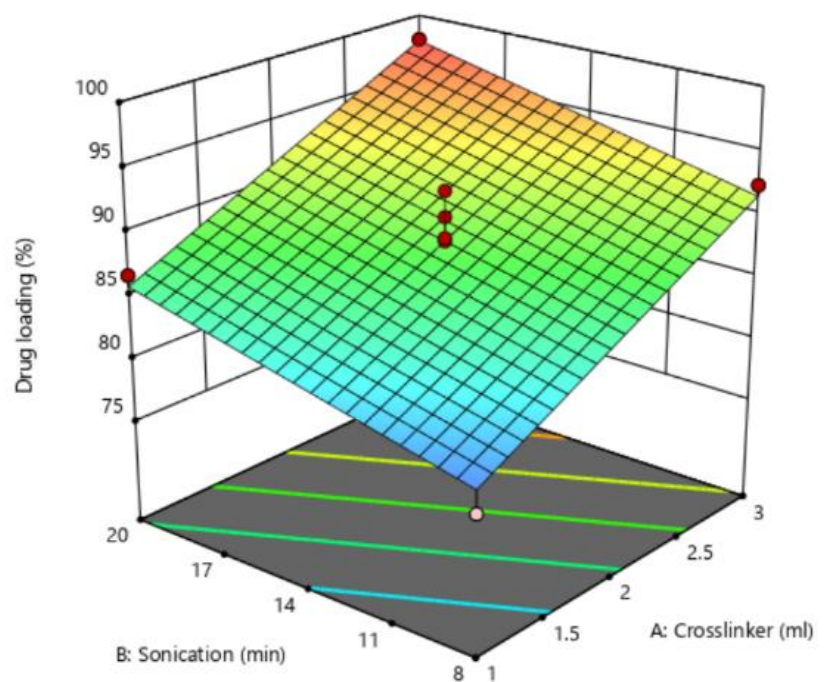


Figure 8: 3D diagrams of guar gum nanoformulation of o-Coumaric acid (NF3): A) Particle size, B) Pdl, C) Zeta Potential values, D) drug loading

6.5 Characterization of Zeta sizer and SEM of guar gum nanoformulation of Syringic acid (NF1), guar gum nanoformulation of Sinapic acid (NF2), guar gum nanoformulation of o-Coumaric acid (NF3)

Figure 9A and 1B display the particle size distribution and zeta potential values of the different nano-formulations (guar gum nanoformulation of Syringic acid (NF1), guar gum nanoformulation of Sinapic acid (NF2), guar gum nanoformulation of o-Coumaric acid (NF3)). The nanoformulations exhibit particle sizes within the 25 to 30 nm range, as shown in Figure 9A. The zeta potential values ranged from -16 to -24 mV, as shown in Figure 9B. Analysis using Field Emission Scanning Electron Microscopy (FESEM) provided valuable information about the physical characteristics of the nanoparticles, indicating that they possess a spherical form at the nanoscale. The particle size distribution analysis was carried out using the ImageJ software. The mean particle size was determined to be 25 nm, 28 nm, and 30 nm for guar gum nanoformulation of Syringic acid (NF1), guar gum nanoformulation of Sinapic acid (NF2), and guar gum nanoformulation of o-Coumaric acid (NF3), respectively (Figure 9C).

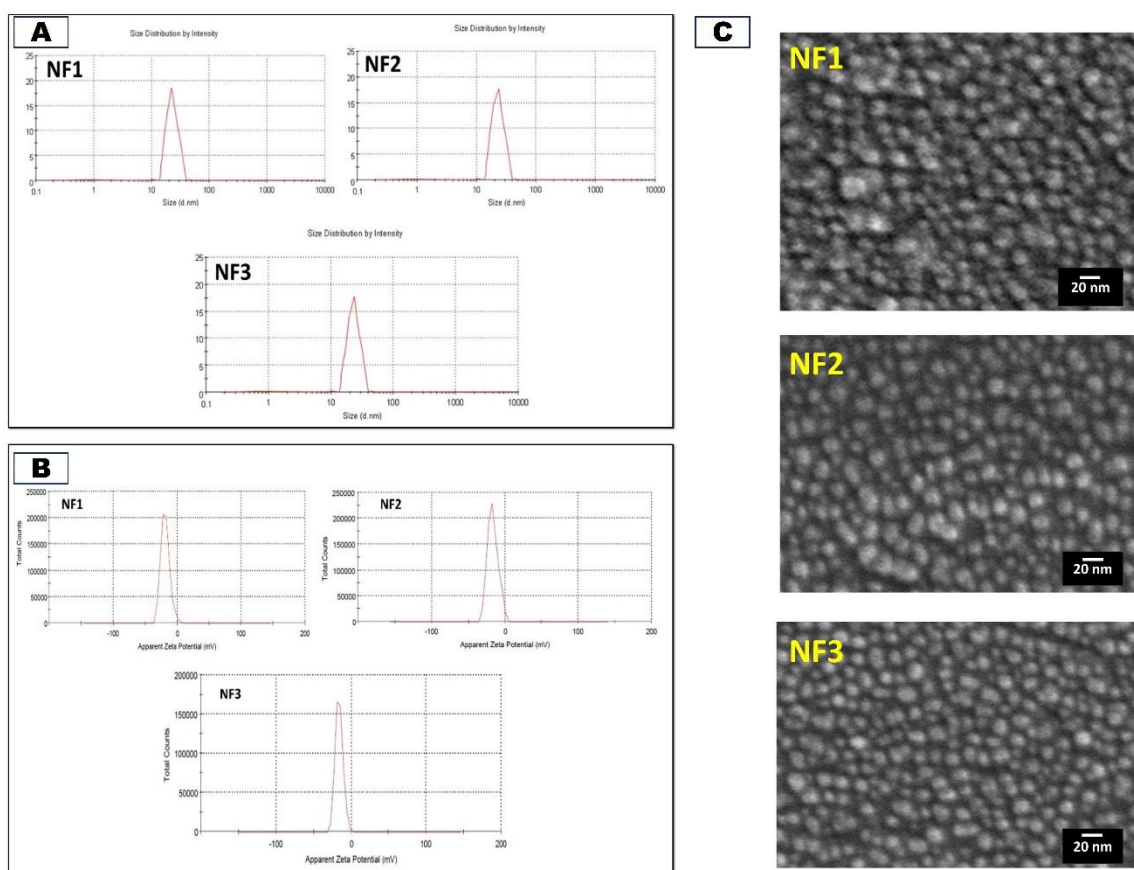


Figure 9: A) Particle size analysis of nanoformulations (measured in nanometers) (Malvern et al.S90). B)Zeta potential measurement of nanoformulations (mV) using Zetasizer (Malvern et al.S 90), C)FESEM of nanoformulations (20nm scale bar, x75,000 magnification) (JEOL-6610). [NF1-guar gum nanoformulation of Syringic acid, NF2-guar gum nanoformulation of Sinapic acid, NF3-guar gum nanoformulation of o-Coumaric acid]

6.6 DSC Analysis and Interpretation

The Differential Scanning Calorimetry (DSC) analysis of NFs provides insight into these materials' thermal properties and stability.

➤ Placebo (Guar gum nanoformulation/GGNP)

The pristine GG and GGNP DSC profile showed that the guar gum has an onset temperature of 29.2°C, an endpoint temperature of 131.13°C, and a peak temperature of 79.75°C. For the guar gum nanoparticles, the onset temperature is 29.33°C, the endpoint temperature is 130.02°C, and the peak temperature is 74.94°C (Figure 10).

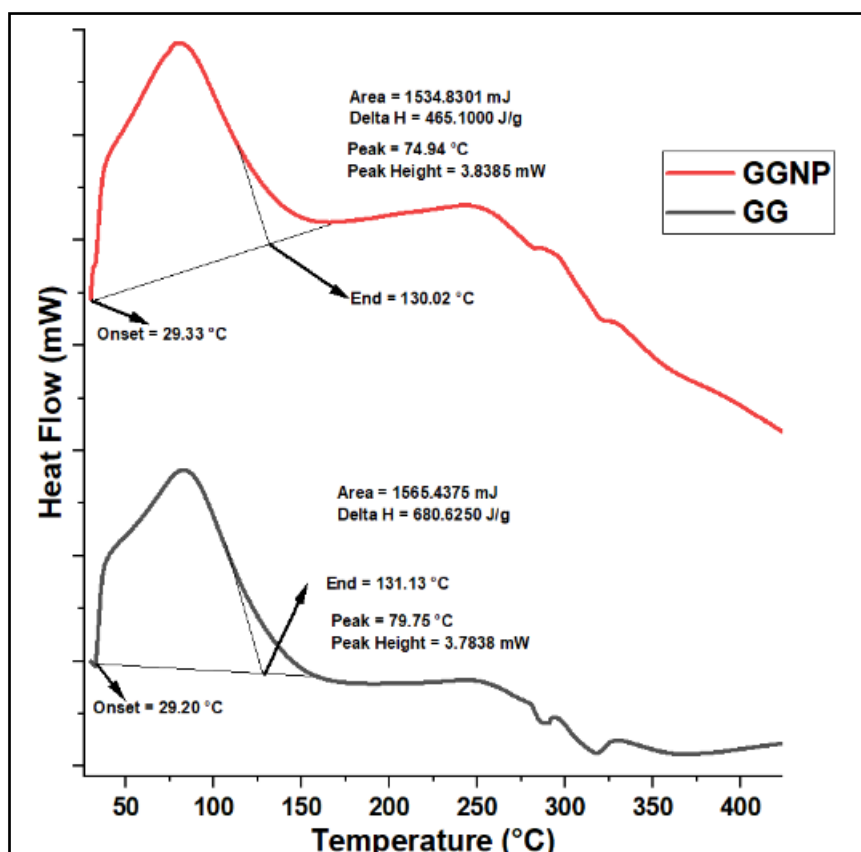


Figure 10: Comparison of Differential Scanning Calorimetry (DSC) graphs of Guar gum (GG) and Guar gum nanoformulations (GGNP)

➤ **Guar gum nanoformulation of Syringic acid (NF1)**

First peak (Onset = 28.42 °C, End = 118.38 °C, Peak = 70.46 °C, Peak Height = 3.8652 mW, Area = 1452.1788 mJ, Delta H = 468.4448 J/g)-The first peak represents a significant endothermic event, likely associated with the loss of moisture or the melting of lower molecular weight components in the nanoformulation. The broad temperature range and substantial area suggest a complex melting process or multiple overlapping transitions (Figure 11).

Second peak: (Onset = 204.95 °C, End = 209.24 °C, Peak = 207.75 °C, Peak Height = 5.5820 mW, Area = 117.9328 mJ, Delta H = 38.0428 J/g)-The second peak is narrower. It occurs at a higher temperature, indicating the melting of the main component in the nanoformulation or a crystallisation event. The lower area and enthalpy than the first peak suggest that this transition involves a smaller quantity of material or less energy-intensive processes.

➤ **SRN**

First peak: (Area = 554.4491 mJ, Delta H = 178.8546 J/g, Peak = 210.13 °C, Peak Height = 35.4810 mW, Onset = 207.77 °C, End = 211.65 °C)-This peak represents the melting point of Syringic acid, occurring within a narrow temperature range, indicative of a well-defined and pure compound. The high peak height and significant area reflect a substantial and sharp endothermic transition, typical of the melting of a crystalline substance (Figure 10B).

Second peak: (Onset = 263.07 °C, End = 279.91 °C, Area = 499.0833 mJ, Delta H = 160.9946 J/g, Peak = 275.70 °C, Peak Height = 5.7210 mW)- The second peak may correspond to the decomposition of Syringic acid or the melting of a higher molecular weight fraction. The broader range and lower peak height indicate a less defined transition than the first peak.

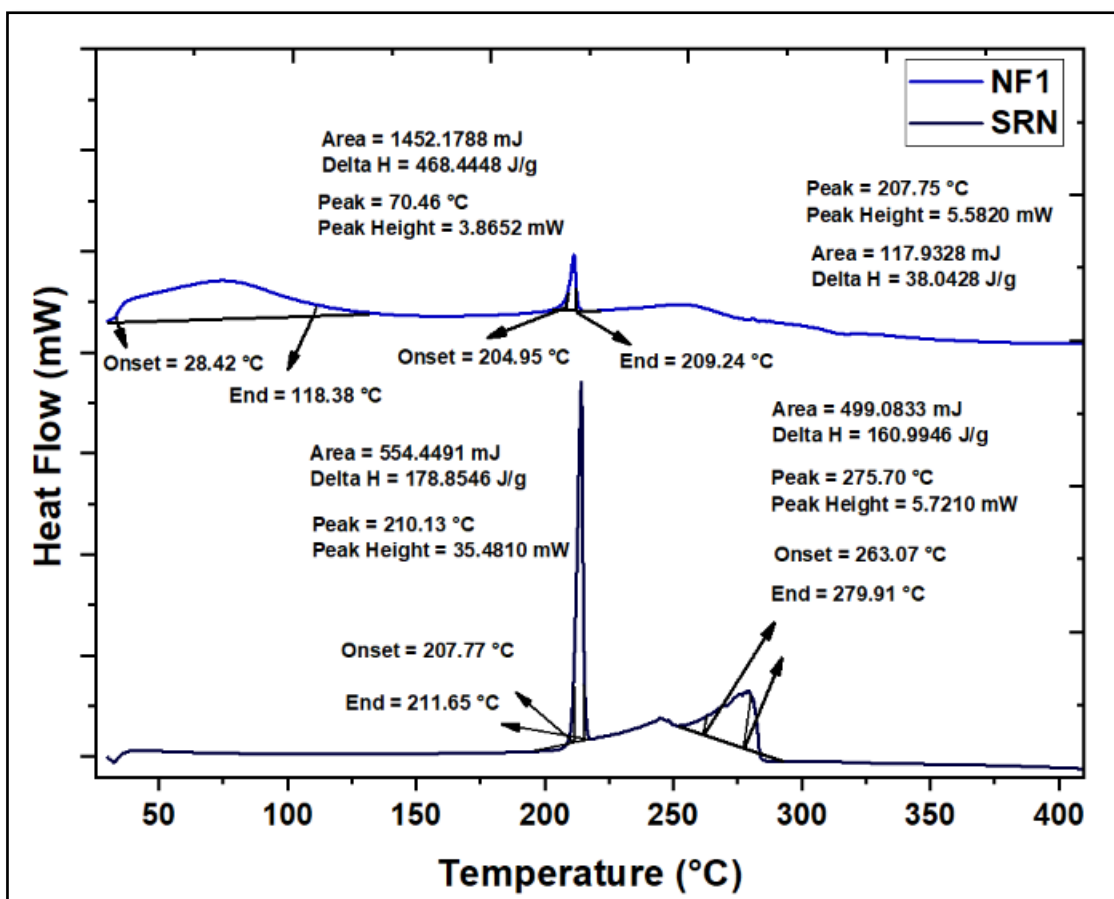


Figure 11: Comparison of Differential Scanning Calorimetry (DSC) graphs of Syringic acid (SRN) and optimized nanoformulation of Syringic acid (NF1)

➤ **Guar gum nanoformulation of Sinapic acid (NF2)**

First peak: (Onset = 32.25 °C, End = 98.95 °C, Peak = 71.61 °C, Peak Height = 3.1872 mW, Area = 1012.1198 mJ, Delta H = 438.7848 J/g)-This first peak represents the loss of bound water or a phase transition, possibly the melting of the polymer matrix in the nanoformulation. The lower peak height and ΔH suggest that the energy required for this transition is relatively modest, indicating a more stable thermal behaviour of the nanoformulation at this stage (Figure 12).

Second peak: (Peak = 205.44 °C, Peak Height = 7.2401 mW, Area = 121.1808 mJ, Delta H = 39.1289 J/g, Onset = 200.48 °C, End = 208.19 °C)-The second peak indicates a significant thermal event, likely related to the degradation or further phase transition within the nanoformulation. The higher peak height than the first peak suggests a more intense thermal process, which could correspond to the breakdown of the nanoformulation or the interaction between the encapsulated drug and the polymer matrix.

- **SNP:** (Onset = 220.54 °C, End = 254.51 °C, Peak = 222.84 °C, Peak Height = 37.6022 mW, Area = 576.5900 mJ, Delta H = 144.1475 J/g)-The single peak for SNP at a higher temperature compared to optimized nanoformulation of Sinapic acid (NF2) indicates the melting point of pure Sinapic acid, reflecting its crystalline nature. The high peak height and ΔH values demonstrate the substantial energy required for this transition, emphasising the thermal stability of SNP at elevated temperatures (Figure 10C).

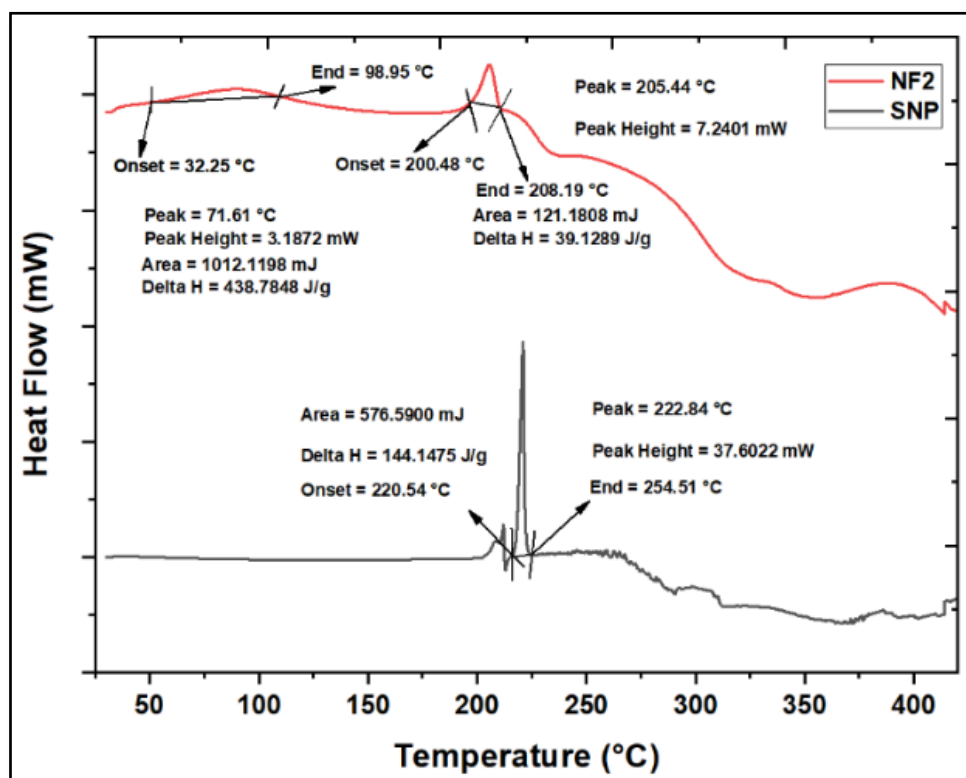


Figure 12: Comparison of Differential Scanning Calorimetry (DSC) graphs of Sinapic acid (SNP) and optimized nanoformulation of Sinapic acid (NF2)

- **Optimized nanoformulation of o-Coumaric acid (NF3)**

First Peak: (Onset: 218.02 °C, End: 227.85 °C, Peak: 214.11 °C, Peak Height: 54.1785 mW, Area: 2142.3119 mJ, ΔH : 361.8022 J/g)-The first peak indicates an endothermic process, possibly corresponding to the melting of a component within the nanoformulation or a phase transition. The significant enthalpy change (ΔH) suggests a notable energy absorption during this transition, indicating the presence of a well-defined crystalline structure or other significant thermal event.

Second Peak: (Onset: 276.95 °C, End: 354.43 °C, Peak: 299.58 °C, Peak Height: -12.0485 mW, Area: -3653.2154 mJ, ΔH : -1405.0828 J/g)-The second peak is

exothermic, as indicated by the negative peak height and ΔH . This might represent a decomposition process, recrystallisation, or some form of thermal degradation, where energy is released. The broad temperature range and substantial energy release suggest significant thermal events occurring within this temperature range (Figure 13).

- **OCA:** (Single Peak: Onset: 216.52 °C, End: 222.26 °C, Peak: 219.61 °C, Peak Height: 58.9196 mW, Area: 2122.4819 mJ, ΔH : 365.9452 J/g). J/g- The DSC curve of o-Coumaric acid shows a single sharp endothermic peak, indicating a well-defined melting point at 219.61 °C. The narrow range between the onset and end temperatures suggests a pure and crystalline material with minimal thermal degradation or other transitions within this temperature range. The energy absorption is consistent with the melting of a crystalline substance (Figure 10D).

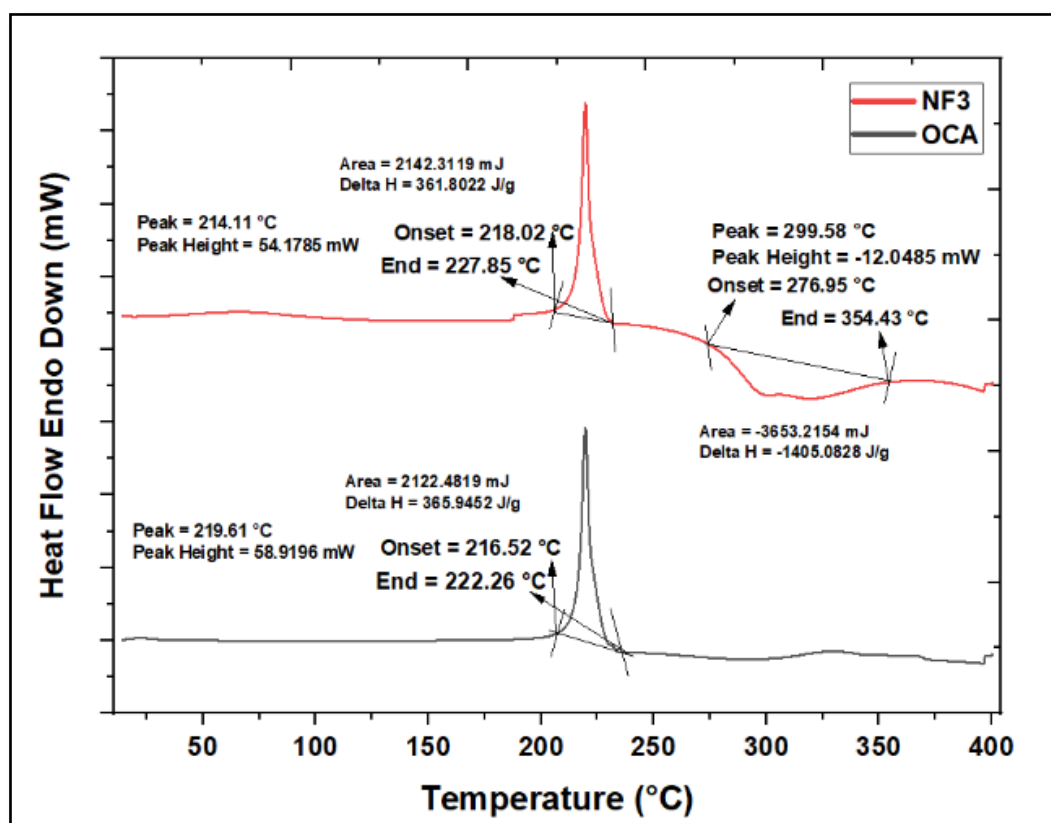


Figure 13: Comparison of Differential Scanning Calorimetry (DSC) graphs of o-Coumaric acid (OCA) and o-Coumaric acid loaded nanoformulations (guar gum nanoformulation of o-Coumaric acid (NF3))

6.7 TGA Analysis and Interpretation

The thermogravimetric analysis (TGA) results indicate the thermal stability and decomposition characteristics of Guar gum, its nanoformulation, Syringic acid, Sinapic acid, Coumaric acid and the nanoformulations guar gum nanoformulation of Syringic acid (NF1), guar gum nanoformulation of Sinapic acid (NF2), and optimized nanoformulation of o-Coumaric acid (NF3) (Figure 11).

➤ **Guar Gum:**

Onset Y (Mass): 7.109 mg, Onset X (Temperature): 307.61 °C. Guar gum's onset of decomposition occurs at 307.61 °C, indicating that it starts losing mass at this temperature. The high onset temperature suggests good thermal stability, typical for biopolymers like Guar gum.

➤ **Placebo (Guar Gum Nanoformulation):**

Onset Y (Mass): 7.005 mg, Onset X (Temperature): 310.83 °C. The Guar gum nanoformulation shows a higher onset temperature of 304.83 °C than pure Guar gum. This increase could indicate that the nanoformulation process increases the material's thermal stability, potentially due to changes in its physical structure or interactions with other components in the formulation.

➤ **Syringic Acid:**

Onset Y (Mass): 2.381 mg, Onset X (Temperature): 260.86 °C. Syringic acid's lower onset temperature of 260.86 °C means it is less thermally stable than gum. This lower thermal stability is expected for small organic molecules like Syringic acid, which decompose at lower temperatures than larger polymeric structures.

➤ **Guar gum nanoformulation of Syringic acid (NF1):**

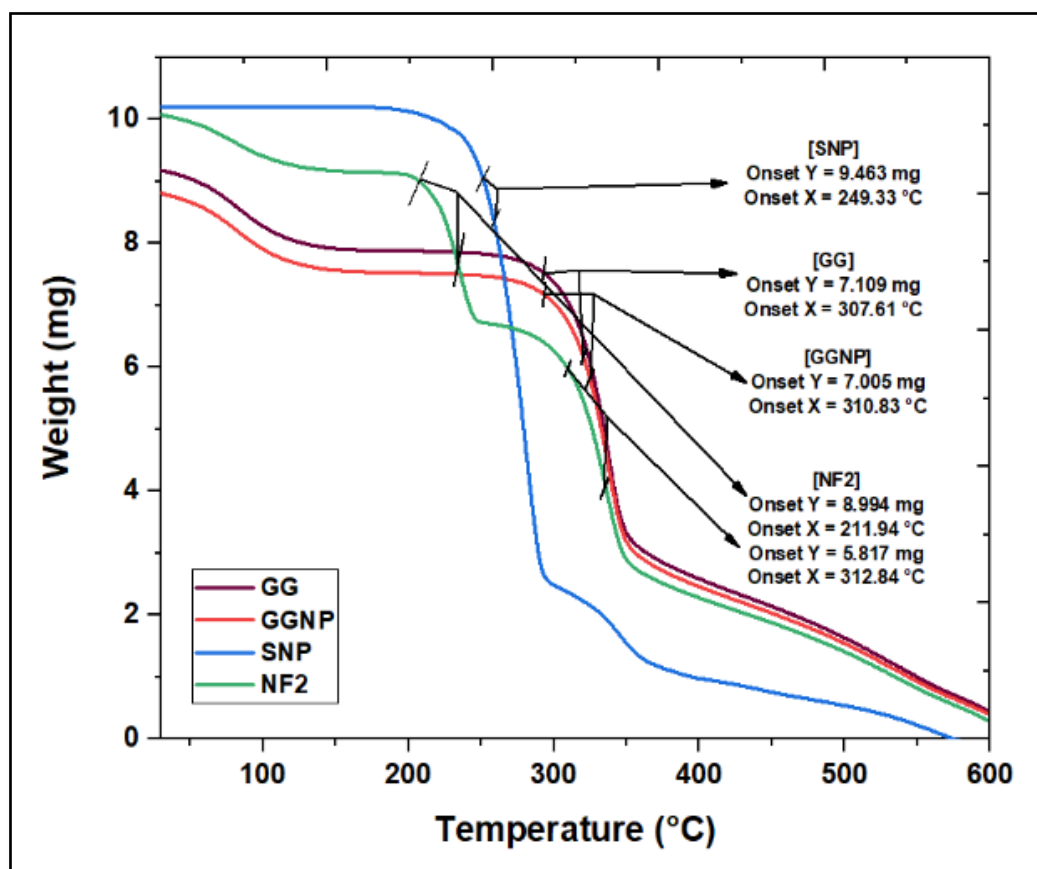
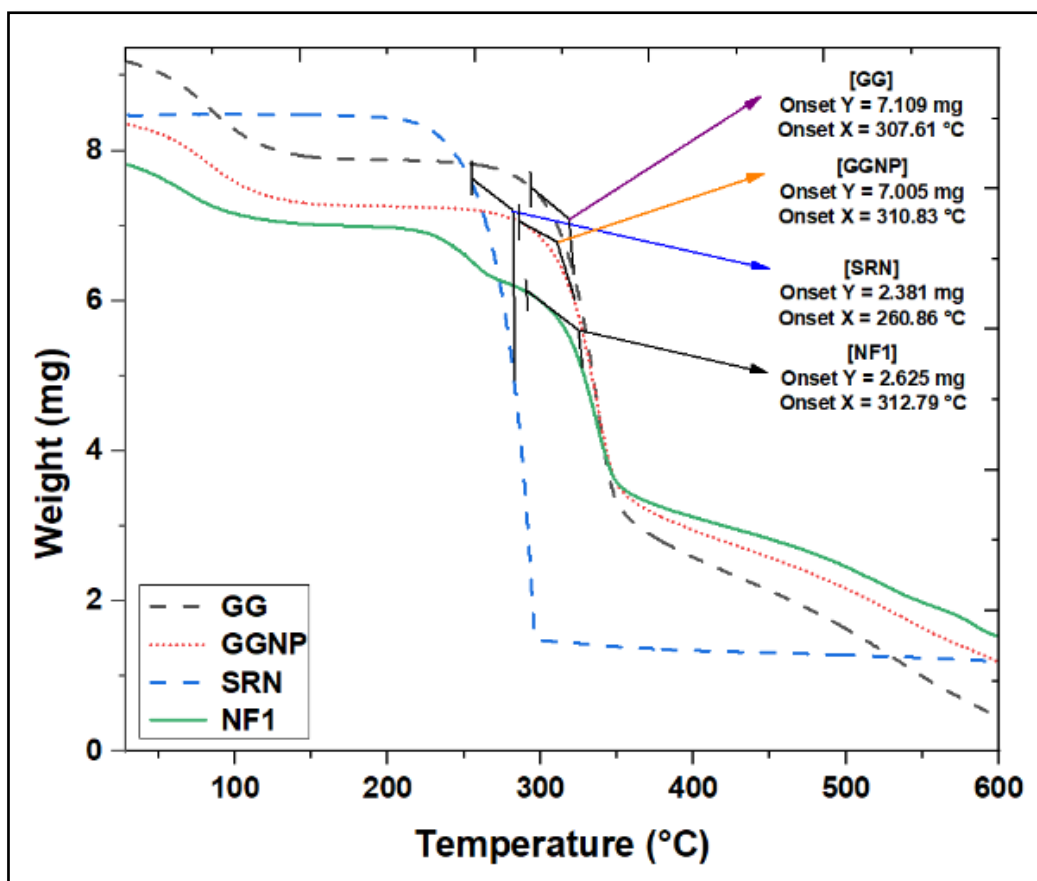
Onset Y (Mass): 2.625 mg, Onset X (Temperature): 312.79 °C. The onset temperature of the optimized nanoformulation of Syringic acid (NF1) is significantly higher at 306.79 °C compared to pure Syringic acid. This suggests that the nanoformulation enhances the thermal stability of Syringic acid, likely due to encapsulation within the Guar gum matrix, which protects it from thermal degradation at lower temperatures.

➤ **Sinapic Acid:**

- Onset Y = 9.463 mg, Onset X = 249.33 °C: Sinapic acid has a significantly lower onset temperature of 249.33 °C, indicating it begins to degrade at a lower temperature than guar gum. The higher initial weight (9.463 mg) suggests the

sample had more mass, but the earlier onset temperature highlights its lower thermal stability.

- **First Peak:** Onset Y = 8.994 mg, Onset X = 211.94 °C: The first peak in the optimized nanoformulation of Sinapic acid (NF2) nanoformulation shows an onset of degradation at 211.94 °C, with a mass of 8.994 mg. This lower onset temperature indicates that the initial component or phase of the formulation begins to degrade earlier than the pure Sinapic acid. **Second Peak:** Onset Y = 5.817 mg, Onset X = 312.84 °C: The second degradation peak occurs at a much higher temperature of 308.84 °C, with a reduced weight of 5.817 mg. This suggests a secondary component in the nanoformulation, possibly the guar gum matrix, which has a higher thermal stability than the pure guar gum or guar gum nanoformulation.
- **O-Coumaric Acid:** Onset X = 242.47 °C: O-Coumaric acid begins to degrade at a much lower temperature of 242.47 °C. This indicates that o-Coumaric acid has lower thermal stability than Guar gum and its nanoformulation. The earlier degradation onset may reflect the inherent chemical structure of o-Coumaric acid, which is more prone to thermal decomposition.
- **First peak** - Onset X = 224.81 °C: The first peak in guar gum nanoformulation of o-Coumaric acid (NF3), with an onset at 224.81 °C, likely corresponds to the initial degradation phase, possibly of the o-Coumaric acid component or other less stable components in the formulation. **Second peak** - Onset X = 314.45 °C: The second peak at 314.45 °C corresponds to a higher thermal stability phase, which may be due to the more stable components such as Guar gum. This higher onset temperature suggests that the nanoformulation effectively enhances the thermal stability of the active compound (o-Coumaric acid), likely through protective interactions within the nano matrix.



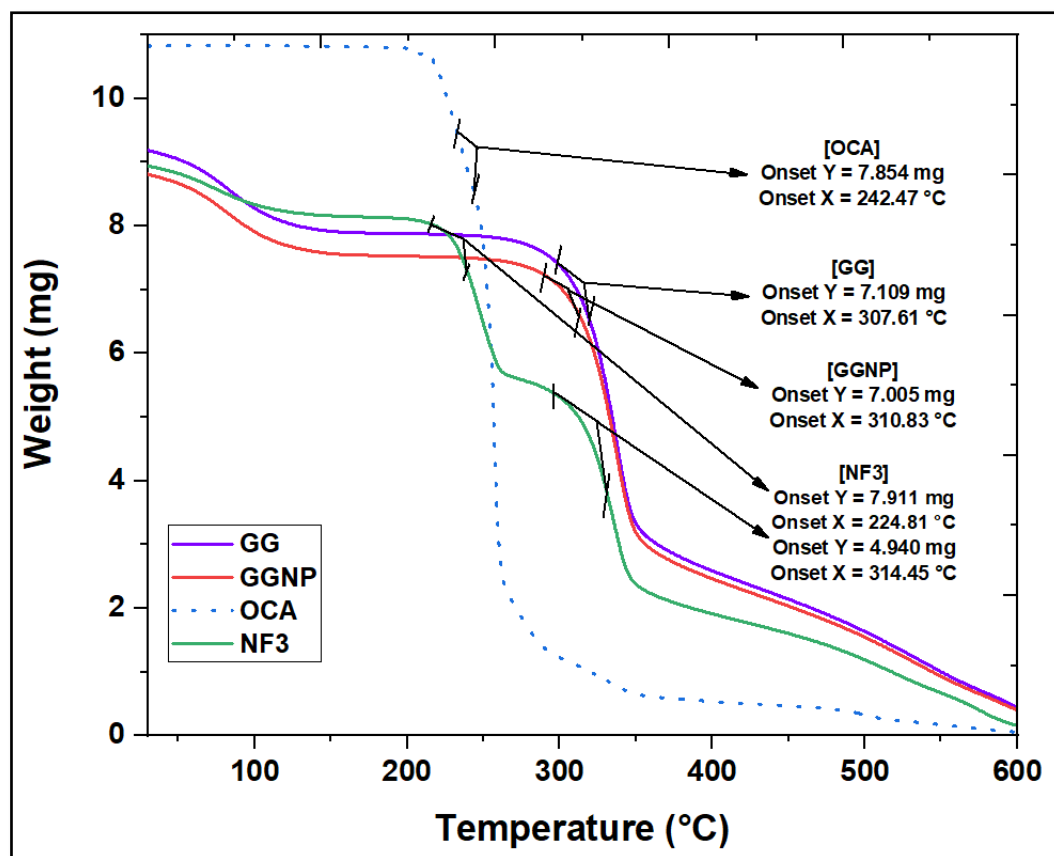


Figure 14: Comparison of Thermogravimetric analysis (TGA) graphs of different formulations

(GG- Guar gum; GGNP-Guar gum nanoformulation; SRN-Syringic acid; SNP-Sinapic acid; OCA-o-Coumaric acid; NF1-optimized nanoformulation of Syringic acid (NF1), NF2-optimized nanoformulation of Sinapic acid, NF3-optimized nanoformulation of o-Coumaric acid (NF3))

6.8 FTIR Analysis and Interpretation

The FTIR spectra provide insights into the chemical structure and interactions within the various samples, including Guar gum (GG), Guar gum nanoparticles (GGNP), Syringic acid (SRN), Sinapic acid (SNP), o-Coumaric acid (OCA) and the nanoformulations (guar gum nanoformulation of Syringic acid (NF1), guar gum nanoformulation of Sinapic acid (NF2), NF3). Below is the analysis based on the provided peak values.

- **Guar Gum (GG) Peaks:** 3290.40, 1637.23, 1375.67, 1016.61, 808.52 (Figure 15)
 - 3290.40 cm^{-1} : This peak corresponds to the O-H stretching vibration, typical of hydroxyl groups in polysaccharides.

- 1637.23 cm^{-1} : Likely associated with the C=O stretching or bending vibrations, indicative of carboxyl or amide groups.
- 1375.67 cm^{-1} : Corresponds to C-H bending, common in alkanes.
- 1016.61 cm^{-1} : Characteristic of C-O-C stretching in polysaccharides.
- 808.52 cm^{-1} : May indicate that C-H bending vibrations are associated with the pyranose ring structure, often found in aromatic compounds.

➤ **Guar Gum Nanoparticles (GGNP) Peaks:** 2973.84, 1381.21, 1059.33, 808.70 (Figure 15)

- 2973.84 cm^{-1} : This peak is related to C-H stretching vibrations, which could indicate the interaction between Guar gum and the encapsulated compound, leading to a shift from the original GG peaks.
- 1381.21 cm^{-1} : A slight shift compared to GG, indicating possible interaction or modification in the C-H bending region.
- 1059.33 cm^{-1} : A shift from the original C-O-C stretching of GG, suggesting structural changes in the glycosidic linkages within the nanoparticles.
- 808.70 cm^{-1} : Similar to the peak in GG, indicating that some structural elements of GG remain intact in the nanoparticle form.

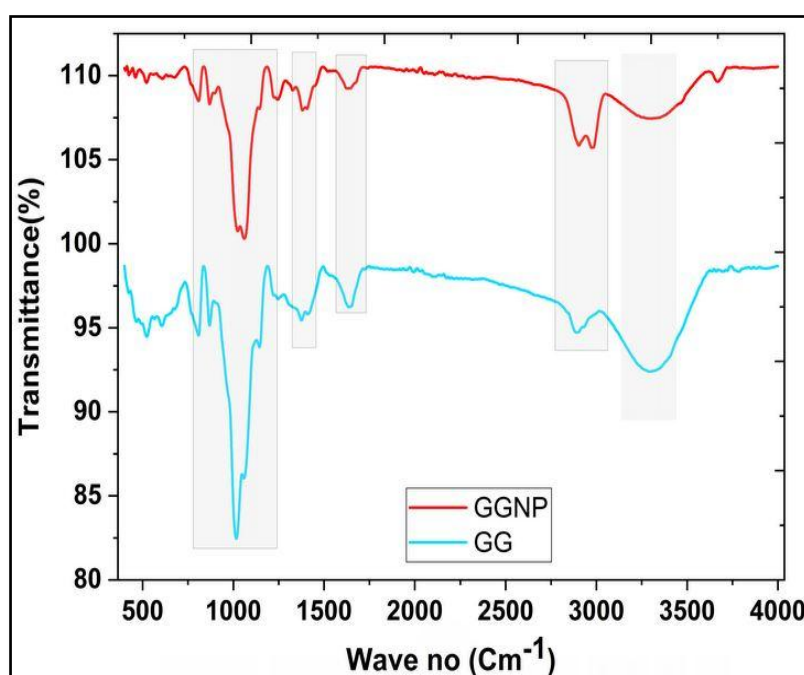


Figure 15: Comparison of FTIR spectra of GG (Guar gum) and GGNP (Guar gum nanoformulation)

- **Syringic Acid (SRN) Peaks:** 3224.17, 2971.87, 1694.06, 1614.33, 1518.60, 1372.05, 1174.66, 1197.49, 1103.03 (Figure 16: A, B)
- 3224.17 cm^{-1} : Corresponds to O-H stretching, indicative of hydroxyl groups.
 - 2971.87 cm^{-1} : Related to C-H stretching in aromatic rings.
 - 1694.06 cm^{-1} : Represents C=O stretching, typical of carboxylic acid groups.
 - 1614.33 cm^{-1} : Associated with C=C stretching in aromatic rings.
 - 1518.60 cm^{-1} : Likely corresponds to the aromatic C=C stretch.
 - 1372.05 cm^{-1} : Indicates C-H bending in methyl groups.
 - 1174.66 cm^{-1} & 1197.49 cm^{-1} : Correspond to C-O stretching in esters or phenolic compounds.
 - 1103.03 cm^{-1} : Suggests C-O stretching, common in alcohols and phenols.
- **Nanoformulation (guar gum nanoformulation of Syringic acid (NF1))Peaks (cm^{-1}):** 3246.21, 2972.27, 1695.06, 1616.03, 1519.33, 1372.05, 1200.83, 1071.8 (Figure 16: A, B)
- 3246.21 cm^{-1} : This peak, close to the O-H stretching region of SRN and GG, suggests successful incorporation of Syringic acid within the Guar gum matrix, with a slight shift indicating interaction between the components.
 - 2972.27 cm^{-1} : C-H stretching, showing a similar pattern to GGNP and SRN, indicating the preservation of aromatic structures.
 - 1695.06 cm^{-1} : C=O stretching, slightly shifted compared to SRN, indicating interaction within the nanoformulation.
 - 1616.03 cm^{-1} : C=C stretching in aromatic rings, closely resembling SRN, showing that the aromatic structure remains intact.
 - 1519.33 cm^{-1} : Similar to SRN, further confirming the incorporation of Syringic acid.

- 1372.05 cm^{-1} : Matches SRN, indicating that the C-H bending in methyl groups is preserved.
- 1200.83 cm^{-1} : A shift from SRN, possibly due to interaction between the Syringic acid and the Guar gum matrix in the nanoformulation.
- 1071.80 cm^{-1} : A shift from the GGNP C-O-C stretching, indicating changes in the polysaccharide structure due to the incorporation of Syringic acid.

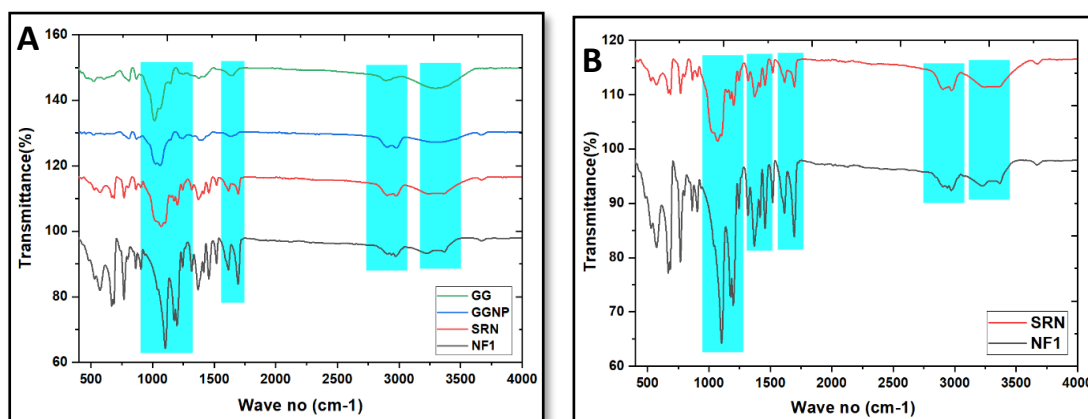


Figure 16: A) Comparison of FTIR spectra of Syringic acid (SRN) and Syringic acid loaded nanoformulation (guar gum nanoformulation of Syringic acid (NF1)) along with Guar gum (GG) and Guar gum nanoformulation (GGNP); B) Comparison of Enlargement view of FTIR spectra of SRN, guar gum nanoformulation of Syringic acid (NF1)

➤ **Sinapic Acid (SNP) Peaks (cm^{-1}):**

3302.99, 2836.54, 2528.59, 1621.10, 1658.71, 1515.08, 1214.78, 1295.97, 1117.61, 971.76, 832.03 (Figure 16: A, B)

- Interpretation:
 1. 3302.99 cm^{-1} : O-H stretching, joint in phenolic acids.
 2. 2836.54 cm^{-1} and 2528.59 cm^{-1} : C-H stretching, possibly from aromatic and aliphatic C-H groups.
 3. 1621.10 cm^{-1} and 1658.71 cm^{-1} : C=O stretching and C=C stretching, typical of carboxyl and aromatic rings in Sinapic acid.
 4. 1515.08 cm^{-1} : Aromatic C=C stretching.

5. 1214.78 cm^{-1} , 1295.97 cm^{-1} , 1117.61 cm^{-1} : C-O stretching in carboxyl and ester groups.
6. 971.76 cm^{-1} , 832.03 cm^{-1} : C-H out-of-plane bending, characteristic of substituted aromatic rings.

Key Observations: The distinct peaks confirm the presence of characteristic functional groups in Sinapic acid, such as hydroxyl, carbonyl, and aromatic rings.

➤ **Nanoformulation optimized nanoformulation of Sinapic acid (NF2) Peaks (cm^{-1}):**
 3305.18, 2837.17, 1659.53, 1621.91, 1515.51, 1266.53, 1296.37, 1265.79, 1116.56, 972.29, 1334.14, 815.23 ((Figure 17: A, B)

○ Interpretation:

1. 3305.18 cm^{-1} : O-H stretching, similar to SNP, indicates hydroxyl groups' presence.
2. 2837.17 cm^{-1} : C-H stretching, consistent with the aliphatic groups in the nanoformulation.
3. 1659.53 cm^{-1} and 1621.91 cm^{-1} : Retained C=O and C=C stretching, indicating the presence of aromatic and carbonyl groups, likely from Sinapic acid.
4. 1515.51 cm^{-1} : Aromatic C=C stretching, indicating the presence of the aromatic ring structure.
5. 1266.53 cm^{-1} , 1296.37 cm^{-1} : C-O stretching, slightly shifted, suggesting interactions between Sinapic acid and the nanoformulation matrix.
6. 972.29 cm^{-1} and 815.23 cm^{-1} : C-H out-of-plane bending, consistent with the aromatic ring structure.

The retention and slight shifts in characteristic peaks from SNP in the optimized nanoformulation of the Sinapic acid (NF2) spectrum suggest that Sinapic acid has been successfully incorporated into the nanoformulation. The interactions between Sinapic acid and the nano matrix are evident from the shifts in the O-H, C-O, and C-H stretching vibrations.

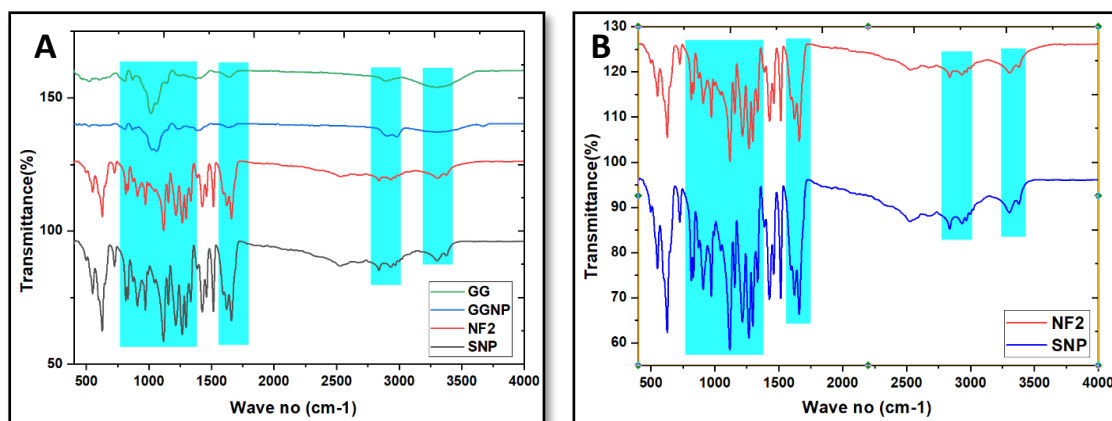


Figure 17: A) Comparison of FTIR spectra of Sinapic acid (SNP) and Sinapic acid loaded nanoformulation (NF2) along with Guar gum (GG) and Guar gum nanoformulation (GGNP); B) Comparison of Enlargement view of FTIR spectra of SNP, guar gum nanoformulation of Sinapic acid (NF2)

➤ **o-Coumaric Acid (OCA):**

Peaks (cm^{-1}): 3348.08, 2971.63, 2607.90, 1660.99, 1613.85, 1595.83, 1459.92, 1325.26, 1214.84, 1092.05, 977.69, 908.12, 747.52, 697.14 (Figure 18: A, B)

○ Interpretation:

1. 3348.08 cm^{-1} : O-H stretching indicates hydroxyl groups in phenolic compounds.
2. 2971.63 cm^{-1} : C-H stretching, associated with aromatic and aliphatic groups.
3. 2607.90 cm^{-1} : Broad peak, possibly indicating the presence of carboxylic acid dimers.
4. 1660.99 cm^{-1} and 1613.85 cm^{-1} : C=O and C=C stretching, characteristic of the carboxyl group and aromatic ring in o-Coumaric acid.
5. 1595.83 cm^{-1} : Aromatic ring C=C stretching.
6. 1459.92 cm^{-1} : C-H bending, typically seen in aromatic compounds.
7. 1325.26 cm^{-1} , 1214.84 cm^{-1} , 1092.05 cm^{-1} : C-O stretching in carboxyl and phenolic groups.

8. 977.69 cm^{-1} , 908.12 cm^{-1} : C-H out-of-plane bending, indicative of aromatic rings.
9. 747.52 cm^{-1} , 697.14 cm^{-1} : C-H bending, common in aromatic systems.

Key Observations: The distinct peaks reflect the characteristic functional groups of o-Coumaric acid, including hydroxyl, carboxyl, and aromatic rings, indicating its structural integrity.

➤ **Nanoformulation guar gum nanoformulation of o-Coumaric acid (NF3):** Peaks (cm^{-1}):

3337.02, 2971.78, 1661.01, 1596.91, 1459.86, 1426.78, 1326.12, 1218.02, 1066.01, 993.27, 867.59, 810.96, 748.29, 697.52 (Figure 18: A, B)

○ **Interpretation:**

1. 3337.02 cm^{-1} : O-H stretching, similar to OCA, indicates hydroxyl groups' presence.
2. 2971.78 cm^{-1} : C-H stretching, consistent with the spectrum of OCA and suggesting retained aromatic/aliphatic groups.
3. 1661.01 cm^{-1} and 1596.91 cm^{-1} : C=O and C=C stretching, retained from OCA, indicating the presence of the carboxyl and aromatic groups.
4. 1459.86 cm^{-1} : C-H bending, retained from OCA, consistent with aromatic structures.
5. 1326.12 cm^{-1} , 1218.02 cm^{-1} : C-O stretching, slightly shifted from OCA, indicating potential interactions with the nanoformulation matrix.
6. 1066.01 cm^{-1} : C-O-C stretching, indicative of the polysaccharide backbone, possibly influenced by interactions within the nanoformulation.
7. 993.27 cm^{-1} , 867.59 cm^{-1} , 810.96 cm^{-1} : C-H out-of-plane bending, indicating aromatic ring structures.
8. 748.29 cm^{-1} , 697.52 cm^{-1} : C-H bending, consistent with the aromatic system.

The retention of critical peaks from OCA in the optimized nanoformulation of o-Coumaric acid (NF3) spectrum and slight shifts suggest the successful incorporation of o-Coumaric acid into the nanoformulation. The shifts in the C-O and C-H stretching regions imply interactions between o-Coumaric acid and the Guar gum matrix. This indicates effective encapsulation and possible hydrogen bonding or other interactions within the nanoformulation.

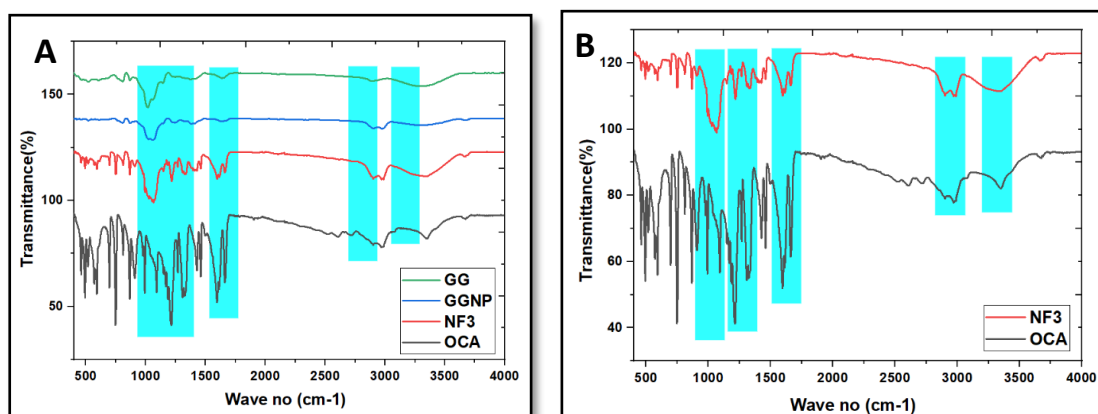


Figure 18: A) Comparison of FTIR spectra of o-Coumaric acid (OCA) and o-Coumaric acid loaded nanoformulation (NF3) along with Guar gum (GG) and Guar gum nanoformulation (GGNP); B) Enlargement view of FTIR spectra of OCA, guar gum nanoformulation of o-Coumaric acid (NF3)

6.9 Drug Loading Release Models

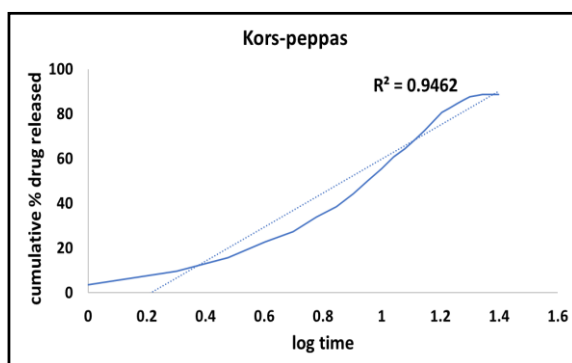
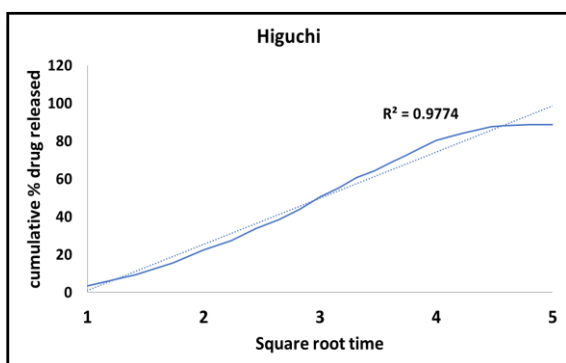
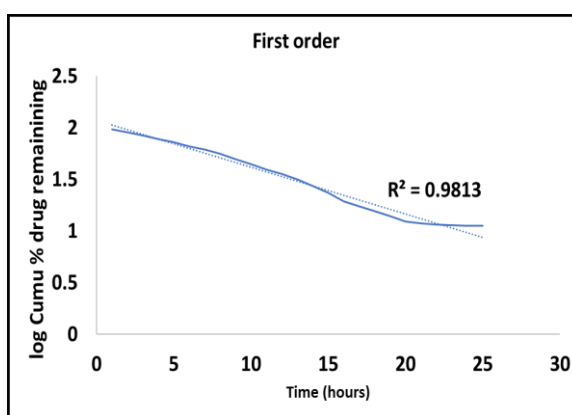
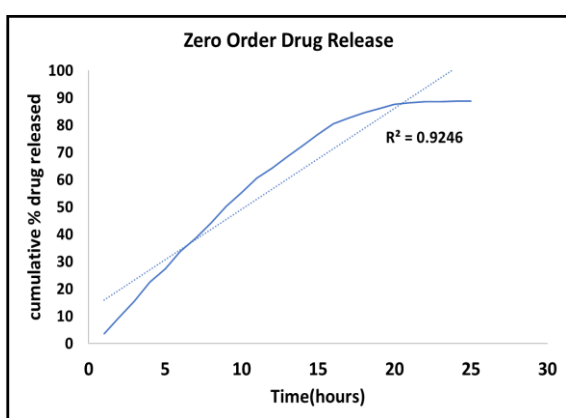
The drug loading rates of optimized nanoformulation of Syringic acid (NF1), optimized nanoformulation of Sinapic acid (NF2), and optimized nanoformulation of o-Coumaric acid (NF3) were 83.2%, 88.8%, and 92.3%, correspondingly.

➤ Release kinetics of optimized nanoformulation of Syringic acid (NF1)

The drug release kinetics study for optimized nanoformulation of Syringic acid (NF1) (the Syringic acid-loaded guar gum nanoformulation) (Figure 19) reveals a consistent and robust correlation between the experimental data and various mathematical models. The Zero-Order Kinetics model, with an R^2 value of 0.9246, indicates that the drug release from the nanoformulation is characterised by a constant rate over time, providing stability in the release profile. The First-Order Kinetics model, exhibiting an impressive R^2 value of 0.9813, suggests that the release of Syringic acid is proportional to the remaining drug concentration. This implies a controlled and predictable drug release pattern from the guar gum nanoformulation. The Higuchi Model, with an R^2 value of 0.9774, aligns well with the experimental data,

indicating that the drug release is diffusion-controlled. This suggests that the release mechanism involves the diffusion of Syringic acid through the guar gum matrix. The Korsmeyer-Peppas Model demonstrates a good fit with an R^2 value of 0.9462, emphasising the influence of polymeric properties on drug release. This model provides insights into the release mechanism, particularly in polymeric systems. The Hixson-Crowell Model, with an R^2 value of 0.9752, indicates a strong correlation, suggesting that changes in the surface area of the guar gum nanoformulation may contribute to the observed drug release profile.

The values obtained for each model affirm their suitability for describing the release behaviour of the encapsulated drug.



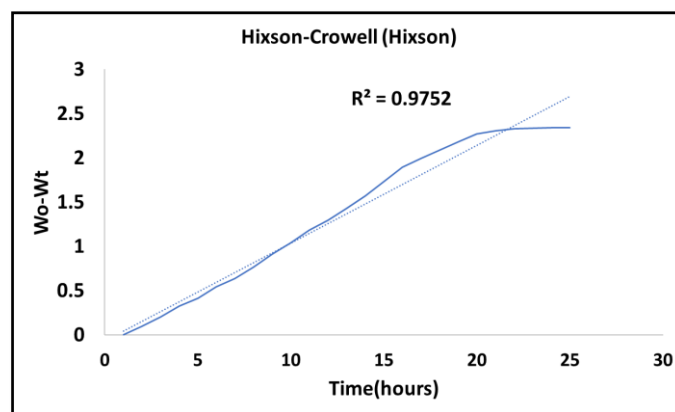


Figure 19: Different kinetics models of optimized guar gum nanoformulation of Syringic acid (NF1)

➤ **Release kinetics of optimized nanoformulation of Sinapic acid (NF2)**

The drug release study of optimized nanoformulation of Sinapic acid (NF2) (nanoformulated Sinapic acid-loaded guar gum), intended for wound healing applications, reveals promising results across various release models. The formulations were analysed using kinetic models to understand the release behaviour (Figure 20). The R^2 values obtained indicate good fits for most models, suggesting that the release kinetics are well-described by these mathematical frameworks. Specifically, the first-order model shows the highest correlation with an R^2 value of 0.9762, indicating that the release rate predominantly depends on the drug concentration remaining in the formulation. The zero-order model also demonstrates a strong fit with an R^2 value of 0.8912, suggesting that the drug release occurs constantly over time, independent of its concentration in the formulation. This could be beneficial for achieving a consistent therapeutic effect over a prolonged period, which is crucial for wound healing applications. Additionally, the Hixson model ($R^2 = 0.9595$), Korsmeyer-Peppas model ($R^2 = 0.9526$), and Higuchi model ($R^2 = 0.9623$) all show good fits, indicating that different aspects of the release mechanism, such as matrix erosion or diffusion, contribute to the overall release profile. These findings suggest that the nanoformulation of Sinapic acid-loaded guar gum has a controlled and predictable release profile, essential for optimising its therapeutic efficacy in wound healing. The high R^2 values across multiple models validate the robustness of the formulation and its potential suitability for clinical applications where precise control over drug release is critical.

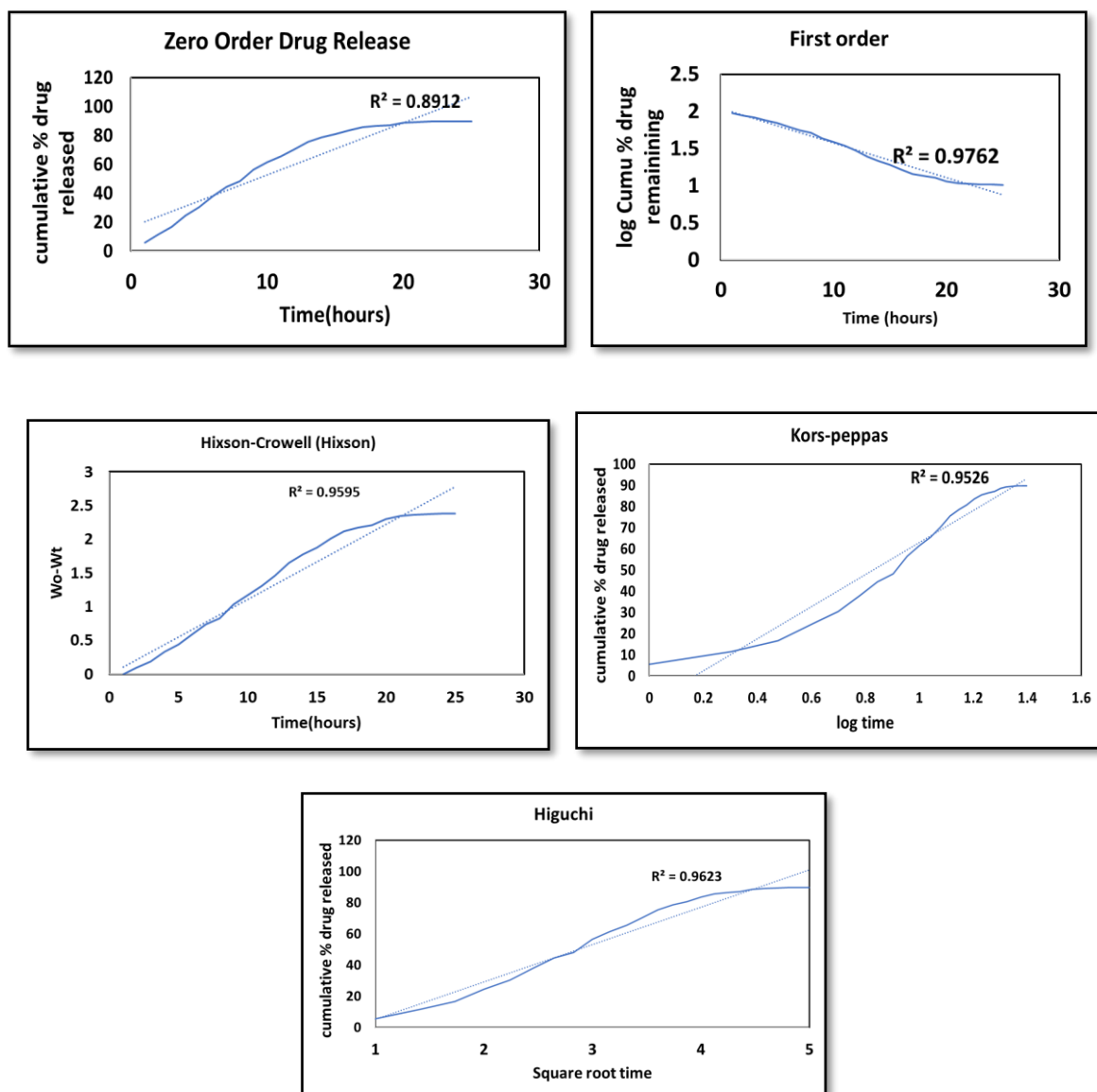
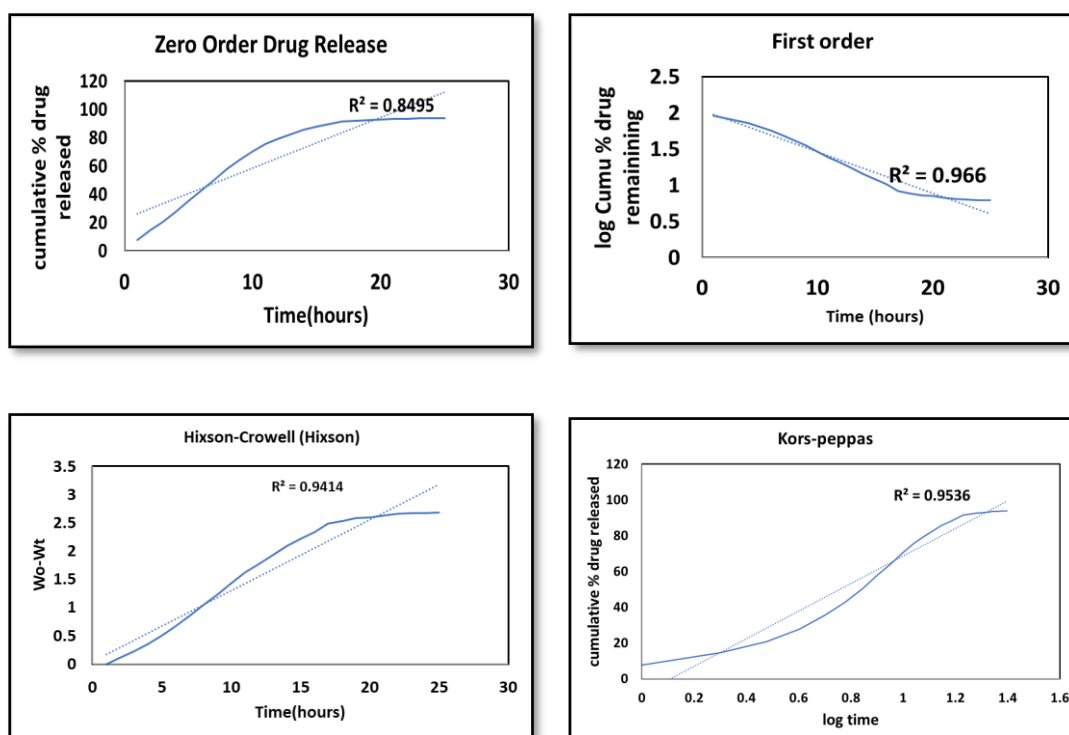


Figure 20: Different kinetics models of optimized guar gum nanoformulation of Sinapic acid (NF2)

➤ **Release kinetics of optimized nanoformulation of o-Coumaric acid (NF3)**

The drug release study of the NF3 (OCA-loaded guar gum nanoformulation) for wound healing was analysed using various kinetic models to understand the release mechanism. The results of fitting the data to different models yielded distinct R^2 values, indicating how well each model describes the drug release behaviour. The Zero Order model, with an R^2 value of 0.8495, suggests that the drug release rate is relatively constant over time, though the fit is imperfect. This indicates that the release rate is not entirely independent of the drug concentration. In contrast, the First Order model showed an R^2 value of 0.966, indicating a strong correlation. This suggests that the drug release rate is concentration-dependent,

decreasing exponentially as the drug concentration decreases. The Hixson-Crowell model, which yielded an R^2 value of 0.9414, implies that the drug release is influenced by changes in the surface area and diameter of the particles, pointing towards erosion or dissolution over time. The Korsmeyer-Peppas model had an R^2 value of 0.9536, indicating a good fit and suggesting a complex release mechanism involving diffusion and erosion. This model benefits polymeric systems where the release mechanism is not straightforward. Finally, the Higuchi model, with an R^2 value of 0.9392, indicates that the drug release is predominantly controlled by diffusion. This model describes the release from a matrix system where the drug diffuses through the polymer matrix over time. In summary, the drug release from the OCA-loaded guar gum nanoformulation is best described by the First Order model, followed closely by the Korsmeyer-Peppas model. This indicates that the release is primarily concentration-dependent, with significant contributions from diffusion and erosion mechanisms. The strong fits to the Hixson-Crowell and Higuchi models further suggest that particle erosion and diffusion through the polymer matrix play essential roles in drug release (Table 16) (Figure 21).



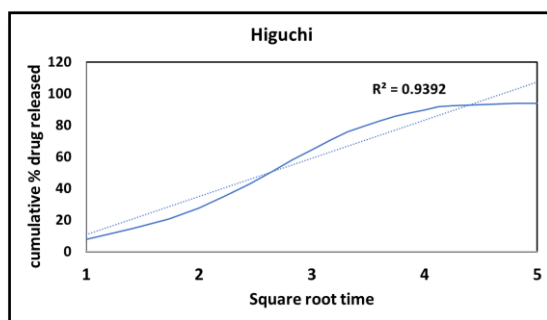


Figure 21: Different kinetics models of optimized guar gum nanoformulation of o-Coumaric acid (NF3)

Table 16: Kinetics Models of guar gum nanoformulation of Syringic acid (NF1), guar gum nanoformulation of Sinapic acid (NF2), optimized nanoformulation of o-Coumaric acid (NF3) (coefficient of regression R^2)

Drug Release model	R^2 Value optimized nanoformulation of Syringic acid (NF1)	R^2 Value-optimized nanoformulation of Sinapic acid (NF2)	R^2 Value-optimized nanoformulation of o-Coumaric acid (NF3)
Zero-order	0.9246	0.8912	0.8495
First order	0.9813	0.9762	0.966
Hixson model	0.9774	0.9595	0.9414
Kros-peppas model	0.9462	0.9526	0.9536
Higuchi model	0.9752	0.9623	0.9392

6.10 Determination of pH

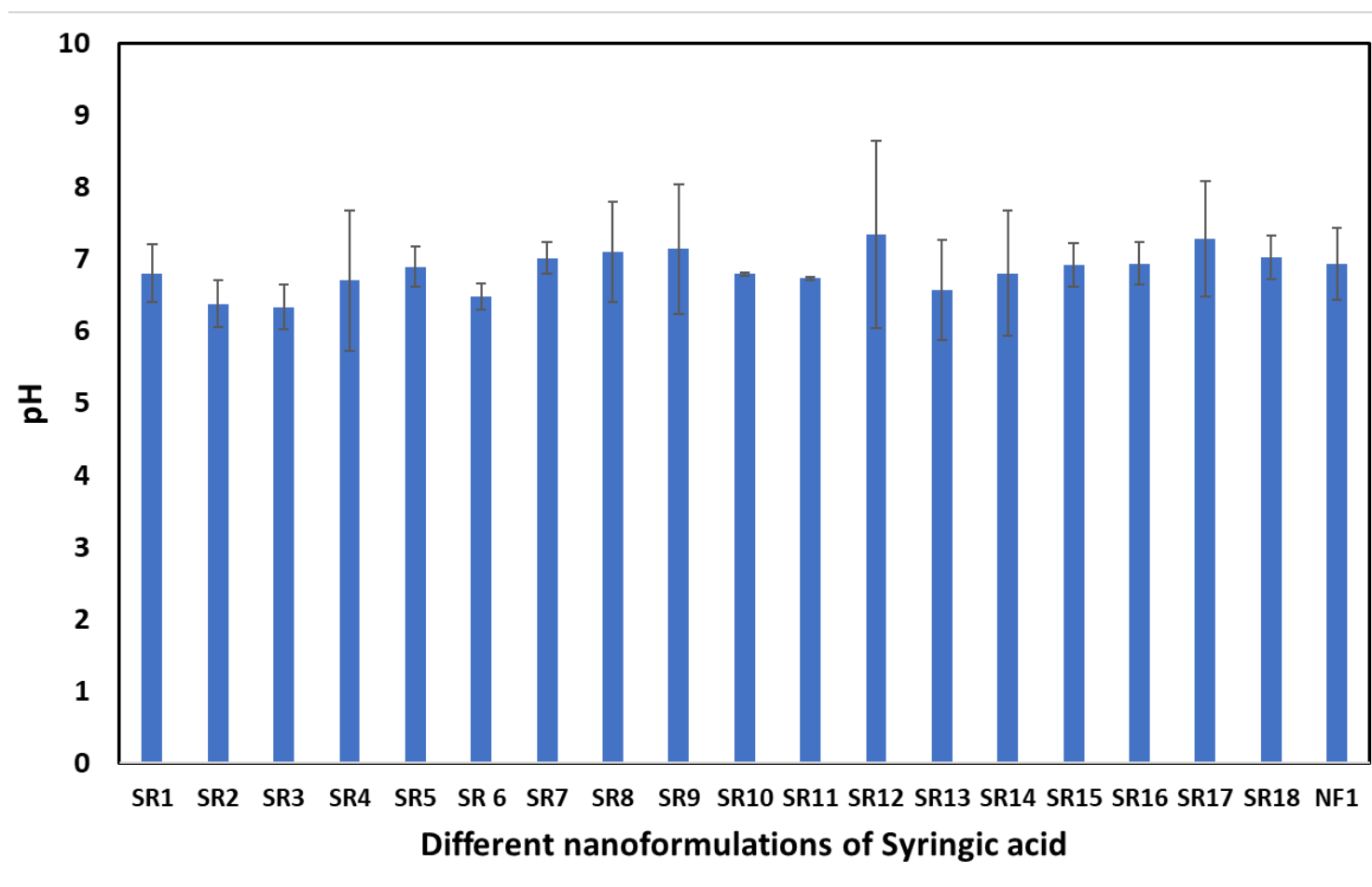


Figure 22: pH values of different run samples for optimized nanoformulation of Syringic acid (NF1) and optimized optimized nanoformulation of Syringic acid (NF1) (SR-Standard run used in BBD model). All values are expressed as mean \pm standard error of the mean (SEM) (n=3).

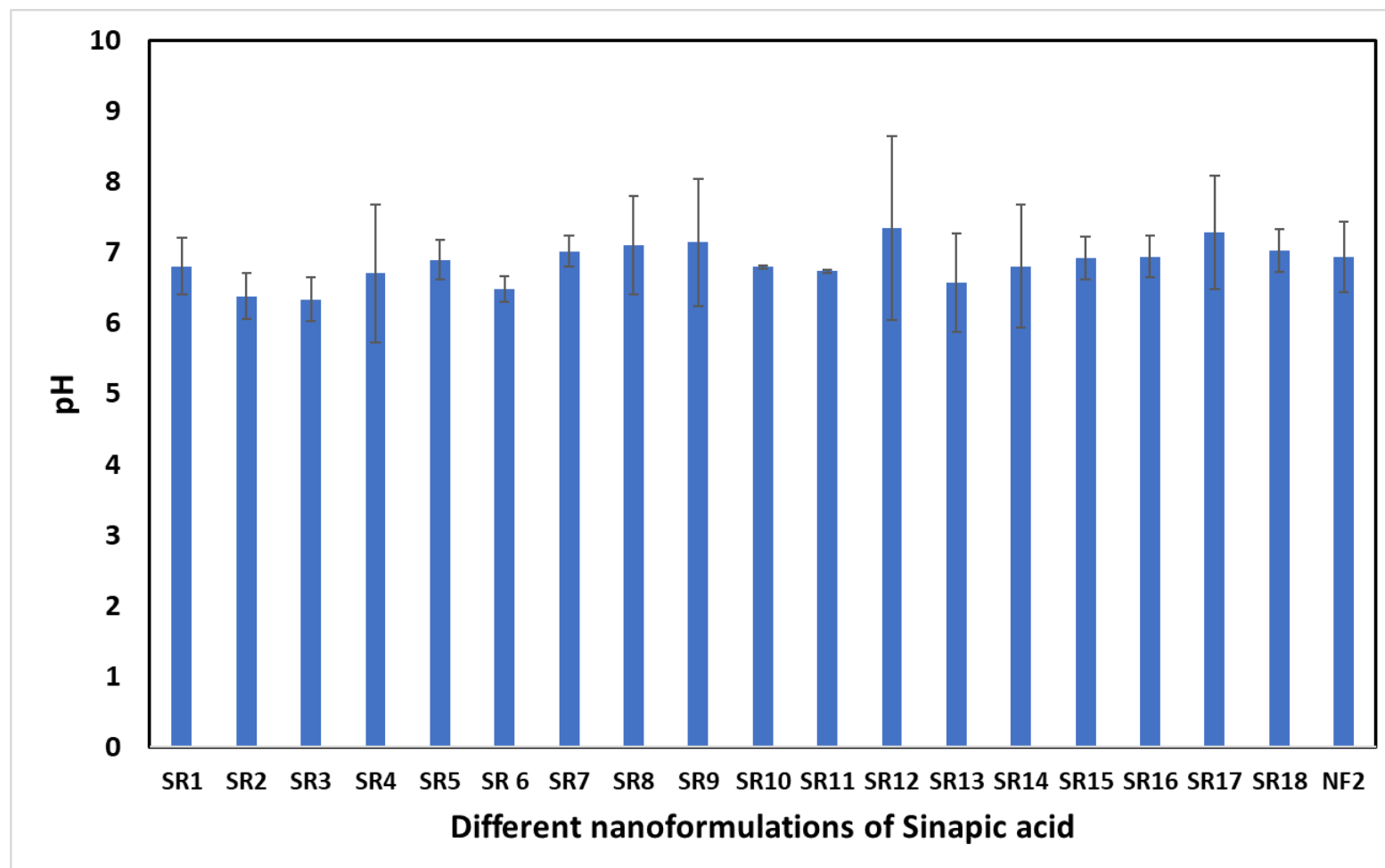


Figure 23: pH values of different run samples for optimized nanoformulation of Sinapic acid (NF2) and optimized nanoformulation of Sinapic acid (NF2). All values are expressed as mean \pm standard error of the mean (SEM) (n=3).

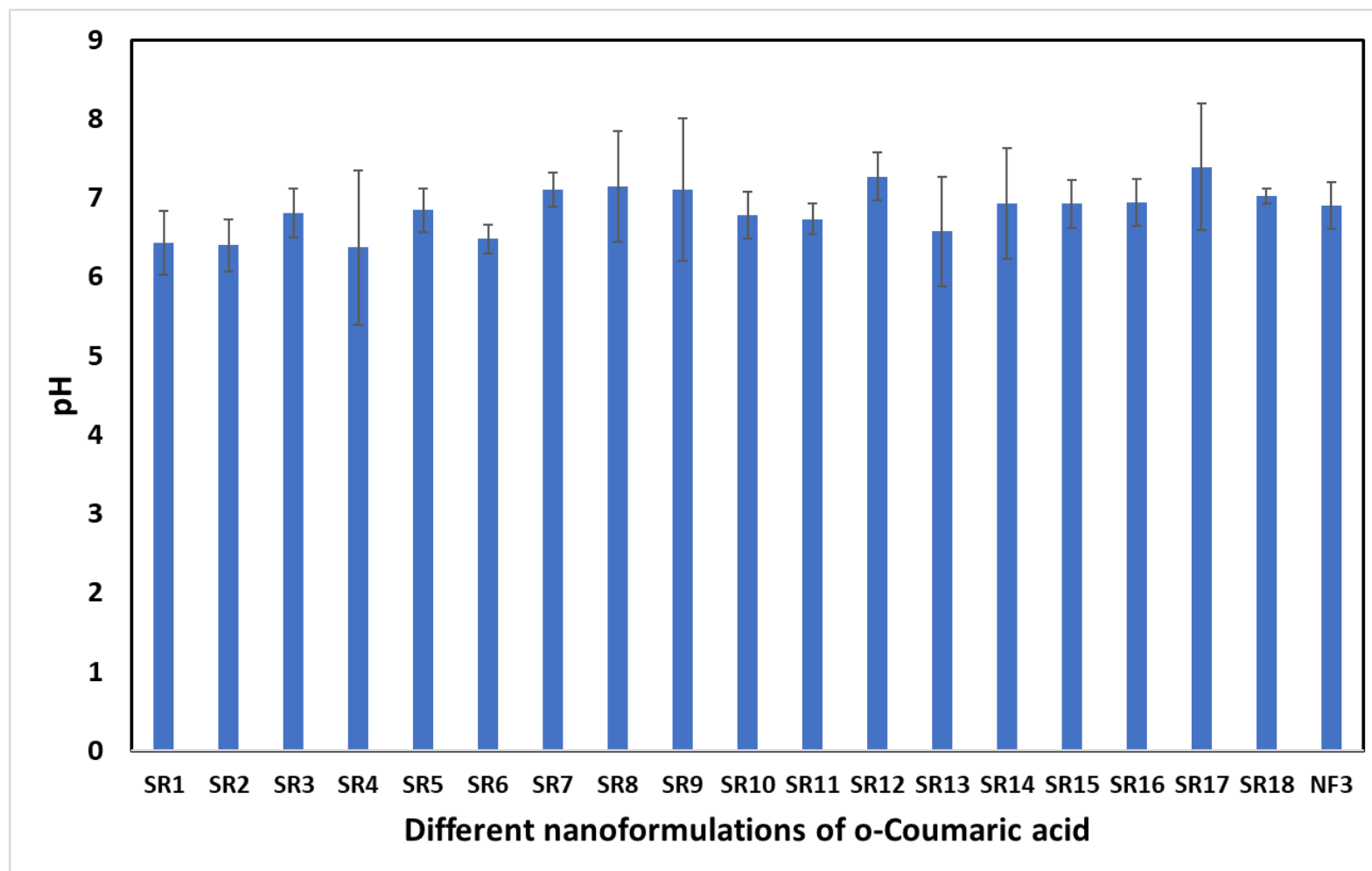


Figure 24: pH values of different run samples for nanoformulation of Sinapic acid (NF2) and optimized nanoformulation of o-Coumaric acid (NF3) All values are expressed as mean \pm standard error of the mean (SEM) (n=3).

For optimized nanoformulation of Syringic acid (NF1), pH values ranging between 6.28 to 7.35 in the nanoformulations suggest a slightly acidic to neutral nature, a characteristic that is anticipated to positively impact their skin application for wound healing (Figure 22).

For guar gum nanoformulation of Sinapic acid (NF2), the pH values of the formulations range from 6.33 to 7.28, which falls within the mildly acidic to neutral range. Most of the formulations, including SR 1 (6.8), SR 5 (6.89), SR 6 (6.48), SR 10 (6.79), SR 11 (6.73), SR 14 (6.8), SR 15 (6.92), SR 16 (6.94), and optimized nanoformulation of Sinapic acid (NF2) (6.93), have pH values closer to neutral (around 7.0) (Figure 23).

For guar gum nanoformulation of o-Coumaric acid (NF3), the formulations exhibit a pH range of 6.4 to 7.39. pH levels can significantly influence chemical stability and skin compatibility in cosmetic and pharmaceutical applications. SR17 shows the highest pH at 7.3, indicating a more alkaline nature that may enhance preservative efficacy but could be less suitable for sensitive skin. Conversely, SR1, with a pH of 6.33, falls at the lower end, potentially offering milder properties suitable for sensitive skin formulations. guar gum nanoformulation of o-Coumaric acid (NF3) at pH 6.9 maintains a neutral to slightly acidic range, ideal for applications requiring skin balance and stability (Figure 24).

6.11 Determination of Spreadability

For the first NF, the Spreadability measurements range from 41.7 gm.cm/sec to gm.cm/sec. Notably, formulations SR12 and SR15 stand out with relatively higher spreadability values, indicating their capacity to cover larger surface areas more efficiently. In contrast, formulations SR 6, SR 7, and SR 8 display lower Spreadability values. The optimized formulation with a higher spreadability value (83.33 gm.cm/sec) suggests greater ease of application (Figure 25).

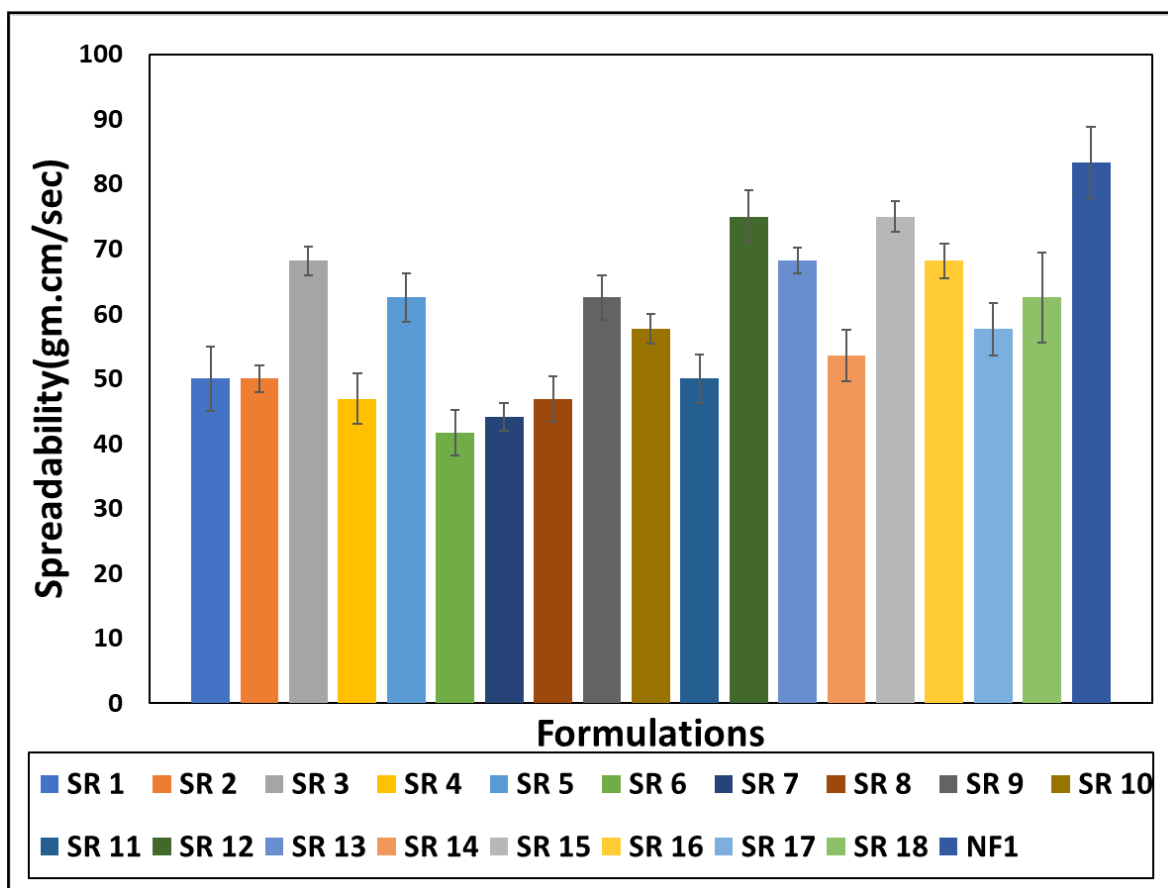


Figure 25: Spreadability values of different run samples for optimized nanoformulation of Syringic acid (NF1) and optimized nanoformulation of Syringic acid (NF1) (SR-Standard run used in BBD model). All values are expressed as mean \pm standard error of the mean (SEM) (n=3).

The spreadability values of optimized nanoformulation of Sinapic acid (NF2) of the samples ranged from 41.7 to 83.33 gm.cm/sec, with several samples (SR 3; SR 13; SR 16) showing similar high spreadability values of 68.18 gm.cm/sec, and sample SR 15 showing the highest individual spreadability at 77.69 gm.cm/sec. However, the optimized nanoformulation of Sinapic acid (NF2) formulation exhibited the highest spreadability value of 83.33 gm.cm/sec among all tested samples (Figure 26).

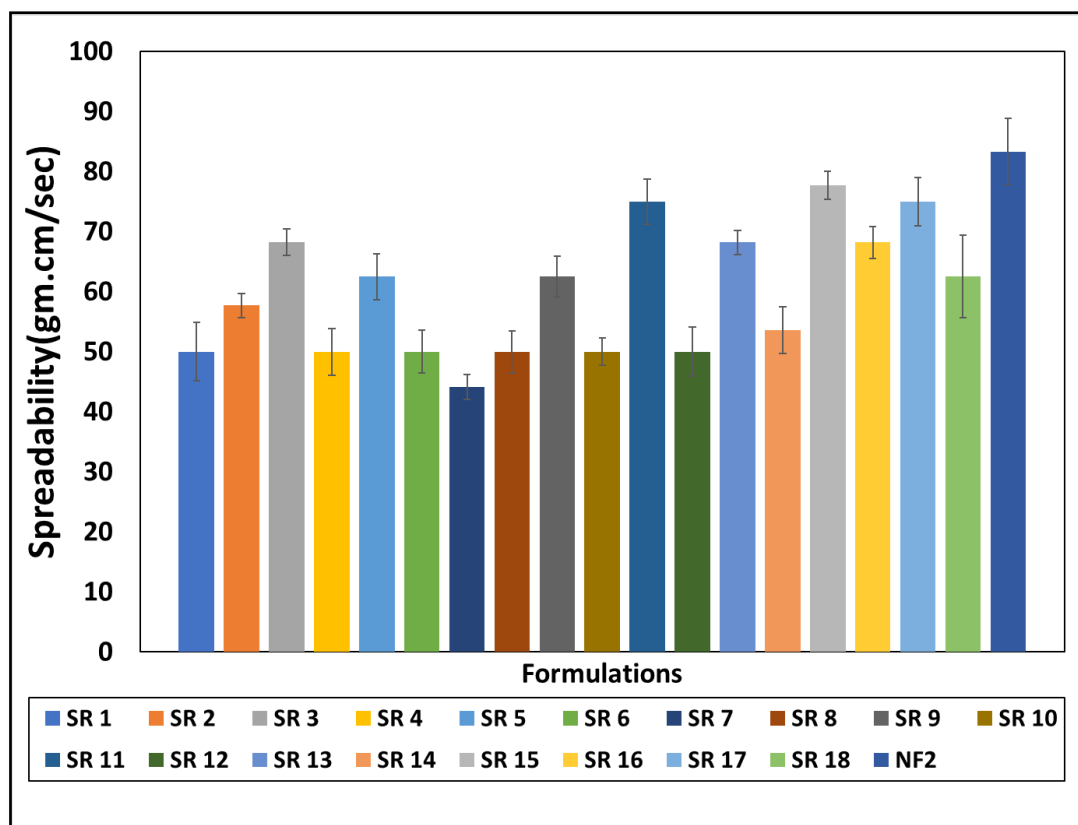


Figure 26: Spreadability values of different run samples for optimized nanoformulation of Sinapic acid (NF2) and optimized optimized nanoformulation of Sinapic acid (NF2) (SR-Standard run used in BBD model) All values are expressed as mean \pm standard error of the mean (SEM) (n=3).

The spreadability values of the optimized nanoformulation of o-Coumaric acid (NF3) samples ranged from 44.11 to 93.75 gm.cm/sec, with several samples (SR 3; SR 13) showing similar high spreadability values of 68.18 gm.cm/sec, and samples SR 12 and SR 15 showing the highest individual spreadability at 75 gm.cm/sec. However, the optimized nanoformulation of o-Coumaric acid (NF3) formulation exhibited the highest spreadability value of 93.75 gm.cm/sec among all tested samples (Figure 27).

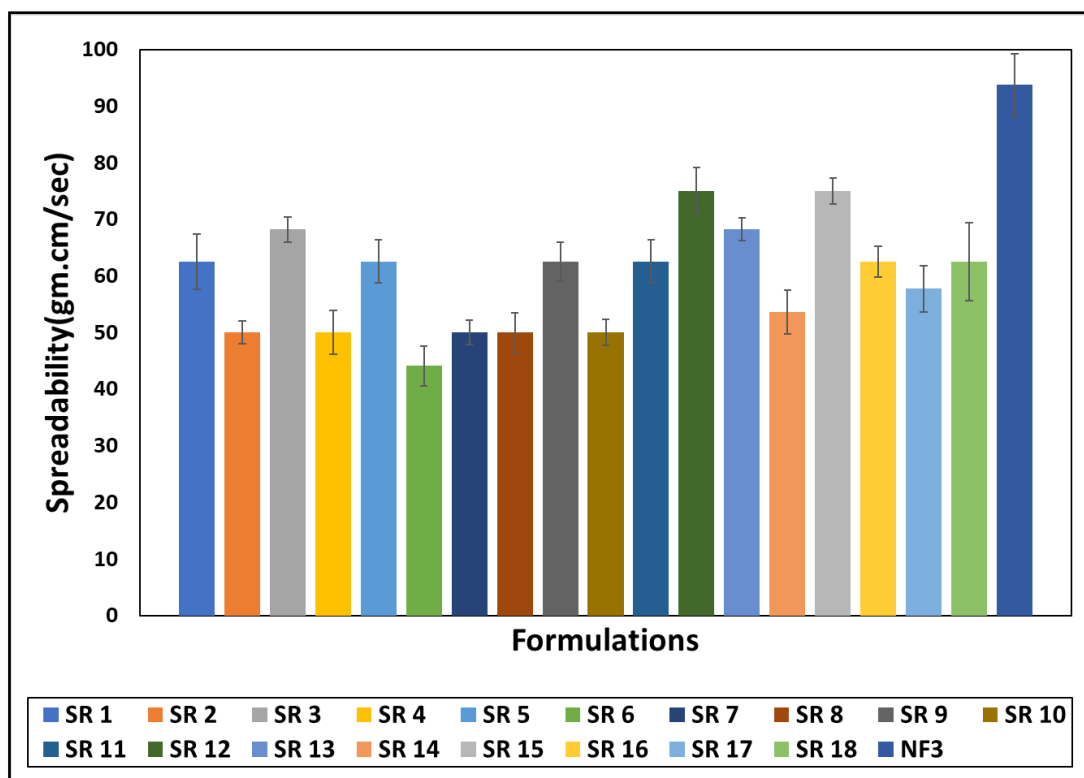


Figure 27: Spreadability values of different run samples for optimized nanoformulation of o-Coumaric acid (NF3) and optimized optimized nanoformulation of o-Coumaric acid (NF3) (SR-Standard run used in BBD model) All values are expressed as mean \pm standard error of the mean (SEM) (n=3).

6.12 Determination of Viscosity

Viscosity values for the formulations (SR1 to SR18) range from 7910 to 8980 cP. The optimized formulation optimized Syringic acid (NF1) nanoformulation had shown a moderate viscosity of 8230 cP (Figure 28).

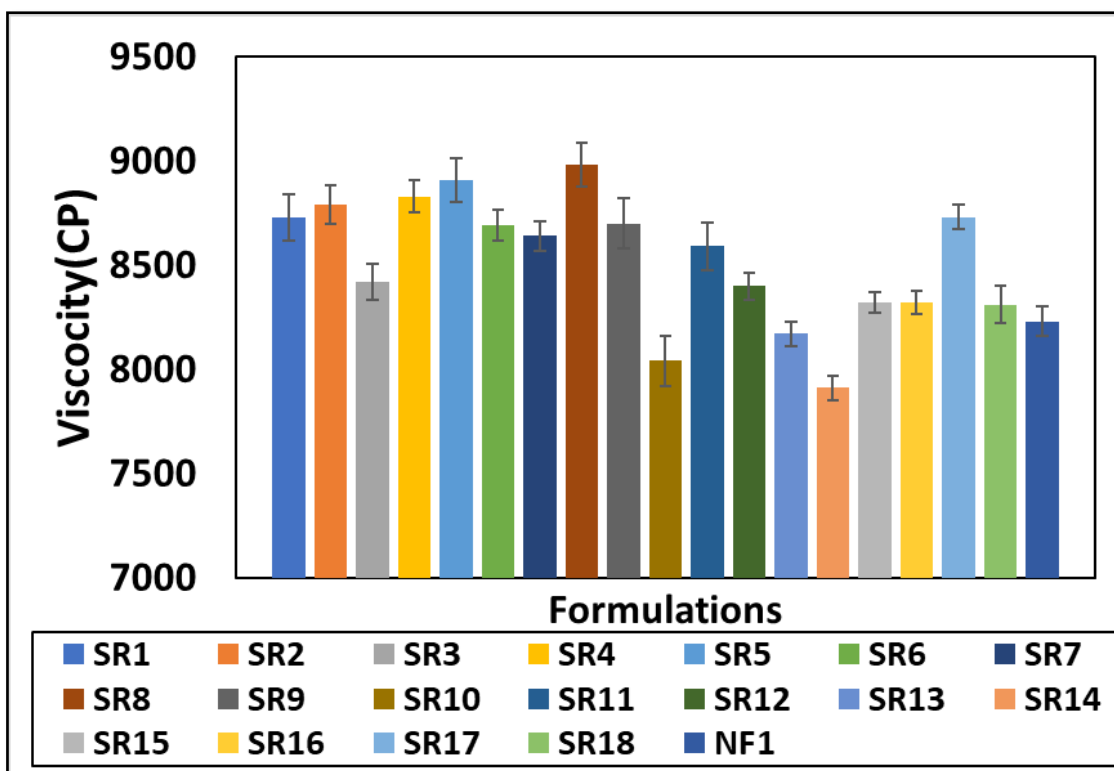


Figure 28: Viscosity values of different run samples for optimized nanoformulation of Syringic acid (NF1) and optimized optimized nanoformulation of Syringic acid (NF1) (SR-Standard run used in BBD model) All values are expressed as mean \pm standard error of the mean (SEM) (n=3).

The viscosity analysis of 18 different formulations and the optimized nanoformulation of Sinapic acid (NF2) formulation reveals significant flow characteristics and thickness variations. The viscosity values range from 7910 cP to 8880 cP. SR 1 and 5, with 8830 cP and 8810 cP, respectively, fall into the high viscosity category. In contrast, the formulation SR 14 has the lowest viscosity at 7910 cP, indicating a thinner consistency. SR 10, with a viscosity of 8040 cP, also fits into this category of lighter formulations. The majority of the formulations, including SR 2 (8790 cP), SR 4 (8700 cP), SR 6 (8420 cP), SR 7 (8330 cP), SR 9 (8720 cP), SR 11 (8590 cP), SR 17 (8700 cP), and optimized nanoformulation of Sinapic acid (NF2) (8220 cP), have viscosities in the mid-to-high range, around 8220 cP to 8790 Cp (Figure 29).

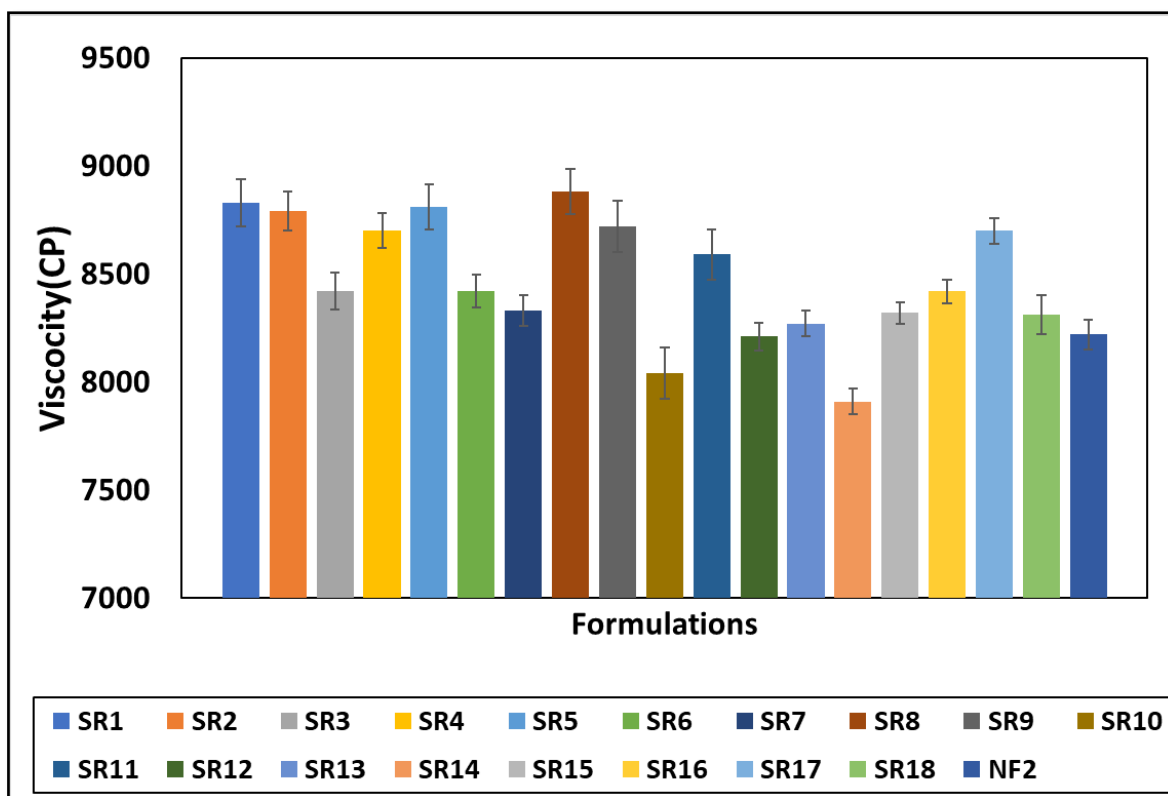


Figure 29: Viscosity values of different run samples for optimized nanoformulation of Sinapic acid (NF2) and optimized optimized nanoformulation of Sinapic acid (NF2) (SR-Standard run used in BBD model) All values are expressed as mean \pm standard error of the mean (SEM) (n=3).

The viscosity values range from 8020 cP to 8710 cP. The formulation SR16 has the lowest viscosity at 8020 cP, indicating a thinner consistency. The formulation SR8 has the highest viscosity at 8880 cP, indicating a very thick consistency. The majority of the formulations, including SR3 (8720 cP), SR4 (8530 cP), SR6 (8650 cP), SR7 (8540 cP), SR9 (8590 cP), SR11 (8590 cP), SR17 (8530 cP), and SR18 (8390 cP), have viscosities in the mid-to-high range, around 8390 cP to 8720 cP. The optimized nanoformulation of o-Coumaric acid (NF3) formulation has a viscosity of 8300 cP, placing it in the moderate viscosity range (Figure 30).

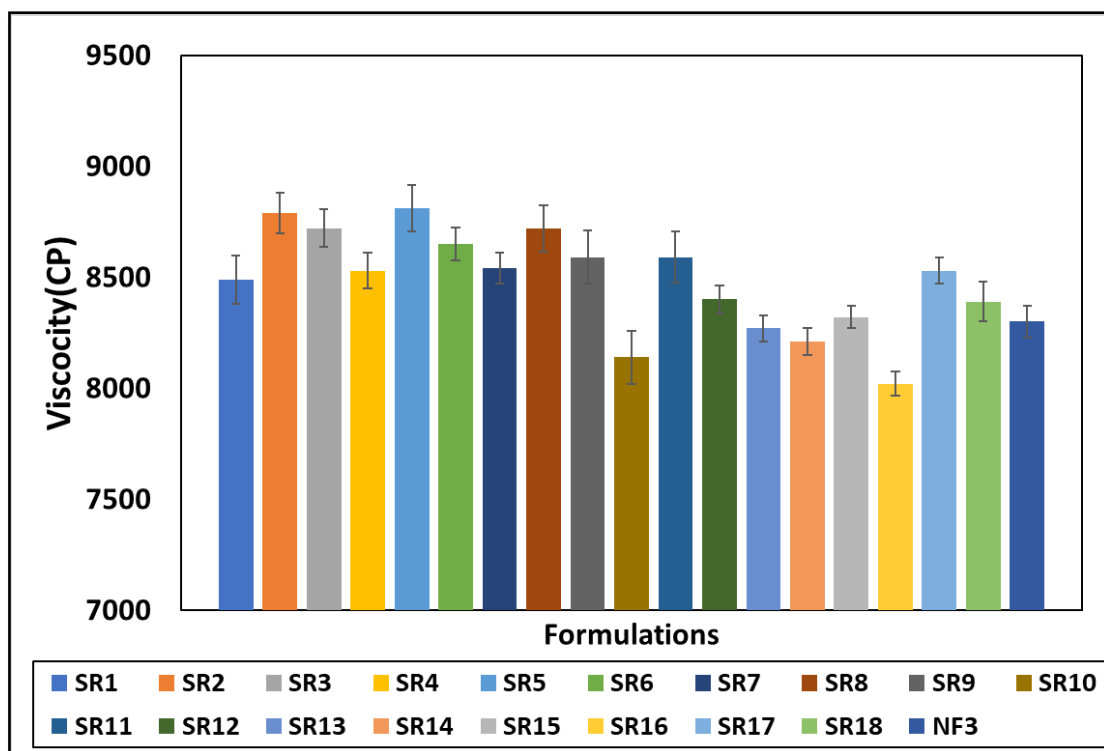


Figure 30: Viscosity values of different run samples for optimized nanoformulation of o-Coumaric acid (NF3) and optimized optimized nanoformulation of o-Coumaric acid (NF3) (SR-Standard run used in BBD model) All values are expressed as mean \pm standard error of the mean (SEM) (n=3).

6.13 Determination of RI

The refractive index values across formulations exhibit a relatively consistent range from 1.233 to 1.456 for the first nanoformulations (Figure 31).

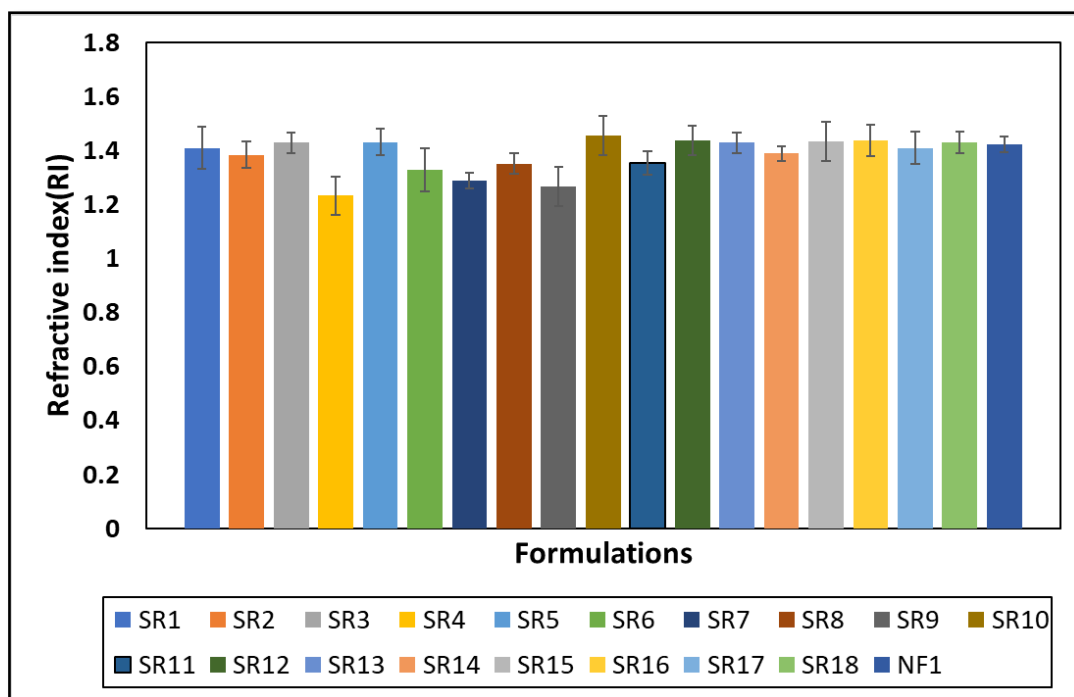


Figure 31: RI values of different run samples for optimized nanoformulation of Syringic acid (NF1) and optimized nanoformulation of Syringic acid (NF1) (SR-Standard run used in BBD model) All values are expressed as mean \pm standard error of the mean (SEM) (n=3).

For the second nanoformulations, The RI values of the 18 formulations ranged broadly from 1.89 to 1.632, indicating a wide diversity in their compositions and optical characteristics. The formulation with the highest refractive index was SR 5, at 1.632. Formulations such as SR 10 (1.456), SR 16 (1.438), SR 18 (1.432), and SR 13 (1.490) had relatively high refractive indices, similar to SR 5 but slightly lower. The optimized nanoformulation of Sinapic acid (NF2) formulation, with an RI of 1.4, falls into the upper-middle range of the measured values.

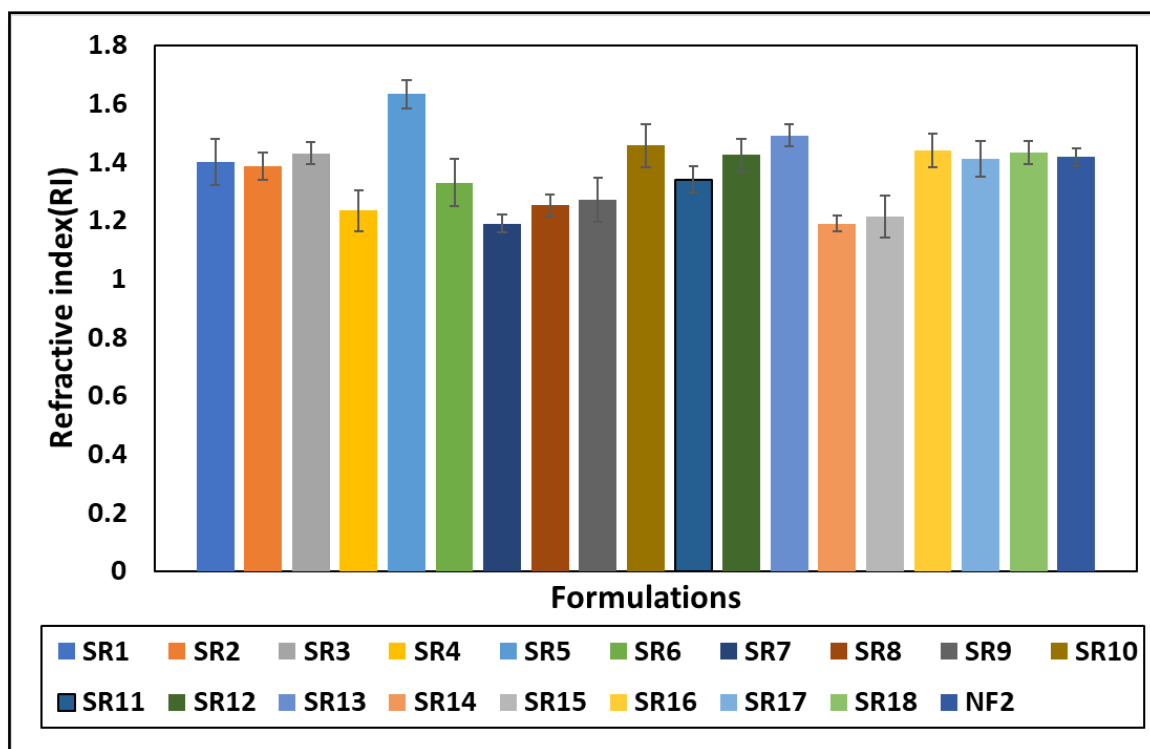


Figure 32: RI values of different run samples for optimized nanoformulation of Sinapic acid (NF2) and optimized optimized nanoformulation of Sinapic acid (NF2) (SR-Standard run used in BBD model) All values are expressed as mean \pm standard error of the mean (SEM) (n=3).

The refractive index (RI) values of the 18 formulations ranged from 1.189 to 1.738, indicating diverse optical characteristics. SR5 had the highest RI of 1.738, suggesting high optical density suitable for cosmetic applications. Formulations like SR7 and SR14, with RI values of 1.189, offer minimal light interaction, which is ideal for natural or matte finishes. guar gum nanoformulation of o-Coumaric acid (NF3), with an RI of 1.404, balances optical properties, making it suitable for wound healing applications where moderate light interaction is beneficial (Figure 33).

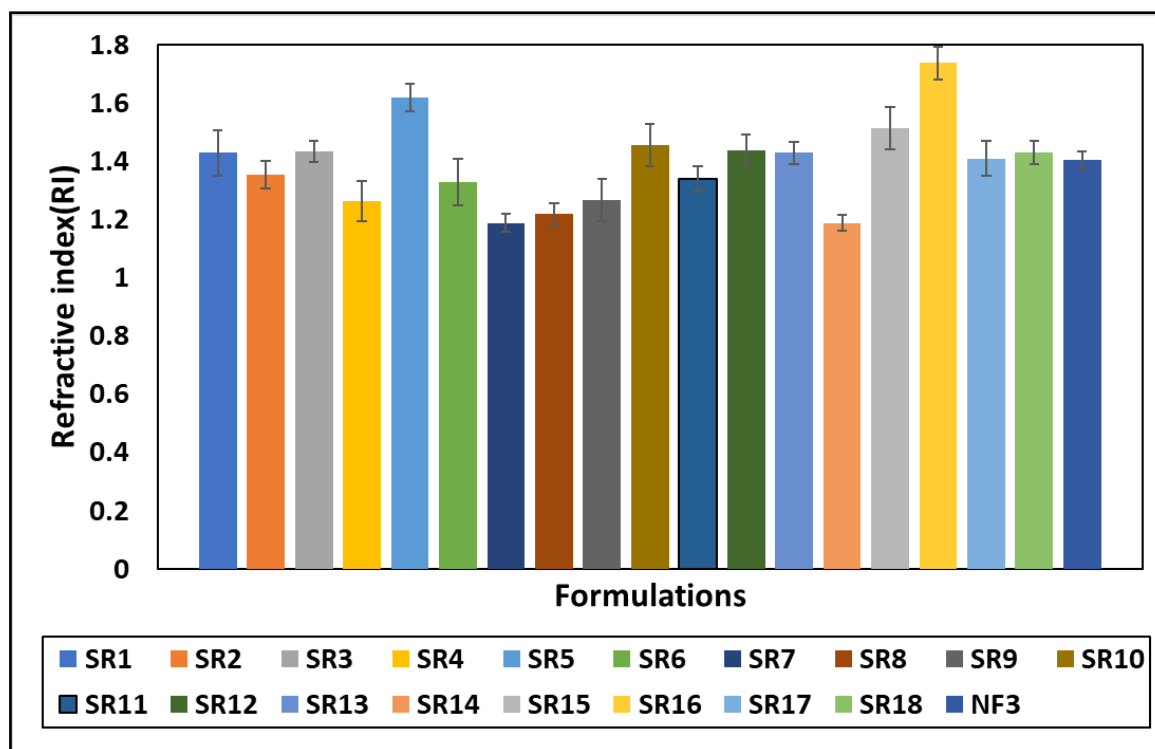


Figure 33: RI values of different run samples for optimized nanoformulation of o-Coumaric acid (NF3) and optimized nanoformulation of o-Coumaric acid (NF3) (SR-Standard run used in BBD model) All values are expressed as mean \pm standard error of the mean (SEM) (n=3).

6.14 In vitro

6.14.1 Free radical scavenging activity

➤ DPPH

The DPPH assay results demonstrate the antioxidant activities of different samples, including ascorbic acid, GGNP, SRN, guar gum nanoformulation of Syringic acid (NF1), SNP, guar gum nanoformulation of Sinapic acid (NF2), OCA, and guar gum nanoformulation of o-Coumaric acid (NF3), at doses between 20 and 100 $\mu\text{g/ml}$. The % DPPH inhibition was observed following different treatments compared to the control. Ascorbic acid, used as a standard, shows the highest antioxidant activity across all concentrations, starting at 51.96% at 20 $\mu\text{g/ml}$ and reaching 88.48% at 100 $\mu\text{g/ml}$. This indicates a robust and concentration-dependent increase in antioxidant capacity. GGNP exhibits the lowest antioxidant activity among the samples, with a modest increase from 14.4% at 20 $\mu\text{g/ml}$ to 32.53% at 100 $\mu\text{g/ml}$. Similarly, SRN shows a gradual increase in activity, from 15.87% to 45.89% across the same concentration range. SNP and OCA show moderate antioxidant activities, with SNP increasing from 18.87% to 47.89% and OCA from 20.87% to 48.89% as concentration increases from 20

to 100 $\mu\text{g/ml}$. The guar gum nanoformulation of Syringic acid (NF1), guar gum nanoformulation of Sinapic acid (NF2), and optimized nanoformulation of o-Coumaric acid (NF3) nanoformulations display significantly higher antioxidant activities than GGNP and other raw drugs. At 20 $\mu\text{g/ml}$, optimized nanoformulation of Syringic acid (NF1) starts at 32.41%, optimized nanoformulation of Sinapic acid (NF2) at 34.41%, and optimized nanoformulation of o-Coumaric acid (NF3) at 36.41%. At the highest 100 $\mu\text{g/ml}$ concentration, these values rise to 72.49%, 74.49%, and 75.49%, respectively. These nanoformulations thus demonstrate a robust and concentration-dependent increase in antioxidant activity, nearing the efficacy of ascorbic acid at higher concentrations (Figure 34).

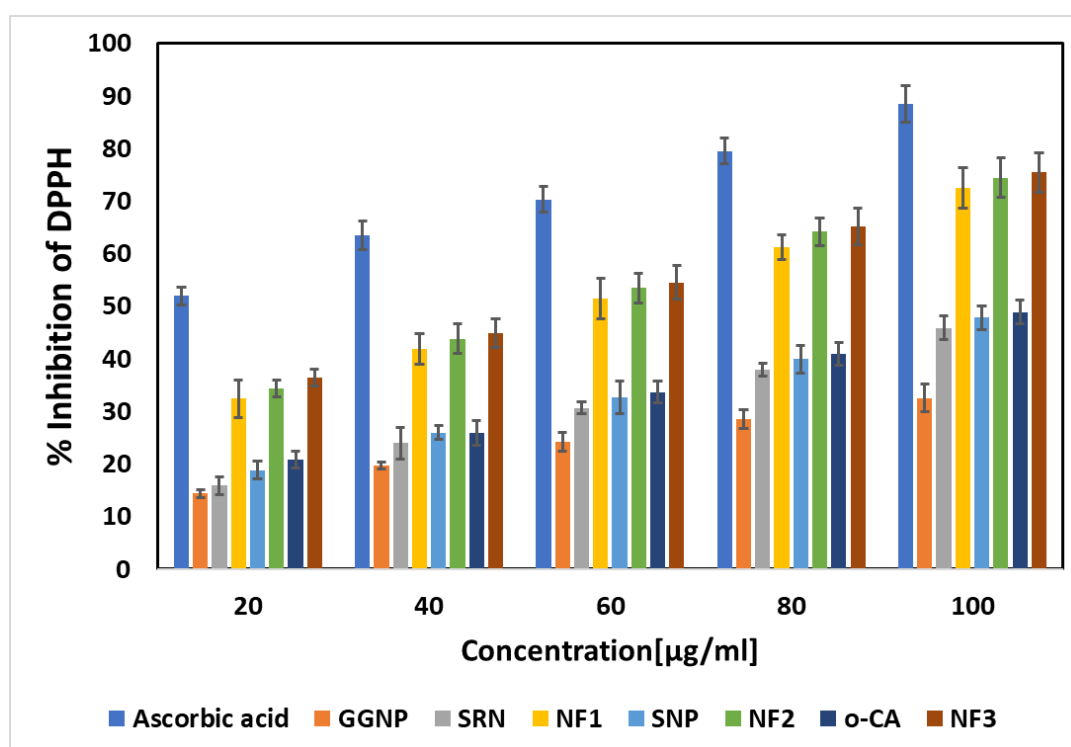


Figure 34: DPPH free radical scavenging activity of formulations All values are expressed as mean \pm standard error of the mean (SEM) (n=3).

(GG- Guar gum; GGNP-Guar gum nanoformulation; SRN-Syringic acid; SNP-Sinapic acid; OCA-o-Coumaric acid; NF1-optimized nanoformulation of Syringic acid (NF1), NF2-optimized nanoformulation of Sinapic acid, NF3-optimized nanoformulation of o-Coumaric acid)

➤ ABTS

The ABTS assay results demonstrate the antioxidant activities of various samples, including ascorbic acid, GGNP, SRN, guar gum nanoformulation of Syringic acid (NF1), SNP, guar gum nanoformulation of Sinapic acid (NF2), OCA, and guar gum nanoformulation of o-Coumaric acid (NF3), at doses between 20 and 100 µg/ml. Ascorbic acid, the standard, exhibits the highest antioxidant activity across all concentrations, starting at 58.53% at 20 µg/ml and increasing to 87.95% at 100 µg/ml. This indicates a robust and consistent increase in antioxidant capacity with concentration. GGNP shows lower antioxidant activity than ascorbic acid, rising from 21.38% at 20 µg/ml to 42.19% at 100 µg/ml. SRN also demonstrates a gradual increase in activity, from 28.55% to 50.4% over the same concentration range. SNP and OCA show moderate antioxidant activities, with SNP increasing from 29.55% to 51.4% and OCA from 30.55% to 55.4% as concentration increases from 20 to 100 µg/ml. Nanoformulations guar gum nanoformulation of Syringic acid (NF1), guar gum nanoformulation of Sinapic acid (NF2), and optimized nanoformulation of o-Coumaric acid (NF3) exhibit significantly higher antioxidant activities than GGNP. At 20 µg/ml, optimized nanoformulation of Syringic acid (NF1) starts at 51.59%, optimized nanoformulation of Sinapic acid (NF2) at 50.59%, and optimized nanoformulation of o-Coumaric acid (NF3) at 54.59%. At 100 µg/ml, these values increase to 77.27%, 78.27%, and 79.27%, respectively. These nanoformulations thus show a robust and concentration-dependent increase in antioxidant activity, approaching the efficacy of ascorbic acid at higher concentrations (Figure 35).

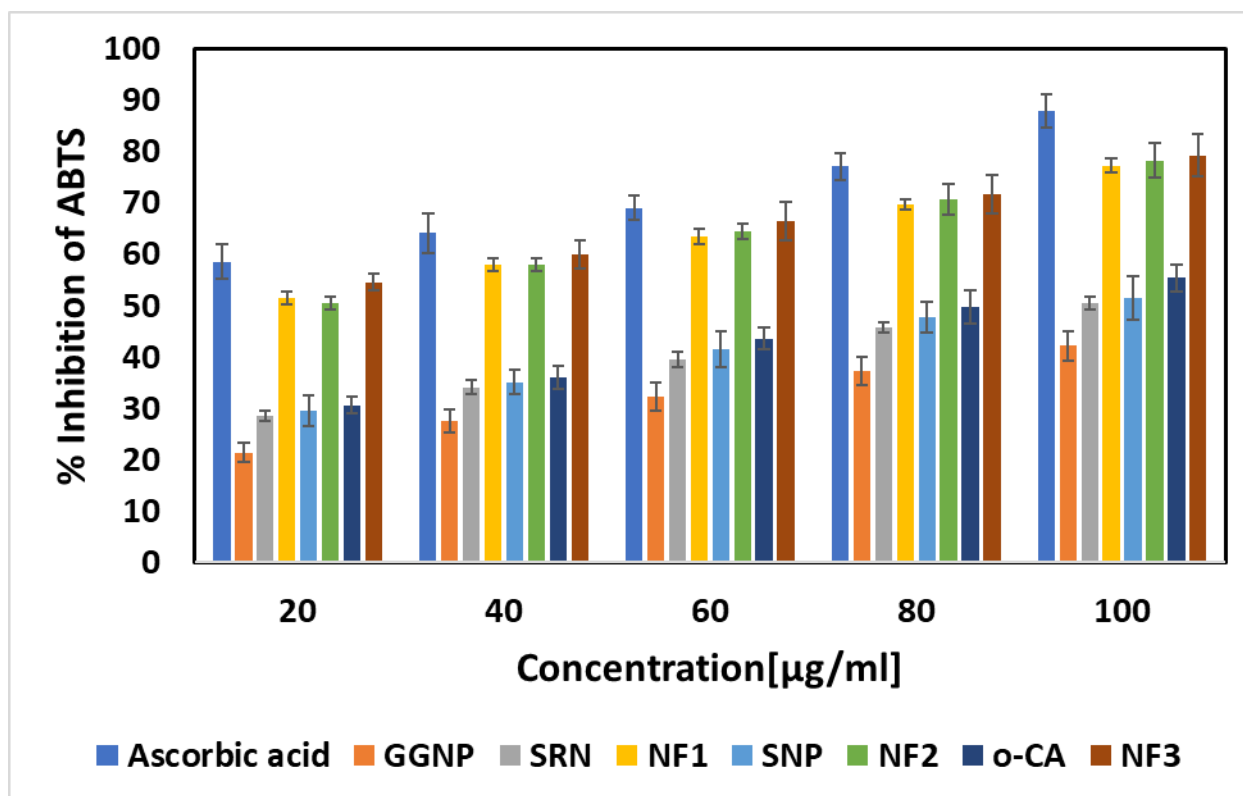


Figure 35: ABTS free radical scavenging activity of formulations. All values are expressed as mean \pm standard error of the mean (SEM) (n=3).

(GG- Guar gum; GGNP-Guar gum nanoformulation; SRN-Syringic acid; SNP-Sinapic acid; OCA-o-Coumaric acid; NF1-optimized nanoformulation of Syringic acid (NF1), NF2-optimized nanoformulation of Sinapic acid, NF3-optimized nanoformulation of o-Coumaric acid)

6.14.2 Anti-diabetic enzyme activity

➤ α -Glucosidase

The α -glucosidase assay results demonstrate the inhibitory activities of various samples, including acarbose (standard α -glucosidase inhibitor), GGNP, SRN, guar gum nanoformulation of Syringic acid (NF1), SNP, guar gum nanoformulation of Sinapic acid (NF2), OCA, and guar gum nanoformulation of o-Coumaric acid (NF3), at doses between 20 and 100 μ g/ml. Acarbose showed the highest inhibitory activity across all concentrations, starting at 68.19% at 20 μ g/ml and increasing to 90.3% at 100 μ g/ml. This indicates a robust and concentration-dependent increase in alpha-glucosidase inhibition. GGNP exhibits the lowest inhibitory activity among the samples, rising from 10.95% at 20 μ g/ml to 34.32% at 100 μ g/ml. SRN shows a gradual increase in activity, from 24.25% to 40.54% over the same

concentration range. SNP and OCA show moderate inhibitory activities, with SNP increasing from 25.25% to 41.54% and OCA from 22.25% to 47.54% as concentration increases from 20 to 100 $\mu\text{g/ml}$. Nanoformulations guar gum nanoformulation of Syringic acid (NF1), guar gum nanoformulation of Sinapic acid (NF2), and optimized nanoformulation of o-Coumaric acid (NF3) exhibit significantly higher inhibitory activities than GGNP and SRN. At 20 $\mu\text{g/ml}$, optimized nanoformulation of Syringic acid (NF1) starts at 37.94%, optimized nanoformulation of Sinapic acid (NF2) at 39.94%, and optimized nanoformulation of o-Coumaric acid (NF3) at 40.94%. At 100 $\mu\text{g/ml}$, these values increase to 61.44%, 63.4%, and 64.44%, respectively. These nanoformulations show a robust and concentration-dependent increase in alpha-glucosidase inhibition, although they do not reach the efficacy of acarbose (Figure 36).

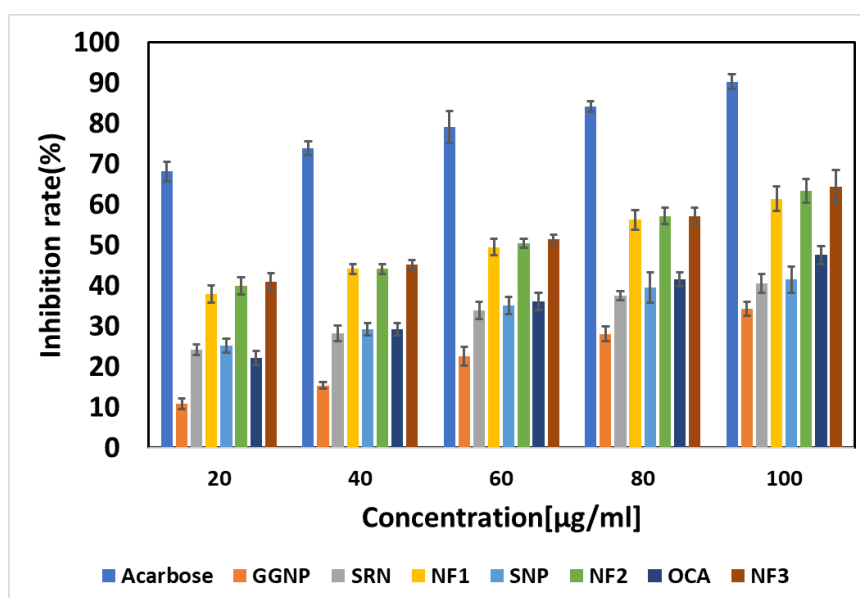


Figure 36: α -glucosidase enzyme activity of formulations All values are expressed as mean \pm standard error of the mean (SEM) (n=3).

(GG- Guar gum; GGNP-Guar gum nanoformulation; SRN-Syringic acid; SNP-Sinapic acid; OCA-o-Coumaric acid; NF1-optimized nanoformulation of Syringic acid (NF1), NF2-optimized nanoformulation of Sinapic acid, NF3-optimized nanoformulation of o-Coumaric acid)

➤ α -Amylase

The alpha-amylase assay results indicate the inhibitory activities of various samples, including acarbose, GGNP, SRN, guar gum nanoformulation of Syringic acid (NF1), SNP, guar gum nanoformulation of Sinapic acid (NF2), OCA, and guar gum nanoformulation of o-Coumaric

acid (NF3), at doses between 20 and 100 $\mu\text{g/ml}$. Acarbose, used as the standard, exhibits the highest inhibitory activity across all concentrations, starting at 56.65% at 20 $\mu\text{g/ml}$ and increasing to 82.14% at 100 $\mu\text{g/ml}$. This demonstrates a robust and concentration-dependent increase in alpha-amylase inhibition. GGNP shows lower inhibitory activity than acarbose, rising from 15.27% at 20 $\mu\text{g/ml}$ to 30.13% at 100 $\mu\text{g/ml}$. SRN also exhibits a gradual increase in activity, from 12.88% to 27.2% across the same concentration range. Nanoformulations guar gum nanoformulation of Syringic acid (NF1), guar gum nanoformulation of Sinapic acid (NF2), and optimized nanoformulation of o-Coumaric acid (NF3) display significantly higher inhibitory activities than GGNP, SNP, OCA and SRN. At 20 $\mu\text{g/ml}$, optimized nanoformulation of Syringic acid (NF1) starts at 29.76%, optimized nanoformulation of Sinapic acid (NF2) at 31.4%, and optimized nanoformulation of o-Coumaric acid (NF3) at 33.24% at 20 $\mu\text{g/ml}$. SNP and OCA begin at 14.88% and 16.88%, respectively. At 100 $\mu\text{g/ml}$, these values increase to 47.69% for guar gum nanoformulation of Syringic acid (NF1), 48.88% for optimized nanoformulation of Sinapic acid (NF2) and 53.5% for guar gum nanoformulation of o-Coumaric acid (NF3). SNP and OCA also show increased inhibition, reaching 31.2% and 34.2% at the highest concentration, respectively. These samples demonstrate a robust and concentration-dependent increase in alpha-amylase inhibition, with optimized nanoformulation of o-Coumaric acid (NF3) showing the highest activity among them, approaching the efficacy of acarbose at higher concentrations (Figure 37).

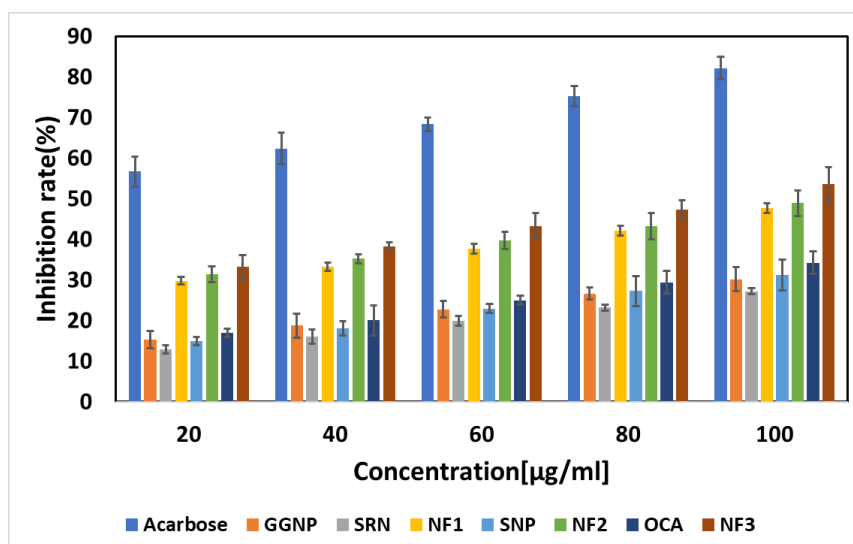


Figure 37: α -amylase enzyme activity of formulations

(GG- Guar gum; GGNP-Guar gum nanoformulation; SRN-Syringic acid; SNP-Sinapic acid; OCA-o-Coumaric acid; NF1-optimized nanoformulation of Syringic acid (NF1), NF2-

optimized nanoformulation of Sinapic acid, NF3-optimized nanoformulation of o-Coumaric acid)

All the values are represented as mean \pm S.E.M. (n=3)

6.14.3 MTT assay

In the L929 cell line, GGNP demonstrates a gradual decrease in cell viability from 90.41% at the lowest concentration to 65.72% at the highest concentration. SRN shows a significant reduction in viability, starting at 61.79% and dropping to 31.45%. optimized nanoformulation of Syringic acid (NF1) maintains high viability, starting at 97.67% and decreasing to 71.7%. SNP shows the lowest viability among the formulations, decreasing values from 58.7% to 40.45%. optimized nanoformulation of Sinapic acid (NF2) also begins with high viability at 98.38% and ends at 75.58%. OCA exhibits a similar trend to SNP, decreasing viability from 59.79% to 36.45%. Optimized nanoformulation of o-Coumaric acid (NF3) maintains relatively high viability throughout, from 95.33% to 78.7%. Overall, guar gum nanoformulation of Syringic acid (NF1), guar gum nanoformulation of Sinapic acid (NF2), and optimized nanoformulation of o-Coumaric acid (NF3) show higher cell viability across all concentrations, indicating lower cytotoxicity. In contrast, SRN and SNP exhibit higher cytotoxicity with significantly lower cell viability as the concentration increases (Figure 38: A).

With the HaCaT cell line, GGNP shows a slight decrease in cell viability from 95.74% at 6.25 $\mu\text{g/ml}$ to 83.88% at 100 $\mu\text{g/ml}$. SRN exhibits a significant reduction in viability, starting at 56.34% and dropping to 33.02% as the concentration increases. optimized nanoformulation of Syringic acid (NF1) maintains high viability, with cell proliferation observed at lower concentrations, showing 108.8% viability at 6.25 $\mu\text{g/ml}$ and decreasing to 85.77% at 100 $\mu\text{g/ml}$. SNP shows a decline in viability from 80.4% to 62.22% across the concentration range. optimized nanoformulation of Sinapic acid (NF2) demonstrates high viability with cell proliferation at the lower concentration (112.38% at 6.25 $\mu\text{g/ml}$), reducing to 90.97% at 100 $\mu\text{g/ml}$. OCA shows a moderate decline in viability from 84.38% to 63.72%. optimized nanoformulation of o-Coumaric acid (NF3) maintains the highest cell viability, with proliferation at lower concentrations (115.24% at 6.25 $\mu\text{g/ml}$) and decreasing to 95.7% at the highest concentration. Overall, formulations guar gum nanoformulation of Syringic acid (NF1), guar gum nanoformulation of Sinapic acid (NF2), and optimized nanoformulation of o-Coumaric acid (NF3) show higher cell viability and cell proliferation at lower concentrations, indicating lower cytotoxicity (Figure 38: B).

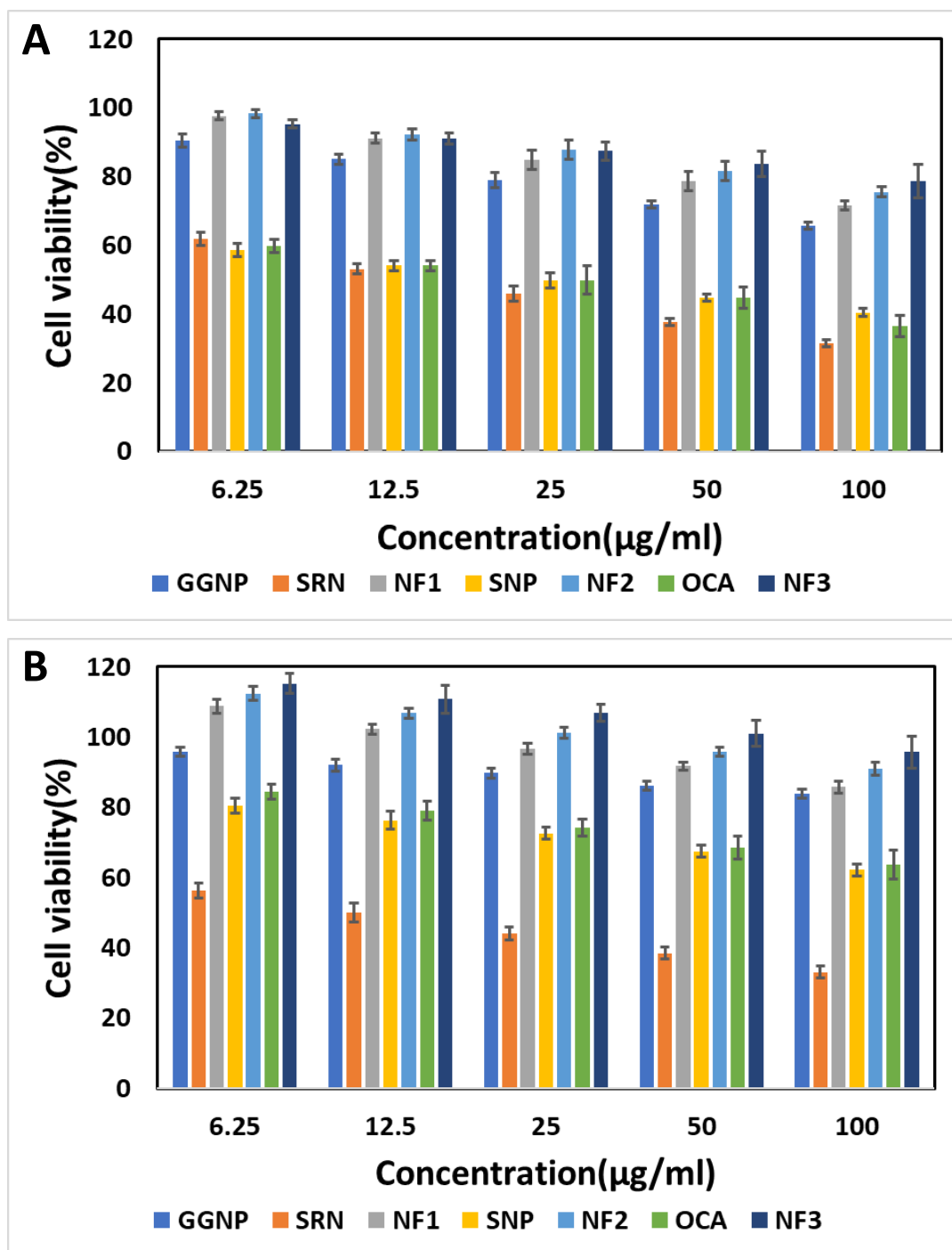


Figure 38: Cytotoxicity assay of formulations A) L929 cells; B) HaCaT. All values are expressed as mean \pm standard error of the mean (SEM) (n=3).

(GG- Guar gum; GGNP-Guar gum nanoformulation; SRN-Syringic acid; SNP-Sinapic acid; OCA-o-Coumaric acid; NF1-optimized nanoformulation of Syringic acid (NF1), NF2-optimized nanoformulation of Sinapic acid, NF3-optimized nanoformulation of o-Coumaric acid)

6. 13.4 Scratch assay

The scratch assay results indicate the percentage of wound healing (increased cell migration) for different formulations compared to a control. The control group shows 36.6% wound healing. GGNP substantially increases healing at 60.6% (Figure 39). SRN shows 24.5% healing, while optimized nanoformulation of Syringic acid (NF1) demonstrates a significantly higher healing rate at 92.6% (Figure 40). SNP shows 29.8% healing (Figure 41). optimized nanoformulation of Sinapic acid (NF2) and optimized nanoformulation of o-Coumaric acid (NF3) achieve complete scratch healing, whereas OCA displays 31.4% healing (Figure 42). NF2 and optimized nanoformulation of o-Coumaric acid (NF3) exhibit the highest wound healing efficacy, followed by optimized nanoformulation of Syringic acid (NF1) and GGNP, with SRN and SNP showing minor effectiveness (Figure 43).

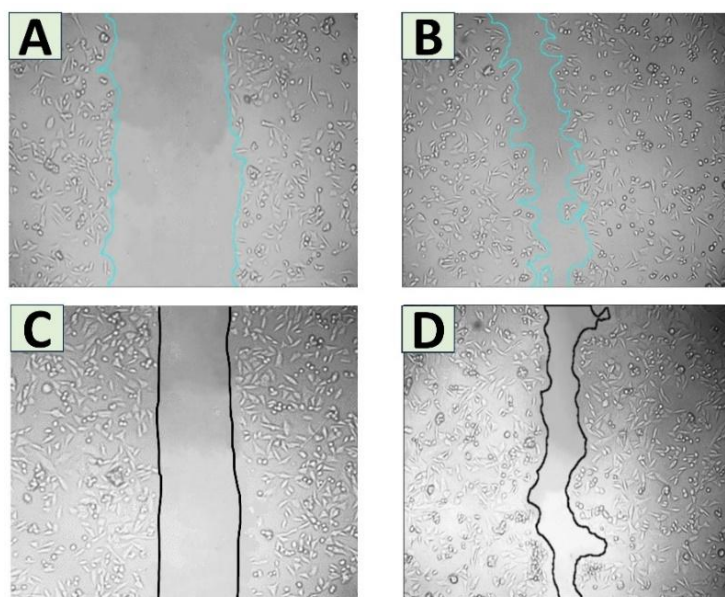


Figure 39: In vitro scratch assay A-D) In vitro scratch assay (A= Before treatment with GGNP, 0hr; B=after treatment with GGNP, 24hr; C, D= Control/no treatment)

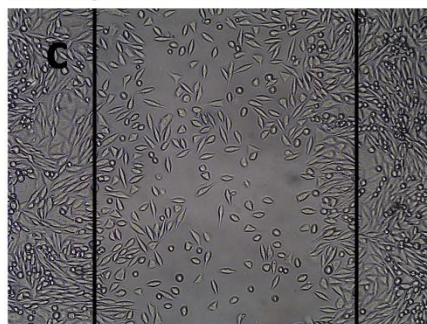
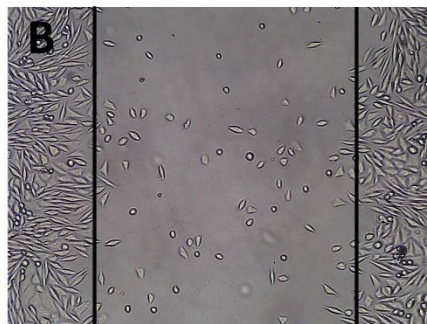


Figure 40: In vitro scratch assay A-D) In vitro scratch assay (A= Before treatment, 0hr; B=after treatment with SRN, 24hr;C= after treatment with guar gum nanoformulation of Syringic acid (NF1);24hr) * $p < 0.05$

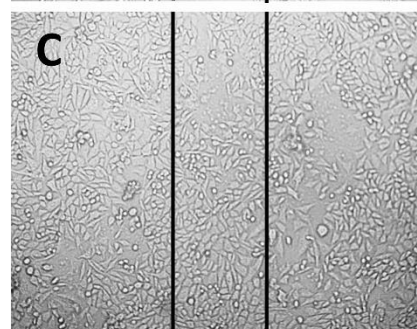
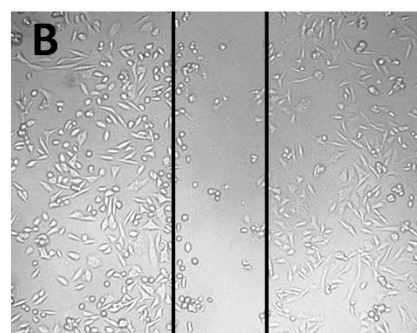
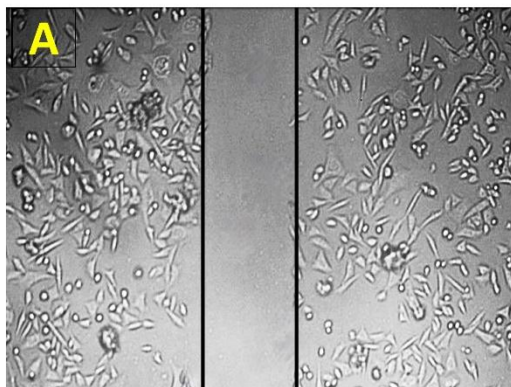


Figure 41: In vitro scratch assay A-D) In vitro scratch assay (A= Before treatment, 0hr; B=after treatment with SNP, 24hr;C= after treatment with guar gum nanoformulation of Sinapic acid (NF2);24 hr) * $p < 0.05$

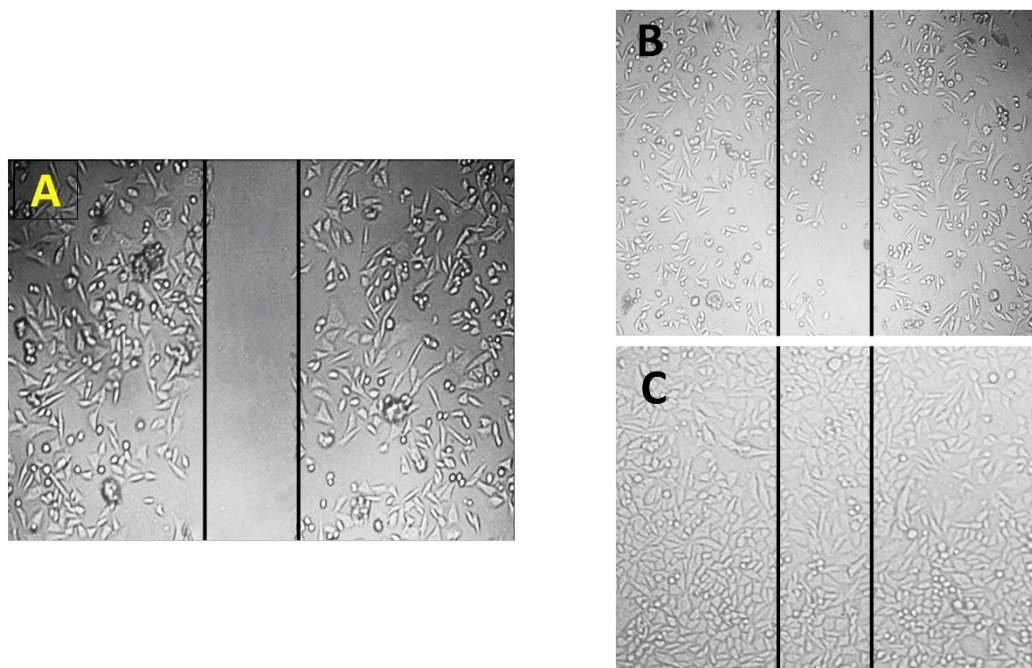


Figure 42: In vitro scratch assay A-D) In vitro scratch assay (A= Before treatment, 0hr; B=after treatment with OCA, 24hr; C= after treatment with guar gum nanoformulation of o-Coumaric acid (NF3);24 hr) * $p < 0.05$

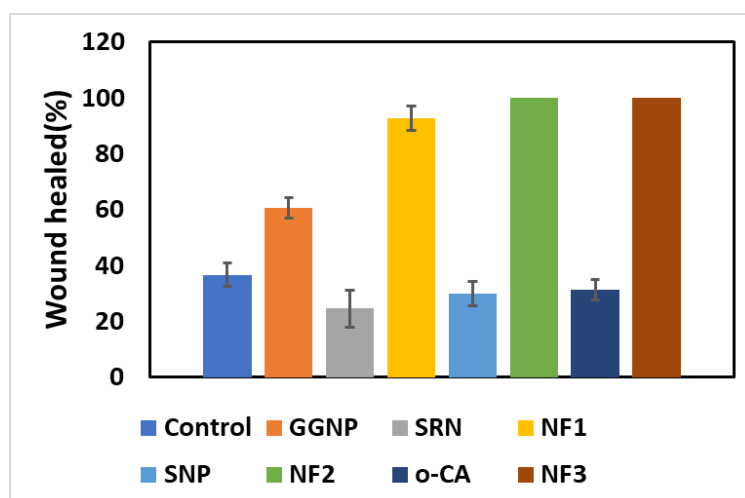


Figure 43: Graphical representation of in-vitro scratch assay of all samples. All values are expressed as mean \pm standard error of the mean (SEM) (n=3). * $p < 0.05$

6.14.5 Tube formation assay

The tube formation assay results show the tube lengths (in μm) for different formulations compared to a control. The control group has a tube length of 115.99 μm . SRN has a similar tube length at 112.34 μm . optimized nanoformulation of Syringic acid (NF1) shows an increased tube length of 192.53 μm , and SNA has a tube length of 131.43 μm . optimized

nanoformulation of Sinapic acid (NF2) exhibits a tube length of 209.37 μm , and OCA measures 123.43 μm (Figure 44). optimized nanoformulation of o-Coumaric acid (NF3) demonstrates the most extended tube length at 241.6 μm . These results suggest that guar gum nanoformulation of Syringic acid (NF1), guar gum nanoformulation of Sinapic acid (NF2), and optimized nanoformulation of o-Coumaric acid (NF3) significantly enhance tube formation compared to the control and other formulations. The tube formation assay results show the number of meshes and tubes formed for different formulations compared to a control. The control group has three meshes and seven tubes. SRN has a similar number of meshes at 3, with six tubes. Optimized nanoformulation of Syringic acid (NF1) significantly increases in ten meshes and 19 tubes. SNA has four meshes and eight tubes, while optimized nanoformulation of Sinapic acid (NF2) shows ten and 21 tubes. OCA results in 6 meshes and ten tubes. optimized nanoformulation of o-Coumaric acid (NF3) exhibits the highest values, with 14 meshes and 25 tubes. Overall, guar gum nanoformulation of Syringic acid (NF1), guar gum nanoformulation of Sinapic acid (NF2), and optimized nanoformulation of o-Coumaric acid (NF3) demonstrate a higher capacity for tube formation than the control (Figure 45).

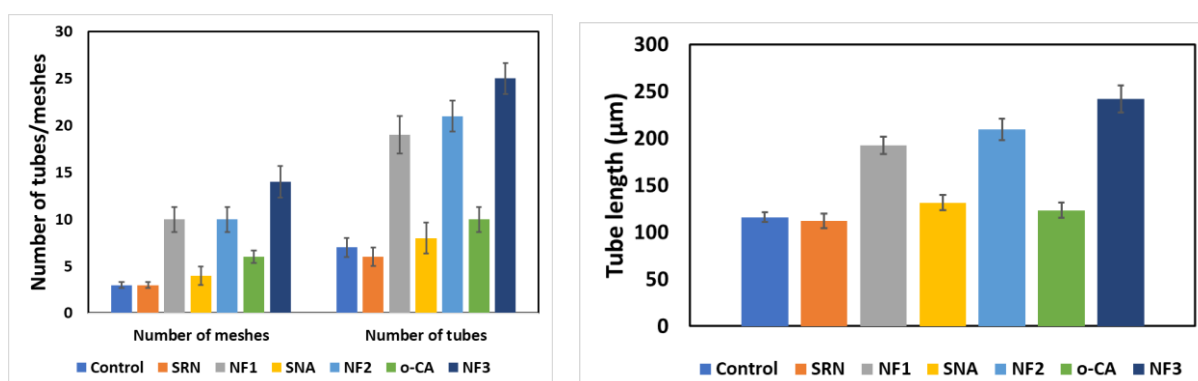


Figure 44: Graphical representation of all tube-formation assay. All values are expressed as mean \pm standard error of the mean (SEM) (n=3). *p<0.05

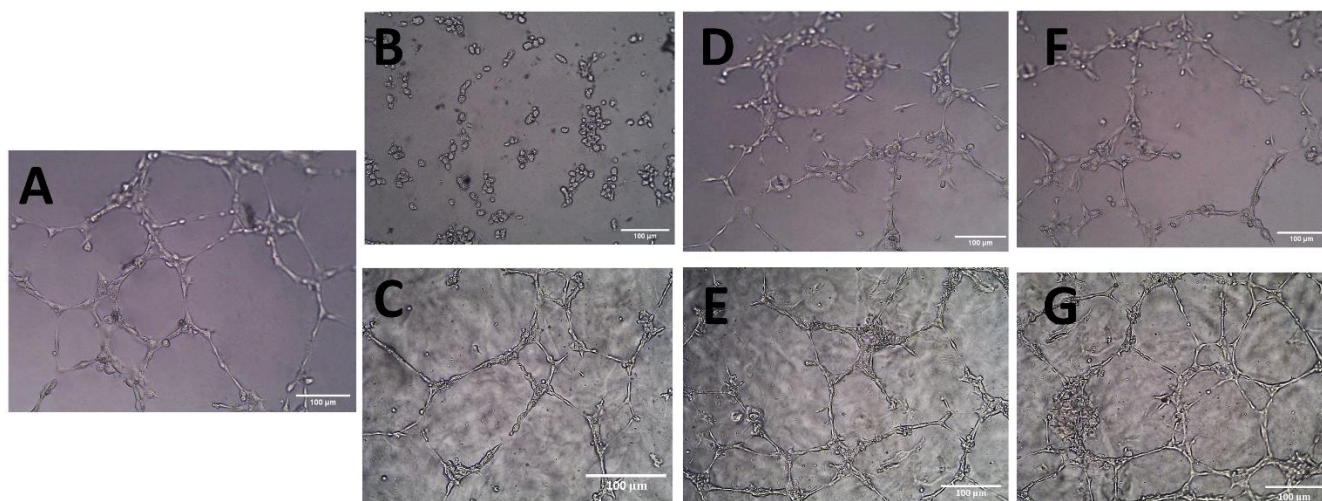


Figure 45: Photographs of Tube formation after being treated with different samples (A-Control, B-SRN, C-guar gum nanoformulation of Syringic acid (NF1), D-SNP, E-guar gum nanoformulation of Sinapic acid (NF2), F-OCA, G-guar gum nanoformulation of o-Coumaric acid (NF3))* $p < 0.05$

6.14.6 In vitro oxidative biomarkers analysis

The protein content (BSA) was quantified using the procedure described by Lowry et al.1951, employing a standard curve established with BSA (Figure 46). Assessing the quantity of total protein in the sample before initiating the assay is crucial, as the percentage of total protein content serves as a parameter for defining enzyme activity.

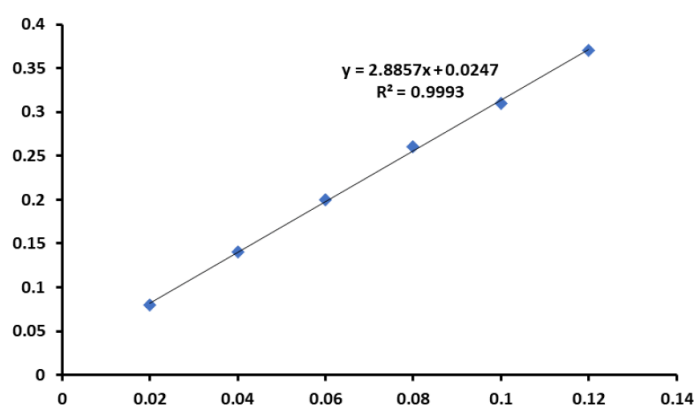


Figure 46: Protein estimation using the Lowry method

➤ Lipid peroxidation (LPO) activity

The in vitro lipid peroxidation (LPO) activity was measured in various treated groups. The control group exhibited the lowest LPO activity at 4.88 µMoles MDA/mg protein, while the

hyperglycaemic group showed significantly higher activity at 37.37 μ Moles MDA/mg protein. Guar gum nanoparticles (GGNP) under hyperglycaemic conditions demonstrated reduced LPO activity, with high-dose (HD) and low-dose (LD) treatments showing 12.76 and 15.63 μ Moles MDA/mg protein, respectively. Similarly, SRN under hyperglycaemic conditions showed LPO activities of 24.33 μ Moles MDA/mg protein (HD) and 27.53 μ Moles MDA/mg protein (LD). SNP treatments also reduced LPO activity, with high-dose and low-dose groups exhibiting 19.57 and 23.2 μ Moles MDA/mg protein, respectively. OCA treatments showed LPO activities of 20.23 μ Moles MDA/mg protein (HD) and 22.97 μ Moles MDA/mg protein (LD). Nanoformulations (guar gum nanoformulation of Syringic acid (NF1), guar gum nanoformulation of Sinapic acid (NF2), and guar gum nanoformulation of o-Coumaric acid (NF3)) under hyperglycaemic conditions showed significantly reduced LPO activities. For guar gum nanoformulation of Syringic acid (NF1), the high and low doses resulted in LPO activities of 4.53 and 5.43 μ Moles MDA/mg protein, respectively. optimized nanoformulation of Sinapic acid (NF2) had activities of 5.26 (HD) and 6.33 (LD) μ Moles MDA/mg protein, while optimized nanoformulation of o-Coumaric acid (NF3) showed 5.67 (HD) and 6.4 (LD) μ Moles MDA/mg protein (Figure 47).

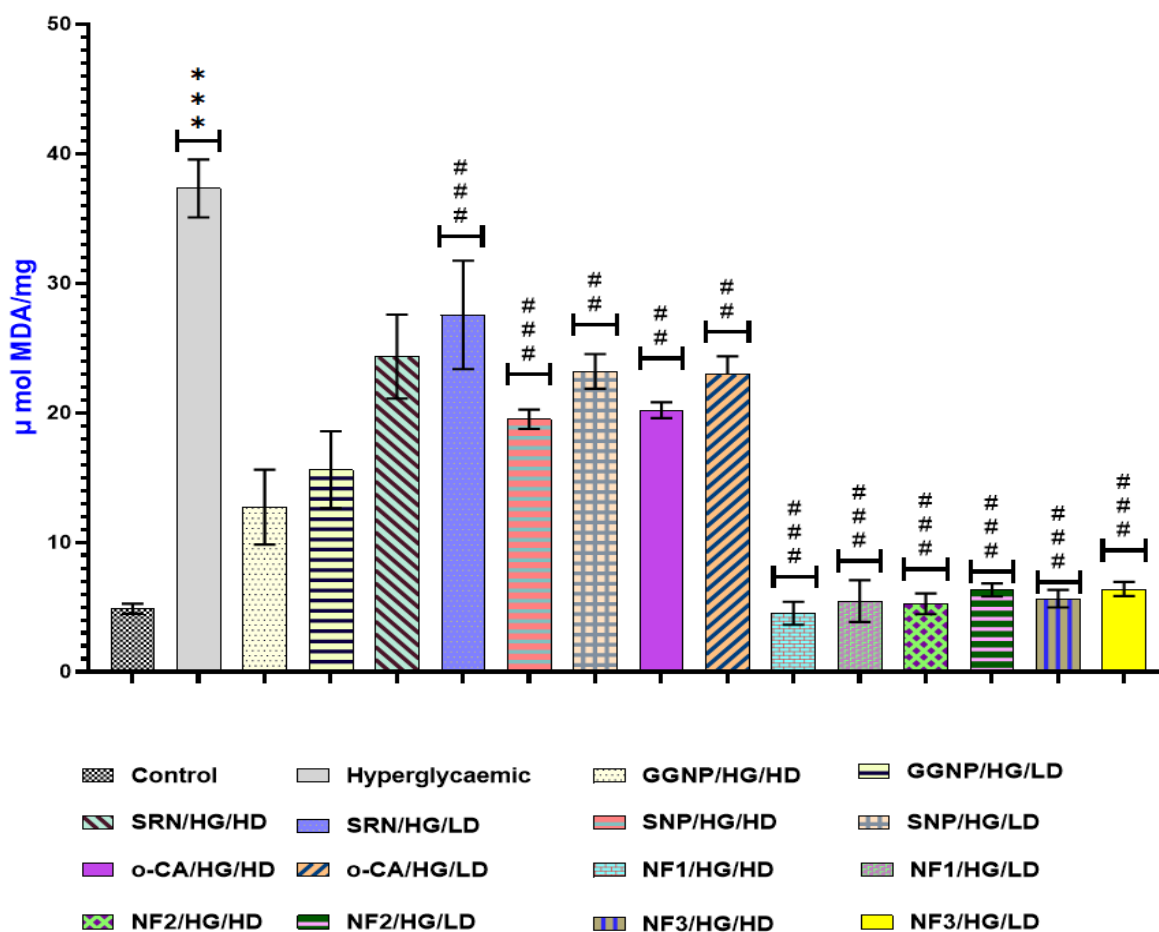


Figure 47: In vitro Lipid peroxidation (LPO) activity of different experimental samples with L929 cell line (All the values are represented as mean \pm S.E.M. (n=3) ***p<0.001, **p<0.01, and *p<0.05, compared to control (Group 1).###p<0.001, ##p<0.01, and #p<0.05, compared to Hyperglycaemic (Group 2)

➤ Catalase

The in vitro catalase activity was measured across various groups, with results expressed in units per milligram (U/mg). The control group had the highest catalase activity at 70.4 U/mg, while the hyperglycaemic group exhibited the lowest activity at 6.67 U/mg. Guar gum nanoparticles (GGNP) in hyperglycaemic conditions showed increased catalase activity, with high-dose (HD) and low-dose (LD) treatments yielding 39.09 and 31.53 U/mg, respectively. SRN treatments under hyperglycaemic conditions had catalase activities of 21.57 U/mg (HD) and 15.29 U/mg (LD). SNP treatments also elevated catalase activity, with high-dose and low-dose groups showing 27.7 and 21.43 U/mg, respectively. OCA treatments resulted in 30.03 U/mg (HD) catalase activities and 21.29 U/mg (LD). Under hyperglycaemic conditions,

nanoformulations (guar gum nanoformulation of Syringic acid (NF1), guar gum nanoformulation of Sinapic acid (NF2), and guar gum nanoformulation of o-Coumaric acid (NF3)) significantly boosted catalase activity. For guar gum nanoformulation of Syringic acid (NF1), high and low doses resulted in activities of 57.85 and 47.48 U/mg, respectively. Optimized nanoformulation of Sinapic acid (NF2) had activities of 64.83 (HD) and 56.15 (LD) U/mg, while optimized nanoformulation of o-Coumaric acid (NF3) showed 66.19 (HD) and 59.15 (LD) U/mg (Figure 48). The results indicate that various treatments, especially nanoformulations, significantly enhance catalase activity compared to the hyperglycaemic condition, suggesting potential antioxidative benefits.

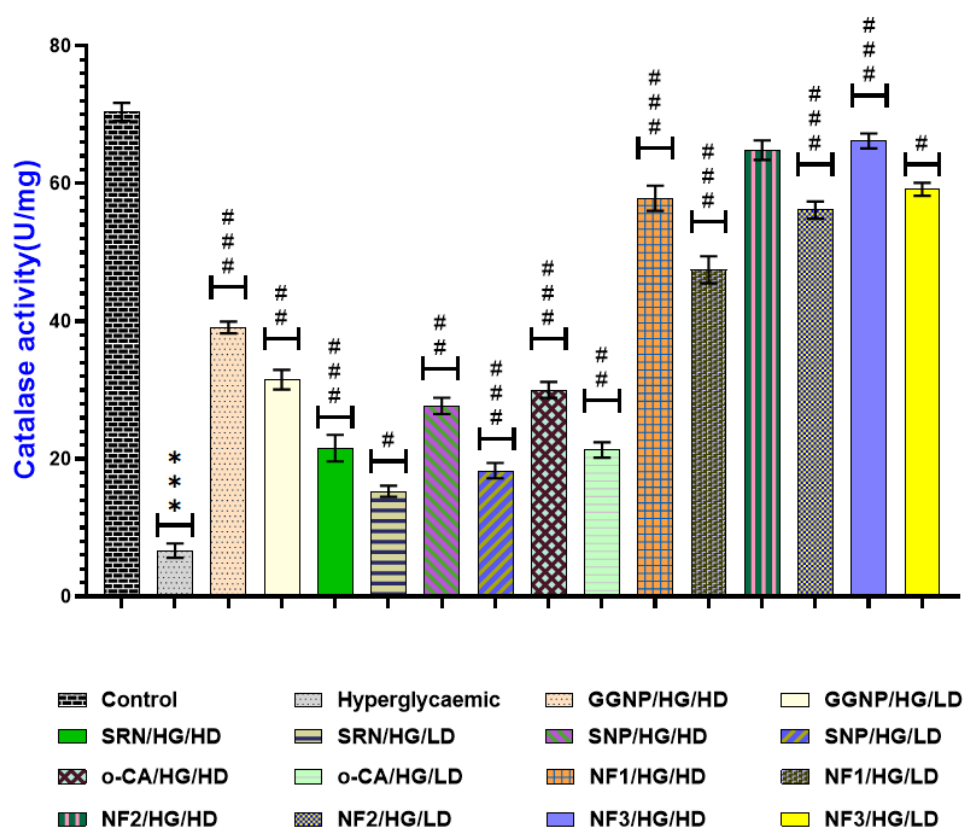


Figure 48: In vitro Catalase activity of different experimental samples with L929 cell line (All the values are represented as mean \pm S.E.M. (n=3) ***p<0.001, **p<0.01 and *p<0.05, vs control (Group 1), ###p<0.001, ##p<0.01 and #p<0.05, vs Hyperglycaemic (Group 2))

➤ Superoxide dismutase (SOD)

The in vitro superoxide dismutase (SOD) activity was assessed across various groups, with the results expressed in units per milligram (U/mg). The control group demonstrated the highest SOD activity at 210.07 U/mg, whereas the hyperglycaemic group had the lowest

activity at 29.37 U/mg. Guar gum nanoparticles (GGNP) under hyperglycaemic conditions showed increased SOD activity, with high-dose (HD) and low-dose (LD) treatments resulting in 130.77 and 122.93 U/mg, respectively. SRN treatments in hyperglycaemic conditions had SOD activities of 92.53 U/mg (HD) and 75.53 U/mg (LD). SNP treatments also enhanced SOD activity, with high-dose and low-dose groups exhibiting 101.37 and 86.83 U/mg, respectively. OCA treatments resulted in SOD activities of 107.61 U/mg (HD) and 97.54 U/mg (LD). Nanoformulations (guar gum nanoformulation of Syringic acid (NF1), guar gum nanoformulation of Sinapic acid (NF2), and guar gum nanoformulation of o-Coumaric acid (NF3)) under hyperglycaemic conditions significantly boosted SOD activity. optimized nanoformulation of Syringic acid (NF1) showed activities of 188.47 U/mg (HD) and 184.69 U/mg (LD), optimized nanoformulation of Sinapic acid (NF2) demonstrated 185.13 (HD) and 177.69 (LD) U/mg, while optimized nanoformulation of o-Coumaric acid (NF3) exhibited 192.46 (HD) and 186.36 (LD) U/mg (Figure 49). These results indicate that various treatments, particularly nanoformulations, significantly enhance SOD activity compared to the hyperglycaemic condition, suggesting potential antioxidative properties.

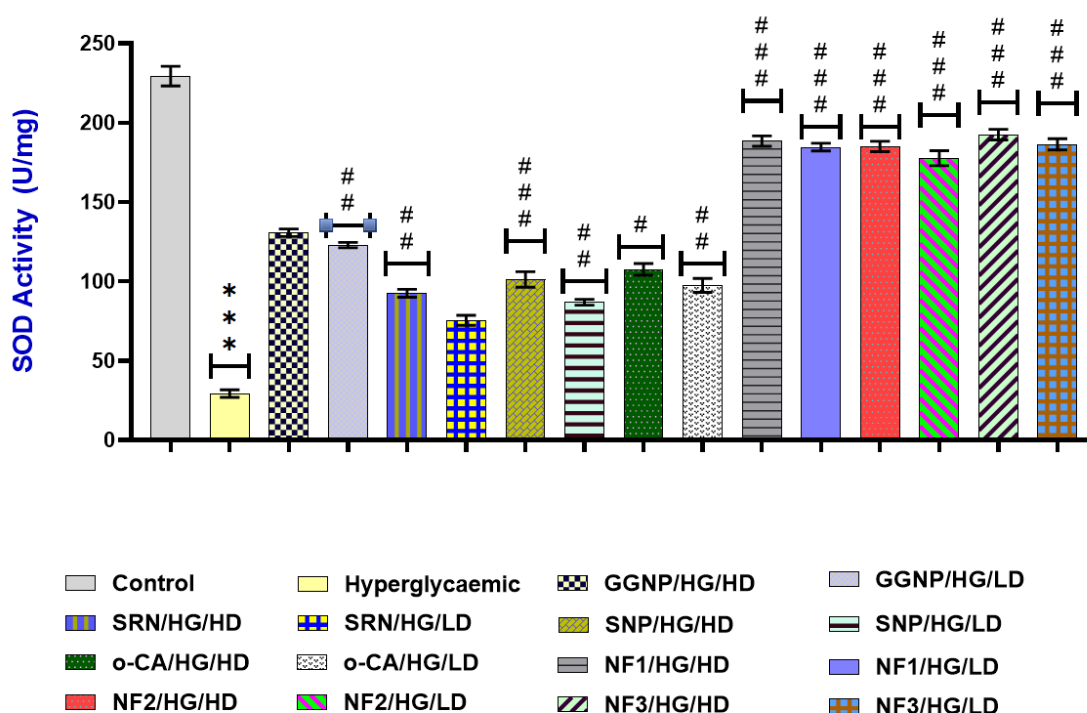


Figure 49: In vitro Superoxide dismutase (SOD) activity of different experimental samples with L929 cell line (All the values are represented as mean \pm S.E.M. (n=3) ***p<0.001, **p<0.01, and *p<0.05, compared to control (Group 1).###p<0.001, ##p<0.01, and #p<0.05, compared to Hyperglycaemic (Group 2))

➤ **Glutathione S-transferase (GST)**

The in vitro glutathione S-transferase (GST) activity was measured across various groups, with results expressed in units per milligram (U/mg). The control group exhibited the highest GST activity at 27.02 U/mg, while the hyperglycaemic group showed significantly reduced activity at 5.13 U/mg. Guar gum nanoparticles (GGNP) in hyperglycaemic conditions increased GST activity, with high-dose (HD) and low-dose (LD) treatments resulting in 16.02 and 14.19 U/mg, respectively. SRN treatments under hyperglycaemic conditions had GST activities of 11.65 U/mg (HD) and 10.26 U/mg (LD). SNP treatments showed slightly elevated GST activity, with high-dose and low-dose groups displaying 10.88 and 9.60 U/mg, respectively. OCA treatments had GST activities of 12.88 U/mg (HD) and 10.26 U/mg (LD). Under hyperglycaemic conditions, nanoformulations (guar gum nanoformulation of Syringic acid (NF1), guar gum nanoformulation of Sinapic acid (NF2), and guar gum nanoformulation of o-Coumaric acid (NF3)) significantly enhanced GST activity. optimized nanoformulation of Syringic acid (NF1) showed activities of 24.86 U/mg (HD) and 19.60 U/mg (LD), optimized nanoformulation of Sinapic acid (NF2) exhibited 22.19 (HD) and 18.23 (LD) U/mg, while optimized nanoformulation of o-Coumaric acid (NF3) demonstrated 24.16 (HD) and 20.13 (LD) U/mg (Figure 50). The results indicate that various treatments, especially nanoformulations, markedly increase GST activity compared to the hyperglycaemic condition, suggesting their potential antioxidative properties.

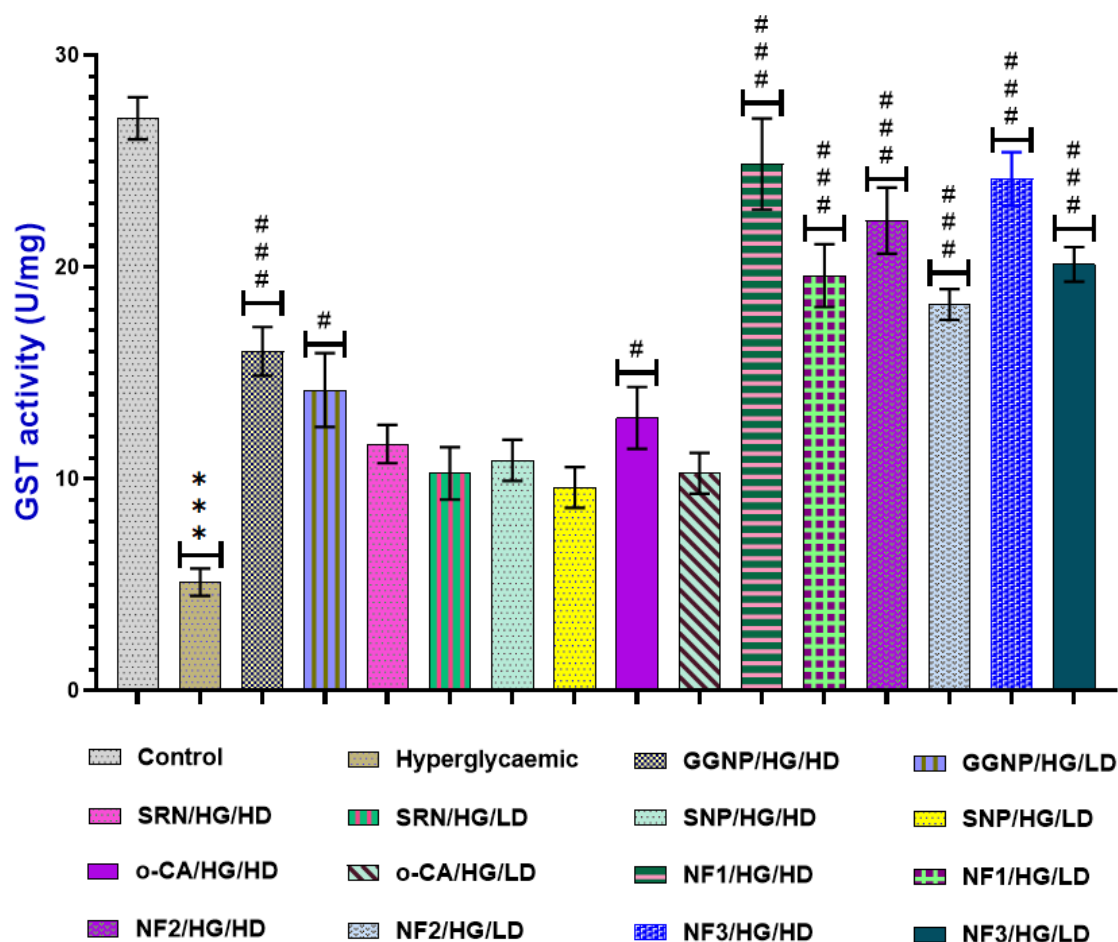


Figure 50: In vitro Glutathione S-transferase (GST) activity of different experimental samples with L929 cell line (All the values are represented as mean \pm S.E.M. (n=3) ***p<0.001, **p<0.01, and *p<0.05, compared to control (Group 1).###p<0.001, ##p<0.01, and #p<0.05, compared to Hyperglycaemic (Group 2))

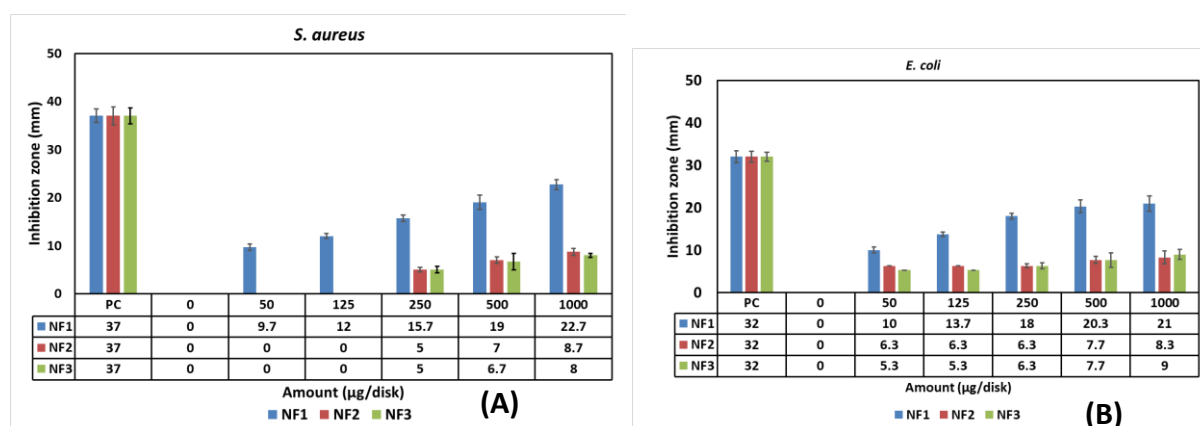
6.15 Antimicrobial tests

6.15.1 Antimicrobial assay

All the nanoformulations exhibited inhibition against *S. aureus* that varied depending on the concentration. Significant inhibition zones were observed where the concentration was evaluated at its highest point of 1000 μ g/disk. The average diameters for guar gum nanoformulation of Syringic acid (NF1), guar gum nanoformulation of Sinapic acid (NF2), and optimized nanoformulation of o-Coumaric acid (NF3) were 22.7 mm, 8.7 mm, and 8 mm, respectively. A little reduction was observed at lower concentrations of 50 μ g/disk and 125 μ g/disk, indicating an average range of inhibitory zones of 9.7 mm to 12 mm with guar gum

nanoformulation of Syringic acid (NF1). Nevertheless, no inhibitions were observed with optimized nanoformulation of Sinapic acid (NF2) and guar gum nanoformulation of o-Coumaric acid (NF3), as depicted in Figures 51A and 52A.

The mean diameter of the inhibitory zones for *E. coli* was approximately 21 mm, 8.3 mm, and 9 mm for guar gum nanoformulation of Syringic acid (NF1), guar gum nanoformulation of Sinapic acid (NF2), and guar gum nanoformulation of o-Coumaric acid (NF3), correspondingly, at 1000 µg/disk. Figures 51B and 52B show that at a lower concentration of 50 µg/disk, the average inhibition zones for guar gum nanoformulation of Syringic acid (NF1), guar gum nanoformulation of Sinapic acid (NF2), and optimized nanoformulation of o-Coumaric acid (NF3) were 10 mm, 6.3 mm, and 5.3 mm, respectively. For *Candida albicans*, the positive control exhibited a maximal inhibition zone of 23 mm when a dosage of 1000 µg/disk was used. At the maximum dosage, the mean zone inhibitions were approximately 5.7 mm, 19.7 mm, and 5.8 mm for guar gum nanoformulation of Syringic acid (NF1), guar gum nanoformulation of Sinapic acid (NF2), and guar gum nanoformulation of o-Coumaric acid (NF3), respectively. The mean zone of inhibition for guar gum nanoformulation of Syringic acid (NF1), guar gum nanoformulation of Sinapic acid (NF2), and optimized nanoformulation of o-Coumaric acid (NF3) was 5 mm, 17 mm, and 5 mm, correspondingly, at the lowest concentration (50 µg/disk), as demonstrated in Figures 51C and 52C.



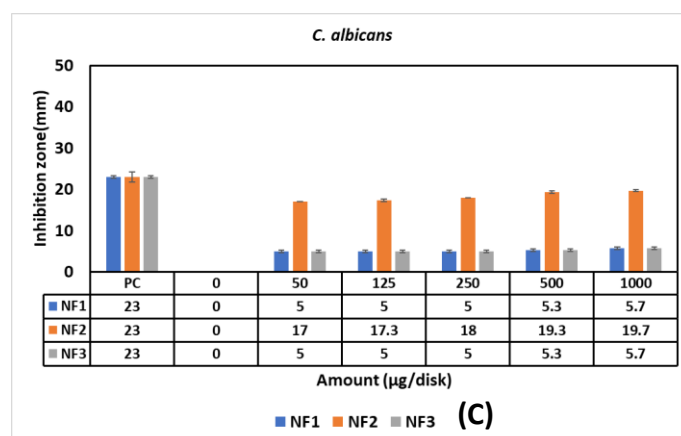


Figure 51- Antimicrobial activity graph of (A): *S. aureus*; (B): *E. coli*; (C): *C. albicans* (All values are expressed as mean \pm standard error of the mean (SEM) (n=3).

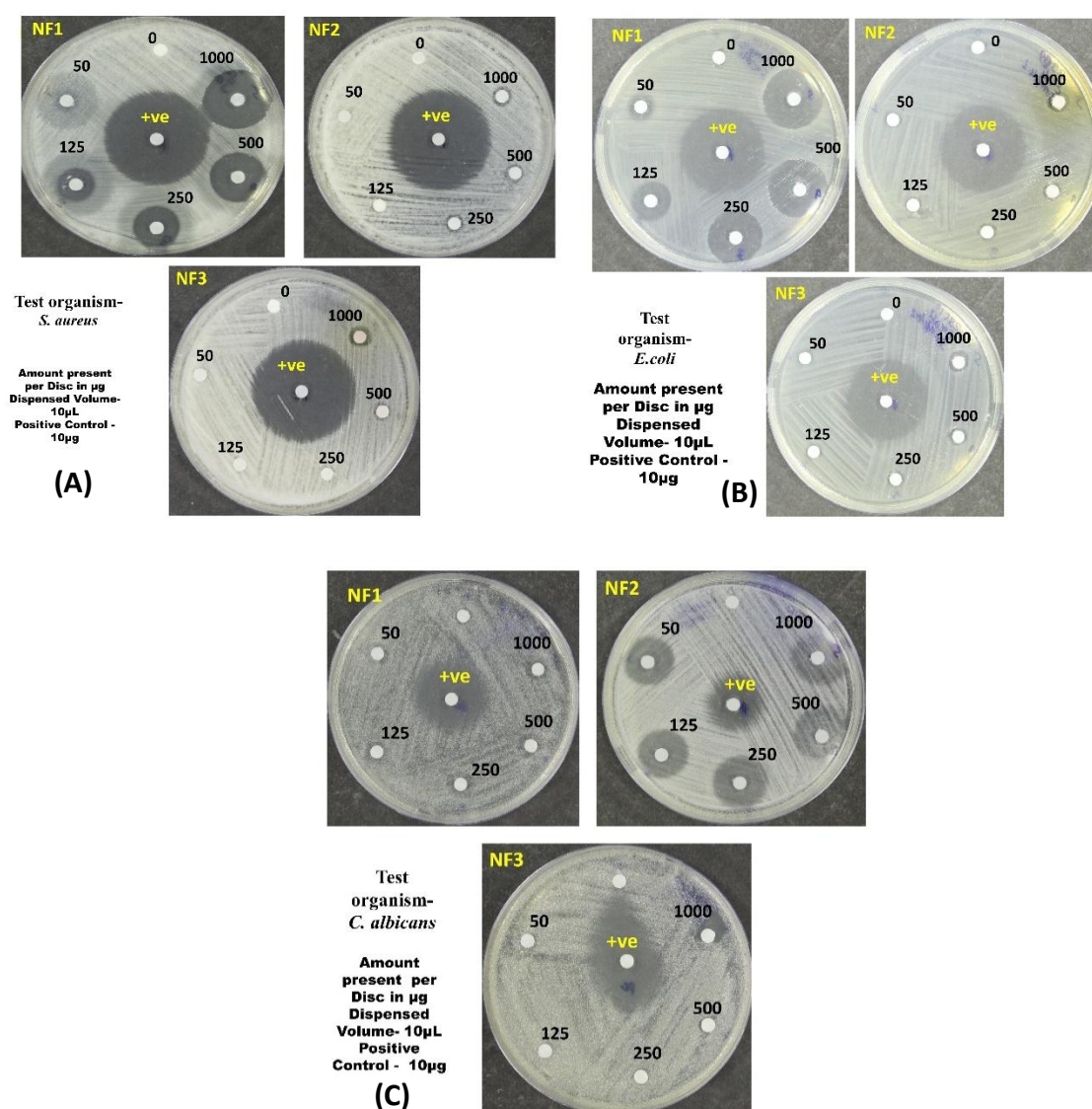


Figure 52- Antimicrobial activity plate of (A) *S. aureus* ; (B) *E. coli*; (C) *C. albicans*. All values are expressed as mean \pm standard error of the mean (SEM) (n=3).

6.15.2 Assessment of Cox-II Activity

The results indicate that the different nanoformulations exhibited varying degrees of Cox-II inhibition at different dosages, as illustrated in Figure 53. optimized nanoformulation of Syringic acid (NF1) consistently showed substantial suppression of Cox-II compared to the control at all doses. The inhibition percentages are 123.67% at a concentration of 50 $\mu\text{g/ml}$, 174.16% at 100 $\mu\text{g/ml}$, and 213.30% at 200 $\mu\text{g/ml}$. Similarly, optimized Sinapic acid (NF2) nanoformulation inhibited Cox-II activity at all doses, although it was slightly less potent than the guar gum nanoformulation of Syringic acid (NF1). Specifically, optimized nanoformulation of Sinapic acid (NF2) inhibited Cox-II activity by 57.34% at 50 $\mu\text{g/ml}$ dosage, 67.50% at 100 $\mu\text{g/ml}$, and 73.80% at 200 $\mu\text{g/ml}$. The nanoformulation optimized nanoformulation of o-Coumaric acid (NF3) had the most inhibitory effectiveness compared to other formulations, with inhibition rates of 189.74% at a concentration of 50 $\mu\text{g/ml}$, 257.16% at 100 $\mu\text{g/ml}$ and 333.30% at 200 $\mu\text{g/ml}$ (Figure 53).

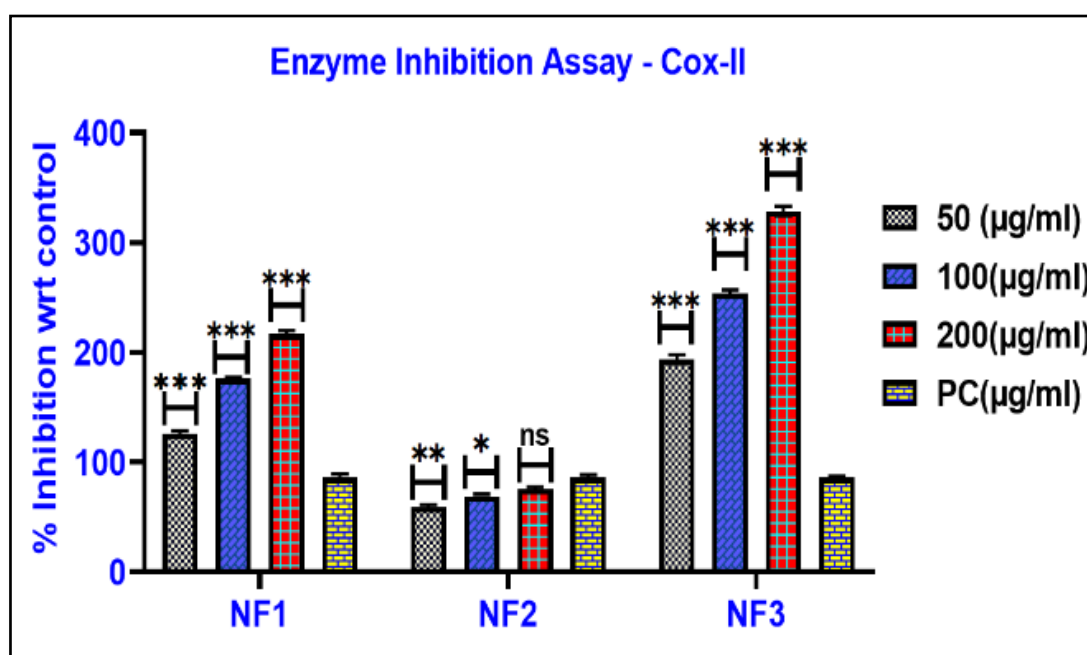


Figure 53: Enzyme Inhibition Assay for Cox-II (All the values are represented as mean \pm S.E.M. (n=3) ***p<0.001, **p<0.01 and *p<0.05, vs control)

6.15.3 TNF- α expression

Unlike the control group, guar gum nanoformulation of Syringic acid (NF1), guar gum nanoformulation of Sinapic acid (NF2), and optimized nanoformulation of o-Coumaric acid (NF3) decrease TNF- α expression to different levels (Figure 54A-D). In the absence of LPS treatment, the TNF- α down-regulation percentage seems to be highest in optimized nanoformulation of o-Coumaric acid (NF3) (38.9%), followed by optimized nanoformulation of Sinapic acid (NF2) (25.9%) and optimized nanoformulation of Syringic acid (NF1) (25.3%) (Figure 35 A, B). In contrast, Figure 35 C, D indicates that the positive control group (LPS-treated cells) had markedly greater levels of TNF- α in comparison to the negative control group (without LPS treatment). Application of NF-1, NF-2, and NF-3 resulted in a substantial decrease in the production of TNF- α . guar gum nanoformulation of Syringic acid (NF1), guar gum nanoformulation of Sinapic acid (NF2), and optimized nanoformulation of o-Coumaric acid (NF3) exhibit significantly more downregulation in TNF- α expression after bacterial infections, with downregulation percentages of 25.9%, 34.7%, and 46.9%, respectively, compared to the control group.

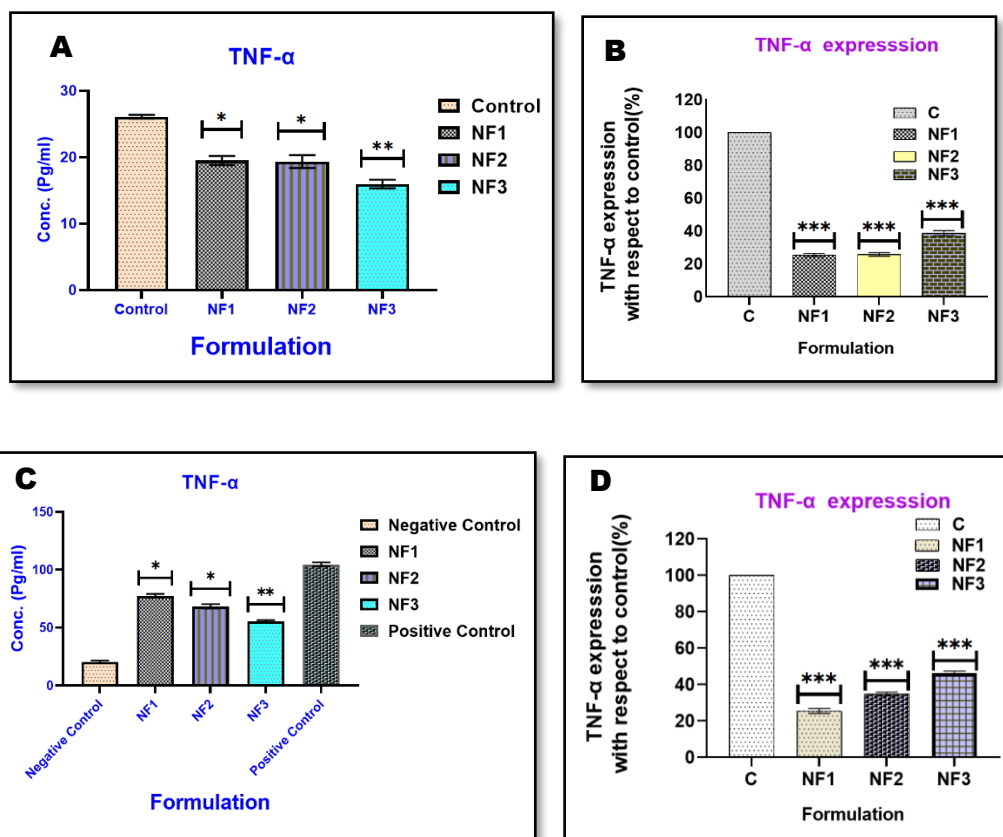


Figure 54: A)-B) The protein expression of TNF- α is decreased in the presence of bacterial infection compared to the control group without infection, C)-D) Protein Expression (downregulation) of TNF- α concerning (wrt) control (with bacterial infection) (positive control group (with LPS treatment), the negative control group (cells without LPS treatment)) (All the values are represented as mean \pm S.E.M. (n=3) ***p<0.001, **p<0.01 and *p<0.05, vs control)

6.16 In vivo results

Given the promising antioxidant, anti-diabetic, and wound-healing properties demonstrated by both formulations in our in vitro findings, we opted to evaluate the potential of only the two best formulations, nanoformulation of Sinapic acid (guar gum nanoformulation of Sinapic acid (NF2)) and nanoformulation of o-Coumaric acid (guar gum nanoformulation of o-Coumaric acid (NF3)), in the animal model, as these exhibited more significant results than nanoformulation of Syringic acid (guar gum nanoformulation of Syringic acid (NF1)). For the in vivo study, 60 SD rats were procured and divided into nine groups, and various nutritional supplements, including NPD and HFD, were administered.

6.16.1 Evaluation of DM parameters

➤ Body weight estimation

The body weights were recorded on the 3rd, 7th, 14th, and 29th days, as depicted in Figure 36. The first group with NPD showed less increase in body weight compared to the rest of the HFD feeding groups. Body weight decreased after the induction of diabetes with STZ. The reduced body weights were recorded on the 14th and 29th day in STZ-treated groups, as shown in Figure 55.

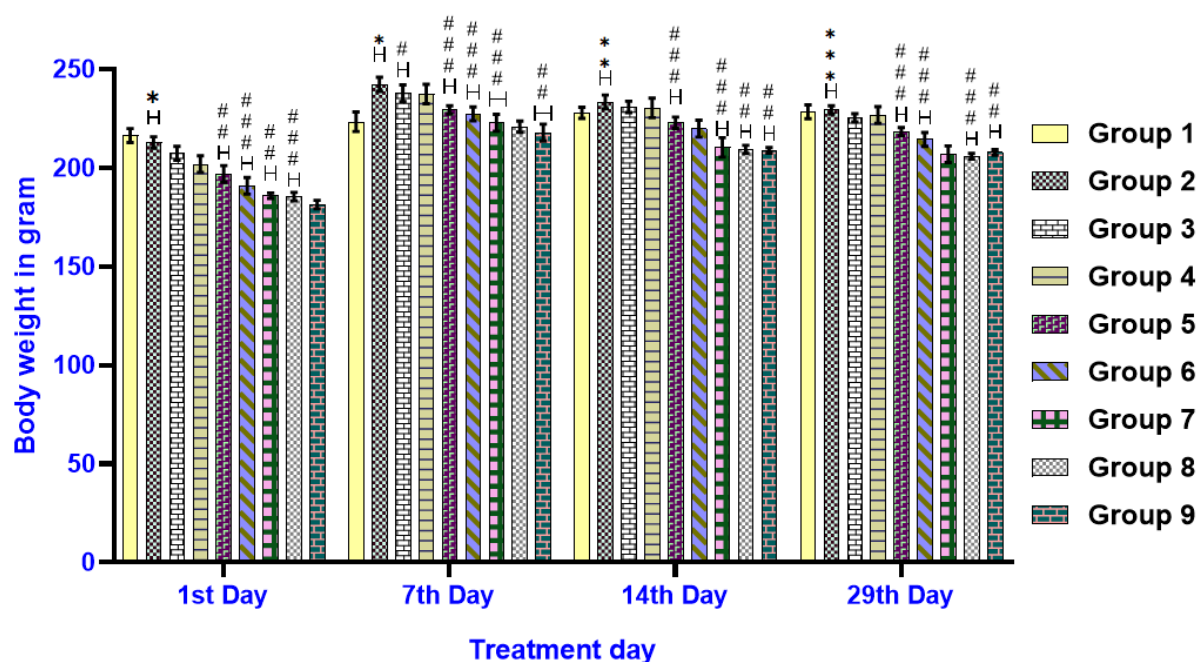


Figure 55: Body weight of groups in different days (All the values are represented as mean \pm S.E.M. (n=3) ***p<0.001, **p<0.01 and *p<0.05, vs control (Group 1), ###p<0.001, ##p<0.01 and #p<0.05, vs placebo (Group 2))

➤ Blood glucose

Blood glucose levels were measured at the initiation of the study (prior to treatment) and its conclusion (treatment) utilising a glucometer (ACCU-CHEK Instant S). In the HFD/STZ-induced diabetic rats, the 40 mg/kg, i.p. dose of STZ led to heightened hyperglycaemia, with blood glucose levels exceeding 250 mg/dl, indicating the onset of diabetes. After the 29th day, the optimized nanoformulation of Sinapic acid (NF2) and guar gum nanoformulation of o-Coumaric acid (NF3) (both high and low dose) exhibited a significant decline in blood glucose levels compared to both control and positive control (Figure 56).

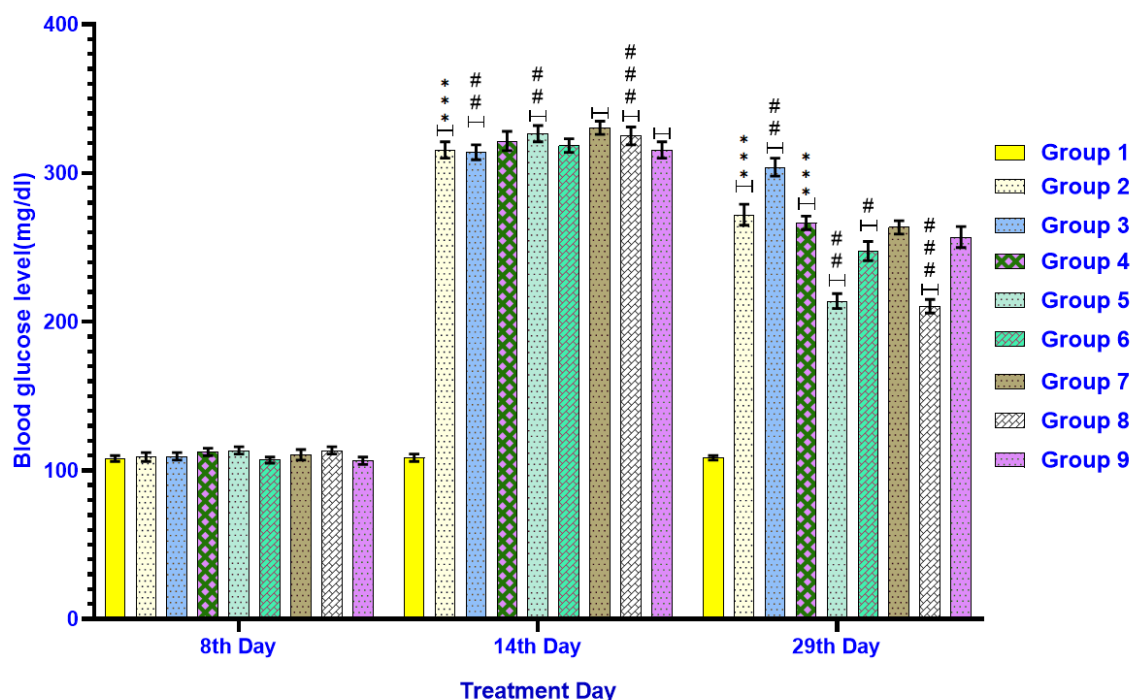


Figure 56: Evaluation of blood glucose on different days (All the values are represented as mean \pm S.E.M. (n=3) ***p<0.001, **p<0.01 and <0.05, vs control (Group 1), ###p<0.001, ##p<0.01 and #p<0.05, vs placebo (Group 2))

6.16.2 Evaluation of Wound Healing Parameters

➤ Effect of nanoformulations on wound contraction

The healing percentages for each group show a clear upward trend from the 3rd to the 14th day of wound creation, indicating the natural progression of wound healing over time. Nanoformulation treatment groups had shown significant improvement with both the high and low doses as compared to control as well as raw drug treatment groups. The healing percentages were relatively low on the 3rd day across all groups. Group 2, treated with placebo nanoformulation, showed the lowest healing percentage at 8.63% and Group 8, i.e., guar gum nanoformulation of Sinapic acid (NF2), the highest at 24%. By the 7th day, significant improvement was evident across all groups. Group 8 leads with 55.63%, while Group 4 has the lowest percentage at 38.75%. This day marks a substantial increase in healing for most groups, suggesting that the treatments became more effective as time progressed. The trend continues on the 10th day, where Group 8 maintains the highest healing percentage at 85.13%, closely followed by Group 5 at 83.13%. Group 4, despite showing improvement, remains the lowest at 57.5%. This stage indicated that most groups are experiencing rapid healing, likely due to the cumulative effect of the treatments administered. By the 14th day, several groups have

achieved near-complete or complete healing. Groups 1, 5 and 8 reach 100% healing, highlighting their effective healing processes. In contrast, Group 2, despite improving significantly from its initial stages, records the lowest percentage of 73.5%. Groups 6 and 9 also had shown impressive healing percentages of 96.88% and 97.38%, respectively (Figure 57).

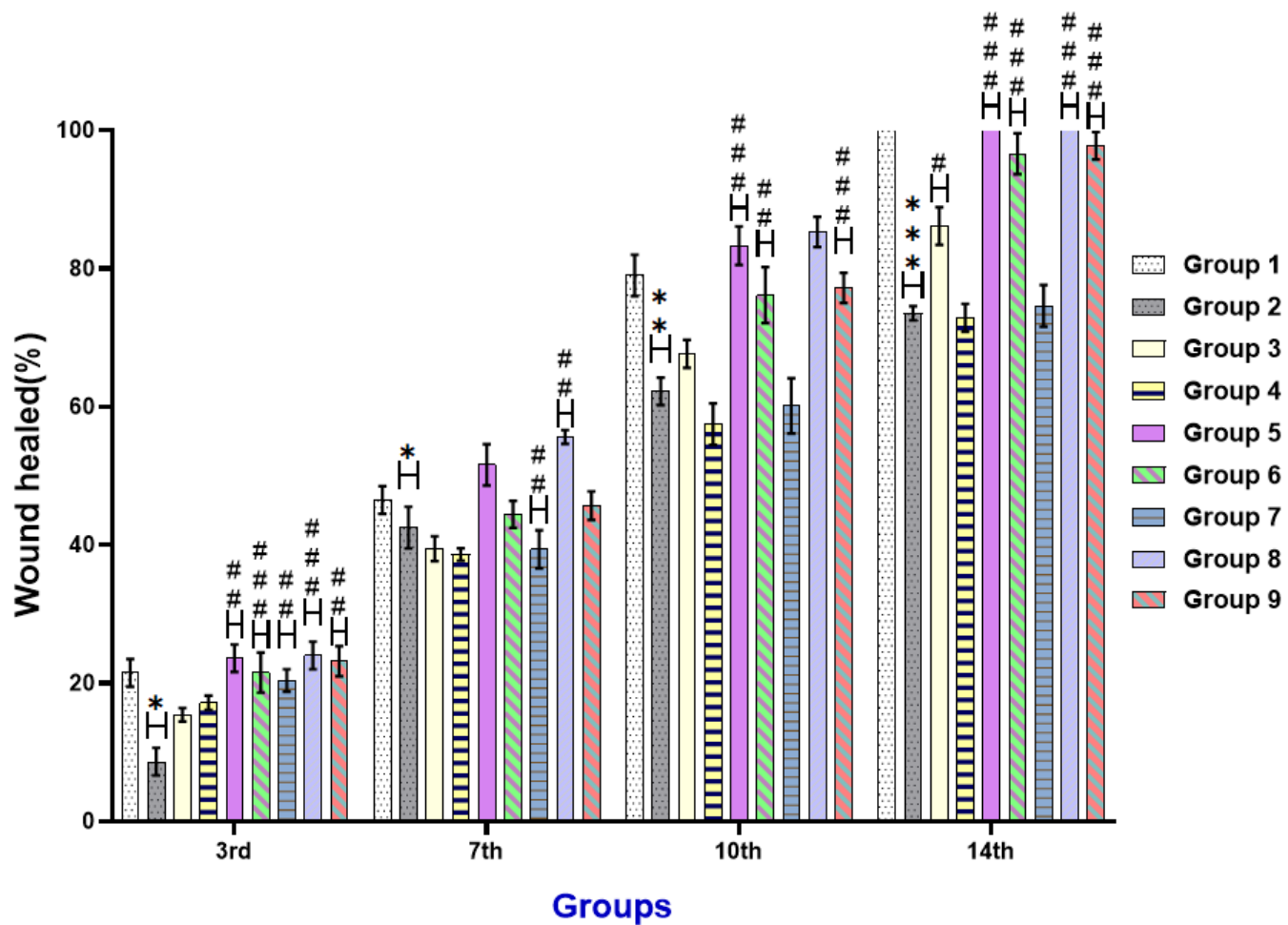




















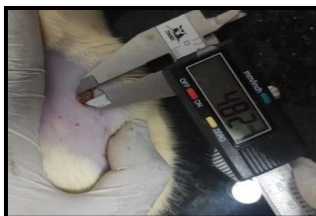


Figure 57: Graphical representation of wound healing in different in vivo experimental groups (All the values are represented as mean \pm S.E.M. (n=3) ***p<0.001, **p<0.01 and *p<0.05, vs control (Group 1), ###p<0.001, ##p<0.01 and #p<0.05, vs placebo (Group 2))

Table 17.1: Photographic representation of wound healing on different days (0, 3rd, 7th)

Group	Day 0	Day 3	Day 7
Group 1			
Group 2			
Group 3			
Group 4			
Group 5			
Group 6			
Group 7			








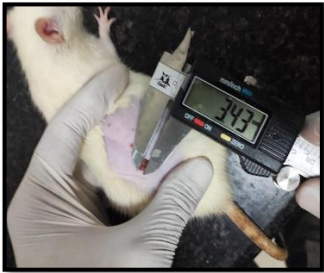











Group 8			
Group 9			

Table 17.2: Photographic representation of wound healing on different days (10th, 14th)

Groups	Day 10	Day 14
Group 1		
Group 2		
Group 3		

Group 4		
Group 5		
Group 6		
Group 7		
Group 8		
Group 9		

➤ Tensile strength

The non-diabetic control group (Group 1) demonstrated a tensile strength of 27 MPa. In contrast, the placebo-treated group had a lower tensile strength of 12.965 MPa. The positive control group displayed a slightly higher tensile strength of 18.825 MPa than the placebo group, indicating modest improvement. The raw drug-treated groups (Groups 4 and 7) showed improved tensile strength of 15.12 MPa and 18.19 MPa, respectively, compared to the placebo and positive control groups. Conversely, the nanoformulation-treated groups exhibited significant improvements. The guar gum nanoformulation of Sinapic acid (NF2)-treated groups demonstrated tensile strengths of 25.38 MPa and 23.845 MPa for high and low doses, respectively. The guar gum nanoformulation of o-Coumaric acid (NF3)-treated groups showed even better tensile strengths of 26.23 MPa and 24.78 MPa for high and low doses. These findings underscore the superior efficacy of optimized nanoformulation of Sinapic acid (NF2) and optimized nanoformulation of o-Coumaric acid (NF3) in enhancing tensile strength, highlighting its potential for improving wound healing outcomes.

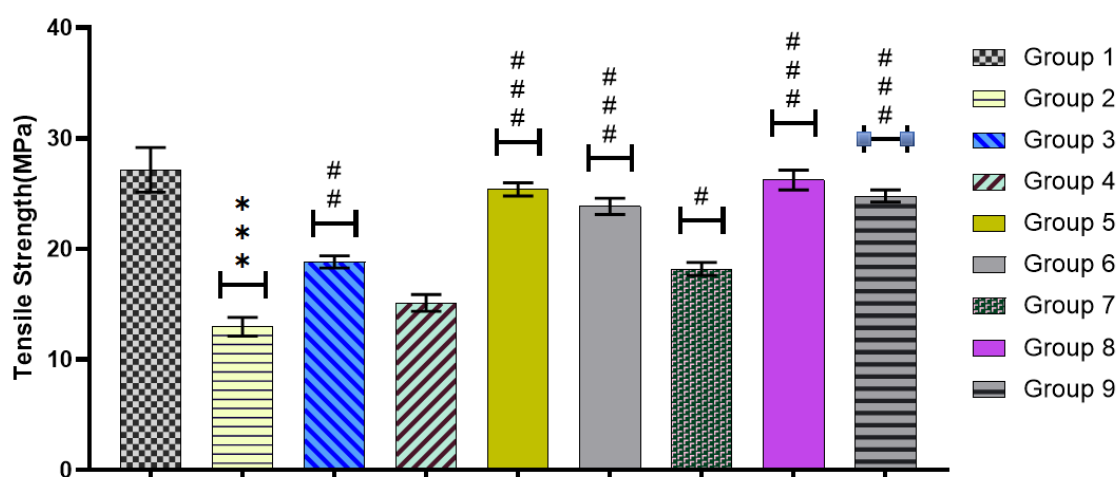


Figure 58: Graphical representation of tensile strength of wound healing in different in vivo experimental groups (All the values are represented as mean \pm S.E.M. (n=3) ***p<0.001, **p<0.01 and *p<0.05, vs control (Group 1), ###p<0.001, ##p<0.01 and #p<0.05, vs placebo (Group 2))

6.16.3 Protein estimation in tissue homogenate using Lowry's method

The total protein content, crucial for expressing enzyme-specific activity, is determined using the established technique described by Lowry et al. (Figure 59)

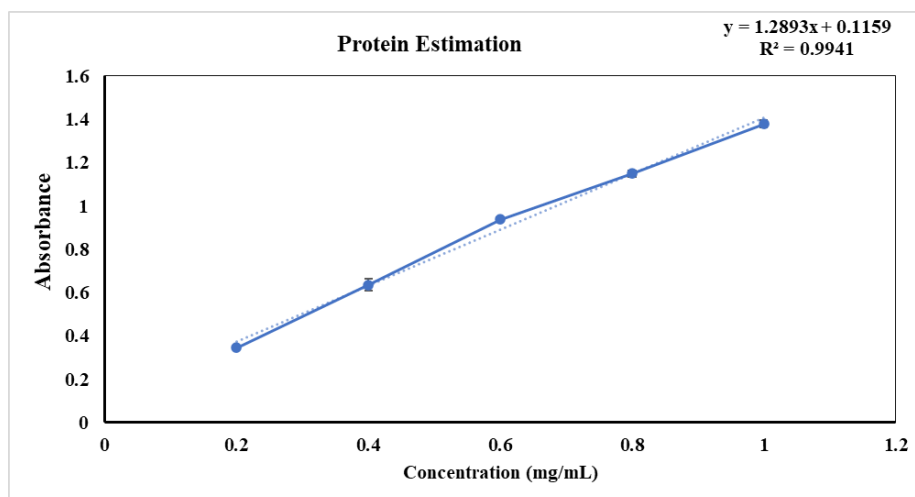


Figure 59: Protein estimation using the Lowry method

6.16.4 In vivo oxidative biomarkers analysis

➤ LPO

Excessive LPO can result from hyperglycaemia. Consequently, we aimed to assess the extent of LPO in the skin tissues of experimental groups. The non-diabetic control group exhibited a relatively low lipid peroxidation (LPO) level, precisely 0.0291 $\mu\text{mol MDA/mg}$. In contrast, all diabetic groups demonstrated elevated LPO levels. Notably, the placebo nanoformulation group (Group 2) exhibited the highest LPO activity among all treatment groups. The positive control group, group three, effectively reduced the LPO level to 0.0591 $\mu\text{mol MDA/mg}$, indicating a moderate improvement. Treatment with the raw drug (Groups 4 and 7) slightly reduced LPO levels to 0.0625 and 0.0593 $\mu\text{mol MDA/mg}$, respectively. In comparison, the nanoformulation treatment groups significantly decreased LPO levels. Specifically, the guar gum nanoformulation of Sinapic acid (NF2)-treated groups achieved LPO levels of 0.0338 and 0.03635 $\mu\text{mol MDA/mg}$ for high and low doses, respectively. The guar gum nanoformulation of o-Coumaric acid (NF3)-treated groups demonstrated LPO levels of 0.03125 and 0.0329 $\mu\text{mol MDA/mg}$ for high and low doses, respectively. These results indicate that treatment with optimized nanoformulation of Sinapic acid (NF2) and optimized nanoformulation of o-Coumaric acid (NF3) at both dosage levels significantly mitigated oxidative stress by reducing LPO (MDA levels) in diabetic rats (Figure 60).

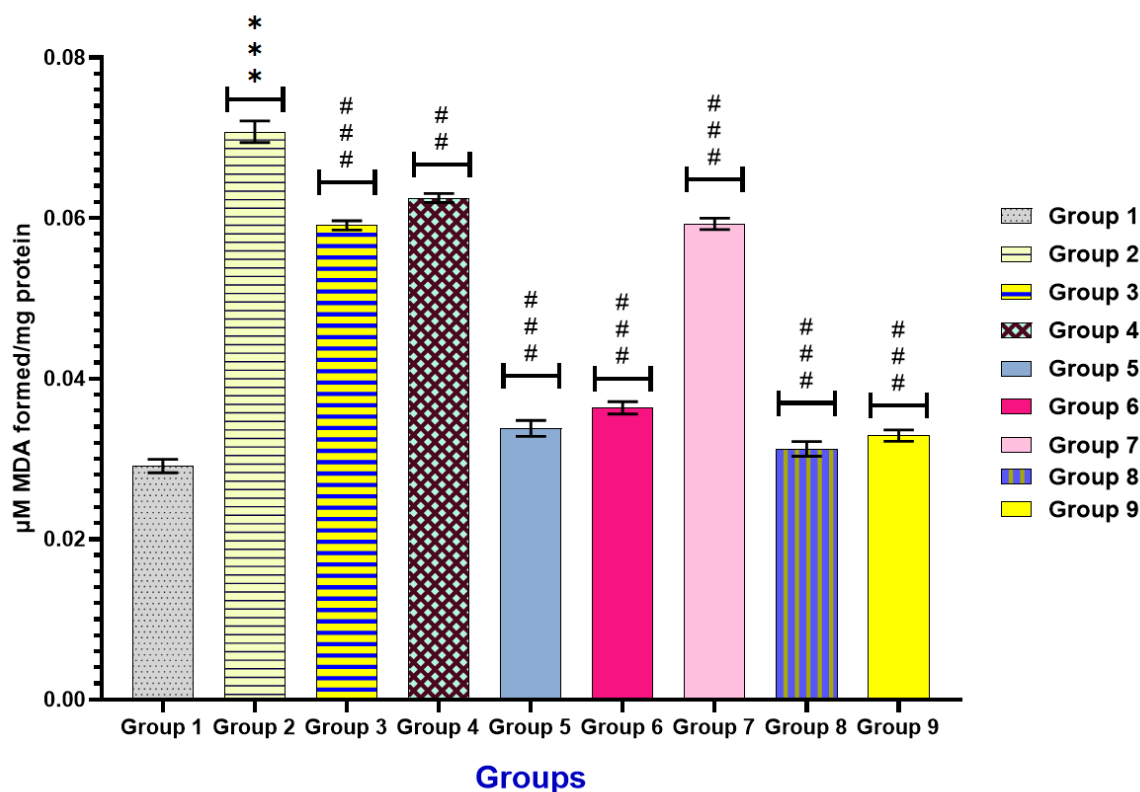


Figure 60: In vivo Lipid peroxidation (LPO) activity of skin of different experimental groups (All the values are represented as mean \pm S.E.M. (n=3) ***p<0.001, **p<0.01 and *p<0.05, vs control (Group 1), ###p<0.001, ##p<0.01 and #p<0.05, vs placebo (Group 2))

➤ Catalase

Chronic hyperglycaemia has been linked to reduced catalase levels. Thus, we aimed to examine the catalase levels in the skin tissues of the treatment groups.

The non-diabetic control group (Group 1) exhibited a significantly high catalase activity of 3.655 U/mg compared to the other groups. The placebo-treated group displayed a lower catalase activity of 2.455 U/mg, attributed mainly to oxidative stress under diabetic conditions. The positive control group showed a slightly higher catalase activity of 2.495 U/mg than the placebo group.

In contrast, the nanoformulation-treated groups demonstrated a marked improvement in catalase activity. The guar gum nanoformulation of Sinapic acid (NF2)-treated groups exhibited catalase activity of 3.265 and 3.165 U/mg for high and low doses, respectively. The guar gum nanoformulation of o-Coumaric acid (NF3)-treated groups showed catalase activity of 3.345 and 3.22 U/mg for high and low doses, respectively. These findings indicate that the

optimized nanoformulation of o-Coumaric acid (NF3) treatment nearly restored normal catalase levels and significantly reduced the risk of oxidative stress by enhancing catalase activity in diabetic rats (Figure 61).

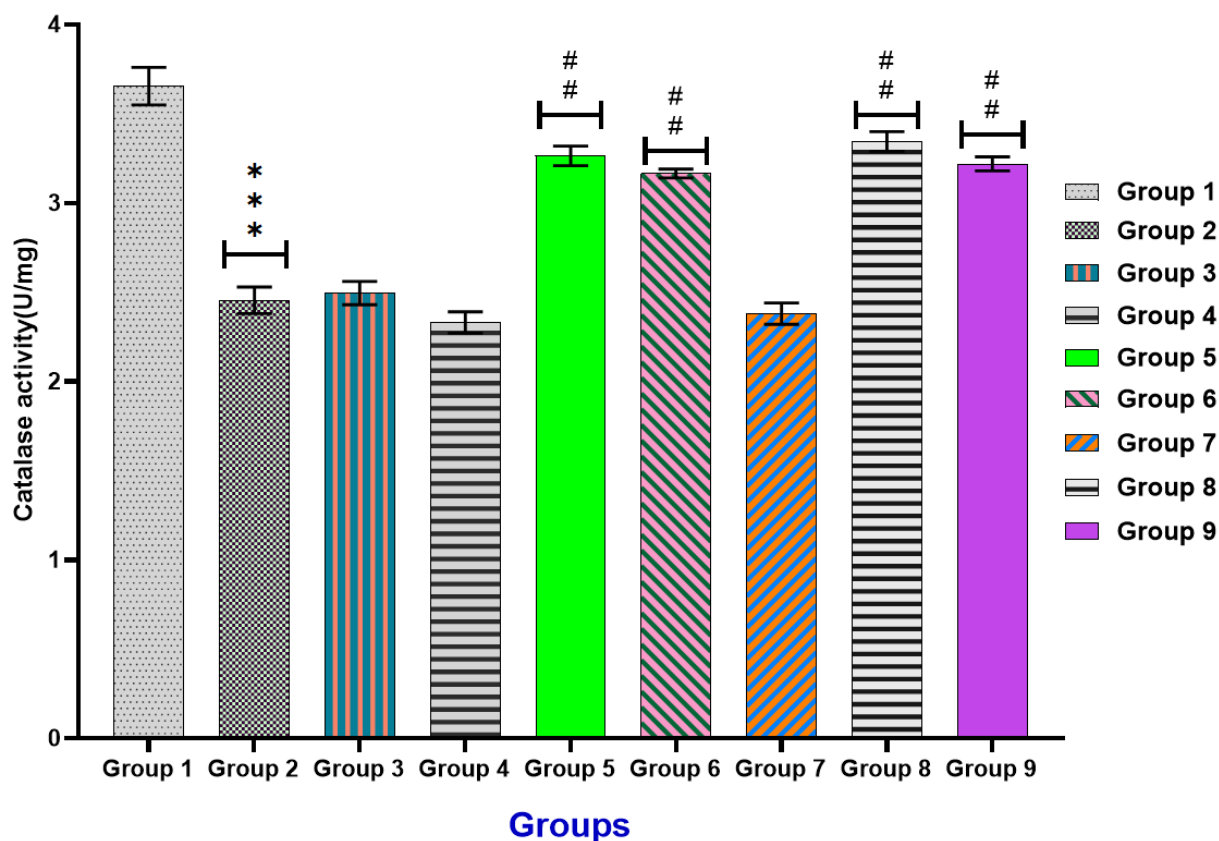


Figure 61: In vivo Catalase activity of different experimental samples with wounded skin (All the values are represented as mean \pm S.E.M. (n=3) ***p<0.001, **p<0.01 and *p<0.05, vs control (Group 1), ###p<0.001, ##p<0.01 and #p<0.05, vs placebo (Group 2))

➤ SOD estimation

Chronic hyperglycaemia has been associated with decreased levels of superoxide dismutase (SOD). Therefore, we focused on evaluating the SOD activity in the skin tissues of the experimental groups. The non-diabetic control group (Group 1) exhibited an SOD activity of 8.055 U/mg. In comparison, the placebo-treated group displayed a lower SOD level of 4.065 U/mg, primarily due to oxidative stress under diabetic conditions. The positive control group showed a slightly higher SOD activity of 4.18 U/mg, indicating some improvement following treatment. In contrast, the nanoformulation-treated groups demonstrated significant improvements in SOD activity. The guar gum nanoformulation of Sinapic acid (NF2)-treated groups exhibited SOD activity of 11.35 and 11.155 U/mg for high and low doses, respectively.

The guar gum nanoformulation of o-Coumaric acid (NF3)-treated groups showed SOD activity of 11.725 and 11.285 U/mg for high and low doses, respectively. These findings indicate that optimized nanoformulation of o-Coumaric acid (NF3) treatment produced superior results compared to other groups and significantly mitigated the risk of oxidative stress by enhancing SOD activity in diabetic rats (Figure 62).

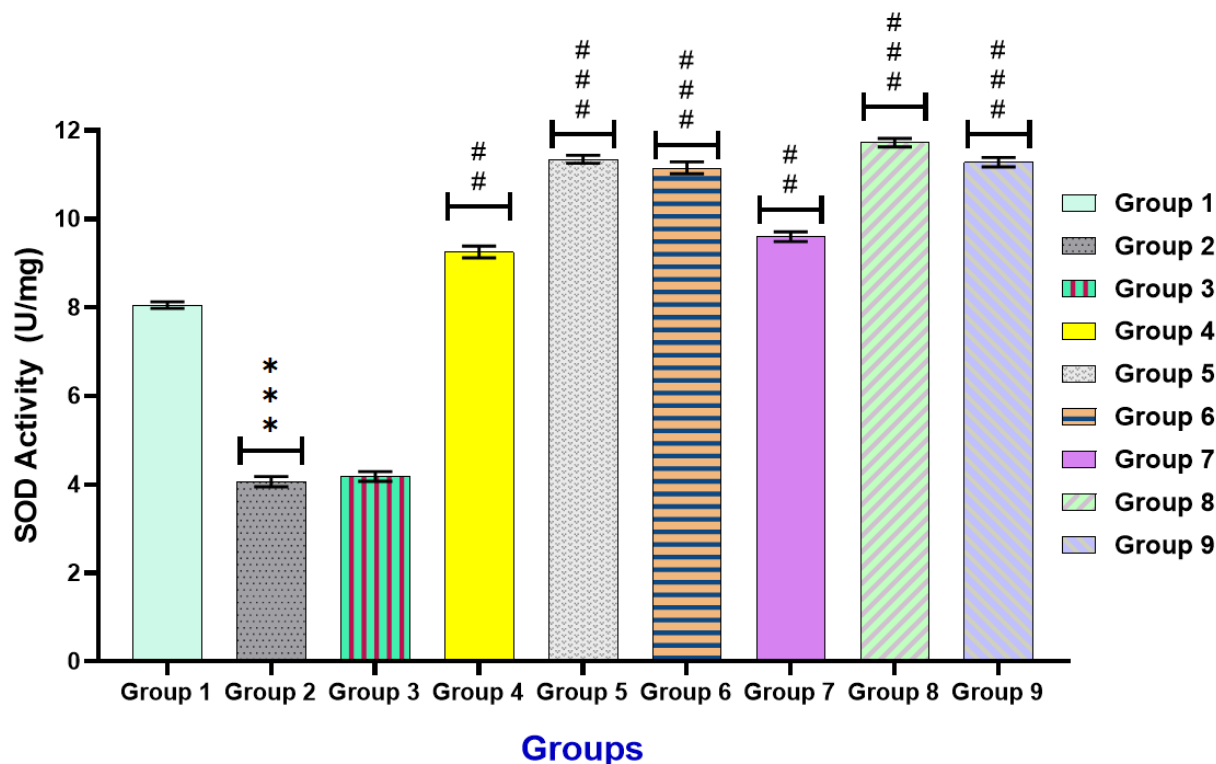


Figure 62: In vivo Superoxide dismutase (SOD) activity of different experimental samples with wounded skin (All the values are represented as mean \pm S.E.M. (n=3) ***p<0.001, **p<0.01 and *p<0.05, vs control (Group 1), ####p<0.001, ##p<0.01 and #p<0.05, vs placebo (Group 2))

➤ GST estimation

Chronic hyperglycaemia has been associated with decreased glutathione S-transferase (GST) levels. Consequently, we aimed to thoroughly examine the GST activity in the various experimental groups' skin tissues to better understand the impact of hyperglycaemia on antioxidant defences. The non-diabetic control group (Group 1) exhibited a GST activity of 1.965 U/mg. The placebo-treated group had a lower GST activity of 1.275 U/mg, primarily due to oxidative stress under diabetic conditions. The positive control group displayed a slightly higher GST activity of 1.475 U/mg than the placebo group, indicating some improvement. The raw drug-treated groups (Groups 4 and 7) showed improved GST activity of 1.765 U/mg and

1.89 U/mg, respectively, compared to the placebo and positive control groups. In contrast, the nanoformulation-treated groups demonstrated significant improvements in GST activity. The guar gum nanoformulation of Sinapic acid (NF2)-treated groups exhibited GST activity of 2.31 and 2.18 U/mg for high and low doses, respectively. The guar gum nanoformulation of o-Coumaric acid (NF3)-treated groups showed GST activity of 2.465 and 2.37 U/mg for high and low doses, respectively. These findings suggest that optimized nanoformulation of o-Coumaric acid (NF3) treatment nearly restored regular GST activity and significantly mitigated oxidative stress by enhancing GST activity in diabetic rats (Figure 63).

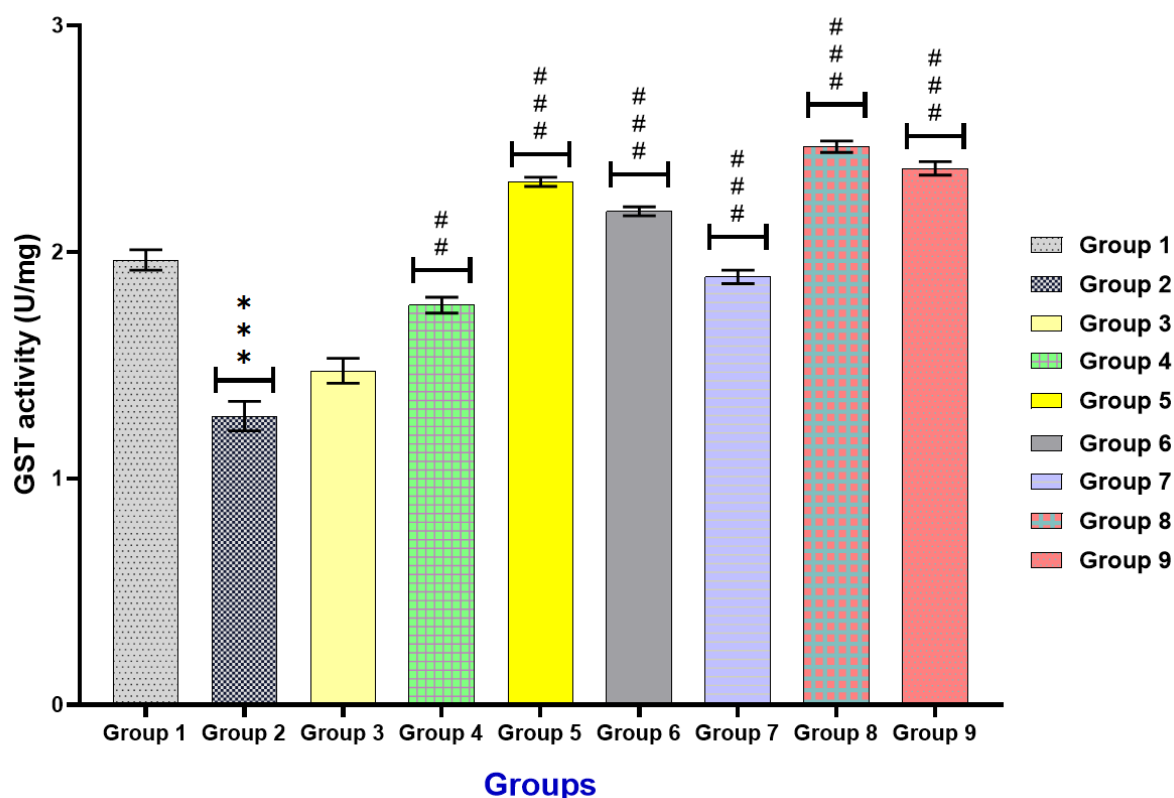


Figure 63: In vivo Glutathione S-transferase (GST) activity of different experimental samples with wounded skin (All the values are represented as mean \pm S.E.M. (n=3) ***p<0.001, **p<0.01 and *p<0.05, vs control (Group 1), ###p<0.001, ##p<0.01 and #p<0.05, vs placebo (Group 2))

6.16.5 Estimation of hydroxyproline

All experimental groups were analysed for hydroxyproline content, an essential collagen constituent. A non-proteinogenic amino acid, hydroxyproline, is mainly restricted to collagen and is measured as a collagen content indicator. Collagen is crucial in reconstructing the injured or disrupted tissue, as it restores the mechanical strength, anatomical structure, and function of

repaired skin. The hydroxyproline content (mg/g tissue) was measured across nine groups on the 3rd, 7th, and 10th days to assess collagen deposition and wound healing. The results revealed an overall increase in hydroxyproline content across all groups as time progressed. On the 3rd day, Group 1 had a hydroxyproline content of 42.45 mg/g, steadily increasing to 97.25 mg/g by the 10th day. Group 2 started with a lower hydroxyproline content of 23.5 mg/g on the 3rd day, reaching 48.65 mg/g on the 10th day. Group 3 increased from 34.55 mg/g on the 3rd day to 75.05 mg/g by the 10th day. Group 4 had hydroxyproline levels of 31.4 mg/g on the 3rd day, increasing to 62.4 mg/g on the 10th day. Group 5 demonstrated the most significant rise in hydroxyproline content, starting at 46.95 mg/g on the 3rd day and reaching 110.5 mg/g by the 10th day. Similarly, Group 6 increased from 40.9 mg/g on the 3rd day to 92.85 mg/g on the 10th day. Group 7 had moderate levels, starting at 32.5 mg/g on the 3rd day and increasing to 65.9 mg/g by the 10th day. Group 8 exhibited the highest overall hydroxyproline content, rising from 49.75 mg/g on the 3rd day to 120.45 mg/g by the 10th day. Lastly, Group 9 increased from 43.8 mg/g on the 3rd day to 102.75 mg/g on the 10th day. Overall, the data reflect varying collagen synthesis rates, with Groups 5 and 8 showing the most substantial increases, suggesting more effective wound healing processes in these groups (Figure 64).

The results showed that the hydroxyproline percentage content increased on the seventh and tenth days compared to the third day after treatment. There was a noticeable and significant percentage increase of 38.71% on the seventh day and 129.22% on the tenth day in the non-diabetic control group (Group 1). The placebo-treated group showed a smaller percentage rise of 25.62% and 107.17% on the seventh and tenth days. Compared to the placebo group, the positive control group had a slightly higher rise of 32.87% and 117.31%.

In contrast, the nanoformulation-treated groups showed a considerable rise in the percentage of hydroxyproline. The high-dose guar gum nanoformulation of Sinapic acid (NF2)-treated groups increased by 43.49% on the 7th day and 135.4% on the 10th day after treatment. The low-dose guar gum nanoformulation of Sinapic acid (NF2)-treated groups showed increases of 41.77% and 127.09% on the 7th and 10th days, respectively. The high-dose guar gum nanoformulation of o-Coumaric acid (NF3)-treated groups showed an increase of 46.76 % on the 7th day and 142.05 % on the 10th day, whereas the low-dose guar gum nanoformulation of o-Coumaric acid (NF3)-treated groups exhibited increases of 41.49% and 134.63 % on the 7th and 10th days, respectively (Figure 65).

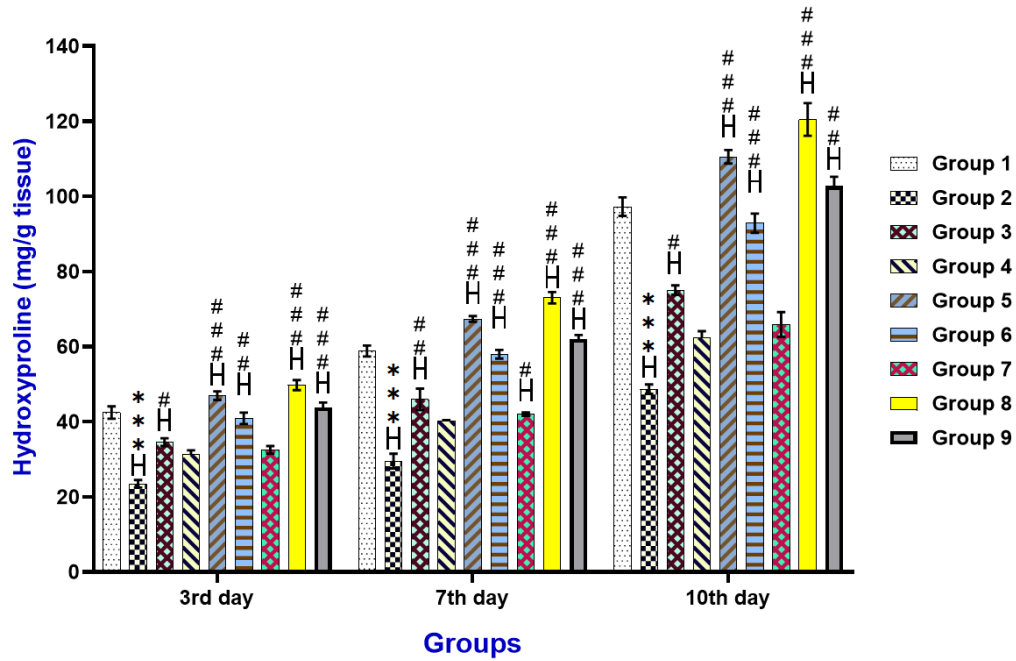


Figure 64: Estimation of hydroxyproline content in wounded/healed skin tissue (All the values are represented as mean \pm S.E.M. (n=3) ***p<0.001, **p<0.01 and *p<0.05, vs control (Group 1), ###p<0.001, ##p<0.01 and #p<0.05, vs placebo (Group 2))

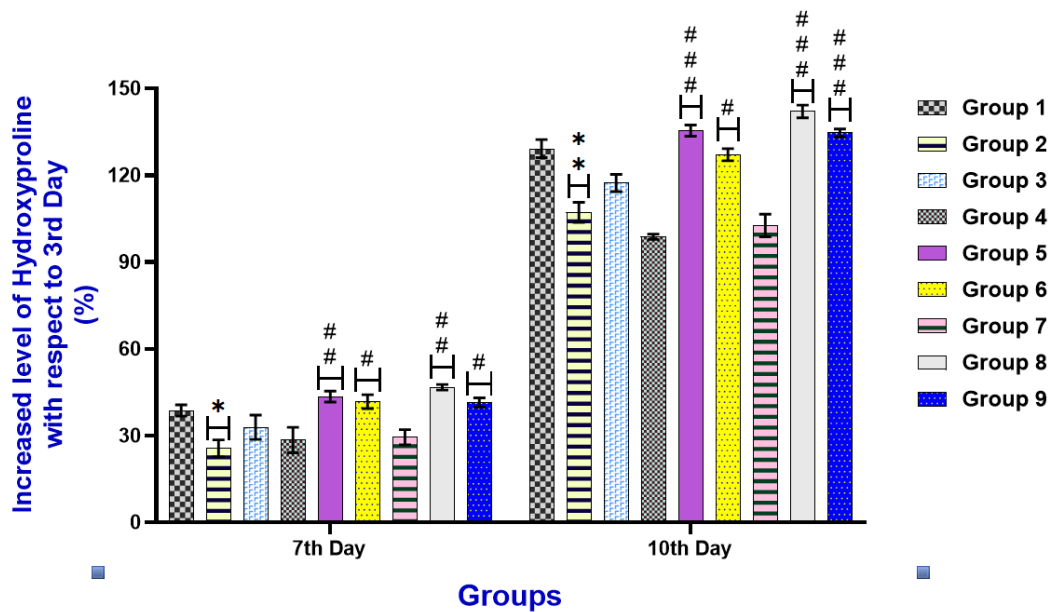


Figure 65: Comparison of hydroxyproline content in wounded/healed skin tissue (All the values are represented as mean \pm S.E.M. (n=3) ***p<0.001, **p<0.01 and *p<0.05, vs control (Group 1), ###p<0.001, ##p<0.01 and #p<0.05, vs placebo (Group 2))

6.16.6 Estimation of Hexosamine

The analysis of hexosamine content revealed that Groups 1, 5, 6, 8, and 9 exhibited significantly better tissue responses than Groups 2 and 3. Group 1 showed a consistent increase in hexosamine levels, starting at 0.305 mg/100 mg on the 3rd day and rising to 0.74 mg/100 mg by the 10th day, indicating strong tissue regeneration. Group 5 demonstrated impressive results, with hexosamine content increasing from 0.37 mg/100 mg on the 3rd day to 0.95 mg/100 mg by the 10th day, suggesting highly effective tissue repair. Similarly, Group 6 showed a steady and robust increase, reaching 0.77 mg/100 mg by the 10th day, reflecting good tissue healing. Group 8 consistently outperformed all other groups, beginning with the highest initial hexosamine content of 0.4 mg/100 mg on the 3rd day and reaching a peak of 1.07 mg/100 mg by the 10th day, highlighting its superior tissue response. Group 9 also showed strong results, with levels rising from 0.355 mg/100 mg to 0.885 mg/100 mg over the same period, indicating effective tissue regeneration. In contrast, Groups 2 and 3 displayed lower hexosamine content and more modest increases. Group 2, which started at 0.23 mg/100 mg, only reached 0.51 mg/100 mg by the 10th day. Group 3, beginning at 0.275 mg/100 mg, ended at 0.635 mg/100 mg. The hexosamine content is presented in Figure 66. There is a noticeable increase in hexosamine content from the 7th to the 10th day across all groups. The mean values also reflect this trend. The increase pattern is consistent, indicating that the experimental conditions likely influenced hexosamine production similarly across different groups. The findings indicated the percentage increase (on the 7th and 10th day after treatment) of hexosamine content relative to the 3rd day. In the non-diabetic control group (Group 1), there was a markedly high percentage increase of 94.07% on the 7th day and 143.05% on the 10th day. The placebo-treated group exhibited a lower percentage increase of 82.38% and 121.59% on the 7th and 10th days after treatment, respectively. The positive control group showed a slightly higher increase of 83.68% and 131.1% compared to the placebo group. Conversely, the nanoformulation-treated groups displayed a significant enhancement in hexosamine percentage increase. The high-dose guar gum nanoformulation of Sinapic acid (NF2)-treated groups demonstrated an increase of 97.36% on the 7th day and 156.79% on the 10th day. The low-dose guar gum nanoformulation of Sinapic acid (NF2)-treated groups exhibited an increase of 93.97% and 136.85% on the 7th and 10th days, respectively. The high dose guar gum nanoformulation of o-Coumaric acid (NF3)-treated groups showed an increase of 103.78% on the 7th day and 167.60% on the 10th day, whereas the low dose guar gum nanoformulation of o-Coumaric acid (NF3)-treated groups

exhibited an increase of 100.23% and 149.44% on the 7th and 10th days, respectively (Figure 67).

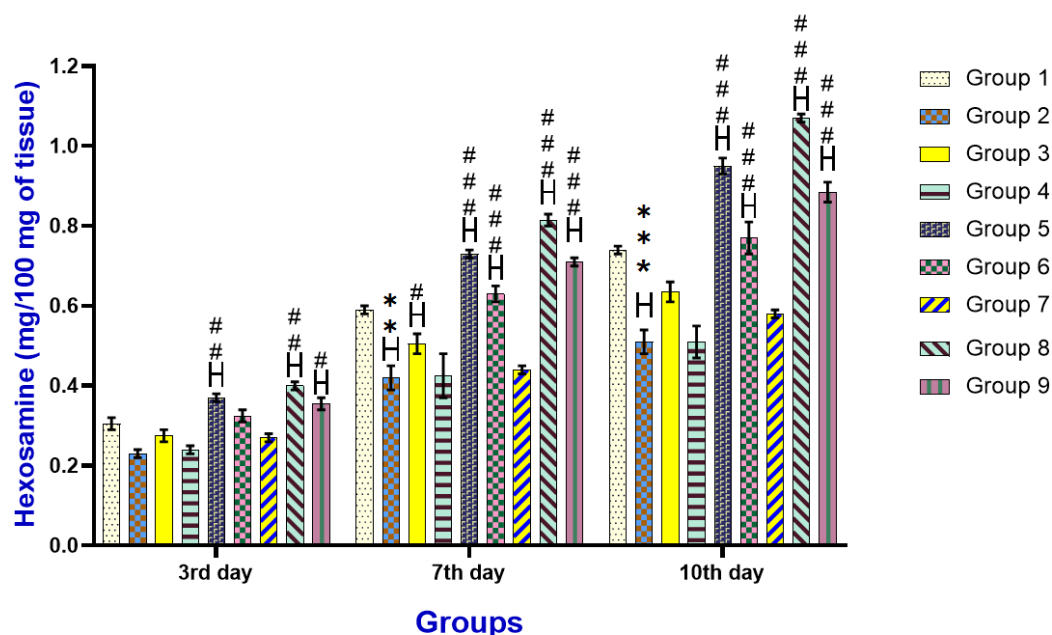


Figure 66: Estimation of hexosamine content in wounded/healed skin tissue (All the values are represented as mean \pm S.E.M. (n=3) ***p<0.001, **p<0.01 and *p<0.05, vs control (Group 1), ###p<0.001, ##p<0.01 and #p<0.05, vs placebo (Group 2))

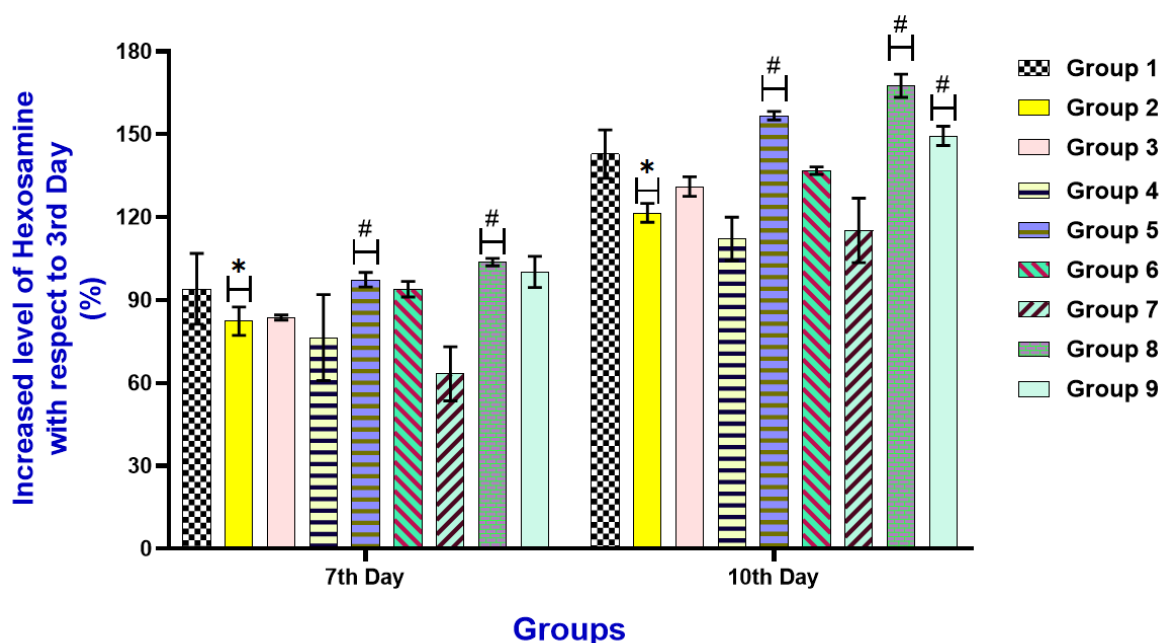
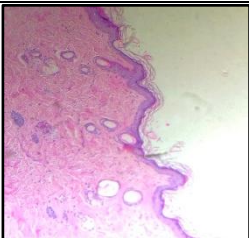
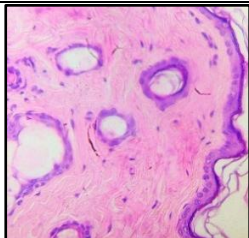
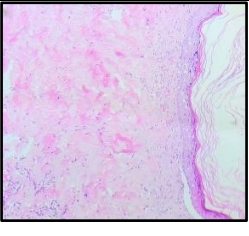
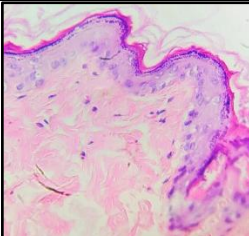
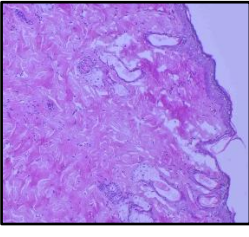
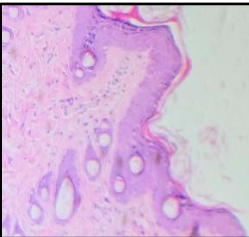
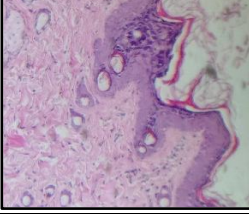
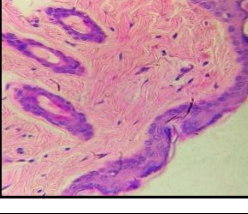


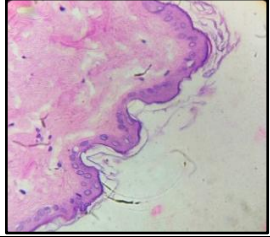
Figure 67: Comparison of hexosamine content in wounded/healed skin tissue (All the values are represented as mean \pm S.E.M. (n=3) ***p<0.001, **p<0.01 and *p<0.05, vs control (Group 1), ###p<0.001, ##p<0.01 and #p<0.05, vs placebo (Group 2))

6.16.7 Histopathology

Histopathological analysis was conducted on the wounded tissues from different groups to assess the extent of healing. The tissues were stained with H&E dye, examined with a 10X magnification, and edited. The results revealed that Groups 1, 5, 6, 8 and 9 exhibited complete dermal remodelling, including thickening and stratification of the epithelium. In contrast, Groups 2, 3, 4 and 7 showed less dermal remodelling and minimal thickening, indicating comparatively reduced healing. Key parameters essential for effective wound healing, such as re-epithelialization, thickening of the epidermis and dermis, and maturation of fully developed granulation tissues, were notably disturbed in the diabetic wounded control group. However, treatment with NF at varying doses (20 mg/kg and 40 mg/kg) resulted in enhanced re-epithelialization, mature and well-developed granulation tissues, and new blood vessels in the wounded tissues. Both low and high doses of NF effectively restored these critical parameters and accelerated wound healing.

Table 18: Histopathological evaluation of diabetic wound healing process before and after treatment in different groups (Hematoxylin and eosin (H&E) staining)

Group 1		Group 5	
Group 2		Group 6	
Group 3		Group 7	
Group 4		Group 8	

		Group 9	
--	--	----------------	--

Chapter 7

Discussion

According to prevalence estimates from the International Diabetes Federation (IDF), there were 537 million individuals aged 20–79 with diabetes worldwide in 2021. This number is projected to increase to 643 million by 2030 and 783 million by 2045. Alarming, one in five deaths globally in 2021 was attributed to diabetes. T2DM is a widespread metabolic disorder characterised by the intricate interaction between insulin resistance and impaired insulin secretion, leading to chronic hyperglycaemia. T2DM manifests as a persistent medical condition where blood glucose levels remain elevated due to insufficient insulin production by the pancreas or the body's inability to utilise the insulin produced effectively. The rising global prevalence of T2DM underscores its significant public health implications, necessitating an in-depth examination of its diverse complications. Impaired wound healing is a remarkably complex and clinically significant issue among these.

Wounds are defined as tissue structure and cellular integrity disruptions caused by various injuries, including physical, chemical, thermal, or immunological assaults. Wound healing, often associated with skin repair, involves a series of automatic physiological responses collectively called the “healing cascade”. However, in individuals with diabetes, these injuries can lead to severe health complications. Diabetes impairs wound healing through a multifaceted interplay of physiological and biochemical disturbances. The complex pathophysiology of diabetes encompasses elevated blood glucose levels, chronic inflammation, impaired immune responses, and compromised vascular function, all of which contribute to delayed or impaired wound healing.

Diabetic individuals often experience wounds that are slow to heal, heal improperly, or fail to heal altogether, potentially leading to infections. Such infections can spread to nearby tissues and bones or distant body parts. Without prompt medical intervention, these infections can become life-threatening or fatal. Moreover, even in the absence of infection, slow wound healing can significantly impact a person's overall health and quality of life.

Conventional medications like metformin or povidone-iodine are widely used to treat and manage diabetic wound healing, yet these synthetic drugs often come with a significant array of adverse effects. To address these challenges, our research focuses on a novel approach: developing a biodegradable polymer-based nanoformulation utilising guar gum.

This formulation is embedded with bioactive phytochemicals, including Syringic acid, Sinapic acid, or o-Coumaric acid. By employing a comprehensive research strategy that includes optimisation of nanoformulation, in vitro, and in vivo experiments, we aim to create a more effective and safer alternative for diabetic wound healing treatment.

Following screening of the initial emulsifying and stabilising agent concentrations, we utilised the Box-Behnken Design (BBD) to optimise our nanoformulation. Subsequent characterizations confirmed the formulation's nanoscale production, drug loading capacity, and overall efficacy.

Given their critical role in nanoformulation production, initial trials were conducted to screen formulation variables. The screening results identified cross-linker concentration, sonication time, and emulsifier percentage as critical variables influencing the formulation. To optimise the nanoformulations efficiently, reducing cost, time, and the number of experiments, the Box-Behnken Design (BBD) was selected for this study. A total of 18 experiments were designed according to BBD, with each formulation characterised individually for particle size, polydispersity index (PDI), zeta potential (ZP), and drug loading. These characterisations were essential for evaluating the impact of cross-linker concentration, sonication time, and emulsifier percentage on the formulation's physicochemical properties and drug loading efficiency.

The blank nanoformulation (placebo) results highlight the significant impact of emulsifier amount and ultrasonication time on particle size. Increasing sonication time from 8 to 10 minutes reduced the average particle diameter for S2 from 36 nm to 32 nm (Figure 68), but further increases in sonication time led to larger particle sizes, which may be due to more energy and possibly more collisions among the particles which can lead to agglomeration and further increase in particle size (Kole et al., 2012; Taylor et al., 1998). Similarly, varying the emulsifier amount from 5 to 25 mg showed that particle diameter decreased from 36.9 nm to 32.4 nm with an emulsifier amount increased from 5 to 10 mg, then increased with higher emulsifier amounts (Figure 68b). The larger particle size for S1 may be due to insufficient emulsifier coverage, while excess emulsifier in S3 might have accelerated Ostwald ripening (Taylor et al., 1998; Mandal et al., 2024). Sample S2 was chosen for further analysis and applications based on these observations.

The polydispersity index (PDI) values, ranging from 0.09 to 0.21, indicate a relatively narrow size distribution. A PDI closer to 0 suggests a more monodispersed system with uniform

particle sizes, while the negative zeta potential enhances nanoparticle stability by introducing repulsive forces, reducing aggregation likelihood (Mandal et al., 2024). A high negative zeta potential indicates strong electrostatic repulsive forces, contributing to nanoparticle stability, whereas a lower negative zeta potential can improve drug payload in the nanoparticles (Mandal et al., 2024; Shao et al., 2015). Based on these results, formulation S2 was optimized due to its small particle size and suitable zeta potential. Compared to the previous method, the smaller nanoparticle size is attributed to the synergistic effects of the emulsifier blend, Transcutol P, and ultrasonication. Further investigation is warranted to confirm these preliminary results.

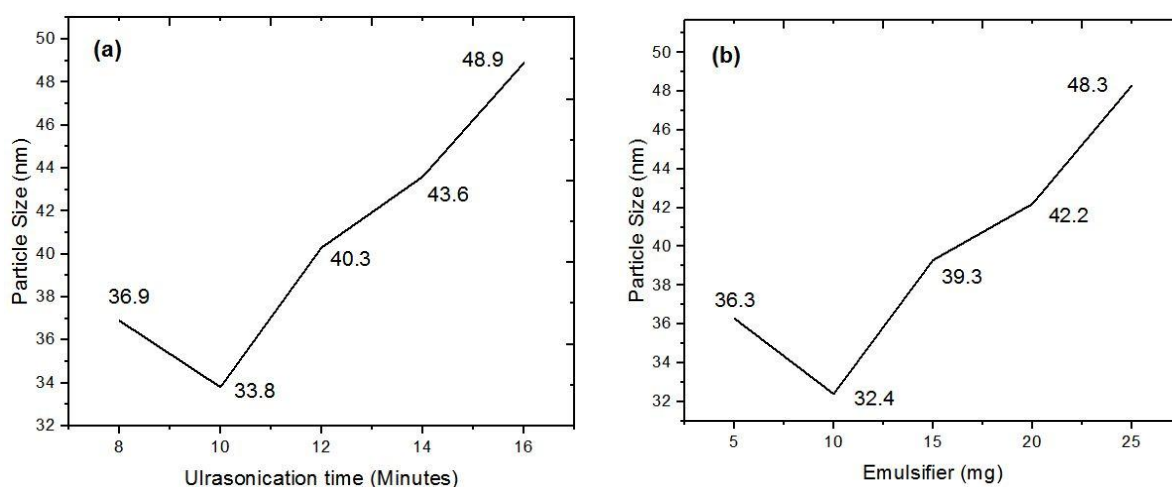


Figure 68: Particle size variation in (a) Ultrasonication time and (b) emulsifier amount at 10 min ultrasonication.

For guar gum nanoformulation of Syringic acid (NF1), factor B exerts a synergistic effect on particle size, while factors A and C individually demonstrate antagonistic effects. However, when combined (AB, BC, and AC), these factors collectively exhibit an antagonistic influence on size. All factors A, B, and C have synergistic effects on PDI individually, whereas in combination show antagonistic effects. Factor A and B have an antagonistic effect, and C has a synergistic effect on ZP. Further, factors A, B, and C have synergistic effects individually. In the case of guar gum nanoformulation of Sinapic acid (NF2), size factor B has a synergistic effect, and A and C have an antagonistic effect individually. However, in the case of combination, it has an antagonistic effect on size. Factors A, B, C, AB, and AC have synergistic effects on PDI individually, whereas BC has shown antagonistic effects. Factors A, B, and C have an antagonistic effect on ZP. Further, factors A, B, and C have synergistic effects individually. In the case of drug loading, all A, B, and C have a synergistic effect. In the guar gum nanoformulation of o-Coumaric acid (NF3), size factor B has a synergistic effect, and A and C have an antagonistic effect individually. However, in the case of combination (AB

and BC), they have an antagonistic effect on size, and AC has a synergistic effect. Factors A, B, C, AB, and BC synergistically affect PDI individually, whereas AC has shown antagonistic effects. Factors A, B, and C have an antagonistic effect on ZP. In drug loading, all A and B had a synergistic effect, and C had an antagonistic effect. AB and BC have a synergistic effect, and AC has an antagonistic effect—this effect, i.e., synergistic effect, indicates a slight change in the factor (A, B, and C) influences the change in dependent variables and vice versa, in the case of an antagonistic effect in all nanoformulations.

All the pH values ranging between 6 and 7.5 in the nanoformulations suggest a slightly acidic to neutral nature. This characteristic is anticipated to positively impact their skin application for wound healing. This pH range aligns well with the skin's natural acidity, promoting compatibility and potentially enhancing the formulations' efficacy in supporting the healing process (Ramadan et al., 2016; Uzun et al., 2012; Karwal et al., 2023)

Higher spreadability implies that the formulation can be applied more smoothly and effortlessly (Estanqueiro et al., 2016). This characteristic benefits user compliance, as individuals are more likely to use products that are easy to apply without excessive effort. Better spreadability can improve bioavailability for formulations containing active pharmaceutical or cosmetic ingredients (de Lafuente et al., 2020). This is because a well-spread formulation enhances the contact between the active agents and the skin, potentially leading to better therapeutic or cosmetic outcomes. A well-spread formulation can enhance the contact of active ingredients with the skin, potentially facilitating better absorption. The optimized formulation with a higher spreadability value (83.33 gm.cm/sec) for optimized nanoformulation of Syringic acid (NF1) and guar gum nanoformulation of Sinapic acid (NF2), 93.75 gm.cm/sec for optimized nanoformulation of o-Coumaric acid (NF3) suggests a greater ease of application (Estanqueiro et al., 2016). This characteristic is advantageous as it facilitates a more uniform distribution of the topical product, ensuring that active ingredients are evenly spread across the skin. In practical terms, higher spreadability enhances the user experience and the effectiveness of the formulated product by promoting consistent coverage on the skin surface (Simoes et al., 2019)

The viscosity measurements of these formulations indicate a thicker consistency, which could present challenges in flow and skin application (Somagoni et al., 2014). However, specific formulations may provide benefits in terms of easier spreading and application. The observed variations in viscosity underscore the importance of this parameter in customising the product for specific uses. Formulations guar gum nanoformulation of Syringic acid (NF1), guar gum

nanoformulation of Sinapic acid (NF2), and optimized nanoformulation of o-Coumaric acid (NF3) exhibit viscosities of 8320 cP, 8220 cP, and 8300 cP, respectively, within a moderate viscosity range. This suggests that NF can offer a balanced consistency—neither too thick nor too thin—likely enhancing its spreadability while retaining sufficient thickness to effectively deliver active ingredients and ensure a positive user experience (Ali et al., 2022).

The refractive index values across formulations exhibit a relatively consistent range from 1.2 to 1.5. This uniformity suggests a well-controlled and consistent composition among the nanoemulsion. Maintaining such consistency is crucial for quality control and ensuring reproducibility in manufacturing processes. The refractive index data analysis indicates that the nanoemulsion formulations have consistent optical characteristics. This consistency can contribute to these formulations' overall quality, stability, and cosmetic acceptability in topical applications, making them potentially well-suited for skincare or cosmetic products (Maxon et al., 2016).

The analysis of the distribution of particle sizes, zeta potential, and loading efficacy indicates that the creation of stable nanoformulations could be advantageous in wound healing therapies (Tyavambiza et al., 2022). The particle size analysis indicated that the average diameters of the nanoparticles guar gum nanoformulation of Syringic acid (NF1), guar gum nanoformulation of Sinapic acid (NF2), and optimized nanoformulation of o-Coumaric acid (NF3) were 25 nm, 28 nm, and 30 nm, respectively. This was further confirmed by FESEM, which displayed spherical particles. Typically, these particles' small and consistent sizes enable more efficient absorption and movement into biological tissues, making them very suitable for application to wounds on the skin's surface (Kalashnikova et al., 2015). The zeta potential values, which range from -16 mV to -24 mV, indicate a high level of colloidal stability and a slight possibility of nanoparticle agglomeration and suspension uniformity. This stability is essential for anti-bacterial activity in wound areas (Kumari et al., 2022). The drug loading efficiencies for guar gum nanoformulation of Syringic acid (NF1), guar gum nanoformulation of Sinapic acid (NF2), and optimized nanoformulation of o-Coumaric acid (NF3) are 83.24%, 88.76% and 92.26%, respectively, indicating a significant integration of compounds. Having this ability is crucial for attaining optimal levels of medication at the sites of infection (Sharma et al., 2016).

The DSC spectrum differences between guar gum and guar gum nanoformulation in thermal properties indicate changes in the material's thermal behaviour due to nanoparticle formation (Verma et al., 2021). The nanoformulation (guar gum nanoformulation of Syringic acid (NF1))

shows a more complex thermal behaviour with two distinct peaks, suggesting the presence of multiple components or phases. The first peak occurs at a much lower temperature range, which could be attributed to the excipients or matrix materials in the nanoformulation. In contrast, the second peak aligns more closely with the melting behaviour observed in pure Syringic acid (SRN). The SRN shows sharp, well-defined peaks characteristic of a pure crystalline substance. The absence of a lower temperature peak in SRN, as seen in the guar gum nanoformulation of Syringic acid (NF1), indicates that the nanoformulation introduces additional components or modifications to the thermal profile of Syringic acid. The difference in ΔH values between the nanoformulation and pure Syringic acid provides insight into the interaction between Syringic acid and the excipients within the nanoformulation. The significant reduction in enthalpy in the second peak of optimized nanoformulation of Syringic acid (NF1) compared to SRN suggests a potential alteration in the crystalline structure or stability of Syringic acid when incorporated into the nanoformulation (Sweety et al., 2020; Neves et al., 2013).

The first thermal event in optimized nanoformulation of Sinapic acid (NF2) occurs at a lower temperature range than the melting of SNP, suggesting that the nanoformulation undergoes initial phase transitions well before the decomposition of Sinapic acid. The second peak of optimized nanoformulation of Sinapic acid (NF2) is lower in temperature than the melting point of SNP, which may indicate the interactions within the nanoformulation that affect the thermal stability of the encapsulated Sinapic acid. The significantly lower ΔH values for optimized nanoformulation of Sinapic acid (NF2) in both thermal events compared to SNP suggest that the nanoformulation alters the thermal properties of Sinapic acid, possibly due to the encapsulation and distribution within the polymer matrix. Overall, the DSC analysis highlights that the nanoformulation (guar gum nanoformulation of Sinapic acid (NF2)) exhibits distinct thermal behaviour compared to pure Sinapic acid, which may influence its performance and stability in applications like drug delivery (Singh et al., 2015).

The first peak of optimized nanoformulation of o-Coumaric acid (NF3) occurs at a slightly lower temperature than pure OCA, suggesting a potential interaction between OCA and other components within the nanoformulation, possibly leading to a slight reduction in melting temperature. The second, more complex exothermic peak in the optimized nanoformulation of o-Coumaric acid (NF3) is absent in the pure OCA, which implies that this peak is related to the nanoformulation matrix or interactions within the optimized nanoformulation of o-Coumaric acid (NF3) system rather than the OCA alone. The thermal events observed in the optimized nanoformulation of o-Coumaric acid (NF3) indicate that the nanoformulation has altered the

thermal stability and decomposition characteristics of OCA, likely due to the encapsulation or interaction with the carrier matrix (Omwoyo et al., 2014; Sohail et al., 2022; Hanmantrao et al., 2022)

The TGA analysis collectively demonstrates that the nanoformulation process significantly impacts the thermal stability of the components involved (Smruthi et al., 2022). The Guar gum nanoformulation exhibits an increase in thermal stability compared to the pure polymer, indicating successful encapsulation and protection of the active compounds within the Guar gum matrix. Specifically, the Syringic acid-loaded nanoformulation (guar gum nanoformulation of Syringic acid (NF1)) shows a marked increase in thermal stability, which is beneficial for applications requiring higher temperature resistance. The Sinapic acid-loaded nanoformulation (guar gum nanoformulation of Sinapic acid (NF2)) displays a complex thermal degradation pattern with two distinct peaks, reflecting the combined properties of Sinapic acid and the Guar gum matrix. Similarly, the o-Coumaric acid-loaded nanoformulation (guar gum nanoformulation of o-Coumaric acid (NF3)) shows improved thermal stability compared to the pure compound, with a higher onset temperature for the second degradation peak. Overall, these results highlight the effectiveness of the nanoformulation process in enhancing the thermal stability of the active ingredients, making these formulations suitable for potential applications involving exposure to heat (Dodi et al., 2016; Bostanudin et al., 2021)

The Guar gum nanoformulation (GGNP) shows modifications in its spectral profile of FTIR compared to pure Guar gum, suggesting successful incorporation of the components. The FTIR analysis collectively confirms the successful incorporation of Syringic acid, Sinapic acid, and o-Coumaric acid into their respective Guar gum nanoformulations (guar gum nanoformulation of Syringic acid (NF1), guar gum nanoformulation of Sinapic acid (NF2), and guar gum nanoformulation of o-Coumaric acid (NF3)). The observed shifts in peak positions compared to the individual components (GG, GGNP, and the active compounds) indicate interactions between the functional groups of Guar gum and the active compounds. These interactions likely enhance the stability and efficacy of the nanoformulations. The retention of critical functional group peaks, with slight modifications in the spectral profiles, suggests effective nano-encapsulation and compatibility between the components while preserving the essential properties of the active compounds within the nano matrix. This structural integrity and interaction within the nanoformulations are crucial for their intended biomedical and therapeutic applications (George et al., 2019; Dodi et al., 2016; Bostanudin et al., 2021).

DPPH assay revealed that the nanoformulations guar gum nanoformulation of Syringic acid (NF1), guar gum nanoformulation of Sinapic acid (NF2), and optimized nanoformulation of o-Coumaric acid (NF3) exhibit robust and significant ($p < 0.05$) antioxidant activities, comparable to ascorbic acid at higher concentrations, indicating their potential effectiveness in therapeutic applications. GGNP, while showing the lowest activity, still presents a concentration-dependent increase in antioxidant capacity. The other samples, SRN, SNP, and OCA, demonstrate moderate antioxidant activities, improving with higher concentrations. These findings suggest that the nanoformulations have enhanced antioxidant defences, which may offer significant benefits for diabetic wound healing (Dodi et al., 2023; Wagner et al., 2008). This enhanced activity is likely due to the hydroxyl groups in guar gum and the increased surface area of nanoparticles (Sharma et al., 2009; Brighente et al., 2007).

The ABTS assay results confirm that the nanoformulations guar gum nanoformulation of Syringic acid (NF1), guar gum nanoformulation of Sinapic acid (NF2), and optimized nanoformulation of o-Coumaric acid (NF3) display robust antioxidant activities, closely matching the standard ascorbic acid at higher concentrations, indicating their potential effectiveness in antioxidant applications. GGNP, while showing lower activity, still presents a concentration-dependent increase in antioxidant capacity. SRN, SNP, and OCA also demonstrate moderate antioxidant activities, improving with higher concentrations. These ABTS activities are likely due to hydroxyl groups donating hydrogen atoms to ABTS radicals, enhancing antioxidant defences and aiding diabetic wound healing (Farooq et al., 2022; Josh et al., 2015; Salvatore et al., 1996; Yang et al., 2021; Yee et al., 1996).

The nanoformulations guar gum nanoformulation of Syringic acid (NF1), guar gum nanoformulation of Sinapic acid (NF2), and optimized nanoformulation of o-Coumaric acid (NF3) display robust alpha-glucosidase inhibitory activities, indicating their potential effectiveness in managing glucose levels. However, they do not match the standard acarbose at higher concentrations. Similarly, the nanoformulations guar gum nanoformulation of Syringic acid (NF1), guar gum nanoformulation of Sinapic acid (NF2), and optimized nanoformulation of o-Coumaric acid (NF3) exhibit alpha-amylase inhibitory activities, closely matching the standard acarbose at higher concentrations, indicating their potential effectiveness in managing starch digestion. The strong performance of guar gum nanoformulation of o-Coumaric acid (NF3), guar gum nanoformulation of Sinapic acid (NF2), and optimized nanoformulation of Syringic acid (NF1) highlights their potential use in therapeutic applications for controlling blood sugar levels that can benefit wound healing. This

superior inhibitory activity against α -glucosidase and α -amylase is likely achieved by competitively binding to the enzyme's active site, causing structural alterations or denaturation (Miller et al., 2022; Cano Sanchez et al., 2018; Bolajoko et al., 2022). These results support the theory that nanoformulations enhance bioactivity due to increased surface area and improved interaction with biological targets, as seen in previous research on competitive inhibition and denaturation by nanoparticles (Wang et al., 2024; Avwioroko et al., 2020)

It is essential to investigate the cytotoxic potential of the compound on normal and malignant cells before animal studies. Although predicting the toxicity of compounds in animal models has pre-clinical significance, as it leads to the introduction of tested compounds in human clinical settings for disease treatment, it is recommended to predict toxicity under in vitro conditions. Cytotoxicity results show that nanoformulations positively impact cell viability, demonstrating higher biocompatibility with fibroblast and keratinocyte cells, which is crucial for wound healing (Veeraraghavan et al., 2021; Alven et al., 2020; Shafique et al., 2021).

Since wound healing is a complex process, a series of events is initiated at the injury site to facilitate the restoration of the skin's original shape and structure. A critical stage in this process involves cell migration, a pivotal factor in tissue repair and regeneration. The migration of epithelial cells toward the injured site fosters wound healing and serves as a protective barrier, preventing infections in the affected area. Furthermore, a vital cellular component, the fibroblast, plays a crucial role in wound healing by producing granulation tissue. Significantly, it has been noted that granulation tissue is marked by a substantial presence of blood vessels, promoting angiogenesis at the injury site and contributing to the swift healing of wounds. The Scratch assay results indicate significant ($p < 0.05$) enhancement in cell migration and wound healing with nanoformulation treatment compared to controls, highlighting their potential to promote cell migration (Alven et al., 2020; Kumbhar et al., 2023). Hence, our findings align with prior research indicating a decrease in cell migration at wounded sites under diabetic conditions (Xuan et al., 2014).

Angiogenesis forms new blood vessels essential for developing tissues and organs (Mariotti et al., 2006). These newly formed blood vessels, composed of endothelial cells, provide crucial nutrients and oxygen to tissues, promoting wound healing. However, in diabetic conditions, particularly under hyperglycaemia, angiogenesis and endothelial function are compromised. For example, the insufficient supply of nutrients and oxygen, along with reduced proliferation and migration of endothelial cells to the wound site, impairs angiogenesis, leading to prolonged

wound exposure (Everts et al., 2023). Therefore, it is essential to investigate the effects of nanoformulations on endothelial cells to better understand their role. Results from the tube formation assay demonstrated a significant enhancement in angiogenesis following nanoformulation treatment, evidenced by a notable increase in tube number and capillary/tube thickness, thereby supporting angiogenesis and facilitating diabetic wound healing.

Maintaining an equilibrium between oxidants and antioxidants is essential for the biological system to function adequately. However, an imbalance in these factors leads to the progression of oxidative stress by intensifying the generation of free radicals. Elevated levels of ROS disrupt the balance of antioxidants and the normal physiological functioning of biological macromolecules, including DNA, lipids, and proteins. In addition, increased LPO (MDA levels) and rupturing of the mitochondrial membrane due to breakage of lipids impact the cell membrane fluidity and permeability (Dix et al., 1993). Lipid peroxidation (LPO) is a chemical process in which oxidising agents, such as free radicals, degrade lipids containing carbon-carbon double bonds, emphasising polyunsaturated fatty acids (PUFAs). This study/assay examines the assessment of the protective efficacy of different developed nanoformulations against oxidative stress.

The lipid peroxidation activity in the context of diabetic wound healing was measured to understand oxidative stress levels under different treatment conditions. Low lipid peroxidation (LPO) levels are beneficial, indicating reduced oxidative stress and potentially better wound healing. In contrast, high LPO levels suggest increased oxidative stress and poorer healing outcomes (Pessoa et al., 2016). The results suggest that nanoformulation treatments significantly reduce lipid peroxidation compared to the hyperglycaemic condition, indicating their potential protective effects against oxidative stress, suggesting improved oxidative microenvironment, and potential wound healing benefits. These results align with prior research on natural polymer-based nanoparticles in wound healing applications (Ebaid et al., 2013; Algandaby et al., 2023; Anushree et al., 2023; Deng et al., 2021)

Catalase, an enzyme, aids in the removal of hydrogen peroxide (H_2O_2) from live cells. Elevated levels of H_2O_2 lead to an imbalance in insulin synthesis and signalling by impairing pancreatic cells (Martins et al., 2014). Consequently, this disturbance hinders the process of glucose metabolism and plays a role in the development of diabetes and wound healing (Netto et al., 2013). The catalase assay revealed that the control group had the highest catalase activity at 70.4 U/mg, indicating optimal antioxidant defence under normal conditions. In contrast, the

hyperglycaemic group exhibited a substantial decrease in catalase activity to 6.68 U/mg, reflecting impaired antioxidant defence and reduced wound healing potential due to elevated H_2O_2 levels. However, the groups treated with the nanoformulation showed a significant increase in catalase activity, suggesting an enhanced antioxidant defence and improved wound healing potential (Hu et al., 2017; Kurahashi et al., 2015)

The glutathione S-transferase (GST) activity was measured to assess the detoxification and antioxidant defence in the context of diabetic wound healing (Shukla et al., 1997). Higher GST activity indicates better detoxification and oxidative stress management, which is beneficial for wound healing (Arya et al., 2011). The control group demonstrated the highest GST activity at 27.02 U/mg, indicating optimal detoxification and antioxidant defence under normal conditions. In contrast, the hyperglycaemic group showed a marked decrease in GST activity to 5.13 U/mg, reflecting impaired detoxification and reduced wound healing potential. Nanoformulations significantly enhanced GST activity at both high and low doses. Among them, optimized nanoformulation of o-Coumaric acid (NF3) proved to be the most effective in boosting GST activity, thereby improving detoxification and antioxidant defence for diabetic wound healing, followed by optimized nanoformulation of Sinapic acid (NF2) and optimized nanoformulation of Syringic acid (NF1) when compared to the control and hyperglycaemic groups (Daggett et., 1998, Mukherjee et al., 2014). These results correlate with existing data (Cano Sanchez et al., 2018; Schäfer et al., 2008)

Maintaining cellular health is a crucial role of SOD, as it safeguards cells from harmful free radicals, excessive oxygen radicals, and other substances that hasten cellular ageing or death. The superoxide dismutase (SOD) activity was measured to assess the antioxidant defence in the context of diabetic wound healing. Higher SOD activity indicates better management of oxidative stress, which is beneficial for wound healing. The control group exhibited the highest SOD activity at 210.07 U/mg, representing the optimal antioxidant defence under normal conditions. The hyperglycaemic group showed a significant reduction in SOD activity to 29.3 U/mg, indicating impaired antioxidant defence and poor wound healing potential due to elevated oxidative stress. The groups treated with the nanoformulation demonstrated a significant increase in SOD activity. Among them, optimized nanoformulation of o-Coumaric acid (NF3) proved to be the most effective in enhancing SOD activity and strengthening antioxidant defence in diabetic wound healing, followed by optimized nanoformulation of Sinapic acid (NF2) and guar gum nanoformulation of Syringic acid (NF1). These findings align with existing data (Kurahashi et al., 2015; Kant et al., 2014).

The nano-formulations possess compact dimensions, a consistent zeta potential, and a high capacity for drug loading, indicating notable effectiveness against microbial organisms. optimized nanoformulation of Syringic acid (NF1) demonstrated the highest potency against *Staphylococcus aureus* and *Escherichia coli*, with significant inhibition zones at high and low concentrations. optimized nanoformulation of Sinapic acid (NF2) showed vigorous antifungal activity against *Candida albicans*, even at lower concentrations, but was less effective against *S. aureus* and *E. coli*. The optimized nanoformulation of o-Coumaric acid (NF3) exhibited the least inhibitory effect across all tested microorganisms and concentrations. These findings underscore that optimized nanoformulation of Syringic acid (NF1) and optimized nanoformulation of Sinapic acid (NF2) are promising candidates for further development in antimicrobial therapies, with optimized nanoformulation of Syringic acid (NF1) ideal for treating bacterial infections and optimized nanoformulation of Sinapic acid (NF2) for combating fungal infections (Neto et al., 2021). The presence of TNF- α can indicate inflammation in wounds (Sunayana et al., 2020; Serra et al., 2017). The healing process cannot begin without severe inflammation, as shown by elevated levels of TNF- α . However, too much can make fixing the problem more difficult. Conversely, when TNF- α is intentionally reduced, inflammation stops, allowing for the progression to stages of tissue regeneration such as revascularisation and collagen formation, eventually leading to the wound closing (Premarathna et al., 2019). Therefore, the equilibrium between the inflammatory response and tissue repair is illustrated by the levels and regulation of TNF- α , a crucial factor for successful wound healing. The results of the TNF- α expression experiment demonstrate the impact of various nanoformulations on inflammation in wound healing. The impact of nanoformulations on TNF- α indicates that optimized nanoformulation of o-Coumaric acid (NF3) is the most potent formulation in reducing TNF- α expression, with optimized nanoformulation of Sinapic acid (NF2) and optimized nanoformulation of Syringic acid (NF1) following closely behind in normal conditions. The nanoformulations demonstrated a downregulation of TNF- α expression in LPS-treated cells, indicating that these formulations enhance the inflammatory response in the presence of bacteria in the wound. The nanoformulations can mitigate inflammation in wounds by decreasing TNF- α expression. By modulating the inflammatory response, these nanoformulations can potentially improve the conditions required for tissue repair and regeneration (Tutar et al., 2018; Ashcroft et al., 2012; Eming et al., 2007).

Cox-II enzyme activity was measured to determine the suppression of prostaglandin synthesis and other relevant substances. The detected level of inhibition demonstrates the effectiveness

of the nanoformulations in regulating inflammatory pathways associated with wound healing (Mihai et al., 2019). The nano-formulations guar gum nanoformulation of Syringic acid (NF1), guar gum nanoformulation of Sinapic acid (NF2), and optimized nanoformulation of o-Coumaric acid (NF3) exhibited substantial and dosage-dependent suppression of Cox-II enzyme activity, suggesting their potential as efficacious anti-inflammatory agents for promoting wound healing. optimized nanoformulation of o-Coumaric acid (NF3) effectively inhibited Cox-II activity even at lower concentrations, outperforming optimized nanoformulation of Syringic acid (NF1) and guar gum nanoformulation of Sinapic acid (NF2). This suggests that optimized nanoformulation of o-Coumaric acid (NF3) is highly effective in regulating the inflammatory pathways crucial for wound healing. The results suggest that the nanoformulations can match or exceed the efficacy of conventional drugs in managing inflammation and promoting wound healing (Mayet et al., 2014; Pochapski et al., 2021)

After successfully developing the optimized nanoformulation, we evaluated its effects under in vitro conditions by inducing hyperglycaemic states. Based on the results of the cytotoxicity and antioxidant enzyme studies, we concluded that these nanoformulations exhibit minimal to no cytotoxicity. Additionally, they demonstrate strong cell migration and antioxidant potential, effectively enhancing epithelial cell migration and increasing the levels of antioxidant enzymes necessary for maintaining homeostasis in the body.

As previously noted, many synthetic anti-diabetic and wound-healing medications come with significant drawbacks. These include high costs, side effects, the need for frequent dosing, and potential interference with human metabolic pathways (Bharti et al., 2018; Chaudhury et al., 2017; Alam et al., 2022)

This highlights the crucial requirement for exploring an alternative plant-based natural therapy that is easily accessible to humans, can enhance wound healing, and minimises side effects. Consequently, we conducted an in vivo study to assess their potential to mitigate delayed diabetic wound healing and oxidative stress following the completion of in vitro studies. Since the results of optimized nanoformulation of Sinapic acid (NF2) and optimized nanoformulation of o-Coumaric acid (NF3) were better than those of guar gum nanoformulation of Syringic acid (NF1), optimized nanoformulation of Sinapic acid (NF2) and optimized nanoformulation of o-Coumaric acid (NF3) were chosen as the test compounds for in vivo studies.

For the in vivo study, 60 female Sprague-Dawley (SD) rats were obtained from NIPER-Mohali and divided into nine groups. These groups were administered different nutritional supplements, including a regular pellet diet (NPD) and a high-fat diet (HFD). HFD can contribute to the development of obesity and diabetes through various physiological mechanisms.

Consuming a high-fat meal can promptly result in an excess of calories, causing weight gain and diabetes. Body weight was monitored according to a predetermined timeline throughout the study, from onset to completion. In the early stages, the body weight of the NPD-fed group remained stable compared to the HFD-fed group, where weight gain was observed. However, following treatment with streptozotocin (STZ), a decrease in body weight was recorded. During the final week of HFD administration, a decrease in the rats' body weight was observed.

Blood glucose levels were measured using a glucometer at the initiation of the study (prior to treatment) and its conclusion (posttreatment). In the HFD/STZ-induced diabetic rats, the 40 mg/kg, i.p. dose of STZ led to heightened hyperglycaemia, with blood glucose levels exceeding 250 mg/dl, indicating the onset of diabetes (Jarrett et al., 1976).

In the initial stage, all groups had an average blood glucose level. After applying STZ, the blood glucose level increased. During the treatment phase, the glucose levels slightly decreased in nanoformulation-treated groups compared to the placebo and positive control groups. In the initial stage of the study, the blood glucose levels in all groups were within the normal range. However, after administering streptozotocin (STZ), a well-known diabetogenic agent, the blood glucose levels significantly increased, indicating the successful induction of hyperglycaemia. During the treatment phase, the nanoformulation-treated groups exhibited a slight decrease in blood glucose levels compared to the placebo and positive control groups. This observation suggests that the nanoformulation may be therapeutic in managing hyperglycaemia and wound healing.

The healing percentages for each group show a clear upward trend from the 3rd to the 14th day, indicating the natural progression of wound healing over time. Nanoformulation treatment groups showed significant improvement with both the high and low doses compared to control and raw drug treatment groups.

Wound contraction refers to the process by which the edges of a wound gradually pull together, reducing its size. Diabetes can lead to peripheral vascular disease, characterized by reduced blood flow to the limbs (Soyoye et al., 2021). This decreased blood flow can limit the delivery

of oxygen and nutrients to the wound site, hindering the healing process and slowing down wound contraction (Singh et al., 2017). Angiogenesis, forming new blood vessels from existing ones, is crucial for wound healing, as it ensures the damaged tissues receive the necessary nutrients, oxygen, and immune cells for proper recovery. Myofibroblasts, specialised cells that draw the wound edges together, contract in response to the new blood vessels, aiding healing (Eming et al., 2007). Effective wound contraction depends on the activity of white blood cells, new blood vessel formation, and collagen synthesis—all of which can be impaired by elevated glucose levels (Pawar et al., 2021). Therefore, managing diabetes and controlling blood sugar levels is vital for optimising wound healing. The *in vivo* study on diabetic wound healing revealed a clear progression in healing percentages across all groups from day 3 to day 14, demonstrating the natural course of wound repair over time. The study's findings highlight the efficacy of the nanoformulation treatments, particularly when comparing the results with those of the control and raw drug treatment groups. On the 3rd day, healing percentages were relatively low across all groups, which is expected during the initial phase of wound healing. Group 2, treated with the placebo nanoformulation, exhibited the lowest healing percentage (8.625%), underscoring the limited efficacy of the placebo. In contrast, Group 8, treated with the high dose of guar gum nanoformulation of Sinapic acid (NF2), showed the highest healing percentage (24%). This early advantage suggests that the nanoformulation, particularly at higher doses, may accelerate the initial wound healing process, possibly due to enhanced bioavailability and targeted active compound delivery. By the 7th day, significant improvements were observed across all groups, reflecting the body's increased healing activity. Group 8 maintained its lead with a healing percentage of 55.625%, indicating sustained effectiveness of the high-dose nanoformulation. The lowest healing percentage was recorded in Group 4 (38.75%), highlighting potential variability in treatment response. The notable increase in healing percentages by this stage suggests that the treatments are becoming more effective as the healing process progresses, likely due to cumulative effects and the body's enhanced physiological response to the treatments. On the 10th day, most groups exhibited rapid healing, with Group 8 still at the forefront (85.125%), followed closely by Group 5 (83.125%). Group 4, while improving, continued to show the lowest healing percentage (57.5%), which may indicate a slower response to treatment in this group. The rapid healing observed in most groups at this stage suggests that the nanoformulation, especially in higher doses, may significantly enhance wound repair, potentially through mechanisms such as improved angiogenesis, increased collagen synthesis, and better wound contraction. By the 14th day, several groups achieved near-complete or complete healing, with Groups 1, 5, 6, and 8 reaching 100% healing.

This outcome emphasizes the effectiveness of the nanoformulation, particularly in the high-dose groups. The lowest healing percentage at this stage was recorded in Group 2 (73.5%), treated with the placebo nanoformulation, underscoring the superior efficacy of the active treatments.

Additionally, Groups 6 and 9 demonstrated impressive healing percentages of 96.8% and 97.75%, respectively, further validating the nanoformulation's potential to promote efficient wound healing.

The study's results strongly suggest that the nanoformulation, especially at higher doses, significantly enhances wound healing in diabetic conditions. The improved healing observed in the nanoformulation-treated groups may be attributed to several factors, including better drug delivery to the wound site, increased drug stability, and prolonged release, which collectively enhance the bioavailability of the active compound (Hamam et al., 2020). The accelerated wound contraction and rapid tissue regeneration in the high-dose groups also indicate that the nanoformulation may positively influence critical processes such as angiogenesis and collagen synthesis. Overall, the findings from this *in vivo* study demonstrate that nanoformulation offers a promising therapeutic approach for enhancing diabetic wound healing. The clear advantage of the nanoformulation over the control and raw drug treatments highlights its potential as an effective treatment option.

The *in vivo* wound healing tensile strength study reveals several critical insights into the effectiveness of various treatments for diabetic wound healing (Dogan et al., 2009). The *in vivo* tensile strength study results provide valuable insights into the effectiveness of different treatments for diabetic wound healing. The non-diabetic control group, which achieved a tensile strength of 27 MPa, sets a benchmark for optimal wound healing. In contrast, the placebo-treated group demonstrated a markedly lower tensile strength of 12.965 MPa. This significant reduction underscores diabetes's challenges to wound healing, where impaired tissue repair and compromised strength are prevalent (Perez G. et al., 2005). The positive control group, with a tensile strength of 18.825 MPa, showed a modest improvement over the placebo group. This suggests that while the positive control treatment has some beneficial effects, it cannot match the strength seen in the non-diabetic control. Similarly, the raw drug-treated groups, with tensile strengths of 15.12 MPa and 18.19 MPa, improved over the placebo and positive control groups. However, these strengths still fall short of those observed in the non-diabetic control, indicating that while the raw drugs contribute positively to wound

healing, they do not fully address the complexities of diabetic wounds. In contrast, the nanoformulation treatments demonstrated a significant enhancement in tensile strength. The guar gum nanoformulation of Sinapic acid (NF2)-treated groups achieved tensile strengths of 25.38 MPa and 23.845 MPa for high and low doses, respectively, while the guar gum nanoformulation of o-Coumaric acid (NF3)-treated groups showed even greater improvements with tensile strengths of 26.23 MPa and 24.78 MPa for high and low doses, respectively. These results highlight the superior efficacy of the nanoformulations compared to both the raw drugs and the positive control. The enhanced performance of optimized nanoformulation of Sinapic acid (NF2) and optimized nanoformulation of o-Coumaric acid (NF3) can be attributed to several factors inherent in nanoformulations. These include improved bioavailability, which allows for better delivery and sustained release of therapeutic agents at the wound site; enhanced cellular uptake, which facilitates more effective interaction with wound tissues; and targeted action, which minimises off-target effects and maximizes therapeutic impact specifically at the wound site (Bitar et al., 1996; Yue et al., 1987). Overall, the significant improvements observed with the nanoformulation treatments underscore their potential for bettering wound healing outcomes in diabetic conditions. Their efficacy surpasses conventional treatments and raw drugs, making them promising candidates for further development and clinical application. These findings suggest that continued research into nanoformulations could offer even more effective strategies for addressing the challenges associated with diabetic wound healing (Özay et al., 2019).

The connection between antioxidants and oxidative stress is intricate, particularly when considering cellular and physiological functions (Rahal et al., 2014). Prolonged or excessive oxidative stress is linked to various diseases, including wound healing and neurological issues, leading to cellular damage (Schäfer et al., 2008). The immune system uses a complex network of non-enzymatic and enzymatic antioxidants to fight oxidative damage. Enzymatic systems like catalase and SOD promptly neutralize free radicals, while non-enzymatic antioxidants eliminate and capture them. By neutralizing ROS and lipid peroxides, antioxidant enzymes (such as glutathione peroxidase, catalase, and SOD), along with non-enzymatic antioxidants (such as vitamins C and E), work to prevent LPO in cells. Comprehending the interaction between antioxidants and oxidative stress is essential for improving overall health and reducing the risk of diseases associated with excessive oxidative damage (Sharifi-Rad et al., 2020; Jomova et al., 2023). Lipid peroxidation is a marker of oxidative stress, where free radicals attack lipids in cell membranes, leading to cell damage and inflammation. In diabetic

conditions, this process is typically accelerated due to chronic hyperglycaemia, which generates excessive reactive oxygen species (ROS). The high levels of ROS damage cellular structures and impair the normal function of key cells involved in wound healing, such as fibroblasts and keratinocytes (Volpe et al., 2018). Consistent with our *in vitro* results, our *in vivo* lipid peroxidation (LPO) assay results demonstrate that the nanoformulation effectively restored the oxidative balance to a normal state in diabetic wound healing. This finding is particularly significant because diabetes is often associated with elevated oxidative stress, which can exacerbate tissue damage and impair the wound-healing process. The ability of our nanoformulation to restore normal LPO levels suggests that it has potent antioxidant properties, likely due to the bioactive compounds encapsulated within the nanoparticle matrix (Ashok et al., 2018). By neutralizing excess ROS, the nanoformulation reduces oxidative damage, creating a more favourable environment for wound healing. This improved oxidative balance can enhance the function of cells critical for tissue repair, promote collagen synthesis, and support angiogenesis, all of which are essential for effective wound contraction and closure (Wang et al., 2024; Zhang et al., 2022). Additionally, restoring normal oxidative conditions may help reduce inflammation at the wound site, further facilitating the healing process. Combining these effects likely underlies the observed improvement in wound healing outcomes with the nanoformulation, making it a promising therapeutic option for managing diabetic wounds (Cano Sanchez et al., 2018).

The *in vivo* assays for catalase, glutathione S-transferase (GST), and superoxide dismutase (SOD) have provided insightful data regarding the efficacy of the nanoformulation in promoting diabetic wound healing (Shukla et al., 1997). The results indicate that the nanoformulation has nearly restored these antioxidant enzyme levels to customary conditions, suggesting a significant improvement in the oxidative stress environment within the wound healing process.

Catalase is an enzyme responsible for decomposing hydrogen peroxide, a reactive oxygen species (ROS) that can cause cellular damage if accumulated (Jomova et al., 2023). In diabetic conditions, the overproduction of ROS can overwhelm the antioxidant defences, leading to increased oxidative stress and impaired wound healing. The near-normal levels of catalase observed in the treated group indicate that the nanoformulation effectively mitigates oxidative stress by enhancing the breakdown of hydrogen peroxide, thus creating a more conducive environment for wound healing (Birben et al., 2012).

Glutathione S-transferase (GST) is critical in detoxifying reactive intermediates and protecting cells from oxidative damage. Elevated GST levels are often a marker of increased oxidative stress and the need for detoxification. The restoration of GST levels toward normal in the presence of the nanoformulation suggests that it may have helped to rebalance the oxidative stress state in diabetic wounds, enhancing the detoxification processes and potentially contributing to improved healing (Hellou et al., 2012).

Superoxide dismutase (SOD) is another crucial enzyme that catalyzes the conversion of superoxide radicals into less harmful molecules. The normalisation of SOD levels in the nanoformulation-treated group implies that the formulation may enhance the overall antioxidant defence system. This is particularly important in diabetic wounds, where high superoxide radicals can exacerbate tissue damage and delay healing (Bafana et al., 2011).

The significant improvement in these antioxidant enzyme levels following treatment with the nanoformulation underscores its potential in addressing the oxidative imbalance commonly observed in diabetic wounds. By restoring catalase, GST, and SOD levels close to normal, the nanoformulation appears to reduce oxidative stress and support the wound healing process. These findings highlight the effectiveness of nanoformulation in counteracting oxidative damage and promoting a more favourable wound-healing environment. This improvement in enzymatic activity suggests that nanoformulation may play a vital role in managing diabetes-related complications and enhancing wound repair through its antioxidant properties.

Hydroxyproline, a non-proteinogenic amino acid predominantly found in collagen, serves as a critical indicator of collagen content and thus reflects the extent of tissue repair and regeneration (Mavropalias et al., 2023). Collagen is crucial in restoring injured skin's mechanical strength, anatomical structure, and functional integrity (Balasubramanian et al., 2013). The *in vivo* hydroxyproline study provides valuable insights into the effects of various treatments on collagen synthesis in diabetic wound healing.

The study revealed notable differences in hydroxyproline content across different treatment groups over time. Specifically, hydroxyproline content increased significantly by the seventh and tenth days in all experimental groups compared to the third day. Notably, the non-diabetic control group exhibited significant improvements in hydroxyproline levels, with increases of 38.71% on the seventh day and 129.22% on the tenth day. This substantial rise aligns with the natural healing process observed in non-diabetic conditions, where collagen production and tissue repair are typically more effective (Mavropalias et al., 2023).

In contrast, the placebo-treated group showed a smaller increase in hydroxyproline, with a rise of 25.62% on the seventh day and 107.17% on the tenth day. This suggests that the placebo treatment has a limited impact on collagen synthesis, highlighting the need for more effective interventions in wound healing. The positive control group, which received a standard treatment for diabetic wounds, demonstrated a moderate increase in hydroxyproline levels—32.87% on the seventh day and 117.31% on the tenth day. While this indicates some level of efficacy, the results suggest that the positive control is less effective than the nanoformulation treatments. The most pronounced effects were observed in the nanoformulation-treated groups. Both high and low doses of optimized nanoformulation of Sinapic acid (NF2) and optimized nanoformulation of o-Coumaric acid (NF3) significantly increased hydroxyproline levels, indicating a strong potential for these treatments to enhance collagen synthesis (Bai et al., 2020). High-dose optimized nanoformulation of Sinapic acid (NF2) led to a 43.49% increase on the seventh day and a 135% increase on the tenth day, while low-dose optimized nanoformulation of Sinapic acid (NF2) showed an increase of 41.77% and 127.09%, respectively. High-dose optimized nanoformulation of o-Coumaric acid (NF3) resulted in a 46.76% increase on the seventh day and a 142.05% increase on the tenth day, with low-dose optimized nanoformulation of o-Coumaric acid (NF3) showing rises of 41.49% and 134.63%. These findings suggest that nanoformulations are highly effective in promoting collagen deposition and accelerating wound healing in diabetic conditions (Bai et al., 2020). The significant increases in hydroxyproline levels observed in the nanoformulation groups may be attributed to their enhanced delivery of active compounds to the wound site, improving the availability of growth factors and nutrients essential for collagen synthesis and tissue repair. This superior performance of nanoformulations over traditional treatments underscores their potential as a promising approach for managing diabetic wounds. Overall, the results highlight the potential of nanoformulations to offer a more effective solution for diabetic wound healing than conventional treatments.

Hexosamines play a crucial role in tissue repair, as they are key components of glycosaminoglycans and proteoglycans that contribute to the extracellular matrix (Menezes et al., 2023). Their progressive increase suggests an improvement in the wound-healing process (Honnegowda et al., 2016). The results from the hexosamine content analysis in diabetic wound healing models offer valuable insights into the efficacy of various treatments. The observed increase in hexosamine content from the 7th to the 10th day across all groups indicates a general trend towards enhanced wound healing. In the non-diabetic control group, the substantial rise

in hexosamine content—94.07% on the 7th day and 143.05% on the 10th day—reflects an optimal healing environment without the complications associated with diabetes. This result underscores the robust nature of the healing process under normal conditions. In contrast, the placebo-treated group demonstrated a lower increase in hexosamine content, with percentages of 82.38% on the 7th day and 121.59% on the 10th day. This lesser increase suggests that the placebo alone is less effective in stimulating hexosamine production and promoting wound healing. It highlights the need for more active therapeutic interventions in the management of diabetic wounds. The positive control group showed slightly higher increases in hexosamine levels (83.68% on the 7th day and 131.1% on the 10th day) compared to the placebo group, indicating that the positive control has a moderate impact on enhancing hexosamine production. However, these results still fall short of the improvements observed with the nanoformulation treatments. The nanoformulation-treated groups, particularly those receiving high and low doses, exhibited significant enhancements in hexosamine content. The high-dose guar gum nanoformulation of Sinapic acid (NF2)-treated groups showed increases of 97.36% on the 7th day and 156.79% on the 10th day, while the low-dose guar gum nanoformulation of Sinapic acid (NF2)-treated groups had increases of 93.97% and 136.85%, respectively. The guar gum nanoformulation of o-Coumaric acid (NF3)-treated groups demonstrated even greater improvements, with the high dose showing 103.78% on the 7th day and 167.60% on the 10th day, and the low dose showing 100.23% and 149.44%, respectively. The superior performance of the nanoformulation-treated groups indicates that these treatments significantly enhance hexosamine production and, by extension, wound healing. The high-dose nanoformulations (optimized nanoformulation of Sinapic acid (NF2) and guar gum nanoformulation of o-Coumaric acid (NF3)) were particularly effective, likely due to their increased bioavailability and efficacy. This suggests that nanoformulations hold promise as effective therapeutic agents for diabetic wound healing (Im et al., 2009). Overall, the findings highlight the potential of nanoformulations to offer improved treatment options for diabetic wounds. The marked increase in hexosamine content with these treatments suggests they could address the shortcomings of conventional therapies, leading to better healing outcomes and potentially enhancing patient quality of life (Shetlar et al., 1959; Ashkani-Esfahani et al., 2012).

The *in vivo* study and histopathological analysis results are closely interlinked, providing a detailed perspective on wound healing. By the 14th day, several groups achieved near-complete or complete healing, with Groups 1, 6, and 8 reaching 100% healing (Table 17.1). This high

level of healing was corroborated by histopathological findings, which revealed complete dermal remodelling, including significant thickening and stratification of the epithelium in these groups. Similarly, Groups 6 and 9, which showed impressive healing percentages of 96.875% and 97.375%, respectively, also demonstrated thorough tissue recovery and well-developed granulation tissues in the histopathological examination (Table 17.2). In contrast, Group 2, despite showing improvement, had the lowest healing percentage at 73.5%. This lower percentage of healing was reflected in the histopathological analysis, which showed less dermal remodelling and minimal thickening, indicating less effective healing than the higher-performing groups. The diabetic wounded control group exhibited disturbed healing parameters, such as poor re-epithelialization and incomplete granulation tissue maturation, aligning with their lower healing percentages. This correlation underscores the impact of the diabetic condition on wound healing (Singla et al., 2017). NF treatment at doses of 20 mg/kg and 40 mg/kg resulted in enhanced healing, as evidenced by improved re-epithelialization, mature granulation tissues, and new blood vessel formation (Table 18). This improvement in healing was reflected in the higher healing percentages observed in the treated groups. The efficacy of NF treatment in restoring critical healing parameters and accelerating wound recovery was thus validated by the quantitative healing percentages and the qualitative histopathological observations (Singla et al., 2017; Dwivedi et al., 2017).

Chapter 8: Conclusion

Type 2 diabetes mellitus (T2DM) is a prevalent metabolic disorder characterised by insulin resistance and impaired insulin secretion, leading to chronic hyperglycaemia. This condition results in elevated blood glucose levels due to either inadequate insulin production or ineffective utilisation of insulin. The increasing global prevalence of T2DM highlights its significant public health impact, particularly concerning its complications, such as impaired wound healing. Wounds, which disrupt tissue structure and integrity due to various injuries, usually heal through a physiological process known as the "healing cascade". However, in diabetic individuals, wound healing is often impaired due to elevated blood glucose levels, chronic inflammation, weakened immune responses, and compromised vascular function. This can lead to slow or incomplete healing, increasing the risk of infections that can spread and become life-threatening if untreated. Even in the absence of infection, poor wound healing can significantly affect a person's health and quality of life. In 2021, the International Diabetes Federation estimated 537 million people aged 20–79 with diabetes, with projections reaching 643 million by 2030 and 783 million by 2045. Diabetes was responsible for one in five global deaths in 2021. Conventional treatments like metformin and povidone-iodine, while familiar, often come with adverse effects. To address these issues, our research explores a novel approach using a biodegradable polymer-based nanoformulation with guar gum, incorporating bioactive phytochemicals such as Syringic acid, Sinapic acid, and o-Coumaric acid. Through optimisation and comprehensive testing, we aim to develop a more effective and safer alternative for managing diabetic wound healing.

After conducting initial trials, we optimized the compositions and parameters of our nanoformulations using a BBD design model. The subsequent characterisation of these formulations confirmed that they achieved nanoscale dimensions with optimal drug loading and controlled release kinetics. The efficacy of the nanoformulations was further validated through various assays. Free radical scavenging assays, such as DPPH and ABTS, demonstrated the nanoformulations' capacity to effectively neutralise free radicals, which is advantageous for promoting wound healing. Additionally, antidiabetic assays, including glucosidase and amylase activity tests, yielded promising results, indicating that all three nanoformulations had beneficial effects on glucose metabolism. In vitro cytotoxicity tests revealed that the nanoformulations exhibited minimal or negligible toxicity, which is crucial

for their safety profile. Significant improvements were observed in wound healing and angiogenesis, as evidenced by the enhanced performance in scratch assays (which measure wound closure) and tube formation assays (which assess new blood vessel development). These results suggest that nanoformulations effectively repair damaged tissues and form new vascular structures. Moreover, in vitro antioxidant assays, including lipid peroxidation (LPO), catalase, superoxide dismutase (SOD), and glutathione S-transferase (GST) tests, showed that the nanoformulations could enhance antioxidant activity, thereby restoring near-normal oxidative conditions in the test systems.

Following these promising in vitro results, we selected the two most effective nanoformulations, the optimized nanoformulation of Sinapic acid (NF2) and the guar gum nanoformulation of o-Coumaric acid (NF3), for in vivo studies. These studies demonstrated that the nanoformulations were highly effective in healing diabetic wounds. Specifically, high doses of the nanoformulations achieved complete wound healing similar to that observed under normal conditions. Even at lower doses, the nanoformulations nearly achieved full wound closure in diabetic conditions. Additionally, the treatments significantly restored tensile strength to levels comparable to those seen in non-diabetic conditions. Consistent with the in vitro antioxidant assays, the in vivo studies also showed that the nanoformulations improved antioxidant activity, helping to normalize oxidative stress conditions in the healing wounds.

In conclusion, the optimized nanoformulations showed strong efficacy in diabetic wound healing. They demonstrated nanoscale properties with controlled drug release and effective free radical scavenging. In vitro tests confirmed minimal toxicity and significant antioxidant activity, wound healing, and angiogenesis improvements. In vivo studies further validated that nanoformulations optimized nanoformulation of Sinapic acid (NF2) and optimized nanoformulation of o-Coumaric acid (NF3) achieved complete wound healing and restored tensile strength, highlighting their potential as effective and safer alternatives to conventional treatments.

Further research and clinical trials will be crucial to confirm these findings and explore the broader applications of nanoformulations in wound care.

References

- Ademiluyi, A. O. , & Oboh, G. (2013). Soybean phenolic-rich extracts inhibit key enzymes linked to type 2 diabetes (α -amylase and α -glucosidase) and hypertension (angiotensin I converting enzyme) in vitro. *Experimental and toxicologic pathology: official journal of the Gesellschaft für Toxikologische Pathologie*, 65 (3), 305–309. <https://doi.org/10.1016/j.etp.2011.09.005>
- Adepu, S., & Ramakrishna, S. (2021). Controlled Drug Delivery Systems: Current Status and Future Directions. *Molecules (Basel, Switzerland)*, 26 (19), 5905. <https://doi.org/10.3390/molecules26195905>
- Aderibigbe, B. A. , & Buyana, B. (2018). Alginate in wound dressings. *Pharmaceutics*, 10 (2), 42.
- Agarwal, P. , Kukrele, R. , & Sharma, D. (2019). Vacuum assisted closure (VAC)/negative pressure wound therapy (NPWT) for difficult wounds: A review. *Journal of clinical orthopaedics and trauma*, 10 (5), 845-848.
- Aguilar, L. M. C. , Silva, S. M. , & Moulton, S. E. (2019). Growth factor delivery: Defining the next generation platforms for tissue engineering. *Journal of Controlled Release*, 306, 40-58.
- Aguilera-Correa, J. J. , Gisbert-Garzarán, M. , Mediero, A. , Carias-Cálix, R. A. , Jiménez-Jiménez, C. , Esteban, J. , & Vallet-Regí, M. (2022). Arabic gum plus colistin coated moxifloxacin-loaded nanoparticles for the treatment of bone infection caused by *Escherichia coli*. *Acta Biomaterialia*, 137, 218-237.
- Ahlqvist, E. , Prasad, R. B. , & Groop, L. (2022). 100 YEARS OF INSULIN: Towards improved precision and a new classification of diabetes mellitus. *Journal of Endocrinology*, 252 (3), R59-R70.
- Ahmed, B. , Sultana, R. , & Greene, M. W. (2021). Adipose tissue and insulin resistance in obese. *Biomedicine & Pharmacotherapy*, 137, 111315.
- Ahmed, K. A. , Korany, R. M. S. , El Halawany, H. A. , & Ahmed, K. S. (2019). *Spirulina platensis* alleviates arsenic-induced toxicity in male rats: biochemical, histopathological and immunohistochemical studies. *Adv Anim Vet Sci*, 7 (8), 701-710.
- Alam, S. , Sarker, M. M. R. , Sultana, T. N. , Chowdhury, M. N. R. , Rashid, M. A. , Chaity, N. I. , . . . & Mohamed, I. N. (2022). Antidiabetic phytochemicals from

medicinal plants: prospective candidates for new drug discovery and development. *Frontiers in endocrinology*, 13, 800714.

- Alavi, M. , & Rai, M. (2020). Topical delivery of growth factors and metal/metal oxide nanoparticles to infected wounds by polymeric nanoparticles: an overview. *Expert Review of Anti-infective Therapy*, 18 (10), 1021-1032.
- Alexandru, V. , Gaspar, A. , Savin, S. , Toma, A. , Tatia, R. , & Gille, E. (2015). Phenolic content, antioxidant activity, and effect on collagen synthesis of a traditional wound healing polyherbal formula. *Studia Universitatis" Vasile Goldis" Arad. Seria Stiintele Vietii (Life Sciences Series)*, 25 (1), 41.
- Algandaby, M. M. , Esmat, A. , Nasrullah, M. Z. , Alhakamy, N. A. , AbdelNaim, A. B. , Rashad, O. M. , . . . & Eltamany, E. E. (2023). LC-MS based metabolic profiling and wound healing activity of a chitosan nanoparticle-loaded formula of *Teucrium polium* in diabetic rats. *Biomedicine & Pharmacotherapy*, 168, 115626.
- Ali, A. , Skedung, L. , Burleigh, S. , Lavant, E. , Ringstad, L. , Anderson, C. D. , . . . & Engblom, J. (2022). Relationship between sensorial and physical characteristics of topical creams: A comparative study on effects of excipients. *International Journal of Pharmaceutics*, 613, 121370.
- Ali, S. S. , Morsy, R. , El-Zawawy, N. A. , Fareed, M. F. , & Bedaiwy, M. Y. (2017). Synthesized zinc peroxide nanoparticles (ZnO₂-NPs): a novel antimicrobial, anti-elastase, anti-keratinase, and anti-inflammatory approach toward polymicrobial burn wounds. *International journal of nanomedicine*, 6059-6073.
- Alizadeh, S. , Seyedalipour, B. , Shafieyan, S. , Kheime, A. , Mohammadi, P. , & Aghdami, N. (2019). Copper nanoparticles promote rapid wound healing in acute full-thickness defects via acceleration of skin cell migration, proliferation, and neovascularization. *Biochemical and biophysical research communications*, 517 (4), 684-690.
- Allu, I. , Kumar Sahi, A. , Kumari, P. , Sakhile, K. , Sionkowska, A. , & Gundu, S. (2023). A brief review on cerium oxide (CeO₂NPs)-based scaffolds: recent advances in wound healing applications. *Micromachines*, 14 (4), 865.
- Alven, S. , Nqoro, X. , & Aderibigbe, B. A. (2020). Polymer-based materials loaded with curcumin for wound healing applications. *Polymers*, 12 (10), 2286.
- Alven, S. , Nqoro, X. , & Aderibigbe, B. A. (2020). Polymer-based materials loaded with curcumin for wound healing applications. *Polymers*, 12 (10), 2286.

- Amalan, V. , Vijayakumar, N. , & Ramakrishnan, A. (2015). p-Coumaric acid regulates blood glucose and antioxidant levels in streptozotocin induced diabetic rats. *J. Chem. Pharm. Res*, 7 (7), 831-839.
- Amaldoss, M. J. N. (2022). Gum-based nanoparticles in cancer therapy. In *Micro-and Nanoengineered Gum-Based Biomaterials for Drug Delivery and Biomedical Applications* (pp. 183-225). Elsevier.
- Amjed, N. , Zeshan, M. , Farooq, A. , & Naz, S. (2023). A comprehensive review on the applications of guar gum as a biopolymer for pharmaceuticle drug delivery. *International Journal of Biological Macromolecules*, 128390.
- André-Lévigne, D. , Modarressi, A. , Pignel, R. , Bochaton-Piallat, M. L. , & Pittet-Cuénod, B. (2016). Hyperbaric oxygen therapy promotes wound repair in ischemic and hyperglycemic conditions, increasing tissue perfusion and collagen deposition. *Wound Repair and Regeneration*, 24 (6), 954-965.
- Anushree, U. , Punj, P. , Vasumathi, & Bharati, S. (2023). Phosphorylated chitosan accelerates dermal wound healing in diabetic wistar rats. *Glycoconjugate Journal*, 40 (1), 19-31.
- Aravindaraj, N. , Suresh, J. , Krishnaswami, V. , & Kandasamy, R. (2022). Guar Gum-Based Novel Nanodrug Delivery Systems. *Nanoengineering of Biomaterials*, 63-89.
- Arnaoutova, I. , & Kleinman, H. K. (2010). In vitro angiogenesis: endothelial cell tube formation on gelled basement membrane extract. *Nature protocols*, 5 (4), 628-635.
- Arya, A. K. , Pokharia, D. , & Tripathi, K. (2011). Relationship between oxidative stress and apoptotic markers in lymphocytes of diabetic patients with chronic nonhealing wounds. *Diabetes research and clinical practice*, 94 (3), 377-384.
- Ashcroft, G. S. , Jeong, M. J. , Ashworth, J. J. , Hardman, M. , Jin, W. , Moutsopoulos, N. , . . . & Wahl, S. M. (2012). Tumor necrosis factor-alpha (TNF- α) is a therapeutic target for impaired cutaneous wound healing. *Wound Repair and Regeneration*, 20 (1), 38-49.
- Ashkani-Esfahani, S. , Emami, Y. , Esmaeilzadeh, E. , Bagheri, F. , & Namazi, M. R. (2012). Glucosamine enhances tissue regeneration in the process of wound healing in rats as animal model: a stereological study. *J Cytol Histol*, 3 (1), 150.
- Ashok, A. , Andrabi, S. S. , Mansoor, S. , Kuang, Y. , Kwon, B. K. , & Labhasetwar, V. (2022). Antioxidant therapy in oxidative stress-induced neurodegenerative diseases:

Role of nanoparticle-based drug delivery systems in clinical translation. *Antioxidants*, 11 (2), 408.

- Ashrafizadeh, M. , Najafi, M. , Orouei, S. , Zabolian, A. , Saleki, H. , Azami, N. , . . . & Ahn, K. S. (2020). Resveratrol modulates transforming growth factor-beta (tgf- β) signaling pathway for disease therapy: a new insight into its pharmacological activities. *Biomedicines*, 8 (8), 261.
- Ashrafizadeh, M. , Zarrabi, A. , Hushmandi, K. , Zarrin, V. , Moghadam, E. R. , Hashemi, F. , . . . & Mirzaei, H. (2020). Toward regulatory effects of curcumin on transforming growth factor-beta across different diseases: a review. *Frontiers in pharmacology*, 11, 585413.
- Atiyeh, B. S. , Dibo, S. A. , & Hayek, S. N. (2009). Wound cleansing, topical antiseptics and wound healing. *International wound journal*, 6 (6), 420-430.
- Augustine, R. , Prasad, P. , & Khalaf, I. M. N. (2019). Therapeutic angiogenesis: from conventional approaches to recent nanotechnology-based interventions. *Materials Science and Engineering: C*, 97, 994-1008.
- Avwioroko, O. J. , Anigboro, A. A. , Atanu, F. O. , Otuechere, C. A. , Alfred, M. O. , Abugo, J. N. , & Omorogie, M. O. (2020). Investigation of the binding interaction of α -amylase with Chrysophyllum albidum seed extract and its silver nanoparticles: a multi-spectroscopic approach. *Chemical Data Collections*, 29, 100517.
- Bafana, A. , Dutt, S. , Kumar, A. , Kumar, S. , & Ahuja, P. S. (2011). The basic and applied aspects of superoxide dismutase. *Journal of Molecular Catalysis B: Enzymatic*, 68 (2), 129-138.
- Bai, Q. , Han, K. , Dong, K. , Zheng, C. , Zhang, Y. , Long, Q. , & Lu, T. (2020). Potential applications of nanomaterials and technology for diabetic wound healing. *International journal of nanomedicine*, 9717-9743.
- Bains, A. , Sharma, P. , Kaur, S. , Yadav, R. , Kumar, A. , Sridhar, K. , . . . & Sharma, M. (2023). Gum arabic/guar gum stabilized Hydnocarpus wightiana oil nanohydrogel: Characterization, antimicrobial, anti-inflammatory, and anti-biofilm activities. *International Journal of Biological Macromolecules*, 239, 124341.
- Balasubramanian, P. , Prabhakaran, M. P. , Sireesha, M. , & Ramakrishna, S. (2013). Collagen in human tissues: structure, function, and biomedical implications from a tissue engineering perspective. *Polymer Composites–Polyolefin Fractionation–Polymeric Peptidomimetics–Collagens*, 173-206.

- Baruah, C. , & Sarmah, J. K. (2022). Guar gum-based hydrogel and hydrogel nanocomposites for biomedical applications. In *Micro-and Nanoengineered Gum-Based Biomaterials for Drug Delivery and Biomedical Applications* (pp. 473-492). Elsevier.
- Baxter, H. (2003). Management of surgical wounds. *Nursing times*, 99 (13), 66-68.
- Beck-Nielsen, H. , Vaag, A. , Poulsen, P. , & Gaster, M. (2003). Metabolic and genetic influence on glucose metabolism in type 2 diabetic subjects—experiences from relatives and twin studies. *Best Practice & Research Clinical Endocrinology & Metabolism*, 17 (3), 445-467.
- Bessereau, J. , Aboab, J. , Hullin, T. , Huon-Bessereau, A. , Bourgeois, J. L. , Brun, P. M. , . . . & Annane, D. (2017). Safety of hyperbaric oxygen therapy in mechanically ventilated patients. *International maritime health*, 68 (1), 46-51.
- Beuge, J. A. , & Aust, S. D. (1978). The thiobarbituric acid assay.
- Beyer Jr, W. F. , & Fridovich, I. (1987). Assaying for superoxide dismutase activity: some large consequences of minor changes in conditions. *Analytical biochemistry*, 161 (2), 559-566.
- Bharti, S. K. , Krishnan, S. , Kumar, A. , & Kumar, A. (2018). Antidiabetic phytoconstituents and their mode of action on metabolic pathways. *Therapeutic Advances in Endocrinology and metabolism*, 9 (3), 81-100.
- Bhubhanil, S. , Talodthaisong, C. , Khongkow, M. , Namdee, K. , Wongchitrat, P. , Yingmema, W. , . . . & Kulchat, S. (2021). Enhanced wound healing properties of guar gum/curcumin-stabilized silver nanoparticle hydrogels. *Scientific Reports*, 11 (1), 21836.
- Bianchera, A. , Catanzano, O. , Boateng, J. , & Elviri, L. (2020). The place of biomaterials in wound healing. *Therapeutic dressings and wound healing applications*, 337-366.
- Biganeh, H. , Dizaji, S. M. , Taghipour, Y. D. , Murtaza, G. , & Rahimi, R. (2023). Nanoformulations of plant-derived compounds as emerging therapeutic approach for colorectal cancer. *Current Drug Delivery*, 20 (8), 1067-1094.
- Bigliardi, P. L. , Alsagoff, S. A. L. , El-Kafrawi, H. Y. , Pyon, J. K. , Wa, C. T. C. , & Villa, M. A. (2017). Povidone iodine in wound healing: A review of current concepts and practices. *International Journal of Surgery*, 44, 260-268.

- Bikowski, J. (1999). Secondarily infected wounds and dermatoses: a diagnosis and treatment guide. *The Journal of emergency medicine*, 17 (1), 197-206.
- Birben, E. , Sahiner, U. M. , Sackesen, C. , Erzurum, S. , & Kalayci, O. (2012). Oxidative stress and antioxidant defense. *World allergy organization journal*, 5, 9-19.
- Bitar, M. S. , & Labbad, Z. N. (1996). Transforming growth factor- β and insulin-like growth factor-I in relation to diabetes-induced impairment of wound healing. *Journal of Surgical Research*, 61 (1), 113-119.
- Blume, P. A. , Walters, J. , Payne, W. , Ayala, J. , & Lantis, J. (2008). Comparison of negative pressure wound therapy using vacuum-assisted closure with advanced moist wound therapy in the treatment of diabetic foot ulcers: a multicenter randomized controlled trial. *Diabetes care*, 31 (4), 631-636.
- Boateng, J. , & Catanzano, O. (2015). Advanced therapeutic dressings for effective wound healing—a review. *Journal of pharmaceutical sciences*, 104 (11), 3653-3680.
- Bolajoko, E. B. , Akinosun, O. M. , & Khine, A. A. (2020). Hyperglycemia-induced oxidative stress in the development of diabetic foot ulcers. In *Diabetes* (pp. 35-48). Academic Press.
- Borges, A. , Ferreira, C. , Saavedra, M. J. , & Simões, M. (2013). Antibacterial activity and mode of action of ferulic and gallic acids against pathogenic bacteria. *Microbial drug resistance*, 19 (4), 256-265.
- Borgquist, O. , Ingemansson, R. , & Malmsjö, M. (2010). Wound edge microvascular blood flow during negative-pressure wound therapy: examining the effects of pressures from -10 to -175 mmHg. *Plastic and reconstructive surgery*, 125 (2), 502-509.
- Bostanudin, M. F. , Salam, A. , Mahmood, A. , Arafat, M. , Kaharudin, A. N. , Sahudin, S. , . . . & Azfaralariff, A. (2021). Formulation and in-vitro characterisation of cross-linked amphiphilic guar gum nanocarriers for percutaneous delivery of arbutin. *Journal of pharmaceutical sciences*, 110 (12), 3907-3918.
- Bostanudin, M. F. , Salam, A. , Mahmood, A. , Arafat, M. , Kaharudin, A. N. , Sahudin, S. , . . . & Azfaralariff, A. (2021). Formulation and in-vitro characterisation of cross-linked amphiphilic guar gum nanocarriers for percutaneous delivery of arbutin. *Journal of pharmaceutical sciences*, 110 (12), 3907-3918.
- Brighente, I. M. C. , Dias, M. , Verdi, L. G. , & Pizzolatti, M. G. (2007). Antioxidant activity and total phenolic content of some Brazilian species. *Pharmaceutical biology*, 45 (2), 156-161.

- Brown, B. C. , McKenna, S. P. , Siddhi, K. , McGrouther, D. A. , & Bayat, A. (2008). The hidden cost of skin scars: quality of life after skin scarring. *Journal of Plastic, Reconstructive & Aesthetic Surgery*, 61 (9), 1049-1058.
- Bruggisser, R. , vonDaeniken, K. , Jundt, G. , Schaffner, W. , &TullbergReinert, H. (2002). Int erference of plant extracts, phytoestrogens and antioxidants with the MTT tetrazolium assay. *Plantamedica*, 68 (05), 445-448.
- Burgess, J. L. , Wyant, W. A. , Abdo Abujamra, B. , Kirsner, R. S. , & Jozic, I. (2021). Diabetic wound-healing science. *Medicina*, 57 (10), 1072.
- Caban, M. , & Lewandowska, U. (2023). Encapsulation of polyphenolic compounds based on hemicelluloses to enhance treatment of inflammatory bowel diseases and colorectal cancer. *Molecules*, 28 (10), 4189.
- Cano Sanchez, M. , Lancel, S. , Boulanger, E. , & Nevieri, R. (2018). Targeting oxidative stress and mitochondrial dysfunction in the treatment of impaired wound healing: a systematic review. *Antioxidants*, 7 (8), 98.
- Cano Sanchez, M. , Lancel, S. , Boulanger, E. , & Nevieri, R. (2018). Targeting oxidative stress and mitochondrial dysfunction in the treatment of impaired wound healing: a systematic review. *Antioxidants*, 7 (8), 98.
- Cano Sanchez, M. , Lancel, S. , Boulanger, E. , &Nevieri, R. (2018). Targeting oxidative stress and mitochondrial dysfunction in the treatment of impaired wound healing: a systematic review. *Antioxidants*, 7 (8), 98.
- Casado-Díaz, A. , Quesada-Gómez, J. M. , & Dorado, G. (2020). Extracellular vesicles derived from mesenchymal stem cells (MSC) in regenerative medicine: applications in skin wound healing. *Frontiers in Bioengineering and Biotechnology*, 8, 146.
- Cavaghan, M. K. , Ehrmann, D. A. , & Polonsky, K. S. (2000). Interactions between insulin resistance and insulin secretion in the development of glucose intolerance. *The Journal of clinical investigation*, 106 (3), 329-333.
- Cavalcanti, G. R. , Duarte, F. I. , Converti, A. , & de Lima, Á. A. (2021). Ferulic acid activity in topical formulations: technological and scientific prospecting. *Current pharmaceutical design*, 27 (19), 2289-2298.
- Cavalu, S. , Pasca, P. M. , & Brocks, M. (2019). Natural Polymeric Film Encapsulating Propolis Nano-Formulation for Cutaneous Wound Healing. *Mater. Plast*, 56 (3).
- Centers for Disease Control and Prevention (CDC. (2017). National Diabetes Statistics Report, 2017-Estimates of Diabetes and Its Burden in the United States Background.

- Chakraborty, R. , Borah, P. , Dutta, P. P. , & Sen, S. (2022). Evolving spectrum of diabetic wound: Mechanistic insights and therapeutic targets. *World Journal of Diabetes*, 13 (9), 696.
- Chance, B. , & Maehly, A. C. (1955). (136) Assay of catalases and peroxidases.
- Chandika, P. , Khan, F. , Heo, S. Y. , Kim, T. H. , Kim, Y. M. , Yi, M. , & Jung, W. K. (2022). Multifunctional dual cross-linked poly (vinyl alcohol)/methacrylate hyaluronic acid/chitoooligosaccharide-Sinapic acid wound dressing hydrogel. *International Journal of Biological Macromolecules*, 222, 1137-1150.
- Chaudhury, A. , Duvoor, C. , Reddy Dendi, V. S. , Kraleti, S. , Chada, A. , Ravilla, R. , . . . & Mirza, W. (2017). Clinical review of antidiabetic drugs: implications for type 2 diabetes mellitus management. *Frontiers in endocrinology*, 8, 6.
- Cherng, J. H. , Lin, C. A. J. , Liu, C. C. , Yeh, J. Z. , Fan, G. Y. , Tsai, H. D. , . . . & Hsu, S. D. (2022). Homostasis and anti-inflammatory abilities of AuNPs-coated chitosan dressing for burn wounds. *Journal of Personalized Medicine*, 12 (7), 1089.
- Cherng, Y. G. , Tsai, C. C. , Chung, H. H. , Lai, Y. W. , Kuo, S. C. , & Cheng, J. T. (2013). Antihyperglycemic action of Sinapic acid in diabetic rats. *Journal of Agricultural and Food Chemistry*, 61 (49), 12053-12059.
- Christenson, J. C. , Korgenski, E. K. , & Relich, R. F. (2018). Laboratory diagnosis of infection due to bacteria, fungi, parasites, and rickettsiae. In *Principles and practice of pediatric infectious diseases* (pp. 1422-1434). Elsevier.
- Chu, Y. , Yu, D. , Wang, P. , Xu, J. , Li, D. , & Ding, M. (2010). Nanotechnology promotes the full-thickness diabetic wound healing effect of recombinant human epidermal growth factor in diabetic rats. *Wound repair and regeneration*, 18 (5), 499-505.
- Çimşit, M. , Uzun, G. , & Yıldız, Ş. (2009). Hyperbaric oxygen therapy as an anti-infective agent. *Expert review of anti-infective therapy*, 7 (8), 1015-1026.
- Contardi, M. , Lenzuni, M. , Fiorentini, F. , Summa, M. , Bertorelli, R. , Suarato, G. , & Athanassiou, A. (2021). Hydroxycinnamic acids and derivatives formulations for skin damages and disorders: A review. *Pharmaceutics*, 13 (7), 999.
- Correa, V. L. R. , Martins, J. A. , de Souza, T. R. , Rincon, G. D. C. N. , Miguel, M. P. , de Menezes, L. B. , & Amaral, A. C. (2020). Melatonin-loaded lecithin-chitosan nanoparticles improved wound healing in diabetic rats. *International Journal of Biological Macromolecules*, 162, 1465-1475.

- Costa, G. , Francisco, V. , C Lopes, M. , T Cruz, M. , & T Batista, M. (2012). Intracellular signaling pathways modulated by phenolic compounds: application for new anti-inflammatory drugs discovery. *Current medicinal chemistry*, 19 (18), 2876-2900.
- Cueva, C. , Moreno-Arribas, M. V. , Martín-Álvarez, P. J. , Bills, G. , Vicente, M. F. , Basilio, A. , . . . & Bartolomé, B. (2010). Antimicrobial activity of phenolic acids against commensal, probiotic and pathogenic bacteria. *Research in microbiology*, 161 (5), 372-382.
- Daggett, D. A. , Oberley, T. D. , Nelson, S. A. , Wright, L. S. , Kornguth, S. E. , & Siegel, F. L. (1998). Effects of lead on rat kidney and liver: GST expression and oxidative stress. *Toxicology*, 128 (3), 191-206.
- Davison, A. M. (2004). The incised wound. In *Essentials of Autopsy Practice: Recent Advances, Topics and Developments* (pp. 187-220). London: Springer London.
- Day, C. M. , Hickey, S. M. , Song, Y. , Plush, S. E. , & Garg, S. (2020). Novel tamoxifen nanoformulations for improving breast cancer treatment: Old wine in new bottles. *Molecules*, 25 (5), 1182.
- de Lafuente, Y. , Ochoa-Andrade, A. , Parente, M. E. , Palena, M. C. , & Jimenez-Kairuz, A. F. (2020). Preparation and evaluation of caffeine bioadhesive emulgels for cosmetic applications based on formulation design using QbD tools. *International Journal of Cosmetic Science*, 42 (6), 548-556.
- DeCicco-Skinner, K. L. , Henry, G. H. , Cataisson, C. , Tabib, T. , Gwilliam, J. C. , Watson, N. J. , . . . & Wiest, J. S. (2014). Endothelial cell tube formation assay for the in vitro study of angiogenesis. *JoVE (Journal of Visualized Experiments)*, 91), e51312.
- DeFronzo, R. A. , Ferrannini, E. , Groop, L. , Henry, R. R. , Herman, W. H. , Holst, J. J. , . . . & Weiss, R. (2015). Type 2 diabetes mellitus. *Nature reviews Disease primers*, 1 (1), 1-22.
- Deng, L. , Du, C. , Song, P. , Chen, T. , Rui, S. , Armstrong, D. G. , & Deng, W. (2021). The role of oxidative stress and antioxidants in diabetic wound healing. *Oxidative medicine and cellular longevity*, 2021 (1), 8852759.
- Derosa, G. , Catena, G. , Gaudio, G. , D'Angelo, A. , & Maffioli, P. (2020). Adipose tissue dysfunction and metabolic disorders: Is it possible to predict who will develop type 2 diabetes mellitus? Role of markErs in the progreSsion of dIabeteS in obese paTieNts (The RESISTIN trial). *Cytokine*, 127, 154947.

- Desta, T. , Li, J. , Chino, T. , & Graves, D. T. (2010). Altered fibroblast proliferation and apoptosis in diabetic gingival wounds. *Journal of dental research*, 89 (6), 609-614.
- Dicpinigaitis, P. A. , Koval, K. J. , Tejawani, N. C. , & Egol, K. A. (2006). Gunshot wounds to the extremities. *Bulletin of the NYU hospital for joint diseases*, 64 (3-4), 139-139.
- Diniz, C. , Suliburska, J. , & Ferreira, I. M. (2017). New insights into the antiangiogenic and proangiogenic properties of dietary polyphenols. *Molecular nutrition & food research*, 61 (6), 1600912.
- Dix, T. A. , & Aikens, J. (1993). Mechanisms and biological relevance of lipid peroxidation initiation. *Chemical research in toxicology*, 6 (1), 2-18.
- Dodi, G. , Pala, A. , Barbu, E. , Peptanariu, D. , Hritcu, D. , Popa, M. I. , & Tamba, B. I. (2016). Carboxymethyl guar gum nanoparticles for drug delivery applications: Preparation and preliminary in-vitro investigations. *Materials Science and Engineering: C*, 63, 628-636.
- Dodi, G. , Sabau, R. E. , Crețu, B. E. B. , & Gardikiotis, I. (2023). Exploring the antioxidant potential of gellan and guar gums in wound healing. *Pharmaceutics*, 15 (8), 2152.
- Dodi, G. , Sabau, R. E. , Crețu, B. E. B. , & Gardikiotis, I. (2023). Exploring the Antioxidant Potential of Gellan and Guar Gums in Wound Healing. *Pharmaceutics*, 15 (8), 2152.
- Dogan, S. , Demirer, S. E. H. E. R. , Kepenekci, I. , Erkek, B. , Kiziltay, A. Y. S. E. L. , Hasirci, N. E. S. R. I. N. , . . . & Kuterdem, E. (2009). Epidermal growth factor-containing wound closure enhances wound healing in non-diabetic and diabetic rats. *International wound journal*, 6 (2), 107-115.
- Du, C. , Liu, J. , Fikhman, D. A. , Dong, K. S. , & Monroe, M. B. B. (2022). Shape memory polymer foams with phenolic acid-based antioxidant and antimicrobial properties for traumatic wound healing. *Frontiers in Bioengineering and Biotechnology*, 10, 809361.
- Du, J. , & Wong, K. K. (2019). Nanomaterials for wound healing: scope and advances. In *Theranostic bionanomaterials* (pp. 211-230). Elsevier.
- Dwivedi, D. , Dwivedi, M. , Malviya, S. , & Singh, V. (2017). Evaluation of wound healing, anti-microbial and antioxidant potential of *Pongamia pinnata* in wistar rats. *Journal of traditional and complementary medicine*, 7 (1), 79-85.

- Eaglstein, W. H. , & Falanga, V. (1998). Tissue engineering and the development of Apligraf®, a human skin equivalent. *Advances in Skin & Wound Care*, 11, 1-8.
- Ebaid, H. , Ahmed, O. M. , Mahmoud, A. M. , & Ahmed, R. R. (2013). Limiting prolonged inflammation during proliferation and remodeling phases of wound healing in streptozotocin-induced diabetic rats supplemented with camel undenatured whey protein. *BMC immunology*, 14 (1), 1-13.
- El-Ela, F. I. A. , Farghali, A. A. , Mahmoud, R. K. , Mohamed, N. A. , & Moaty, S. A. (2019). New approach in ulcer prevention and wound healing treatment using doxycycline and amoxicillin/LDH Nanocomposites. *Scientific reports*, 9 (1), 6418.
- Elsabahy, M. , Heo, G. S. , Lim, S. M. , Sun, G. , & Wooley, K. L. (2015). Polymeric nanostructures for imaging and therapy. *Chemical reviews*, 115 (19), 10967-11011.
- Eming, S. A. , Brachvogel, B. , Odorisio, T. , & Koch, M. (2007). Regulation of angiogenesis: wound healing as a model. *Progress in histochemistry and cytochemistry*, 42 (3), 115-170.
- Eming, S. A. , Krieg, T. , & Davidson, J. M. (2007). Inflammation in wound repair: molecular and cellular mechanisms. *Journal of Investigative Dermatology*, 127 (3), 514-525.
- Eming, S. A. , Martin, P. , & Tomic-Canic, M. (2014). Wound repair and regeneration: mechanisms, signaling, and translation. *Science translational medicine*, 6 (265), 265sr6-265sr6.
- English, B. K. , & Gaur, A. H. (2010). The use and abuse of antibiotics and the development of antibiotic resistance. *Hot topics in infection and immunity in children VI*, 73-82.
- Enoch, S. , & Leaper, D. J. (2008). Basic science of wound healing. *Surgery (Oxford)*, 26 (2), 31-37.
- Estanqueiro, M. , Amaral, M. H. , & Sousa Lobo, J. M. (2016). Comparison between sensory and instrumental characterization of topical formulations: impact of thickening agents. *International journal of cosmetic science*, 38 (4), 389-398.
- Estanqueiro, M. , Amaral, M. H. , & Sousa Lobo, J. M. (2016). Comparison between sensory and instrumental characterization of topical formulations: impact of thickening agents. *International journal of cosmetic science*, 38 (4), 389-398.

- Etebu, E. , & Ariekpar, I. (2016). Antibiotics: Classification and mechanisms of action with emphasis on molecular perspectives. *Int. J. Appl. Microbiol. Biotechnol. Res*, 4 (2016), 90-101.
- Everts, P. A. , Lana, J. F. , Onishi, K. , Buford, D. , Peng, J. , Mahmood, A. , . . . & Podesta, L. (2023). Angiogenesis and tissue repair depend on platelet dosing and bioformulation strategies following orthobiological platelet-rich plasma procedures: a narrative review. *Biomedicines*, 11 (7), 1922.
- Fahimirad, S. , Abtahi, H. , Satei, P. , Ghaznavi-Rad, E. , Moslehi, M. , & Ganji, A. (2021). Wound healing performance of PCL/chitosan based electrospun nanofiber electrospayed with curcumin loaded chitosan nanoparticles. *Carbohydrate polymers*, 259, 117640.
- Falanga, V. , Isseroff, R. R. , Soulika, A. M. , Romanelli, M. , Margolis, D. , Kapp, S. , . . . & Harding, K. (2022). Chronic wounds. *Nature Reviews Disease Primers*, 8 (1), 50.
- Farooq, M. , Ihsan, J. , Mohamed, R. M. , Khan, M. A. , Rehman, T. U. , Ullah, H. , . . . & Siddiq, M. (2022). Highly biocompatible formulations based on Arabic gum Nano composite hydrogels: Fabrication, characterization, and biological investigation. *International Journal of Biological Macromolecules*, 209, 59-69.
- Fathi-Achachelouei, M. , Knopf-Marques, H. , Ribeiro da Silva, C. E. , Barthès, J. , Bat, E. , Tezcaner, A. , & Vrana, N. E. (2019). Use of nanoparticles in tissue engineering and regenerative medicine. *Frontiers in bioengineering and biotechnology*, 7, 113.
- Feldman, E. L. , Callaghan, B. C. , Pop-Busui, R. , Zochodne, D. W. , Wright, D. E. , Bennett, D. L. , . . . & Viswanathan, V. (2019). Diabetic neuropathy. *Nature reviews Disease primers*, 5 (1), 41.
- Frykberg Robert, G. (2015). Challenges in the treatment of chronic wounds. *Advances in wound care*.
- Gadde, S. , Even-Or, O. , Kamaly, N. , Hasija, A. , Gagnon, P. G. , Adusumilli, K. H. , . . . & Farokhzad, O. C. (2014). Development of therapeutic polymeric nanoparticles for the resolution of inflammation. *Advanced healthcare materials*, 3 (9), 1448-1456.
- Garg, S. S. , Dubey, R. , Sharma, S. , Vyas, A. , & Gupta, J. (2023). Biological macromolecules-based nanoformulation in improving wound healing and bacterial biofilm-associated infection: A review. *International Journal of Biological Macromolecules*, 125636.

- Geana, E. I. , Ciucure, C. T. , Tamaian, R. , Marinas, I. C. , Gaboreanu, D. M. , Stan, M. , & Chitescu, C. L. (2023). Antioxidant and Wound Healing Bioactive Potential of Extracts Obtained from Bark and Needles of Softwood Species. *Antioxidants*, 12 (7), 1383.
- George, A. , Shah, P. A. , & Shrivastav, P. S. (2019). Guar gum: Versatile natural polymer for drug delivery applications. *European Polymer Journal*, 112, 722-735.
- George, A. , Shah, P. A. , & Shrivastav, P. S. (2019). Guar gum: Versatile natural polymer for drug delivery applications. *European Polymer Journal*, 112, 722-735.
- George, A. , Shah, P. A. , & Shrivastav, P. S. (2019). Guar gum: Versatile natural polymer for drug delivery applications. *European Polymer Journal*, 112, 722-735.
- Gerstein, H. C. , & Rutty, C. J. (2021). Insulin therapy: the discovery that shaped a century. *Canadian Journal of Diabetes*, 45 (8), 798-803.
- Ghorani, B. , Naji-Tabasi, S. , Bostan, A. , & Emadzadeh, B. (2018). Application of Nanotechnology in the Safe Delivery of Bioactive Compounds. In *Nanotechnology Applications in the Food Industry* (pp. 237-291). CRC Press.
- Gil, C. J. , Tomov, M. L. , Theus, A. S. , Cetnar, A. , Mahmoudi, M. , & Serpooshan, V. (2019). In vivo tracking of tissue engineered constructs. *Micromachines*, 10 (7), 474.
- Goldstein, B. J. (2002). Insulin resistance as the core defect in type 2 diabetes mellitus. *The American journal of cardiology*, 90 (5), 3-10.
- Gonzalez, A. C. D. O. , Costa, T. F. , Andrade, Z. D. A. , & Medrado, A. R. A. P. (2016). Wound healing-A literature review. *Anais brasileiros de dermatologia*, 91 (5), 614-620.
- Gonzalez, A. C. D. O. , Costa, T. F. , Andrade, Z. D. A. , & Medrado, A. R. A. P. (2016). Wound healing-A literature review. *Anais brasileiros de dermatologia*, 91, 614-620.
- Goodarzi, P. , Falahzadeh, K. , Nematizadeh, M. , Farazandeh, P. , Payab, M. , Larijani, B. , . . . & Arjmand, B. (2018). Tissue engineered skin substitutes. *Cell Biology and Translational Medicine*, Volume 3: Stem Cells, Bio-materials and Tissue Engineering, 143-188.
- Gordoís A, Scuffham P, Shearer A, Oglesby A, Tobian JA. The health care costs of diabetic peripheral neuropathy in the US. *Diabetes Care*. 2003;26 (6): 1790-5.
- Gordoís, A. , Scuffham, P. , Shearer, A. , Oglesby, A. , & Tobian, J. A. (2003). The health care costs of diabetic peripheral neuropathy in the US. *Diabetes care*, 26 (6), 1790-1795.

- Grazul-Bilska, A. T. , Johnson, M. L. , Bilski, J. J. , Redmer, D. A. , Reynolds, L. P. , Abdullah, A. , & Abdullah, K. M. (2003). Wound healing: the role of growth factors. *Drugs Today (Barc)*, 39 (10), 787-800.
- Gresta, F. , Sortino, O. , Santonoceto, C. , Issi, L. , Formantici, C. , & Galante, Y. M. (2013). Effects of sowing times on seed yield, protein and galactomannans content of four varieties of guar (*Cyamopsis tetragonoloba* L.) in a Mediterranean environment. *Industrial Crops and Products*, 41, 46-52.
- Guo, S. A. , & DiPietro, L. A. (2010). Factors affecting wound healing. *Journal of dental research*, 89 (3), 219-229.
- Habig, W. H. , Pabst, M. J. , & Jakoby, W. B. (1974). Glutathione S-transferases: the first enzymatic step in mercapturic acid formation. *Journal of biological Chemistry*, 249 (22), 7130-7139.
- Hamad, A. , Khashan, K. S. , & Hadi, A. (2020). Silver nanoparticles and silver ions as potential antibacterial agents. *Journal of Inorganic and Organometallic Polymers and Materials*, 30 (12), 4811-4828.
- Hamam, F. , & Nasr, A. (2020). Curcumin-Loaded Mesoporous Silica Particles as Wound-Healing Agent: An: In vivo: Study. *Saudi journal of medicine & medical sciences*, 8 (1), 17-24.
- Hamdan, S. , Pastar, I. , Drakulich, S. , Dikici, E. , Tomic-Canic, M. , Deo, S. , & Daunert, S. (2017). Nanotechnology-driven therapeutic interventions in wound healing: potential uses and applications. *ACS central science*, 3 (3), 163-175.
- Hameed, H. , Aydin, S. , & Başaran, N. (2016). Sinapic acid: is it safe for humans. *FABAD Journal of Pharmaceutical Sciences*, 41 (1), 39.
- Han, S. K. (2023). Basics of wound healing. In *Innovations and Advances in Wound Healing* (pp. 1-42). Singapore: Springer Nature Singapore.
- Hanmantrao, M. , Chaterjee, S. , Kumar, R. , Vishwas, S. , Harish, V. , Porwal, O. , . . . & Singh, S. K. (2022). Development of guar gum-pectin-based colon targeted solid self-nanoemulsifying drug delivery system of xanthohumol. *Pharmaceutics*, 14 (11), 2384.
- Harish, V. , Almalki, W. H. , Alshehri, A. , Alzahrani, A. , Gupta, M. M. , Alzarea, S. I. , . . . & Singh, S. K. (2023). Quality by design (QbD) based method for estimation of xanthohumol in bulk and solid lipid nanoparticles and validation. *Molecules*, 28 (2), 472.

- Harris, T. L. , & Flaherty, E. G. (2010). Bruises and skin lesions. Child abuse and neglect: diagnosis, treatment, and evidence. 1st Ed. St. Louis (Mo): Elsevier Saunders 2011, 239-51.
- He, J. , Qiao, Y. , Zhang, H. , Zhao, J. , Li, W. , Xie, T. , . . . & Zhou, M. (2020). Gold–silver nanoshells promote wound healing from drug-resistant bacteria infection and enable monitoring via surface-enhanced Raman scattering imaging. *Biomaterials*, 234, 119763.
- He, X. , Xue, J. , Shi, L. , Kong, Y. , Zhan, Q. , Sun, Y. , . . . & Dai, Y. (2022). Recent antioxidative nanomaterials toward wound dressing and disease treatment via ROS scavenging. *Materials Today Nano*, 17, 100149.
- Heilbronn, L. K. , & Campbell, L. V. (2008). Adipose tissue macrophages, low grade inflammation and insulin resistance in human obesity. *Current pharmaceutical design*, 14 (12), 1225-1230.
- Hellou, J. , Ross, N. W. , & Moon, T. W. (2012). Glutathione, glutathione S-transferase, and glutathione conjugates, complementary markers of oxidative stress in aquatic biota. *Environmental Science and Pollution Research*, 19, 2007-2023.
- Hernandez, R. (2006). The use of systemic antibiotics in the treatment of chronic wounds. *Dermatologic therapy*, 19 (6), 326-337.
- Heyboer III, M. , Sharma, D. , Santiago, W. , & McCulloch, N. (2017). Hyperbaric oxygen therapy: side effects defined and quantified. *Advances in wound care*, 6 (6), 210-224.
- Hillel, A. , Shah, P. , & Elisseff, J. (2007). Hydrogels in cell encapsulation and tissue engineering. In *Biomedical polymers* (pp. 57-82). Woodhead Publishing.
- Honnegowda, T. M. , Udupa, E. G. P. , Rao, P. , Kumar, P. , & Singh, R. (2016). Superficial burn wound healing with intermittent negative pressure wound therapy under limited access and conventional dressings. *World journal of plastic surgery*, 5 (3), 265.
- Hosgood, G. (2006). Stages of wound healing and their clinical relevance. *Veterinary Clinics: Small Animal Practice*, 36 (4), 667-685.
- Hou, B. , Qi, M. , Sun, J. , Ai, M. , Ma, X. , Cai, W. , . . . & Qiu, L. (2020). Preparation, characterization and wound healing effect of vaccarin-chitosan nanoparticles. *International journal of biological macromolecules*, 165, 3169-3179.

- Howell-Jones, R. S. , Wilson, M. J. , Hill, K. E. , Howard, A. J. , Price, P. E. , & Thomas, D. W. (2005). A review of the microbiology, antibiotic usage and resistance in chronic skin wounds. *Journal of Antimicrobial Chemotherapy*, 55 (2), 143-149.
- Hu, M. , Korschelt, K. , Daniel, P. , Landfester, K. , Tremel, W. , & Bannwarth, M. B. (2017). Fibrous nanozyme dressings with catalase-like activity for H₂O₂ reduction to promote wound healing. *ACS applied materials & interfaces*, 9 (43), 38024-38031.
- Huang, C. , Dong, L. , Zhao, B. , Lu, Y. , Huang, S. , Yuan, Z. , . . . & Qian, W. (2022). Anti-inflammatory hydrogel dressings and skin wound healing. *Clinical and Translational Medicine*, 12 (11), e1094.
- Huang, S. T. , Yang, R. C. , Wu, H. T. , Wang, C. N. , & Pang, J. H. S. (2011). Zinc-chelation contributes to the anti-angiogenic effect of ellagic acid on inhibiting MMP-2 activity, cell migration and tube formation. *PLoS One*, 6 (5), e18986.
- Huang, S. W. , Wu, Y. F. , Ahmed, T. , Pan, S. C. , & Cheng, C. M. (2023). Point-of-care detection devices for wound care and monitoring. *Trends in biotechnology*.
- Huang, X. , Xi, Y. , Pan, Q. , Mao, Z. , Zhang, R. , Ma, X. , & You, H. (2018). Caffeic acid protects against IL-1 β -induced inflammatory responses and cartilage degradation in articular chondrocytes. *Biomedicine & Pharmacotherapy*, 107, 433-439.
- Hudzicki, J. (2009). Kirby-Bauer disk diffusion susceptibility test protocol. *American society for microbiology*, 15 (1), 1-23.
- Hwang, H. J. , Park, H. J. , Chung, H. J. , Min, H. Y. , Park, E. J. , Hong, J. Y. , & Lee, S. K. (2006). Inhibitory effects of caffeic acid phenethyl ester on cancer cell metastasis mediated by the down-regulation of matrix metalloproteinase expression in human HT1080 fibrosarcoma cells. *The Journal of nutritional biochemistry*, 17 (5), 356-362.
- Hyldig, N. , Birke-Sorensen, H. , Kruse, M. , Vinter, C. , Joergensen, J. S. , Sorensen, J. A. , . . . & Bille, C. (2016). Meta-analysis of negative-pressure wound therapy for closed surgical incisions. *Journal of British Surgery*, 103 (5), 477-486.
- Iacob, A. T. , Drăgan, M. , Ionescu, O. M. , Profire, L. , Ficai, A. , Andronesu, E. , . . . & Lupașcu, D. (2020). An overview of biopolymeric electrospun nanofibers based on polysaccharides for wound healing management. *Pharmaceutics*, 12 (10), 983.
- Im, A. , & Kim, Y. S. (2009). Role of glycosaminoglycans in wound healing. *Archives of Pharmaceutical Sciences and Research*, 1 (2), 106-114.

- International Diabetes Federation. IDF Diabetes Atlas 10th Edition 2021, Global Estimates for the Prevalence of Diabetes for 2019, 2030 and 2045. Available online: <http://www.diabetesatlas.org/> (accessed on 30 January 2024).
- International Diabetes Federation. IDF Diabetes Atlas 9th Edition 2019, Global Estimates for the Prevalence of Diabetes for 2019, 2030 and 2045. Available online: <http://www.diabetesatlas.org/> (accessed on 30 January 2023).
- Jagodzinski, N. A. , Weerasinghe, C. , & Porter, K. (2010). Crush injuries and crush syndrome-a review. Part 2: the local injury. *Trauma*, 12 (3), 133-148.
- Jarrett, R. J. , & Keen, H. (1976). Hyperglycaemia and diabetes mellitus. *The Lancet*, 308 (7993), 1009-1012.
- Jiang, H. , He, K. , Luo, X. , Zhang, M. , Shao, J. , Gan, L. , . . . & Wei, Q. (2022). Chlorogenic acid attenuates inflammation, oxidative stress, apoptosis and protects head kidney macrophage of yellow catfish from ammonia toxicity. *Aquaculture Research*, 53 (1), 168-177.
- Jiang, Z. , Zheng, Z. , Yu, S. , Gao, Y. , Ma, J. , Huang, L. , & Yang, L. (2023). Nanofiber scaffolds as drug delivery systems promoting wound healing. *Pharmaceutics*, 15 (7), 1829.
- John, C. M. , & Arockiasamy, S. (2021). 3, 5-Dimethoxy-4-benzoic acid (Syringic acid) a natural phenolic acid reduces reactive oxygen species in differentiated 3T3-L1 adipocytes. *In Vitro Cellular & Developmental Biology-Animal*, 57, 386-394.
- Jomova, K. , Raptova, R. , Alomar, S. Y. , Alwasel, S. H. , Nepovimova, E. , Kuca, K. , & Valko, M. (2023). Reactive oxygen species, toxicity, oxidative stress, and antioxidants: Chronic diseases and aging. *Archives of toxicology*, 97 (10), 2499-2574.
- Jomova, K. , Raptova, R. , Alomar, S. Y. , Alwasel, S. H. , Nepovimova, E. , Kuca, K. , & Valko, M. (2023). Reactive oxygen species, toxicity, oxidative stress, and antioxidants: Chronic diseases and aging. *Archives of toxicology*, 97 (10), 2499-2574.
- Jones, V. , Grey, J. E. , & Harding, K. G. (2006). Wound dressings. *Bmj*, 332 (7544), 777-780.
- Joshi, S. R. , Standl, E. , Tong, N. , Shah, P. , Kalra, S. , & Rathod, R. (2015). Therapeutic potential of α -glucosidase inhibitors in type 2 diabetes mellitus: an evidence-based review. *Expert opinion on pharmacotherapy*, 16 (13), 1959-1981.
- Kailashiya, J. , & Dash, D. (2022). Effects of nanoceria on human platelet functions and blood coagulation. *International Journal of Nanomedicine*, 273-284.

- Kalachaveedu, M. , Jenifer, P. , Pandian, R. , & Arumugam, G. (2020). Fabrication and characterization of herbal drug enriched Guar galactomannan based nanofibrous mats seeded with GMSC's for wound healing applications. *International journal of biological macromolecules*, 148, 737-749.
- Kalashnikova, I. , Das, S. , & Seal, S. (2015). Nanomaterials for wound healing: scope and advancement. *Nanomedicine*, 10 (16), 2593-2612.
- Kale, D. S. , Karande, G. S. , & Datkhile, K. D. (2023). Diabetic foot ulcer in India: aetiological trends and bacterial diversity. *Indian journal of endocrinology and metabolism*, 27 (2), 107-114.
- Kaltalioglu, K. (2023). Sinapic acid-loaded gel accelerates diabetic wound healing process by promoting re-epithelialization and attenuating oxidative stress in rats. *Biomedicine & Pharmacotherapy*, 163, 114788.
- Kamaly, N. , Yameen, B. , Wu, J. , & Farokhzad, O. C. (2016). Degradable controlled-release polymers and polymeric nanoparticles: mechanisms of controlling drug release. *Chemical reviews*, 116 (4), 2602-2663.
- Kamani, S. , & Singh, P. K. (2017). DIABETES: A LONG WAY TO GO IN INDIA.
- Kang, Y. J. , Mbonye, U. R. , DeLong, C. J. , Wada, M. , & Smith, W. L. (2007). Regulation of intracellular cyclooxygenase levels by gene transcription and protein degradation. *Progress in lipid research*, 46 (2), 108-125.
- Kant, V. , Gopal, A. , Pathak, N. N. , Kumar, P. , Tandan, S. K. , & Kumar, D. (2014). Antioxidant and anti-inflammatory potential of curcumin accelerated the cutaneous wound healing in streptozotocin-induced diabetic rats. *International immunopharmacology*, 20 (2), 322-330.
- Karam, R. A. , Rezk, N. A. , Rahman, T. M. A. , & Al Saeed, M. (2018). Effect of negative pressure wound therapy on molecular markers in diabetic foot ulcers. *Gene*, 667, 56-61.
- Karamanou, M., Protogerou, A., Tsoucalas, G., Androutsos, G., & Poulakou-Rebelakou, E. (2016). Milestones in the history of diabetes mellitus: The main contributors. *World journal of diabetes*, 7(1), 1.
- Kargozar, S. , Baino, F. , Hoseini, S. J. , Hamzehlou, S. , Darroudi, M. , Verdi, J. , . . . & Mozafari, M. (2018). Biomedical applications of nanocerita: new roles for an old player. *Nanomedicine*, 13 (23), 3051-3069.

- Karpiński, T. M. , & Szkaradkiewicz, A. K. (2015). Chlorhexidine–pharmacobiological activity and application. *Eur Rev Med Pharmacol Sci*, 19 (7), 1321-1326.
- Karwal, K. , & Mukovozov, I. (2023). Topical AHA in Dermatology: Formulations, Mechanisms of Action, Efficacy, and Future Perspectives. *Cosmetics*, 10 (5), 131.
- Kaurinovic, B. , & Vastag, D. (2019). Flavonoids and phenolic acids as potential natural antioxidants (pp. 1-20). London, UK: IntechOpen.
- Kaurinovic, B. , & Vastag, D. (2019). *Flavonoids and phenolic acids as potential natural antioxidants* (pp. 1-20). London, UK: IntechOpen.
- Kikuzaki, H. , Hisamoto, M. , Hirose, K. , Akiyama, K. , & Taniguchi, H. (2002). Antioxidant properties of ferulic acid and its related compounds. *Journal of agricultural and food chemistry*, 50 (7), 2161-2168.
- King, K. D. , Jones, J. D. , & Warthen, J. (2005). Microvascular and macrovascular complications of diabetes mellitus. *American journal of pharmaceutical education*, 69 (5).
- Kitabchi, A. E. , Umpierrez, G. E. , Miles, J. M. , & Fisher, J. N. (2009). Hyperglycemic crises in adult patients with diabetes. *Diabetes care*, 32 (7), 1335.
- Kolb, H. , & Martin, S. (2017). Environmental/lifestyle factors in the pathogenesis and prevention of type 2 diabetes. *BMC medicine*, 15 (1), 1-11.
- Kole, M. , & Dey, T. K. (2012). Effect of prolonged ultrasonication on the thermal conductivity of ZnO–ethylene glycol nanofluids. *Thermochimica Acta*, 535, 58-65.
- Kolluru, G. K. , Bir, S. C. , & Kevil, C. G. (2012). Endothelial dysfunction and diabetes: effects on angiogenesis, vascular remodeling, and wound healing. *International journal of vascular medicine*, 2012.
- Kono, Y. (1978). Generation of superoxide radical during autoxidation of hydroxylamine and an assay for superoxide dismutase. *Archives of biochemistry and biophysics*, 186 (1), 189-195.
- Kowluru, R. A. , Kowluru, A. , Mishra, M. , & Kumar, B. (2015). Oxidative stress and epigenetic modifications in the pathogenesis of diabetic retinopathy. *Progress in retinal and eye research*, 48, 40-61.
- Kramer, L. , Nadjem, H. , Glardon, M. , Kneubuehl, B. P. , Pollak, S. , Große Perdekamp, M. , & Pircher, R. (2016). A patterned abrasion caused by the impact of a cartridge case may simulate an atypical muzzle imprint mark. *International journal of legal medicine*, 130 (3), 751–757. <https://doi.org/10.1007/s00414-015-1281-4>

- Kumar, C. S. , Soloman, A. M. , Thangam, R. , Perumal, R. K. , Gopinath, A. , & Madhan, B. (2020). Ferulic acid-loaded collagen hydrolysate and polycaprolactone nanofibres for tissue engineering applications. *IET nanobiotechnology*, 14 (3), 202-209.
- Kumar, N. , & Goel, N. (2019). Phenolic acids: Natural versatile molecules with promising therapeutic applications. *Biotechnology reports*, 24, e00370.
- Kumari, A. , Raina, N. , Wahi, A. , Goh, K. W. , Sharma, P. , Nagpal, R. , . . . & Gupta, M. (2022). Wound-healing effects of curcumin and its nanoformulations: A comprehensive review. *Pharmaceutics*, 14 (11), 2288.
- Kumari, A. , Yadav, S. K. , & Yadav, S. C. (2010). Biodegradable polymeric nanoparticles based drug delivery systems. *Colloids and surfaces B: biointerfaces*, 75 (1), 1-18.
- Kumbhar, S. , Khairate, R. , Bhatia, M. , Choudhari, P. , & Gaikwad, V. (2023). Evaluation of curcumin-loaded chitosan nanoparticles for wound healing activity. *ADMET and DMPK*, 11 (4), 601-613.
- Kurahashi, T. , & Fujii, J. (2015). Roles of antioxidative enzymes in wound healing. *Journal of Developmental Biology*, 3 (2), 57-70.
- Kurahashi, T. , & Fujii, J. (2015). Roles of antioxidative enzymes in wound healing. *Journal of Developmental Biology*, 3 (2), 57-70.
- Kwan, K. H. , Liu, X. , To, M. K. , Yeung, K. W. , Ho, C. M. , & Wong, K. K. (2011). Modulation of collagen alignment by silver nanoparticles results in better mechanical properties in wound healing. *Nanomedicine: Nanotechnology, Biology and Medicine*, 7 (4), 497-504.
- Laato, M. , Kähäri, V. M. , Niinikoski, J. , & Vuorio, E. (1987). Epidermal growth factor increases collagen production in granulation tissue by stimulation of fibroblast proliferation and not by activation of procollagen genes. *Biochemical Journal*, 247 (2), 385-388.
- Lavery, L. A. , Armstrong, D. G. , Wunderlich, R. P. , Mohler, M. J. , Wendel, C. S. , & Lipsky, B. A. (2006). Risk factors for foot infections in individuals with diabetes. *Diabetes care*, 29 (6), 1288-1293.
- Lee, J. H. , Parthiban, P. , Jin, G. Z. , Knowles, J. C. , & Kim, H. W. (2021). Materials roles for promoting angiogenesis in tissue regeneration. *Progress in Materials Science*, 117, 100732.

- LeRoith, D. (2002). β -cell dysfunction and insulin resistance in type 2 diabetes: role of metabolic and genetic abnormalities. *The American journal of medicine*, 113(6), 3-11.
- Li, Q. , Xiao, W. , Zhang, F. , Liu, Q. , Ye, J. , Dong, H. , & Cao, X. (2018). Tannic acid-derived metal-phenolic networks facilitate PCL nanofiber mesh vascularization by promoting the adhesion and spreading of endothelial cells. *Journal of Materials Chemistry B*, 6 (18), 2734-2738.
- Li, X. , Wang, X. , Chen, D. , & Chen, S. (2011). Antioxidant activity and mechanism of protocatechuic acid in vitro. *Functional Foods in Health and Disease*, 1 (7), 232-244.
- Lima, J. E., Moreira, N. C., & Sakamoto-Hojo, E. T. (2022). Mechanisms underlying the pathophysiology of type 2 diabetes: From risk factors to oxidative stress, metabolic dysfunction, and hyperglycemia. *Mutation Research/Genetic Toxicology and Environmental Mutagenesis*, 874, 503437.
- Lin, C. M. , Chiu, J. H. , Wu, I. H. , Wang, B. W. , Pan, C. M. , & Chen, Y. H. (2010). Ferulic acid augments angiogenesis via VEGF, PDGF and HIF-1 α . *The Journal of nutritional biochemistry*, 21 (7), 627-633.
- Lin, D. , Xiao, M. , Zhao, J. , Li, Z. , Xing, B. , Li, X. , . . . & Chen, S. (2016). An overview of plant phenolic compounds and their importance in human nutrition and management of type 2 diabetes. *Molecules*, 21 (10), 1374.
- Liu, X. A. , Yang, Y. , Guo, X. , Liu, L. , Wu, K. , & Yu, M. (2017). The antiangiogenesis effect of pirfenidone in wound healing in vitro. *Journal of Ocular Pharmacology and Therapeutics*, 33 (9), 693-703.
- Liu, Y. , Song, S. , Liu, S. , Zhu, X. , & Wang, P. (2022). Application of nanomaterial in hydrogels related to wound healing. *Journal of Nanomaterials*, 2022 (1), 4656037.
- Lowry, O. H. , Rosebrough, N. J. , Farr, A. L. , & Randall, R. J. (1951). Protein measurement with the Folin phenol reagent. *J biol Chem*, 193 (1), 265-275.
- Ma, Z. , Shou, K. , Li, Z. , Jian, C. , Qi, B. , & Yu, A. (2016). Negative pressure wound therapy promotes vessel destabilization and maturation at various stages of wound healing and thus influences wound prognosis. *Experimental and therapeutic medicine*, 11 (4), 1307-1317.
- Madawi, E. A. , Al Jayoush, A. R. , Rawas-Qalaji, M. , Thu, H. E. , Khan, S. , Sohail, M. , . . . & Hussain, Z. (2023). Polymeric nanoparticles as tunable nanocarriers for targeted delivery of drugs to skin tissues for treatment of topical skin diseases. *Pharmaceutics*, 15 (2), 657.

- Maddaluno, L. , Urwyler, C. , & Werner, S. (2017). Fibroblast growth factors: key players in regeneration and tissue repair. *Development*, 144 (22), 4047-4060.
- Madni, A. , Khalid, A. , Wahid, F. , Ayub, H. , Khan, R. , & Kousar, R. (2021). Preparation and applications of guar gum composites in biomedical, pharmaceutical, food, and cosmetics industries. *Current Nanoscience*, 17 (3), 365-379.
- Man, E. , & Hoskins, C. (2020). Towards advanced wound regeneration. *European Journal of Pharmaceutical Sciences*, 149, 105360.
- Mandal, D. , & Gupta, J. (2023, March). Burgeoning Nanotechnology for Diabetic Wound Healing: A Novel Approach to the Future. In *Medical Sciences Forum* (Vol. 21, No. 1, p. 33). MDPI.
- Mandal, D. , & Gupta, J. (2023, March). Burgeoning Nanotechnology for Diabetic Wound Healing: A Novel Approach to the Future. In *Medical Sciences Forum* (Vol. 21, No. 1, p. 33). MDPI.
- Mandal, D. , Sarmah, J. K. , Harish, V. , & Gupta, J. (2024). Antioxidant, In Vitro Cytotoxicity, and Anti-diabetic Attributes of a Drug-Free Guar Gum Nanoformulation as a Novel Candidate for Diabetic Wound Healing. *Molecular Biotechnology*, 1-15.
- Mandal, D. , Sarmah, J. K. , Harish, V. *et al.* Antioxidant, In Vitro Cytotoxicity, and Anti-diabetic Attributes of a Drug-Free Guar Gum Nanoformulation as a Novel Candidate for Diabetic Wound Healing. *Mol Biotechnol* (2024). <https://doi.org/10.1007/s12033-024-01261-z>
- Mani, A. , Kushwaha, K. , Khurana, N. , & Gupta, J. (2022). p-Coumaric acid attenuates high-fat diet-induced oxidative stress and nephropathy in diabetic rats. *Journal of Animal Physiology and Animal Nutrition*, 106 (4), 872-880.
- Margolis, D. J. , Allen-Taylor, L. , Hoffstad, O. , & Berlin, J. A. (2002). Diabetic neuropathic foot ulcers: the association of wound size, wound duration, and wound grade on healing. *Diabetes care*, 25 (10), 1835-1839.
- Margolis, D. J. , Allen-Taylor, L. , Hoffstad, O. , & Berlin, J. A. (2002). Diabetic neuropathic foot ulcers: the association of wound size, wound duration, and wound grade on healing. *Diabetes care*, 25 (10), 1835-1839.
- Maria Elizabeth, M. P. , Clara, O. C. , & Del Carmen, M. (2017). Pancreatic β -cells and type 2 diabetes development. *Current Diabetes Reviews*, 13 (2), 108-121.
- Mariotti, M. , & Maier, J. A. (2006). Angiogenesis: an overview. *New frontiers in angiogenesis*, 1, 1-29.

- Marko, V. , & Marko, V. (2020). Insulin. From Aspirin to Viagra: Stories of the Drugs that Changed the World, 64-91.
- Martin, P. , & Leibovich, S. J. (2005). Inflammatory cells during wound repair: the good, the bad and the ugly. *Trends in cell biology*, 15 (11), 599-607.
- Martins, D. , & English, A. M. (2014). Catalase activity is stimulated by H₂O₂ in rich culture medium and is required for H₂O₂ resistance and adaptation in yeast. *Redox biology*, 2, 308-313.
- Mary, P. R. , Prashanth, K. H. , Vasu, P. , & Kapoor, M. (2019). Structural diversity and prebiotic potential of short chain β -manno-oligosaccharides generated from guar gum by endo- β -mannanase (ManB-1601). *Carbohydrate research*, 486, 107822.
- Mathieu, D. , Ratzenhofer-Komenda, B. , & Kot, J. (2015). Hyperbaric oxygen therapy for intensive care patients: position statement by the European Committee for Hyperbaric Medicine. *Diving Hyperb Med*, 45 (1), 42-46.
- Mavropalias, G. , Boppart, M. , Usher, K. M. , Grounds, M. D. , Nosaka, K. , & Blazeovich, A. J. (2023). Exercise builds the scaffold of life: muscle extracellular matrix biomarker responses to physical activity, inactivity, and aging. *Biological Reviews*, 98 (2), 481-519.
- Maxon, B. , & Starch, M. (2016). Formulating skin care products with silicones: Approaches and strategies. *Handbook of Formulating Dermal Applications: A Definitive Practical Guide*, 59-114.
- Mayet, N. , Choonara, Y. E. , Kumar, P. , Tomar, L. K. , Tyagi, C. , Du Toit, L. C. , & Pillay, V. (2014). A comprehensive review of advanced biopolymeric wound healing systems. *Journal of pharmaceutical sciences*, 103 (8), 2211-2230.
- McLellan, A. T. , Lewis, D. C. , O'brien, C. P. , & Kleber, H. D. (2000). Drug dependence, a chronic medical illness: implications for treatment, insurance, and outcomes evaluation. *Jama*, 284 (13), 1689-1695.
- Melguizo-Rodríguez, L. , de Luna-Bertos, E. , Ramos-Torrecillas, J. , Illescas-Montesa, R. , Costela-Ruiz, V. J. , & García-Martínez, O. (2021). Potential effects of phenolic compounds that can be found in olive oil on wound healing. *Foods*, 10 (7), 1642.
- Melguizo-Rodríguez, L. , de Luna-Bertos, E. , Ramos-Torrecillas, J. , Illescas-Montesa, R. , Costela-Ruiz, V. J. , & García-Martínez, O. (2021). Potential effects of phenolic compounds that can be found in olive oil on wound healing. *Foods*, 10 (7), 1642.

- Menezes, R. , Vincent, R. , Osorno, L. , Hu, P. , & Arinzeh, T. L. (2023). Biomaterials and tissue engineering approaches using glycosaminoglycans for tissue repair: Lessons learned from the native extracellular matrix. *Acta biomaterialia*, 163, 210-227.
- Mihai, M. M. , Dima, M. B. , Dima, B. , & Holban, A. M. (2019). Nanomaterials for Wound Healing and Infection Control. *Materials* (Basel, Switzerland), 12 (13), 2176. <https://doi.org/10.3390/ma12132176>
- Miller, N. , & Joubert, E. (2022). Critical assessment of in vitro screening of α -glucosidase inhibitors from plants with acarbose as a reference standard. *Planta Medica*, 88 (12), 1078-1091.
- Mir, M. , Ali, M. N. , Barakullah, A. , Gulzar, A. , Arshad, M. , Fatima, S. , & Asad, M. (2018). Synthetic polymeric biomaterials for wound healing: a review. *Progress in biomaterials*, 7, 1-21.
- Mishra, N. , Singh, S. , Maurya, P. , Nisha, R. , & Saraf, S. A. (2020). Recent developments and challenges in nanoformulations targeting various ailments of the colon. *Nanoformulations in Human Health: Challenges and Approaches*, 133-167.
- Moballegh Nasery, M. , Abadi, B. , Poormoghadam, D. , Zarrabi, A. , Keyhanvar, P. , Khanbabaei, H. , . . . & Sethi, G. (2020). Curcumin delivery mediated by bio-based nanoparticles: a review. *Molecules*, 25 (3), 689.
- Monika, P. , Chandraprabha, M. N. , Rangarajan, A. , Waiker, P. V. , & Chidambara Murthy, K. N. (2022). Challenges in healing wound: role of complementary and alternative medicine. *Frontiers in nutrition*, 8, 791899.
- Morachis, J. M. , Mahmoud, E. A. , & Almutairi, A. (2012). Physical and chemical strategies for therapeutic delivery by using polymeric nanoparticles. *Pharmacological reviews*, 64 (3), 505-519.
- Moran, G. J. , Krishnadasan, A. , Mower, W. R. , Abrahamian, F. M. , LoVecchio, F. , Steele, M. T. , . . . & Talan, D. A. (2017). Effect of cephalexin plus trimethoprim-sulfamethoxazole vs cephalexin alone on clinical cure of uncomplicated cellulitis: a randomized clinical trial. *Jama*, 317 (20), 2088-2096.
- Moura, J. , Madureira, P. , Leal, E. C. , Fonseca, A. C. , & Carvalho, E. (2019). Immune aging in diabetes and its implications in wound healing. *Clinical Immunology*, 200, 43-54.

- Mukherjee, N. , Saini, P. , Mukherjee, S. , Roy, P. , & Babu, S. P. S. (2014). In vitro antifilarial activity of Azadirachta indica aqueous extract through reactive oxygen species enhancement. *Asian Pacific Journal of Tropical Medicine*, 7 (11), 841-848.
- Murea, M. , Ma, L. , & Freedman, B. I. (2012). Genetic and environmental factors associated with type 2 diabetes and diabetic vascular complications. The review of diabetic studies: RDS, 9 (1), 6.
- Mutimer, M. N. , Riffkin, C. , Hill, J. A. , & Cyr, G. N. (1956). Modern Ointment Base Technology I. : Properties of Hydrocarbon Gels. *Journal of the American Pharmaceutical Association (Scientific ed.)*, 45 (2), 101-105.
- Nampoothiri, M. , Gurram, P. C. , Bojja, S. L. , & Satarker, S. (2023). Phytochemical Nanoformulations for Neurological Disorders. In *Advances in Phytonanotechnology for Treatment of Various Diseases* (pp. 179-197). CRC Press.
- Nampoothiri, M. , Gurram, P. C. , Bojja, S. L. , & Satarker, S. (2023). Phytochemical Nanoformulations for Neurological Disorders. In *Advances in Phytonanotechnology for Treatment of Various Diseases* (pp. 179-197). CRC Press.
- Neto, J. R. , Lima, G. G. , Fiamingo, A. , Germiniani, L. G. L. , Taketa, T. B. , Bataglioli, R. A. , . . . & Beppu, M. M. (2021). Controlling antimicrobial activity and drug loading capacity of chitosan-based layer-by-layer films. *International Journal of Biological Macromolecules*, 172, 154-161.
- Netto, C. G. , Toma, H. E. , & Andrade, L. H. (2013). Superparamagnetic nanoparticles as versatile carriers and supporting materials for enzymes. *Journal of Molecular Catalysis B: Enzymatic*, 85, 71-92.
- Neves, A. R. , Lúcio, M. , Martins, S. , Lima, J. L. C. , & Reis, S. (2013). Novel resveratrol nanodelivery systems based on lipid nanoparticles to enhance its oral bioavailability. *International Journal of Nanomedicine*, 177-187.
- Nićiforović, N. , & Abramović, H. (2014). Sinapic acid and its derivatives: natural sources and bioactivity. *Comprehensive reviews in food science and food safety*, 13 (1), 34-51.
- Nielsen, J. , & Fogh, K. (2015). Clinical utility of foam dressings in wound management: A review. *Chronic Wound Care Management and Research*, 31-38.
- Nithianantham, K. , Shyamala, M. , Chen, Y. , Latha, L. Y. , Jothy, S. L. , & Sasidharan, S. (2011). Hepatoprotective potential of Clitoria ternatea leaf extract against paracetamol induced damage in mice. *Molecules*, 16 (12), 10134-10145.

- Normandin, S. , Safran, T. , Winocour, S. , Chu, C. K. , Vorstenbosch, J. , Murphy, A. M. , & Davison, P. G. (2021, August). Negative pressure wound therapy: mechanism of action and clinical applications. In *Seminars in Plastic Surgery* (Vol. 35, No. 03, pp. 164-170). 333 Seventh Avenue, 18th Floor, New York, NY 10001, USA: Thieme Medical Publishers, Inc. .
- Nosrati, H. , Heydari, M. , & Khodaei, M. (2023). Cerium oxide nanoparticles: synthesis methods and applications in wound healing. *Materials Today Bio*, 100823.
- Ojalvo, A. G. , Acosta, J. B. , Mari, Y. M. , Mayola, M. F. , Pérez, C. V. , Gutiérrez, W. S. , . . . & Armstrong, D. G. (2017). Healing enhancement of diabetic wounds by locally infiltrated epidermal growth factor is associated with systemic oxidative stress reduction. *International wound journal*, 14 (1), 214-225.
- Okonkwo, U. A. , & DiPietro, L. A. (2017). Diabetes and wound angiogenesis. *International journal of molecular sciences*, 18 (7), 1419.
- Omwoyo, W. N. , Ogutu, B. , Oloo, F. , Swai, H. , Kalombo, L. , Melariri, P. , . . . & Gathirwa, J. W. (2014). Preparation, characterization, and optimization of primaquine-loaded solid lipid nanoparticles. *International Journal of nanomedicine*, 3865-3874.
- Orsu, P. , & Matta, S. (2020). Fabrication and characterization of carboxymethyl guar gum nanocomposite for application of wound healing. *International Journal of Biological Macromolecules*, 164, 2267-2276.
- Özey, Y. , Güzel, S. , Yumrutaş, Ö. , Pehlivanoğlu, B. , Erdoğan, İ. H. , Yildirim, Z. , . . . & Darcan, S. (2019). Wound healing effect of kaempferol in diabetic and nondiabetic rats. *Journal of Surgical Research*, 233, 284-296.
- Padalkar, R. , Madgulkar, A. , & Kharade, R. (2022). Wound Healing Dressing System for Diabetic Wounds Based on Curcumin and Syringic Acid. *Int. J. Pharm. Investig.* , 12, 82-86.
- Padalkar, R. , Madgulkar, A. , & Kharade, R. (2022). Wound Healing Dressing System for Diabetic Wounds Based on Curcumin and Syringic Acid. *Int. J. Pharm. Investig.* , 12, 82-86.
- Padmanabhan, J. , & Kyriakides, T. R. (2015). Nanomaterials, inflammation, and tissue engineering. *Wiley Interdisciplinary Reviews: Nanomedicine and Nanobiotechnology*, 7 (3), 355-370.
- Paladini, F. , & Pollini, M. (2019). Antimicrobial silver nanoparticles for wound healing application: progress and future trends. *Materials*, 12 (16), 2540.

- Pawar, K. B. , Desai, S. , Bhonde, R. R. , Bhole, R. P. , & Deshmukh, A. A. (2021). Wound with diabetes: present scenario and future. *Current diabetes reviews*, 17 (2), 136-142.
- Perez G, R. M. , Vargas S, R. , & Ortiz H, Y. D. (2005). Wound healing properties of *Hylocereus undatus* on diabetic rats. *Phytotherapy Research: An International Journal Devoted to Pharmacological and Toxicological Evaluation of Natural Product Derivatives*, 19 (8), 665-668.
- Pérez-Díaz, M. A. , Prado-Prone, G. , Díaz-Ballesteros, A. , González-Torres, M. , Silva-Bermudez, P. , & Sánchez-Sánchez, R. (2023). Nanoparticle and nanomaterial involvement during the wound healing process: an update in the field. *Journal of Nanoparticle Research*, 25 (2), 27.
- Pessoa, A. F. M. , Florim, J. C. , Rodrigues, H. G. , Andrade-Oliveira, V. , Teixeira, S. A. , Vitzel, K. F. , . . . & Santos, M. F. (2016). Oral administration of antioxidants improves skin wound healing in diabetic mice. *Wound Repair and Regeneration*, 24 (6), 981-993.
- Pfeiffer, A. , & Schatz, H. (1995). Diabetic microvascular complications and growth factors. *Experimental and Clinical Endocrinology & Diabetes*, 103 (01), 7-14.
- Phillips, J. C. (2005). Understanding hyperbaric oxygen therapy and its use in the treatment of compromised skin grafts and flaps. *Plastic and Aesthetic Nursing*, 25 (2), 72-80.
- Pierce, G. F. (2001). Inflammation in nonhealing diabetic wounds: the space-time continuum does matter. *The American journal of pathology*, 159 (2), 399-403.
- Pirvanescu, H. , Balasoiu, M. , Ciurea, M. E. , Balasoiu, A. T. , & Manescu, R. (2014). Wound infections with multi-drug resistant bacteria. *Chirurgia*, 109 (1), 73-9.
- Pivodová, V. , Franková, J. , Galandáková, A. , & Ulrichová, J. (2015). In vitro AuNPs' cytotoxicity and their effect on wound healing. *Nanobiomedicine*, 2, 7.
- Pluemsamran, T. , Onkoksoong, T. , & Panich, U. (2012). Caffeic acid and ferulic acid inhibit UVA-induced matrix metalloproteinase-1 through regulation of antioxidant defense system in keratinocyte HaCaT cells. *Photochemistry and Photobiology*, 88 (4), 961-968.
- Pochapski, D. J. , Carvalho dos Santos, C. , Leite, G. W. , Pulcinelli, S. H. , & Santilli, C. V. (2021). Zeta potential and colloidal stability predictions for inorganic

nanoparticle dispersions: Effects of experimental conditions and electrokinetic models on the interpretation of results. *Langmuir*, 37 (45), 13379-13389.

- Pope, J. (2009). Wound aetiology and classification. In *BSAVA Manual of Canine and Feline Wound Management and Reconstruction* (pp. 15-24). BSAVA Library.
- Pott, F. S. , Meier, M. J. , Stocco, J. G. D. , Crozeta, K. , & Ribas, J. D. (2014). The effectiveness of hydrocolloid dressings versus other dressings in the healing of pressure ulcers in adults and older adults: a systematic review and meta-analysis. *Revista latino-americana de enfermagem*, 22, 511-520.
- Pourshahrestani, S. , Zeimaran, E. , Kadri, N. A. , Mutlu, N. , & Boccaccini, A. R. (2020). Polymeric hydrogel systems as emerging biomaterial platforms to enable hemostasis and wound healing. *Advanced healthcare materials*, 9 (20), 2000905.
- Pradeepa, R. , & Mohan, V. (2002). The changing scenario of the diabetes epidemic implications for India. *Indian Journal of Medical Research*, 116, 121.
- Premarathna, A. D. , Ranaheva, T. H. , Wijesekera, S. K. , Wijesundara, R. R. M. K. K. , Jayasooriya, A. P. , Wijewardana, V. , & Rajapakse, R. P. V. J. (2019). Wound healing properties of aqueous extracts of *Sargassum illicifolium*: An in vitro assay. *Wound Medicine*, 24 (1), 1-7.
- Qin, W. , Wu, Y. , Liu, J. , Yuan, X. , & Gao, J. (2022). A comprehensive review of the application of nanoparticles in diabetic wound healing: therapeutic potential and future perspectives. *International Journal of Nanomedicine*, 17, 6007.
- Rachdaoui, N. (2020). Insulin: the friend and the foe in the development of type 2 diabetes mellitus. *International journal of molecular sciences*, 21 (5), 1770.
- Racz, R. S. , Ramanujam, C. L. , & Zgonis, T. (2010). Puncture wounds of the foot. *Clinics in podiatric medicine and surgery*, 27 (4), 523-534.
- Rahal, A. , Kumar, A. , Singh, V. , Yadav, B. , Tiwari, R. , Chakraborty, S. , & Dhama, K. (2014). Oxidative stress, prooxidants, and antioxidants: the interplay. *BioMed research international*, 2014 (1), 761264.
- Rahman, M. A. , Abul Barkat, H. , Harwansh, R. K. , & Deshmukh, R. (2022). Carbon-based nanomaterials: carbon nanotubes, graphene, and fullerenes for the control of burn infections and wound healing. *Current Pharmaceutical Biotechnology*, 23 (12), 1483-1496.
- Rai, S. , Gupta, T. P. , Shaki, O. , & Kale, A. (2023). Hydrogen Peroxide: Its Use in an Extensive Acute Wound to Promote Wound Granulation and Infection Control–Is it

Better Than Normal Saline?. *The International Journal of Lower Extremity Wounds*, 22 (3), 563-577.

- Rajangam, T. , & An, S. S. A. (2013). Fibrinogen and fibrin based micro and nano scaffolds incorporated with drugs, proteins, cells and genes for therapeutic biomedical applications. *International journal of nanomedicine*, 3641-3662.
- Ramadan, E. , Borg, T. , Abdelghani, G. , & Saleh, N. M. (2016). Transdermal microneedle-mediated delivery of polymeric lamivudine-loaded nanoparticles. *J. Pharm. Technol. Drug Res*, 5 (1), 1.
- Rasheeda, K. , Bharathy, H. , & Fathima, N. N. (2018). Vanillic acid and Syringic acid: Exceptionally robust aromatic moieties for inhibiting in vitro self-assembly of type I collagen. *International journal of biological macromolecules*, 113, 952-960.
- Re, R. , Pellegrini, N. , Proteggente, A. , Pannala, A. , Yang, M. , & Rice-Evans, C. (1999). Antioxidant activity applying an improved ABTS radical cation decolorization assay. *Free radical biology and medicine*, 26 (9-10), 1231-1237.
- Re, R. , Pellegrini, N. , Proteggente, A. , Pannala, A. , Yang, M. , & Rice-Evans, C. (1999). Antioxidant activity applying an improved ABTS radical cation decolorization assay. *Free radical biology & medicine*, 26 (9-10), 1231–1237.
- Reginelli, A. , Pinto, A. , Russo, A. , Fontanella, G. , Rossi, C. , Del Prete, A. , . . . & Brunese, L. (2015). Sharp penetrating wounds: spectrum of imaging findings and legal aspects in the emergency setting. *La radiologia medica*, 120, 856-865.
- Reis, J. P. , Loria, C. M. , Sorlie, P. D. , Park, Y. , Hollenbeck, A. , & Schatzkin, A. (2011). Lifestyle factors and risk for new-onset diabetes: a population-based cohort study. *Annals of internal medicine*, 155 (5), 292-299.
- Ren, J. , Yang, M. , Xu, F. , Chen, J. , & Ma, S. (2019). Acceleration of wound healing activity with Syringic acid in streptozotocin induced diabetic rats. *Life sciences*, 233, 116728.
- Ren, J. , Yang, M. , Xu, F. , Chen, J. , & Ma, S. (2019). Acceleration of wound healing activity with Syringic acid in streptozotocin induced diabetic rats. *Life sciences*, 233, 116728.
- Ren, J. , Yang, M. , Xu, F. , Chen, J. , & Ma, S. (2019). Acceleration of wound healing activity with Syringic acid in streptozotocin induced diabetic rats. *Life sciences*, 233, 116728.

- Rennie, J. K. (1926). The Treatment of Diabetes, with Special Reference to Treatment With Insulin and Its Results (Doctoral dissertation, University of Glasgow (United Kingdom)).
- Rezvani Ghomi, E. , Khalili, S. , Nouri Khorasani, S. , Esmaeely Neisiany, R. , & Ramakrishna, S. (2019). Wound dressings: Current advances and future directions. *Journal of Applied Polymer Science*, 136 (27), 47738.
- Rizeq, A. A. (2008). Diabetes mellitus in Cyprus.
- Rocha, J. , Eduardo-Figueira, M. , Barateiro, A. , Fernandes, A. , Brites, D. , Bronze, R. , . . . & Sepodes, B. (2015). Anti-inflammatory effect of rosmarinic acid and an extract of *Rosmarinus officinalis* in rat models of local and systemic inflammation. *Basic & clinical pharmacology & toxicology*, 116 (5), 398-413.
- Rodrigues, M. , Kosaric, N. , Bonham, C. A. , & Gurtner, G. C. (2019). Wound healing: a cellular perspective. *Physiological reviews*, 99 (1), 665-706.
- Rodrigues, M. , Kosaric, N. , Bonham, C. A. , & Gurtner, G. C. (2019). Wound healing: a cellular perspective. *Physiological reviews*, 99 (1), 665-706.
- Roeckl-Wiedmann, I. , Bennett, M. , & Kranke, P. (2005). Systematic review of hyperbaric oxygen in the management of chronic wounds. *Journal of British Surgery*, 92 (1), 24-32.
- Rooney, A. (2009). The story of medicine. Arcturus Publishing.
- Rostami, A. , Baluchnejadmojarad, T. , & Roghani, M. (2022). Sinapic acid ameliorates paracetamol-induced acute liver injury through targeting oxidative stress and inflammation. *Molecular Biology Reports*, 49 (6), 4179-4191.
- Rozentsvit, A. , Vinokur, K. , Samuel, S. , Li, Y. , Gerdes, A. M. , & Carrillo-Sepulveda, M. A. (2017). Ellagic acid reduces high glucose-induced vascular oxidative stress through ERK1/2/NOX4 signaling pathway. *Cellular Physiology and Biochemistry*, 44 (3), 1174-1187.
- Ruchat, S. M. , Elks, C. E. , Loos, R. J. , Vohl, M. C. , Weisnagel, S. J. , Rankinen, T. , . . . & Pérusse, L. (2009). Association between insulin secretion, insulin sensitivity and type 2 diabetes susceptibility variants identified in genome-wide association studies. *Acta diabetologica*, 46, 217-226.
- Sabarees, G. , Velmurugan, V. , Tamilarasi, G. P. , Alagarsamy, V. , & Raja Solomon, V. (2022). Recent advances in silver nanoparticles containing nanofibers for chronic wound management. *Polymers*, 14 (19), 3994.

- Sadat, Z. , Farrokhi-Hajiabad, F. , Lalebeigi, F. , Naderi, N. , Gorab, M. G. , Cohan, R. A. , . . . & Maleki, A. (2022). A comprehensive review on the applications of carbon-based nanostructures in wound healing: from antibacterial aspects to cell growth stimulation. *Biomaterials Science*, 10 (24), 6911-6938.
- Sadidi, H. , Hooshmand, S. , Ahmadabadi, A. , Javad Hoseini, S. , Baino, F. , Vatanpour, M. , & Kargozar, S. (2020). Cerium oxide nanoparticles (Nanoceria): Hopes in soft tissue engineering. *Molecules*, 25 (19), 4559.
- Sajjad, A. , Ali, H. , & Zia, M. (2023). Fabrication and evaluation of vitamin doped ZnO/AgNPs nanocomposite based wheat gluten films: a promising findings for burn wound treatment. *Scientific Reports*, 13 (1), 16072.
- Salazar, J. J. , Ennis, W. J. , & Koh, T. J. (2016). Diabetes medications: Impact on inflammation and wound healing. *Journal of diabetes and its complications*, 30 (4), 746–752. <https://doi.org/10.1016/j.jdiacomp.2015.12.017>
- Salvatore, T. , &Giugliano, D. (1996). Pharmacokinetic-pharmacodynamic relationships of Acarbose. *Clinical pharmacokinetics*, 30 (2), 94-106.
- Sanders, L. J. (2002). From Thebes to Toronto and the 21st century: an incredible journey. *Diabetes Spectrum*, 15 (1), 56.
- Sandoval, C. , Rios, G. , Sepulveda, N. , Salvo, J. , Souza-Mello, V. , & Farias, J. (2022). Effectiveness of copper nanoparticles in wound healing process using in vivo and in vitro studies: a systematic review. *Pharmaceutics*, 14 (9), 1838.
- Santos, R. , Gomes, D. , Macedo, H. , Barros, D. , Tibério, C. , Veiga, A. S. , . . . & Oliveira, M. (2016). Guar gum as a new antimicrobial peptide delivery system against diabetic foot ulcers *Staphylococcus aureus* isolates. *Journal of Medical Microbiology*, 65 (10), 1092-1099.
- Saravanakumar, K. , Sathiyaseelan, A. , Zhang, X. , Choi, M. , & Wang, M. H. (2023). Bimetallic (Ag and MgO) nanoparticles, Aloe vera extracts loaded xanthan gum nanocomposite for enhanced antibacterial and in-vitro wound healing activity. *International Journal of Biological Macromolecules*, 242, 124813.
- Sargsyan, A. , & Herman, M. A. (2019). Regulation of glucose production in the pathogenesis of type 2 diabetes. *Current diabetes reports*, 19, 1-11.
- Sarkar, P. , Bhattacharya, S. , & Pal, T. K. (2019). Application of statistical design to evaluate critical process parameters and optimize formulation technique of polymeric nanoparticles. *Royal Society open science*, 6 (7), 190896.

- Sarmah, J. K. , Bhattacharjee, S. K. , Mahanta, R. , & Mahanta, R. (2009). Preparation of cross-linked guar gum nanospheres containing tamoxifen citrate by single step emulsion in situ polymer cross-linking method. *Journal of Inclusion Phenomena and Macrocyclic Chemistry*, 65, 329-334.
- Sarmah, J. K. , Dutta, A. , Sarmah, S. , & Ankamwar, B. (2022). Guar gum nanoparticles: A new paradigm in biomedical applications. In *Polysaccharide Nanoparticles* (pp. 119-144). Elsevier.
- Sbraccia, P. , D'Adamo, M. , & Guglielmi, V. (2021). Is type 2 diabetes an adiposity-based metabolic disease? From the origin of insulin resistance to the concept of dysfunctional adipose tissue. *Eating and Weight Disorders-Studies on Anorexia, Bulimia and Obesity*, 1-13.
- Schäfer, M. , & Werner, S. (2008). Oxidative stress in normal and impaired wound repair. *Pharmacological research*, 58 (2), 165-171.
- Schäfer, M. , & Werner, S. (2008). Oxidative stress in normal and impaired wound repair. *Pharmacological research*, 58 (2), 165-171.
- Schiestl, C. , Meuli, M. , Trop, M. , & Neuhaus, K. (2013). Management of burn wounds. *European Journal of Pediatric Surgery*, 23 (05), 341-348.
- Schultz, G. S. , Sibbald, R. G. , Falanga, V. , Ayello, E. A. , Dowsett, C. , Harding, K. , . . . & Vanscheidt, W. (2003). Wound bed preparation: a systematic approach to wound management. *Wound repair and regeneration*, 11, S1-S28.
- Sell, S. , Barnes, C. , Smith, M. , McClure, M. , Madurantakam, P. , Grant, J. , . . . & Bowlin, G. (2007). Extracellular matrix regenerated: tissue engineering via electrospun biomimetic nanofibers. *Polymer International*, 56 (11), 1349-1360.
- Selvakumar, G. , & Lonchin, S. (2023). A bio-polymeric scaffold incorporated with p-Coumaric acid enhances diabetic wound healing by modulating MMP-9 and TGF- β 3 expression. *Colloids and Surfaces B: Biointerfaces*, 225, 113280.
- Selvakumar, G. , & Lonchin, S. (2023). A bio-polymeric scaffold incorporated with p-Coumaric acid enhances diabetic wound healing by modulating MMP-9 and TGF- β 3 expression. *Colloids and Surfaces B: Biointerfaces*, 225, 113280.
- Serra, M. B. , Barroso, W. A. , Silva, N. N. D. , Silva, S. D. N. , Borges, A. C. R. , Abreu, I. C. , & Borges, M. O. D. R. (2017). From inflammation to current and alternative therapies involved in wound healing. *International journal of inflammation*, 2017.

- Shafique, M. , Sohail, M. , Minhas, M. U. , Khaliq, T. , Kousar, M. , Khan, S. , . . . & Shah, S. A. (2021). Bio-functional hydrogel membranes loaded with chitosan nanoparticles for accelerated wound healing. *International Journal of Biological Macromolecules*, 170, 207-221.
- Shah, U. , Chatur, P. , Al-Ali, H. , Ahmad, M. , Gani, A. , Masoodi, F. A. , & Gani, A. (2019). Gum-Based Delivery Systems. In *Food Hydrocolloids as Encapsulating Agents in Delivery Systems* (pp. 29-84). CRC Press.
- Shai, L. J. , Magano, S. R. , Lebelo, S. L. , & Mogale, A. M. (2011). Inhibitory effects of five medicinal plants on rat alpha-glucosidase: Comparison with their effects on yeast alpha-glucosidase. *Journal of Medicinal Plants Research*, 5 (13), 2863-2867.
- Shaikh, A. , Kesharwani, P. , & Gajbhiye, V. (2022). Dendrimer as a momentous tool in tissue engineering and regenerative medicine. *Journal of Controlled Release*, 346, 328-354.
- Shairibha, S. R. , Rajadurai, M. , & Kumar, N. A. (2014). Effect of p-Coumaric acid on biochemical parameters in Streptozotocin-induced diabetic rats. *Journal of Academia and Industrial Research (JAIR)*, 3 (5), 237.
- Shamiya, Y. , Ravi, S. P. , Coyle, A. , Chakrabarti, S. , & Paul, A. (2022). Engineering nanoparticle therapeutics for impaired wound healing in diabetes. *Drug Discovery Today*, 27 (4), 1156-1166.
- Shao, X. R. , Wei, X. Q. , Song, X. , Hao, L. Y. , Cai, X. X. , Zhang, Z. R. , Peng, Q. , & Lin, Y. F. (2015). Independent effect of polymeric nanoparticle zeta potential/surface charge, on their cytotoxicity and affinity to cells. *Cell proliferation*, 48 (4), 465–474. <https://doi.org/10.1111/cpr.12192>
- Sharif, S. , Van der Graaf, Y. , Cramer, M. J. , Kapelle, L. J. , de Borst, G. J. , Visseren, F. L. , . . . & SMART study group R. van Petersen BGF Dinther A. Algra Y. van der Graaf DE Grobbee GEHM Rutten FLJ Visseren GJ de Borst LJ Kappelle T. Leiner HM Nathoe. (2021). Low-grade inflammation as a risk factor for cardiovascular events and all-cause mortality in patients with type 2 diabetes. *Cardiovascular diabetology*, 20, 1-8.
- Sharifi-Rad, M. , Anil Kumar, N. V. , Zucca, P. , Varoni, E. M. , Dini, L. , Panzarini, E. , . . . & Sharifi-Rad, J. (2020). Lifestyle, oxidative stress, and antioxidants: back and forth in the pathophysiology of chronic diseases. *Frontiers in physiology*, 11, 694.

- Sharma, A. K. , Sahoo, P. K. , Majumdar, D. K. , & Panda, A. K. (2016). Topical ocular delivery of a COX-II inhibitor via biodegradable nanoparticles. *Nanotechnology Reviews*, 5 (5), 435-444.
- Sharma, G. , Sharma, S. , Kumar, A. , Ala'a, H. , Naushad, M. , Ghfar, A. A. , . . . & Stadler, F. J. (2018). Guar gum and its composites as potential materials for diverse applications: A review. *Carbohydrate polymers*, 199, 534-545.
- Sharma, G. , Sharma, S. , Kumar, A. , Ala'a, H. , Naushad, M. , Ghfar, A. A. , . . . & Stadler, F. J. (2018). Guar gum and its composites as potential materials for diverse applications: A review. *Carbohydrate polymers*, 199, 534-545.
- Sharma, M. , Malik, R. , Verma, A. , Dwivedi, P. , Banoth, G. S. , Pandey, N. , . . . & Dwivedi, A. K. (2013). Folic acid conjugated guar gum nanoparticles for targeting methotrexate to colon cancer. *Journal of biomedical nanotechnology*, 9 (1), 96-106.
- Sharma, O. P. , & Bhat, T. K. (2009). DPPH antioxidant assay revisited. *Food chemistry*, 113 (4), 1202-1205.
- Shetlar, M. R. , Lacefield, E. G. , White, B. N. , & Schilling, J. A. (1959). Wound healing: glycoproteins of wound tissue. I. Studies of hexosamine, hexose, and uronic acids content. *Proceedings of the Society for Experimental Biology and Medicine*, 100 (3), 501-503.
- Shrestha, R. , Krishan, K. , & Kanchan, T. (2020). Abrasion.
- Shukla, A. , Rasik, A. M. , & Patnaik, G. K. (1997). Depletion of reduced glutathione, ascorbic acid, vitamin E and antioxidant defence enzymes in a healing cutaneous wound. *Free radical research*, 26 (2), 93-101.
- Shukla, A. , Rasik, A. M. , & Patnaik, G. K. (1997). Depletion of reduced glutathione, ascorbic acid, vitamin E and antioxidant defence enzymes in a healing cutaneous wound. *Free radical research*, 26 (2), 93-101.
- Simoes, A. , Veiga, F. , & Vitorino, C. (2019). Developing cream formulations: renewed interest in an old problem. *Journal of Pharmaceutical Sciences*, 108 (10), 3240-3251.
- Singh, H. , Jindal, S. , Singh, M. , Sharma, G. , & Kaur, I. P. (2015). Nano-formulation of rifampicin with enhanced bioavailability: development, characterization and in-vivo safety. *International Journal of Pharmaceutics*, 485 (1-2), 138-151.
- Singh, M. , Tiwary, A. K. , & Kaur, G. (2010). Investigations on interpolymer complexes of cationic guar gum and xanthan gum for formulation of bioadhesive films. *Research in pharmaceutical sciences*, 5 (2), 79.

- Singh, M., Kumar, N., Sood, S., Makkar, B., & Arora, V. (2010). Historical milestones in diabetes. *Australasian Medical Journal (Online)*, 3(13), 860.
- Singh, S. , Young, A. , & McNaught, C. E. (2017). The physiology of wound healing. *Surgery (Oxford)*, 35 (9), 473-477.
- Singla, R. , Soni, S. , Patial, V. , Kulurkar, P. M. , Kumari, A. , Mahesh, S. , . . . & Yadav, S. K. (2017). In vivo diabetic wound healing potential of nanobiocomposites containing bamboo cellulose nanocrystals impregnated with silver nanoparticles. *International journal of biological macromolecules*, 105, 45-55.
- Smith, B. R. , & Gambhir, S. S. (2017). Nanomaterials for in vivo imaging. *Chemical reviews*, 117 (3), 901-986.
- Smruthi, M. R. , Nallamuthu, I. , & Anand, T. (2022). A comparative study of optimized naringenin nanoformulations using nanocarriers (PLA/PVA and zein/pectin) for improvement of bioavailability. *Food Chemistry*, 369, 130950.
- Sohail, M. , Khan, S. A. , Minhas, M. U. , Mahmood, A. , Shah, S. A. , & Mohsin, S. (2022). Chitosan/guar gum-based thermoreversible hydrogels loaded with pullulan nanoparticles for enhanced nose-to-brain drug delivery. *International Journal of Biological Macromolecules*, 215, 579-595.
- Solarte David, V. A. , Güiza-Argüello, V. R. , Arango-Rodríguez, M. L. , Sossa, C. L. , & Becerra-Bayona, S. M. (2022). Decellularized tissues for wound healing: Towards closing the gap between scaffold design and effective extracellular matrix remodeling. *Frontiers in Bioengineering and Biotechnology*, 10, 821852.
- Soltani, M. D. , Meftahizadeh, H. , Barani, M. , Rahdar, A. , Hosseinikhah, S. M. , Hatami, M. , & Ghorbanpour, M. (2021). Guar (*Cyamopsis tetragonoloba* L.) plant gum: From biological applications to advanced nanomedicine. *International Journal of Biological Macromolecules*, 193, 1972-1985.
- Somade, O. T. , Oyinloye, B. E. , Ajiboye, B. O. , & Osukoya, O. A. (2023). Syringic acid demonstrates an anti-inflammatory effect via modulation of the NF-κB-iNOS-COX-2 and JAK-STAT signaling pathways in methyl cellosolve-induced hepato-testicular inflammation in rats. *Biochemistry and Biophysics Reports*, 34, 101484.
- Somagoni, J. , Boakye, C. H. , Godugu, C. , Patel, A. R. , Mendonca Faria, H. A. , Zucolotto, V. , & Singh, M. (2014). Nanomimetic-a novel drug delivery system for topical application-in vitro and in vivo evaluation. *PLoS One*, 9 (12), e115952.

- Sorg, H. , & Sorg, C. G. (2023). Skin wound healing: of players, patterns, and processes. *European Surgical Research*, 64 (2), 141-157.
- Sorg, H. , Tilkorn, D. J. , Hager, S. , Hauser, J. , & Mirastschijski, U. (2017). Skin wound healing: an update on the current knowledge and concepts. *European Surgical Research*, 58 (1-2), 81-94.
- Soyoye, D. O. , Abiodun, O. O. , Ikem, R. T. , Kolawole, B. A. , & Akintomide, A. O. (2021). Diabetes and peripheral artery disease: A review. *World journal of diabetes*, 12 (6), 827.
- Spann, C. T. , Taylor, S. C. , & Weinberg, J. M. (2003). Topical antimicrobial agents in dermatology. *Clinics in dermatology*, 21 (1), 70-77.
- Srinivasulu, C. , Ramgopal, M. , Ramanjaneyulu, G. , Anuradha, C. M. , & Kumar, C. S. (2018). Syringic acid (SA)—a review of its occurrence, biosynthesis, pharmacological and industrial importance. *Biomedicine & Pharmacotherapy*, 108, 547-557.
- Stoica, A. E. , Chircov, C. , & Grumezescu, A. M. (2020). Nanomaterials for wound dressings: an up-to-date overview. *Molecules*, 25 (11), 2699.
- Stone, B. G. , & Van Thiel, D. H. (1985, February). Diabetes mellitus and the liver. In *Seminars in liver disease* (Vol. 5, No. 01, pp. 8-28). © 1985 by Thieme Medical Publishers, Inc. .
- Sun, H. , Saeedi, P. , Karuranga, S. , Pinkepank, M. , Ogurtsova, K. , Duncan, B. B. , . . & Magliano, D. J. (2022). IDF Diabetes Atlas: Global, regional and country-level diabetes prevalence estimates for 2021 and projections for 2045. *Diabetes research and clinical practice*, 183, 109119.
- Sunayana, N. , Uzma, M. , Dhanwini, R. P. , Govindappa, M. , Prakash, H. S. , & Vinay Raghavendra, B. (2020). Green synthesis of gold nanoparticles from Vitex negundo leaf extract to inhibit lipopolysaccharide-induced inflammation through in vitro and in vivo. *Journal of Cluster Science*, 31, 463-477.
- Sweetey, J. P. , Sowparani, S. , Mahalakshmi, P. , Selvasudha, N. , Yamini, D. , Geetha, K. , & Ruckmani, K. (2020). Fabrication of stimuli gated nanoformulation for site-specific delivery of thymoquinone for colon cancer treatment—insight into thymoquinone’s improved physicochemical properties. *Journal of Drug Delivery Science and Technology*, 55, 101334.

- Syarina, P. N. A. , Karthivashan, G. , Abas, F. , Arulselvan, P. , &Fakurazi, S. (2015). Wound healing potential of *Spirulina platensis* extracts on human dermal fibroblast cells. *EXCLI journal*, 14, 385.
- Szablewski, L. (2011). Glucose homeostasis–mechanism and defects. *Diabetes-Damages and Treatments*, 2.
- Tahmouzi, S. , Meftahizadeh, H. , Eyshi, S. , Mahmoudzadeh, A. , Alizadeh, B. , Mollakhalili-Meybodi, N. , & Hatami, M. (2023). Application of guar (*Cyamopsis tetragonoloba* L.) gum in food technologies: A review of properties and mechanisms of action. *Food Science & Nutrition*.
- Taofiq, O. , Calhella, R. C. , Heleno, S. , Barros, L. , Martins, A. , Santos-Buelga, C. , . . . & Ferreira, I. C. (2015). The contribution of phenolic acids to the anti-inflammatory activity of mushrooms: Screening in phenolic extracts, individual parent molecules and synthesized glucuronated and methylated derivatives. *Food Research International*, 76, 821-827.
- Taofiq, O. , González-Paramás, A. M. , Barreiro, M. F. , & Ferreira, I. C. (2017). Hydroxycinnamic acids and their derivatives: Cosmeceutical significance, challenges and future perspectives, a review. *Molecules*, 22 (2), 281.
- Taylor, P. (1998). Ostwald ripening in emulsions. *Advances in colloid and interface science*, 75 (2), 107-163.
- Thackham, J. A. , McElwain, D. S. , & Long, R. J. (2008). The use of hyperbaric oxygen therapy to treat chronic wounds: a review. *Wound Repair and Regeneration*, 16 (3), 321-330.
- Thombare, N. , Jha, U. , Mishra, S. , & Siddiqui, M. Z. (2016). Guar gum as a promising starting material for diverse applications: A review. *International journal of biological macromolecules*, 88, 361-372.
- TrigoGutierrez, J. K. , VegaChacón, Y. , Soares, A. B. , &Mima, E. G. D. O. (2021). Antimicrobial activity of curcumin in nanoformulations: A comprehensive review. *International journal of molecular sciences*, 22 (13), 7130.
- Trott, A. T. (2012). *Wounds and Lacerations: Emergency Care and Closure* (Expert Consult-Online and Print). Elsevier Health Sciences.
- Tsakiroglou, P. , VandenAkker, N. E. , Del Bo', C. , Riso, P. , & Klimis-Zacas, D. (2019). Role of berry anthocyanins and phenolic acids on cell migration and angiogenesis: An updated overview. *Nutrients*, 11 (5), 1075.

- Tsakiroglou, P. , VandenAkker, N. E. , Del Bo', C. , Riso, P. , & Klimis-Zacas, D. (2019). Role of berry anthocyanins and phenolic acids on cell migration and angiogenesis: An updated overview. *Nutrients*, 11 (5), 1075.
- Tutar, U. , Hepokur, C. , Misir, S. E. M. A. , Hepokur, A. I. , & DUMAN, F. (2018). Antimicrobial, Antioxidant, Cytotoxic and Wound Healing Effects of *Thymra sintenisii* Extract. *Indian Journal of Pharmaceutical Sciences*, 80 (5).
- Tyavambiza, C. , Meyer, M. , & Meyer, S. (2022). Cellular and molecular events of wound healing and the potential of silver based nanoformulations as wound healing agents. *Bioengineering*, 9 (11), 712.
- Uzun, M. U. H. A. M. M. E. T. , Anand, S. C. , & Shah, T. (2012). The effect of wound dressings on the pH stability of fluids. *Journal of wound care*, 21 (2), 88-95.
- Veeraraghavan, V. P. , Periadurai, N. D. , Karunakaran, T. , Hussain, S. , Surapaneni, K. M. , & Jiao, X. (2021). Green synthesis of silver nanoparticles from aqueous extract of *Scutellaria barbata* and coating on the cotton fabric for antimicrobial applications and wound healing activity in fibroblast cells (L929). *Saudi journal of biological sciences*, 28 (7), 3633-3640.
- Verma, D. , & Sharma, S. K. (2021). Recent advances in guar gum based drug delivery systems and their administrative routes. *International Journal of Biological Macromolecules*, 181, 653-671.
- Verma, D. , & Sharma, S. K. (2021). Recent advances in guar gum based drug delivery systems and their administrative routes. *International Journal of Biological Macromolecules*, 181, 653-671.
- Verma, D. , & Sharma, S. K. (2021). Recent advances in guar gum based drug delivery systems and their administrative routes. *International Journal of Biological Macromolecules*, 181, 653-671.
- Verma, D. , & Sharma, S. K. (2021). Recent advances in guar gum based drug delivery systems and their administrative routes. *International Journal of Biological Macromolecules*, 181, 653-671.
- Visha, M. G. , & Karunakaran, M. (2019). A review on wound healing. *International Journal of Clinicopathological Correlation*, 3 (2), 50-59.
- Volpe, C. M. O. , Villar-Delfino, P. H. , Dos Anjos, P. M. F. , & Nogueira-Machado, J. A. (2018). Cellular death, reactive oxygen species (ROS) and diabetic complications. *Cell death & disease*, 9 (2), 119.

- Wagner, A. E. , Huebbe, P. , Konishi, T. , Rahman, M. M. , Nakahara, M. , Matsugo, S. , & Rimbach, G. (2008). Free radical scavenging and antioxidant activity of ascorbigen versus ascorbic acid: studies in vitro and in cultured human keratinocytes. *Journal of agricultural and food chemistry*, 56 (24), 11694-11699.
- Wang, G. , Yang, F. , Zhou, W. , Xiao, N. , Luo, M. , & Tang, Z. (2023). The initiation of oxidative stress and therapeutic strategies in wound healing. *Biomedicine & Pharmacotherapy*, 157, 114004.
- Wang, M. , Huang, X. , Zheng, H. , Tang, Y. , Zeng, K. , Shao, L. , & Li, L. (2021). Nanomaterials applied in wound healing: Mechanisms, limitations and perspectives. *Journal of Controlled Release*, 337, 236-247.
- Wang, Y. , Chen, C. , He, C. , Dong, W. , Yang, X. , Wu, Y. , . . . & Yan, B. (2024). A self-healing injectable hydrogel integrated with enzymatic and nonenzymatic antioxidants as artificial antioxidant defense system for diabetic wound healing. *Materials & Design*, 237, 112620.
- Werner, A. H. , & Russell, A. D. (1999). Mupirocin, fusidic acid and bacitracin: activity, action and clinical uses of three topical antibiotics. *Veterinary Dermatology*, 10 (3), 225-240.
- Wing, R. R. , Goldstein, M. G. , Acton, K. J. , Birch, L. L. , Jakicic, J. M. , Sallis Jr, J. F. , . . . & Surwit, R. S. (2001). Behavioral science research in diabetes: lifestyle changes related to obesity, eating behavior, and physical activity. *Diabetes care*, 24 (1), 117-123.
- Wolcott, R. D. , Cutting, K. F. , Dowd, S. E. , & Percival, S. L. (2010). Types of wounds and infections. *Microbiology of wounds*, 219-32.
- World Health Organization. (2016). *Guideline daily iron supplementation in infants and children*. World Health Organization.
- Wu SC, Driver VR, Wrobel JS, Armstrong DG. Foot ulcers in the diabetic patient, prevention and treatment. *Vasc Health Risk Manag*. 2007;3 (1): 65.
- Wynn, M. , & Freeman, S. (2019). The efficacy of negative pressure wound therapy for diabetic foot ulcers: A systematised review. *Journal of Tissue Viability*, 28 (3), 152-160.
- Xu, M. , Qin, H. , Zheng, Y. , Chen, J. , Liang, X. , Huang, J. , . . . & Guan, Y. Q. (2022). Construction of a double-responsive modified guar gum nanoparticles and its

application in oral insulin administration. *Colloids and Surfaces B: Biointerfaces*, 220, 112858.

- Xuan, Y. H. , Huang, B. B. , Tian, H. S. , Chi, L. S. , Duan, Y. M. , Wang, X. , . . . & Jin, L. T. (2014). High-glucose inhibits human fibroblast cell migration in wound healing via repression of bFGF-regulating JNK phosphorylation. *PloS one*, 9 (9), e108182.
- Xue, Y. , Yang, F. , Wu, L. , Xia, D. , & Liu, Y. (2024). CeO₂ nanoparticles to promote wound healing: a systematic review. *Advanced Healthcare Materials*, 13 (6), 2302858.
- Yadav, H. , Maji, B. , & Maiti, S. (2024). Novel succinoylated carboxymethyl guar gum nanocarriers of glimepiride for controlling type-2 diabetes. *Medicine in Novel Technology and Devices*, 100309.
- Yadav, N. , Francis, A. P. , Priya, V. V. , Patil, S. , Mustaq, S. , Khan, S. S. , . . . & Rajagopalan, R. (2022). Polysaccharide-drug conjugates: A tool for enhanced cancer therapy. *Polymers*, 14 (5), 950.
- Yan, L. , Wu, W. , Wang, Z. , Li, C. , Lu, X. , Duan, H. , . . . & Han, Y. (2013). Comparative study of the effects of recombinant human epidermal growth factor and basic fibroblast growth factor on corneal epithelial wound healing and neovascularization in vivo and in vitro. *Ophthalmic research*, 49 (3), 150-160.
- Yang, J. , Li, H. , Wang, X. , Zhang, C. , Feng, G. , & Peng, X. (2021). Inhibition mechanism of α -amylase/ α -glucosidase by silibinin, its synergism with acarbose, and the effect of milk proteins. *Journal of Agricultural and Food Chemistry*, 69 (36), 10515-10526.
- Yang, Q. , Fang, D. , Chen, J. , Hu, S. , Jiang, J. , Zeng, M. , & Luo, M. (2023). LncRNAs associated with oxidative stress in diabetic wound healing: regulatory mechanisms and application prospects. *Theranostics*, 13 (11), 3655.
- Yang, X. , Liu, W. , Li, N. , Wang, M. , Liang, B. , Ullah, I. , . . . & Shi, C. (2017). Design and development of polysaccharide hemostatic materials and their hemostatic mechanism. *Biomaterials Science*, 5 (12), 2357-2368.
- Yang, X. , Wang, D. , Zhou, Q. , Nie, F. , Du, H. , Pang, X. , . . . & Xu, Y. (2019). Antimicrobial susceptibility testing of Enterobacteriaceae: determination of disk content and Kirby-Bauer breakpoint for ceftazidime/avibactam. *BMC microbiology*, 19, 1-7.

- Yang, Z. , Huang, R. , Zheng, B. , Guo, W. , Li, C. , He, W. , . . . & Wang, H. (2021). Highly stretchable, adhesive, biocompatible, and antibacterial hydrogel dressings for wound healing. *Advanced science*, 8 (8), 2003627.
- Yee, H. S. , & Fong, N. T. (1996). A review of the safety and efficacy of acarbose in diabetes mellitus. *Pharmacotherapy: The Journal of Human Pharmacology and Drug Therapy*, 16 (5), 792-805.
- Young, A. , & McNaught, C. E. (2011). The physiology of wound healing. *Surgery (Oxford)*, 29 (10), 475-479.
- Younis, N. S. , El Semary, N. A. , & Mohamed, M. E. (2021). Silver nanoparticles green synthesis via cyanobacterium *Phormidium* sp. : characterization, wound healing, antioxidant, antibacterial, and anti-inflammatory activities. *European Review for Medical & Pharmacological Sciences*, 25 (7).
- Yu, H. , Chen, X. , Cai, J. , Ye, D. , Wu, Y. , Fan, L. , & Liu, P. (2019). Novel porous three-dimensional nanofibrous scaffolds for accelerating wound healing. *Chemical Engineering Journal*, 369, 253-262.
- Yue, D. K. , McLennan, S. , Marsh, M. , Mai, Y. W. , Spaliviero, J. , Delbridge, L. , . . . & Turtle, J. R. (1987). Effects of experimental diabetes, uremia, and malnutrition on wound healing. *Diabetes*, 36 (3), 295-299.
- Yun, K. J. , Koh, D. J. , Kim, S. H. , Park, S. J. , Ryu, J. H. , Kim, D. G. , . . . & Lee, K. T. (2008). Anti-inflammatory effects of Sinapic acid through the suppression of inducible nitric oxide synthase, cyclooxygenase-2, and proinflammatory cytokines expressions via nuclear factor- κ B inactivation. *Journal of agricultural and food chemistry*, 56 (21), 10265-10272.
- Yun, Y. R. , Won, J. E. , Jeon, E. , Lee, S. , Kang, W. , Jo, H. , . . . & Kim, H. W. (2010). Fibroblast growth factors: biology, function, and application for tissue regeneration. *Journal of tissue engineering*, 1 (1), 218142.
- Zafari, F. , Shirian, S. , Sadeghi, M. , Teimourian, S. , & Bakhtiyari, M. (2020). CD93 hematopoietic stem cells improve diabetic wound healing by VEGF activation and downregulation of DAPK-1. *Journal of Cellular Physiology*, 235 (3), 2366-2376.
- Zelinka, A. , Roelofs, A. J. , Kandel, R. A. , & De Bari, C. (2022). Cellular therapy and tissue engineering for cartilage repair. *Osteoarthritis and Cartilage*.

- Zhang, L. , Sang, Y. , Feng, J. , Li, Z. , & Zhao, A. (2016). Polysaccharide-based micro/nanocarriers for oral colon-targeted drug delivery. *Journal of drug targeting*, 24 (7), 579-589.
- Zhang, X. , Wei, P. , Yang, Z. , Liu, Y. , Yang, K. , Cheng, Y. , . . . & Zhang, Z. (2022). Current progress and outlook of nano-based hydrogel dressings for wound healing. *Pharmaceutics*, 15 (1), 68.
- Zhao, Q. , Liu, J. , Liu, S. , Han, J. , Chen, Y. , Shen, J. , . . . & Ma, X. (2022). Multipronged Micelles–Hydrogel for Targeted and Prolonged Drug Delivery in Chronic Wound Infections. *ACS Applied Materials & Interfaces*, 14 (41), 46224-46238.
- Zhao, R. , Liang, H. , Clarke, E. , Jackson, C. , & Xue, M. (2016). Inflammation in chronic wounds. *International journal of molecular sciences*, 17 (12), 2085.
- Zhao, R. , Liang, H. , Clarke, E. , Jackson, C. , & Xue, M. (2016). Inflammation in chronic wounds. *International journal of molecular sciences*, 17 (12), 2085.
- Zheng, K. , Tong, Y. , Zhang, S. , He, R. , Xiao, L. , Iqbal, Z. , . . . & Li, Y. (2021). Flexible bicolorimetric polyacrylamide/chitosan hydrogels for smart real-time monitoring and promotion of wound healing. *Advanced Functional Materials*, 31 (34), 2102599.
- Zheng, Y. , Ley, S. H. , & Hu, F. B. (2018). Global aetiology and epidemiology of type 2 diabetes mellitus and its complications. *Nature reviews endocrinology*, 14 (2), 88-98.
- Zochedh, A. , Priya, M. , Chakaravarthy, C. , Sultan, A. B. , & Kathiresan, T. (2023). Experimental and computational evaluation of Syringic acid–structural, spectroscopic, biological activity and docking simulation. *Polycyclic Aromatic Compounds*, 43 (7), 6516-6548.
- Zou, Y. , Kim, A. R. , Kim, J. E. , Choi, J. S. , & Chung, H. Y. (2002). Peroxynitrite scavenging activity of Sinapic acid (3, 5-dimethoxy-4-hydroxycinnamic acid) isolated from *Brassica juncea*. *Journal of Agricultural and Food Chemistry*, 50 (21), 5884-5890.